

Technical Report Documentation Page

1. Report No. FHWA/TX-08/7-2941-5		2. Government Accession No.		3. Recipient's Catalog No.	
4. Title and Subtitle Comprehensive Report on the Long-Term Behavior of High Performance Concrete Bridges in Texas				5. Report Date December 2007; Revised July 2008	
				6. Performing Organization Code	
7. Author(s) Brian C. Dahm, Dr. Ned Burns, Dr. Ramon Carrasquillo, Dr. David W. Fowler, David Whitney, Christopher Shoemaker				8. Performing Organization Report No. 7-2941-5	
9. Performing Organization Name and Address Center for Transportation Research The University of Texas at Austin 3208 Red River, Suite 200 Austin, TX 78705-2650				10. Work Unit No. (TRAIS)	
				11. Contract or Grant No. 7-2941	
12. Sponsoring Agency Name and Address Texas Department of Transportation Research and Technology Implementation Office P.O. Box 5080 Austin, TX 78763-5080				13. Type of Report and Period Covered 9/1/1999 – 8/31/2004	
				14. Sponsoring Agency Code	
15. Supplementary Notes Project performed in cooperation with the Texas Department of Transportation and the Federal Highway Administration.					
16. Abstract Final report summarizing the work done on Project 7-2941, "Long-term Behavior of High Performance Concrete (HPC) Bridges."					
17. Key Words High Performance Concrete, camber, instrumentation, long-term monitoring			18. Distribution Statement No restrictions. This document is available to the public through the National Technical Information Service, Springfield, Virginia 22161; www.ntis.gov.		
19. Security Classif. (of report) Unclassified	20. Security Classif. (of this page) Unclassified	21. No. of pages 324		22. Price	

Form DOT F 1700.7 (8-72) Reproduction of completed page authorized



Comprehensive Report on the Long-Term Behavior of High Performance Concrete Bridges in Texas

Brian C. Dahm
Dr. Ned Burns
Dr. Ramon Carrasquillo
Dr. David W. Fowler
David Whitney
Christopher Shoemaker

CTR Technical Report:	7-2941-5
Report Date:	December 2007; Revised July 2008
Project:	7-2941
Project Title:	Long-Term Behavior of High Performance Concrete (HPC) Bridges
Sponsoring Agency:	Texas Department of Transportation
Performing Agency:	Center for Transportation Research at The University of Texas at Austin

Project performed in cooperation with the Texas Department of Transportation and the Federal Highway Administration.

Center for Transportation Research
The University of Texas at Austin
3208 Red River
Austin, TX 78705

www.utexas.edu/research/ctr

Copyright (c) 2008
Center for Transportation Research
The University of Texas at Austin

All rights reserved
Printed in the United States of America

Disclaimers

Author's Disclaimer: The contents of this report reflect the views of the authors, who are responsible for the facts and the accuracy of the data presented herein. The contents do not necessarily reflect the official view or policies of the Federal Highway Administration or the Texas Department of Transportation (TxDOT). This report does not constitute a standard, specification, or regulation.

Patent Disclaimer: There was no invention or discovery conceived or first actually reduced to practice in the course of or under this contract, including any art, method, process, machine manufacture, design or composition of matter, or any new useful improvement thereof, or any variety of plant, which is or may be patentable under the patent laws of the United States of America or any foreign country.

Engineering Disclaimer

NOT INTENDED FOR CONSTRUCTION, BIDDING, OR PERMIT PURPOSES.

Project Engineer: Dr. David W. Fowler
Professional Engineer License State and Number: Texas No. 27859
P. E. Designation: Research Supervisor

Acknowledgments

Throughout the course of this research project, numerous people have lent their support and help. Thanks are expressed to all of these people who have provided aid in one form or another. The author wishes to thank several people specifically:

All of the employees we dealt with from the Houston, San Angelo, Lubbock, and Amarillo Districts and the Bridge Division at the Texas Department of Transportation must be thanked, in particular Gerry Fields, Bobby Bridges, Lewis Gamboa, and Sam Harris. Without their work, assistance, and patience much of the work on this project would not have been possible.

The authors also thank the staff of the Construction Materials Research Group (CMRG), Kerry Rothenbach, Michael Rung, and Sherian Williams. Their dedication, suggestions, and assistance were essential in the coordination of this long-term project.

There were numerous structures and materials students from CTR and CMRG who assisted in the project, and who also made it that much more enjoyable. These individuals often spent long hours reading Texas Bridge Inspection reports, loading toolboxes and equipment into vehicles, and traveling across Texas to closely inspect bridge elements and the authors thank them.

Faculty supervisors and consultants included Dr. Ned Burns, our reader and supervisor on the earlier associated projects' reports. His vast knowledge of prestressed concrete was greatly appreciated throughout this project. Dr. David Fowler, too, is appreciated for sharing so much of his time, effort, encouragement, suggestions, and support throughout this project.

Table of Contents

Chapter 1. Introduction.....	1
1.1 Background.....	1
1.2 Research Objectives.....	2
1.3 Outline of This Report	2
Chapter 2. Literature Review	5
2.1 Introduction.....	5
2.2 Definition of High Performance Concrete.....	5
2.3 Sources of Long-Term Prestress Loss	5
2.4 Predicting Long-Term Prestress Loss.....	7
2.5 Sources of Long-Term Camber	11
2.6 Predicting Long-Term Camber	11
2.7 Previous Durability Monitoring.....	12
Chapter 3. Structural HPC Bridge Descriptions and Data Acquisition System.....	15
3.1 Introduction.....	15
3.2 Louetta Road Overpass	15
3.3 TxDOT U54 Beam.....	18
3.4 North Concho River/US 87/South Orient Railroad Overpass	20
3.5 Original Data Acquisition System	23
3.6 Modifications to Data Acquisition System.....	26
3.7 Gauge Durability.....	29
Chapter 4. Monitoring Program	35
4.1 Introduction.....	35
4.2 Durability Monitoring.....	35
4.3 Prestress Loss Measurements	38
4.4 Camber Measurements	38
Chapter 5. Monitoring Results	45
5.1 Introduction.....	45
5.2 Durability Results	45
5.3 Prestress Loss.....	49
5.4 Camber.....	52
Chapter 6. Discussion of Test Results and Field Inspections.....	57
6.1 Introduction.....	57
6.2 Prestress Loss.....	57
6.3 Camber.....	60
6.4 Findings in the Field Performance of HPC Decks.....	64
Chapter 7. Summary, Conclusions, and Recommendations.....	67
7.1 Summary.....	67
7.2 Conclusions.....	68
7.3 Recommendations.....	69
References.....	73

Appendix A: Camber and Prestress Losses.....	75
Appendix B: 2941-2 Report.....	101
Appendix C: Last Bridge Deck Inspection Report	181
Appendix D: PSI Bridge Inspection Reports on Louetta and San Angelo HPC Structures.....	199
Appendix E: Collecting and Downloading Strain and Temperature Data from the Louetta Bridge and San Angelo HPC Bridge Data Loggers.....	259

List of Figures

Figure 3.1: Louetta Road Overpass	16
Figure 3.2: Plan View of Louetta Road Overpass [10].....	17
Figure 3.3: Cross-Section Dimensions of Texas HPC Beams [adapted from 10]	19
Figure 3.4: Strand Pattern of Texas HPC Beams [adapted from 10].....	20
Figure 3.5: North Concho River/US 87/South Orient Railroad Overpass [10]	21
Figure 3.6: Plan View of North Concho River/US 87/South Orient Railroad Overpass [10].....	22
Figure 3.7: Schematic of Original Data Transfer Setup [10].....	26
Figure 3.8: Solar Panel Mounted on San Angelo Bent Cap	28
Figure 3.9: Remote-Monitoring Equipment in DAS Box.....	28
Figure 3.10: Schematic of New Data Transfer Setup	29
Figure 3.11: Percentage of Gauges Working.....	33
Figure 3.12: Percentage of ERSR Gauges Working.....	33
Figure 3.13: Percentage of VW/TR Gauges Working	34
Figure 3.14: Percentage of TC Gauges Working.....	34
Figure 4.1: Instrumented Areas of Louetta Road Overpass [10]	39
Figure 4.2: Instrumented Areas of San Angelo Bridges [10]	40
Figure 4.3: Precise Surveying System Equipment.....	40
Figure 4.4: Location of Survey Points on a Louetta Beam.....	41
Figure 4.5: Camber Measurements at San Angelo	41
Figure 4.6: Bearing Point versus Survey Point.....	43
Figure 5.1: Close-Up of Crack in Louetta Southbound Deck.....	47
Figure 5.2: Severe Crack in Louetta Southbound Deck	48
Figure 5.3: Measured Prestress Loss—Typical Case (Beam N32).....	51
Figure 5.4: Measured Prestress Loss—Worst Case (Beam W14)	52
Figure 5.5: Measured Camber and Deflection—Typical Case (Beam N21)	55
Figure 5.6: Measured Camber and Deflection—Worst Case (Beam E45).....	55

List of Tables

Table 2.1: Crack Mapping Summary [19]	13
Table 3.1: Design Compressive Strengths for Louetta Road Overpass.....	18
Table 3.2: Design Compressive Strengths for San Angelo Bridges	23
Table 3.3: Summary of Gauge Location.....	24
Table 3.4: Travel Summary	27
Table 3.5: Gauge Durability Summary for Louetta Road Overpass.....	31
Table 3.6: Gauge Durability Summary for San Angelo Bridges	32
Table 4.1: Summary of the Bridge Inspection Rating System.....	36
Table 5.1: Summary of Routine Bridge Safety Inspection Report Review	45
Table 5.2: Crack Mapping Summary	46
Table 5.3: Results of Chloride Ion Penetration Tests	49
Table 5.4: Components of Measured Prestress Loss	50
Table 5.5: Louetta Camber Measurements	53
Table 5.6: San Angelo Camber Measurements.....	54
Table 6.1: Comparison of Design versus Measured Parameters [10].....	57
Table 6.2: Comparison of Total Prestress Losses	59
Table 6.3: Long-Term Camber	62
Table 6.4: Analysis of Long-Term Camber	64

Chapter 1. Introduction

1.1 Background

In 1993 the Federal Highway Administration (FHWA) began a program to build high performance concrete (HPC) bridges in the United States. As part of this program, two HPC bridges were built in Texas. The Louetta Road Overpass on Texas State Highway 249 near Houston, TX—commonly referred to as the Louetta Road Overpass or more simply the Louetta bridges—was opened to traffic in May 1998. The North Concho River/US 87/South Orient Railroad Overpass on US 67 in San Angelo, TX—commonly referred to as the San Angelo bridges—was opened to traffic in January 1998.

This report covers the continuation of performance monitoring conducted within three previous projects by the Center for Transportation Research (CTR) at The University of Texas at Austin. Two comprehensive reports detailing work completed under CTR Project 9-580, “Design and Construction of Extra-High Strength Concrete for Bridges,” and 9-589, “High Performance Concrete for Bridges” discussed these bridges from their inception through construction and early structural performance until December 1998 [10, 15]. When Project 9-580 ended, the Louetta bridges were monitored under CTR Project 7-3993. Another report [19] covered the work done under CTR Project 7-3993, “Long-Term Behavior of HPC Louetta Road Overpass.” CTR Project 7-2941, “Long-Term Behavior of HPC Bridges,” began September 1, 1999 to monitor efforts on both Texas HPC bridges. At that time Project 7-3993 was terminated, and its field information and database were incorporated into Project 7-2941. This report discusses the findings and refinements in methods for the early performance stages and long-term monitoring of the Texas HPC bridges, the Louetta Road Overpass, and San Angelo bridges, since 1999.

This research project monitored these two HPC bridges in Texas for long-term performance and durability. Monitoring included collection and interpretation of data from the extensive network of gauges installed in the bridges. Early field evaluations in this project involved measurements of the camber and deflection for specific beams, close inspections for cracking or signs of deterioration in the bridges, and determinations of chloride content in the decks.

Analysis of the collected data included calculating prestress losses and camber and deflection on specific beams. This analysis included data collected from April 1998 to September 1999 during CTR Project 7-3993, as well as data collected from January 2000 to August 2001. Data were only collected during CTR Project 7-3993 and not analyzed as part of that research project. A final status report of the Louetta and San Angelo data acquisition systems (DAS) was also performed.

It is important to note that even during the construction of the Louetta and San Angelo bridges, the accepted definition of HPC rapidly evolved from meaning very high strength or high-early strength to mean an engineered material enhanced to optimize properties associated with durability in the specified applications. Transportation structures, especially in Texas, have increasingly used this HPC concept to construct concrete decks with improved abrasion resistance, reduced chloride penetrability, and improved resistance to freezing and thawing damage. Although benefits from these properties improvements are apparent, it can be difficult to predict how much specific target properties result solely from concrete constituents, and how much those properties are influenced by other construction circumstances. Consequently,

successful efforts to minimize permeability in bridge decks with high substitutions of supplemental cementitious materials such as fly ash, silica fume, or slag resulted in a denser concrete matrix. Unfortunately as the density increased, so did the modulus of elasticity, and early cracking of the brittle deck rapidly became apparent.

Thus it was that the Texas Department of Transportation (TxDOT) became interested in adding several new HPC decks to be regularly monitored for distress as part of this HPC-bridge-monitoring project. Later, as early structural changes became minimal and stabilized on the Louetta and San Angelo bridges, the focus of the project shifted entirely to monitoring and reporting the deteriorating conditions of their decks and of the newly specified bridge decks in the Lubbock and Amarillo Districts.

1.2 Research Objectives

The primary objectives of this research project were to monitor the long-term structural behavior of the pretensioned HPC beams and the durability of the HPC decks, as well as to evaluate the performance of the DAS.

The structural advantages of the HPC beams used in these bridges allowed for longer spans and fewer beams per span. By monitoring prestress loss and camber in the beams, a better understanding of the behavior of HPC beams can be achieved. This information can lead to more appropriate specifications in design codes with respect to HPC. The HPC eastbound bridge and non-HPC westbound bridge in San Angelo allow the unique opportunity to compare their long-term durability and structural performance side by side.

One of the expected advantages of HPC is improved durability. In order to monitor the durability of the bridges, the most recent TxDOT Bridge Inventory, Inspection and Appraisal Program (Bridge Inspection) reports (and later Texas Bridge Inspection Reports, which replaced Bridge Inspection) were reviewed before every annual inspection of the bridges. As part of this inspection, visual observations of the concrete were made and documented with photographs and drawings. The deck concrete was also tested for chloride penetration.

The data acquisition evaluations included recording readings from embedded gauges and monitoring the status of all gauges and the condition of the DAS. In this report, an evaluation of the status of the DAS is made and possible improvements are recommended. By observing the performance of the DAS, field-tried recommendations can be implemented for future long-term monitoring projects.

It should be noted that the emphasis of this report on the structural performance and data acquisition occurred earlier in the project, as most of the structural changes occurred in the early ages of the bridges. Existing durability issues are discussed in this report, but many durability issues cannot be addressed completely because important symptoms may have not yet been manifested and will hopefully occur only much later in the life of these structures. The data acquisition and method of deflection measurement are emphasized because they provide the data by which the research team analyzed the structural performance.

1.3 Outline of This Report

This chapter has introduced the material covered in this report. Chapter 2 provides a literature review of relevant material. Chapter 3 describes the Texas HPC bridges monitored in this project. Chapter 4 describes the test program, and its results are presented in Chapter 5. Chapter 6 discusses the results from the test program. A summary of the findings and conclusions from the research are offered in Chapter 7. Appendix A provides graphs showing

camber and prestress losses. Also, a summary of the bridge deck sites is provided as a short field report in Appendix B, and finally a copy of draft reports from the FHWA-funded inspections of the Louetta and San Angelo bridge decks is provided in Appendix C, as requested by our TxDOT project director.

Chapter 2. Literature Review

2.1 Introduction

The literature was reviewed to determine appropriate definitions for high performance concrete. Over the years, numerous definitions have been proposed and refined, but only the most relevant have been included in Section 2.2. Section 2.3 reviews research regarding prestress loss and camber. Codes and specifications are reviewed, and several methods for predicting prestress loss and camber are presented in Section 2.4. The literature reviewed in this chapter is not exhaustive given the wealth of information on some of the topics, but serves as an introduction to the work performed in this study.

2.2 Definition of High Performance Concrete

Today high performance concrete (HPC) is most simply described as a concrete possessing some characteristic that distinguish it as superior to normal concrete in a given application. Normal concrete can be defined as any concrete made using local materials, without the benefit of high-range water reducers or other admixtures. In recent years, many definitions have been proposed. This section discusses some of those definitions.

The Strategic Highway Research Program (SHRP) developed one of the earlier definitions of high performance concrete in their 1991 state-of-the-art report by Zia, Leming, and Ahmad [21]. They defined HPC based on three criteria: (1) maximum water/cement ratio of 0.35, (2) minimum durability factor of 80 percent, and (3) minimum strength criteria of either (a) 3,000 psi within 4 hours, (b) 5,000 psi within 24 hours, or (c) 10,000 psi within 28 days. The three strength criteria are described as very early strength (VES), high early strength (HES), and very high strength (VHS), respectively.

In 1996, the Federal Highway Administration (FHWA) defined HPC for highway structures. The proposed definition consists of four durability characteristics (freeze-thaw durability, scaling resistance, abrasion resistance, and chloride penetration) and four strength characteristics (compressive strength, modulus of elasticity, shrinkage, and creep). Goodspeed, Vankikar, and Cook [9] provide details on performance criteria, standard tests to evaluate performance, and recommended relationships between performance and exposure conditions for each of the eight characteristics.

Gross and Burns [10] proposed a broad and general definition of HPC in 1998, incorporating many of ideas proposed by the previously mentioned definitions. They defined HPC as follows:

HPC is an engineered concrete whose components are carefully selected and proportioned to produce a material with beneficial properties suitable for a specific application. Beneficial properties may be related to any number of strength and/or durability characteristics, dependent upon the given application.

2.3 Sources of Long-Term Prestress Loss

Prestress losses occur due to a number of phenomena. Sources of prestress loss can be divided into two categories. Instantaneous losses, such as elastic shortening, anchorage set, and friction, occur immediately after the prestressing strands have been cut. The time at which the

strands are cut may be referred to as transfer. Time-dependent losses, such as creep and shrinkage of concrete and relaxation of steel, vary during the life of the structure. All of these phenomena are discussed in detail by several texts [14, 16], and are summarized in this section.

2.3.1 Instantaneous Losses

Instantaneous losses include elastic shortening of the concrete, anchorage set, and friction. All of these losses occur when the tension carried by the strands is transferred to the concrete member.

Once the prestressing strands have been cut, the tension in the strands is transferred to the concrete. This causes a compressive force to act on the member. Due to the typical eccentricity of the strands, a compression force forms in the bottom of the beam and a tension force in the top. *Elastic shortening* occurs due to the compressive force. The change in stress of the strands, or prestress loss due to elastic shortening, can be determined by the calculation shown in Equation 2.1:

$$\Delta f_{ps,ES} = \frac{E_{ps}}{E_{ci}} f_{cgp} \quad 2.1$$

where $\Delta f_{ps,ES}$ = prestress loss due to elastic shortening
 E_{ps} = modulus of elasticity of prestressing steel
 E_{ci} = modulus of elasticity of concrete at time prestress is applied
 f_{cgp} = stress in concrete at the center of gravity of the prestressing steel
 due to self-weight and prestress force

A detailed analysis can be carried out to determine the exact theoretical loss, using the transformed section and the jacking force. However, it is commonly accepted to use gross section properties and estimate the prestress force after transfer, P_0 [14]. The stress in the concrete at the center of gravity of the prestressing strands is:

$$f_{cgp} = \frac{P_0}{A_g} + \frac{P_0 e^2}{I_g} - \frac{M_{sw} e}{I_g} \quad 2.2$$

where P_0 = prestress force after release
 e = eccentricity of the prestressing steel
 A_g = area of the beam based on gross section properties
 I_g = moment of inertia base on gross section properties
 M_{sw} = moment due to the self-weight of the beam

As Equation 2.2 shows, this stress is the result of the prestress force and the self-weight of the beam.

Instantaneous losses due to *friction* and *anchorage set* are most significant in post-tensioned members. They are typically compensated for by overstressing the strands. Friction loss is the sum of two components, caused by the wobble factor of the duct and the intentional curvature of draped strands. Coefficients accounting for these effects have been developed and can be found in the ACI Building Code Commentary [4]. The loss in prestress due to friction can be expressed as:

$$\Delta f_{ps,FR} = f_{pj} (1 - e^{-(KL + \mu\alpha)}) \quad 2.3$$

where $\Delta f_{ps,FR}$ = prestress loss due to friction
 f_{pj} = stress in the strands due to jacking
 K = wobble coefficient

- L = distance of strand from jack
- μ = curvature coefficient
- α = total angle change of the strand path from jacking end

The derivation of Equation 2.3 is carried out in the texts [14,16]

Anchorage set, also referred to as anchorage slip or take-up, is caused by the sudden application of the jacking force to the selected anchorage type holding the strands. This loss can be calculated using Equation 2.4.

$$\Delta f_{ps,AN} = \frac{\Delta L}{L} E_{ps} \quad 2.4$$

where $\Delta f_{ps,FR}$ = prestress loss due to friction

ΔL = amount of slip

L = length of the prestressing steel

The significance of anchorage slip decreases with long members, because the amount of slip, ΔL , is independent of the strand length, L.

2.3.2 Time-Dependent Losses

Time-dependent losses include losses due to creep and shrinkage of concrete, and relaxation of the prestressing steel. These losses are difficult to calculate because they vary with time and are interdependent.

Shrinkage is defined as the decrease in volume of concrete with time. The loss in volume is caused by loss of moisture and chemical changes in the concrete. A large amount of shrinkage occurs early, and the total shrinkage is approached asymptotically. As the concrete member shortens due to the decrease in volume, the prestressed steel decreases in length as well. This causes a reduction in the prestress force.

Creep is defined as the time-dependent increase in strain of concrete under a sustained stress or load. The rate of creep rapidly increases initially, but eventually reaches a constant asymptotically. Creep need only be considered for prestress loss beginning with transfer for pretensioned beams, and after tensioning in post-tensioned beams. Stress changes due to creep can be measured by comparing the stress in the concrete before and after a load has been applied. This change in stress can be used to determine the prestress loss due to creep.

Farrington, Burns, and Carrasquillo [8] investigated creep and shrinkage of the HPC mixes used in the Texas HPC Bridges. The measured data were compared to the prediction methods suggested by ACI Committee 209 [3]. The study found the ultimate shrinkage strain and the ultimate creep coefficient of HPC were 55% and 60% lower, respectively, than the amount suggested by the ACI Committee 209 report.

Relaxation is defined as the gradual reduction of stress in the prestressing steel with time due to sustained strain. Strain change in the prestressing steel is caused by a reduction in length due to creep and shrinkage. Here the interdependence of the time-dependent factors can be seen. The prestress loss due to relaxation depends on the strength of the strands and amount of initial stressing as well as the type of strand.

2.4 Predicting Long-Term Prestress Loss

Knowing prestress loss is seldom important with regards to design strengths. However, prestress loss does play an important role in service conditions, such as camber, deflection, and

cracking. The amount of prestress must be properly balanced with loads, in order to achieve the desired slight upward camber. An upward camber is largely desired for its aesthetic appeal. It is typical to think an overestimation is conservative. This is not true for prestress loss. A high estimate may result in tensile forces in the member at service load and cracking may occur. In addition, excessive camber in a series of simply supported beams can lead to an uncomfortable and bumpy ride for vehicular traffic.

Many methods for predicting prestress loss have been suggested. Methods suggested by the *AASHTO LRFD Bridge Design Specifications* [2] and the *PCI Design Handbook* [17] are described in Sections 2.4.3, 2.4.4, and 2.4.5. These methods are for pretensioned members and cannot be applied to the pretensioned/post-tensioned San Angelo eastbound HPC beams without modification. The loss due to post-tensioning was incorporated in the elastic shortening component [10]. This simplification allows prestress losses in these complex beams to be compared to the simple prediction methods presented in the *AASHTO LRFD Bridge Design Specifications* [2] and the *PCI Design Handbook* [17]. Variable names may have been altered from their appearance in the literature in order to make comparison of the methods simpler. In addition, numerical values for constants may have been substituted in cases where the value was constant for all beams studied in this program.

2.4.1 Incremental Time-Step Method

Time-step methods calculate prestress loss at time intervals throughout the life of the member. The prestressing force for each step is taken as the end result of the previous step. The number and length of the steps depends on the desired accuracy. Typical time steps include the following: at the time of prestressing, at the time when a member is subjected to new loads, at an age of one year, and at the end of service life [18]. Computer programs are often employed when high accuracy and, therefore, a large number of time-steps are required. Gross has developed a time-step program capable of analyzing both the AASHTO Type IV I-beams and TxDOT U54 U-beams [10,12].

2.4.2 Actual Beam Designs

Prestress loss was calculated during the actual beam design by TxDOT engineers. Two programs were used to predict long-term prestress losses. ADAPT-ABI [1] was used to predict losses in the San Angelo eastbound I-beams. ADAPT-ABI is a commercial program developed by the ADAPT Corporation that employs a time-step process to determine prestress loss. PSTRS14 [20] was used to predict losses in the San Angelo westbound I-beams and the Louetta U-beams. PSTRS14 is a design and analysis program developed by TxDOT.

2.4.3 AASHTO LRFD Time-Dependent Lump Sum Method

The AASHTO LRFD Time-Dependent Lump Sum Method [2] is the sum of two components. It is the combination of losses due to elastic shortening and a lump sum estimate for time-dependent losses, as shown in Equation 2.5:

$$\Delta f_{ps,total} = \Delta f_{ps,ES} + \Delta f_{ps,TD} \quad 2.5$$

where $\Delta f_{ps,total}$ = total prestress loss

$\Delta f_{ps,TD}$ = time-dependent prestress loss

Elastic shortening losses are predicted using Equation 2.1. As discussed in Section 2.3.1, the prestress force in equation 2.2 is often calculated using an assumed value. The AASHTO

LRFD Time-Dependent Lump Sum Method recommends the prestress force may be calculated using an assumed prestressing steel stress of seventy percent of the ultimate strength of prestressing steel, $0.70 f_{pu}$, for low relaxation strands.

Time-dependent losses are predicted using a single equation, depending on the type of beam section. These lump sum estimates have been developed from trends observed in a time-step computer analysis for a large number of bridges [2]. For members with no mild steel reinforcement using 270-ksi low-relaxation strands, such as those in the Texas HPC Bridges, the time-dependent losses in ksi are predicted as:

$$\Delta f_{ps,TD} = 33.0 \left[1.0 - 0.15 \frac{f'_c - 6.0}{6.0} \right] \quad 2.6$$

and

$$\Delta f_{ps,TD} = 19 \quad 2.7$$

for I-beams and U-beams, respectively. The 28-day compressive strength of the concrete is given as f'_c .

2.4.4 AASHTO LRFD Component Method

The AASHTO LRFD Component Method [2] is the sum of four components and is intended to lead to a better estimate of time-dependent losses than the lump sum used in the AASHTO LRFD Time-Dependent Lump Sum method. Total prestress loss is given by Equation 2.8:

$$\Delta f_{ps,total} = \Delta f_{ps,ES} + \Delta f_{ps,SH} + \Delta f_{ps,CR} + \Delta f_{ps,RE} \quad 2.8$$

where $\Delta f_{ps,SH}$ = prestress loss due to shrinkage

$\Delta f_{ps,CR}$ = prestress loss due to creep

$\Delta f_{ps,RE}$ = prestress loss due to relaxation

Note that the three time-dependent terms (shrinkage, creep, and relaxation) are now calculated separately, as opposed to a single lump sum.

Loss due to elastic shortening of the concrete is calculated as described in Section 2.4.3. Shrinkage loss is based on the average annual ambient relative humidity RH, which can be obtained from local weather statistics or from figures in the *AASHTO LRFD Bridge Design Specifications* [2].

$$\Delta f_{ps,SH} = 17.0 - 0.015 RH \quad 2.9$$

Prestress loss due to creep is estimated as

$$\Delta f_{ps,CR} = 12.0 f_{cgp} - 7.0 \Delta f_{cdp} \quad 2.10$$

where f_{cgp} = the stress in concrete at the center of gravity of pretensioned strands due to applied loads not acting at release

The two stresses in Equation 2.10 are calculated at the same section. Note that at this point the beam and deck are acting compositely to resist loads carried by the bridge.

Loss due to the relaxation of steel is estimated as the sum of losses at transfer and after transfer:

$$\Delta f_{ps,RE1} = \frac{\log(24.0t)}{40.0} \left[\frac{f_{pj}}{f_{py}} - 0.55 \right] f_{pj} \quad 2.11$$

$$\Delta f_{ps,RE2} = 20.0 - 0.4\Delta f_{ps,ES} - 0.2(\Delta f_{ps,SH} + \Delta f_{ps,CR}) \quad 2.12$$

where t = time in days between stressing and transfer

f_{pj} = stress in the prestressing strand at the end of stressing

f_{py} = yield strength of the prestressing strand

The stress at the end of stressing may be taken as $0.80 f_{pu}$.

2.4.5 PCI Design Handbook Method

The PCI Design Handbook method [17] is based on the work of a task group sponsored by ACI-ASCE Committee 423, Prestressed Concrete [22]. The PCI Design Handbook method estimates prestress loss as the sum of the same four components in the AASHTO LRFD Component method shown in Equation 2.. However, the components are calculated using a different set of equations. The *PCI Design Handbook* point out this method is intended for common design conditions, and therefore may be insufficient for HPC beams. A more detailed analysis is suggested for unusual designs or structures.

Elastic shortening is the same as Equation 2.1. However, it indirectly recommends taking the prestress force after transfer as 90 percent of the initial prestress force after anchorage losses ($P_0 = 0.90 P_i$).

Loss due shrinkage incorporates the volume to surface ratio, V/S , in addition to the average ambient relative humidity as shown in Equation 2.13.

$$\Delta f_{ps,SH} = (8.2 \times 10^{-6}) E_{ps} \left(1 - 0.06 \frac{V}{S} \right) (100 - RH) \quad 2.13$$

Creep prestress loss for normal weight concrete is:

$$\Delta f_{ps,CR} = 2.0 \frac{E_{ps}}{E_c} (f_{cgp} - f_{cdp}) \quad 2.14$$

where the calculation of f_{cdp} is based on gross section properties.

Similar to the AASHTO LRFD Component method, prestress loss from relaxation is calculated using the other components. Equation 2.15 gives the loss due to relaxation using 270 ksi low relaxation strands initially stressed to $0.75 f_{pu}$.

$$\Delta f_{ps,RE} = 5.0 - 0.040(\Delta f_{ps,ES} + \Delta f_{ps,SH} + \Delta f_{ps,CR}) \quad 2.15$$

2.4.6 Suggested Method

A suggested method for calculating long-term prestress loss was presented by Gross and Burns [10], and a thorough discussion of the shortcomings of other prediction methods are presented by the authors. Their suggested method is a component method similar to the AASHTO LRFD Component and *PCI Design Handbook* methods. However, refinements have been made and the suggested method uses measured material properties. It predicts prestress loss as the sum of five components.

$$\Delta f_{ps,total} = \Delta f_{ps,ES} + \Delta f_{ps,SH} + \Delta f_{ps,CR} + \Delta f_{ps,RE} + \Delta f_{ps,PR} \quad 2.16$$

The fifth term accounts for losses that occur before release of the strands due to relaxation and thermal effects.

Elastic shortening loss should be calculated according to Equation 2.1, where the prestressing force is calculated using f_{po} equal to $0.90 f_{pj}$.

Prestress loss caused by creep takes the following form:

$$\Delta f_{ps,CR} = K_{cr} \frac{E_{ps}}{E_c} (f_{cgp} - f_{cdp}) \quad 2.17$$

K_{cr} is a constant, which can be adjusted by any common method based on the volume-to-surface ratio of the beam and the average ambient relative humidity.

The suggested method uses the same equation for relaxation loss as the *PCI Design Handbook* [17].

The fifth term is a combination of relaxation loss before transfer and losses due to thermal effects. These losses are expressed in Equation 2.18.

$$\Delta f_{ps,PR} = \frac{\log(24 t)}{45} \left[\frac{f_{pj}}{f_{py}} - 0.55 \right] f_{pj} + \frac{1}{3} E_{ps} \alpha_{ps} \Delta T \quad 2.18$$

where α_{ps} = coefficient of thermal expansion of prestressing strands

ΔT = change in temperature between peak hydration and stressing

It is suggested that the change in temperature should be estimated based on past experience. The reported change in temperature for beams in this project was about 60° F.

2.5 Sources of Long-Term Camber

Camber is essentially a function of the upward deflection caused by the eccentricity of the prestressing force, and the downward deflection caused by loads. Initial camber is easily calculated using moment-area theory. The initial camber is simply a function of the deflection owing to prestressing force and the deflection due to self-weight of the member. Instantaneous deflections caused by additional loads, such as the weight of the slab and parapets, can be determined using classical methods of mechanics.

Determining long-term camber becomes far more difficult, as prestress losses are time-dependent. Camber is highly dependent on the prestress force; therefore, camber is time-dependent as well. Another difficulty is caused by the increased strength concrete gains with time.

2.6 Predicting Long-Term Camber

The literature provides few procedures for predicting long-term camber. The *AASHTO LRFD Bridge Design Specifications* [2] mentions calculating camber, but no guidelines are given. ACI 318 [4] provides an estimate of long-term deflection for non-prestressed, reinforced concrete members based on multiplying the initial camber by a factor. No multiplier is provided for prestressed concrete. The *PCI Design Handbook* [17] suggests a set of multipliers as a guide to estimate long-term camber. This estimate of long-term camber is determined by multiplying the instantaneous elastic deformations caused by the prestress force and loads by a set of constants. Equation 2.19 presents the *PCI Design Handbook* calculation of long-term camber:

$$\Delta_{long-term} = 2.20\Delta_{ps} - 2.40\Delta_{sw} - 3.00\Delta_{sdl} - 2.30\Delta_{ct} \quad 2.19$$

where Δ_{ps} = deflection due to the prestressing force,

Δ_{sw} = deflection due to the self-weight of the member at transfer,

Δ_{sdl} = deflection due to the superimposed dead load, and

Δ_{ct} = deflection due to the composite topping

Numerous computer programs have been developed to determine long-term camber. The use of a computer makes the complex calculations of time-dependent behavior much easier. The two programs used in the TxDOT design of the Texas HPC beams, ADAPT-ABI [1] and PSRTS14 [20], were both used to predict long-term prestress. Gross and Burns [10] developed a time-dependent program capable of predicting long-term camber of the Texas HPC beams. This program was based on the work of Byle and Burns [5].

2.7 Previous Durability Monitoring

Shepperd and Burns [19] reported on the early results of long-term monitoring of the Louetta Road Overpass, as mentioned in Chapter 1. Their report focused on the durability aspects of the bridge. The report discusses visual inspections, testing on core drilled cylinders, petrographic examinations, and chloride content evaluations. Testing of the cylinders included carbonation, compressive strengths, and chloride ion permeability. Only the results that are related to the limited durability testing performed during this project are summarized here.

The deck cracking was first discovered during an annual inspection performed by researchers in July 1998 [19]. At that time, the cracking patterns were recorded and transferred to AutoCAD for analysis. Cracks were measured in the longitudinal and transverse directions in terms of linear feet. Table 2.1 lists the result of the crack mapping. The crack lengths for longitudinal and transverse cracking are shown for the northbound and southbound bridges. Both cast-in-place decks are considered HPC, but the compressive strengths are 4,000 and 8,000 psi for the northbound and southbound decks, respectively. Compressive strengths for all portions of the bridges can be found in Chapter 3, Table 3.1.

Shepperd and Burns [19] found that cracking in the longitudinal and transverse directions corresponded to the flanges and ends, respectively, of the U-beams. A suggested cause of the longitudinal cracking was inadequate bearing conditions of the precast panels. The transverse cracks were attributed to improper installation of control joints. The skew of the control joints did not properly align with the skew of the bridge. The largest crack width was reported as 0.01 in. This width was observed in numerous locations.

Table 2.1: Crack Mapping Summary [19]

Span	Cracking (ft)	
	Longitudinal	Transverse
<i>Louetta Northbound Normal Strength</i>		
N1	65	25
N2	280	95
N3	190	95
Total	535	215
<i>Louetta Southbound High Strength</i>		
S1	185	65
S2	1005	90
S3	510	55
Total	1700	210

The visual inspection of the underside of the bridge revealed some minor problems. Cracking and spalling were detected around the drain ports in the beams. Hairline cracks were detected in the flanges of six beams. The precast panels were observed to be in good shape. Cracking and efflorescence was detected along the column line in the cast-in-place deck.

Chloride penetration testing was performed on the northbound and southbound decks. This testing method is described in Section 4.2.3. The chloride content was negligible at all levels.

Chapter 3. Structural HPC Bridge Descriptions and Data Acquisition System

3.1 Introduction

This chapter provides a description of the two HPC earliest bridges studied in this project. They were uniquely constructed, because of their specially designed HPC beams, and, due to structural interests, they were the original focus of the monitoring activities. Later bridges in Lubbock and Amarillo were monitored only for HPC deck durability, and a description of each of these bridge locations is presented in the appendix.

The Louetta Road Overpass is discussed first. A description of the bridge layout is presented as well as information on the TxDOT U54 Beam.

The description of the North Concho River/US 67/South Orient Railroad Overpass is next. Details on AASHTO Type IV I-beams are given.

A description of the instrumentation and data acquisition system (DAS) used on these two bridges is presented. Adjustments made to the DAS to allow for remote monitoring are discussed. A discussion of the long-term durability of the different gauges used in DAS concludes the chapter. Details on how the instrumentation was used are presented in Chapter 4.

3.2 Louetta Road Overpass

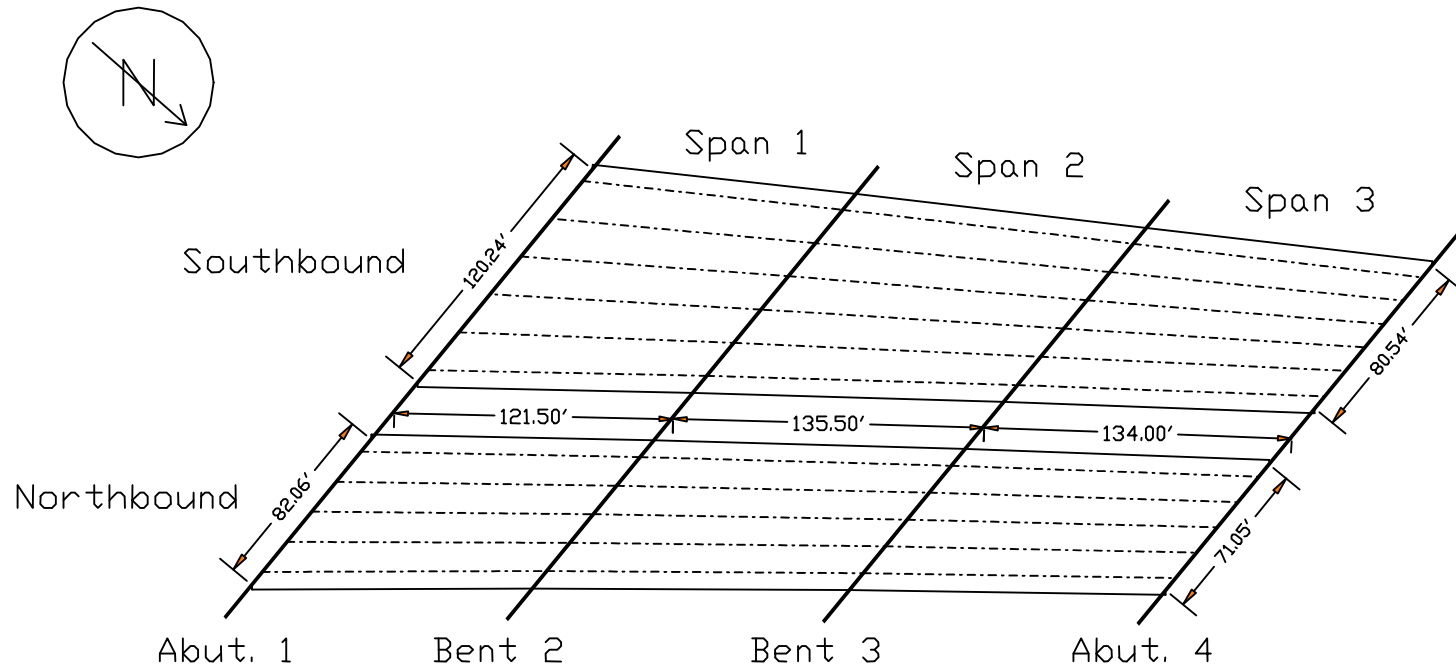
3.2.1 General Description

The Louetta Road Overpass on State Highway 249 is located on the northwest side of Houston, Texas. The overpass is shown in Figure 3.1. The construction of the overpass was part of a 3.0-mile highway improvement project upgrading SH 249 from a four-lane roadway at grade road to an eight-lane freeway. The overpass is 391 ft long, consisting of adjacent northbound and southbound bridges, each with three spans measuring 121.5 ft, 135.5 ft, and 134.0 ft along the centerline of the structure. The overpass was originally planned to carry three lanes of traffic in each direction, northbound and southbound. Before the bridge was open to traffic, both directions were expanded by one lane. The final bridge layout has seven beams in the southbound direction and six beams in the northbound direction. The southbound bridge was built to accommodate an exit ramp, which accounts for the extra beam and larger clear width. The clear width was measured prior to the widening. A plan view of the Louetta Road Overpass is shown in Figure 3.2. Note that the bridge was built with a skew resulting in varying beam lengths.



Figure 3.1: Louetta Road Overpass

The bridge decks are made up of prestressed panels with a cast-in-place topping. The deck is supported by prestressed Texas U-beams, which in turn are simply supported by single piers. The U-beam and pier combination was considered a more aesthetically pleasing option than the typical I-beam, bent cap, and column system. All components of the Louetta Road Overpass are HPC. Table 3.1 lists the design compressive strengths of the different components of the northbound and southbound Louetta Road Overpass bridges. The northbound deck is normal strength HPC.



LOUETTA ROAD OVERPASS (prior to widening)

Figure 3.2: Plan View of Louetta Road Overpass [10]

Table 3.1: Design Compressive Strengths for Louetta Road Overpass

Element	Compressive Strength (psi)	
	Northbound	Southbound
U-Beams		
At Transfer	6,900 - 8,800	6,900 - 8,800
At 56 Days	9,800 - 13,100	9,800 - 13,100
Piers	10,000	10,000
CIP Deck	4,000	8,000
Prestressed Panels	8,000	8,000

3.3 TxDOT U54 Beam

The pretensioned beam used throughout the Louetta Road Overpass was the newly developed TxDOT U54 Beam. The beam is trapezoidal in cross section with an open top. The beam is 54 in. deep, 8 ft across the top, and 4.59 ft across the bottom. The webs are 5 in. thick and the bottom flange is 6.25 in or 8.25 in. thick for the U54A and U54B beams, respectively. The only difference between the two U54 beams is the thickness of the bottom flange, with the U54A allowing for another row of prestressing strands. The beam and its complete dimensions are shown in Figure 3.3. The strand patterns are shown in Figure 3.4. Note that this is a possible strand pattern and not necessarily indicative of all of the beams in this project. Transfer and development length tests were performed to gain approval to use 0.6 in. diameter prestressing strands at 2 in. spacing [11]. A more extensive description of the TxDOT U-beam can be found in Byle and Burns [5] and Gross and Burns [10]. These reports provide such details as strength, strand pattern, and debonding length for each beam in the bridge.

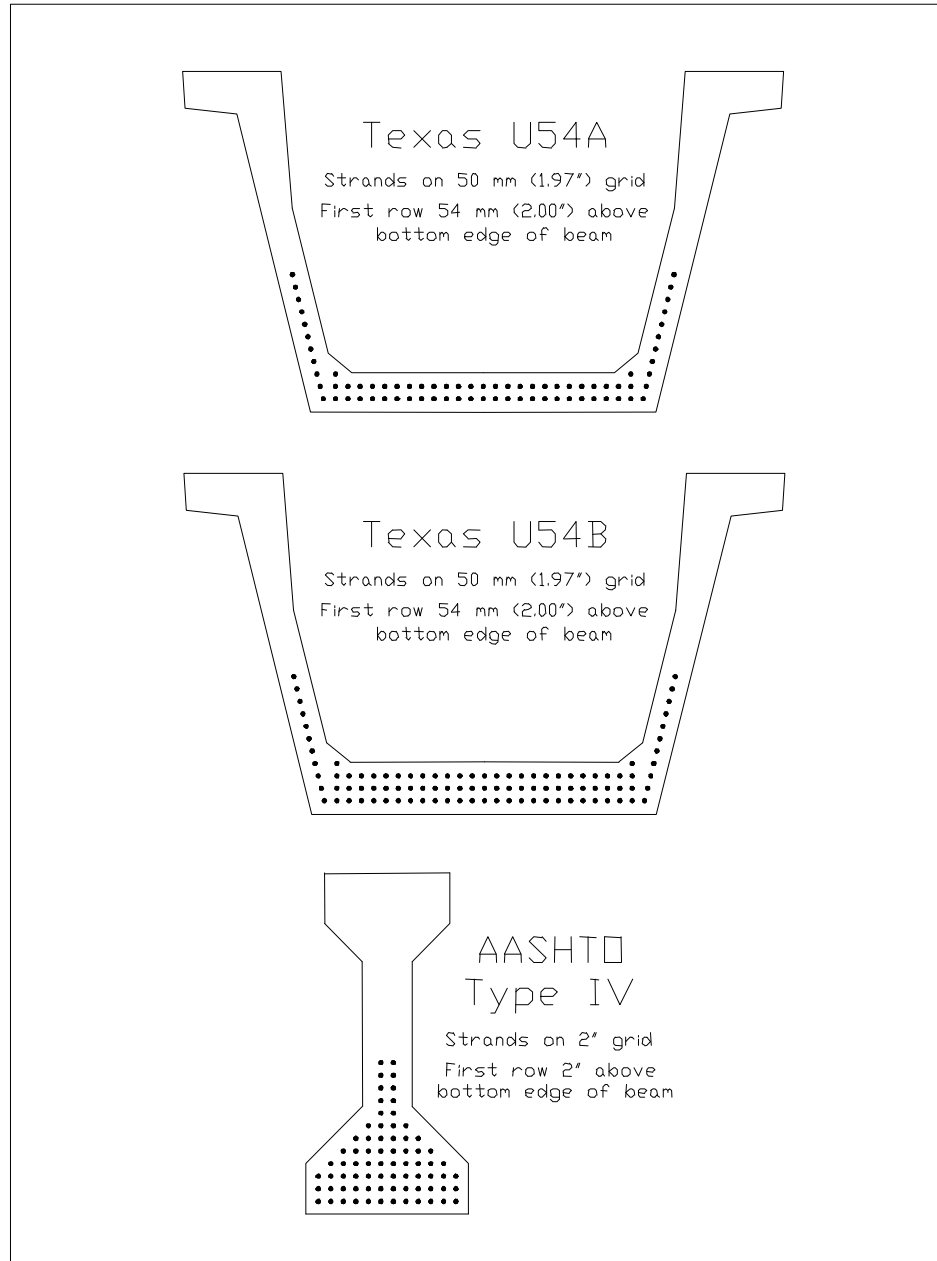


Figure 3.4: Strand Pattern of Texas HPC Beams [adapted from 10]

3.4 North Concho River/US 87/South Orient Railroad Overpass

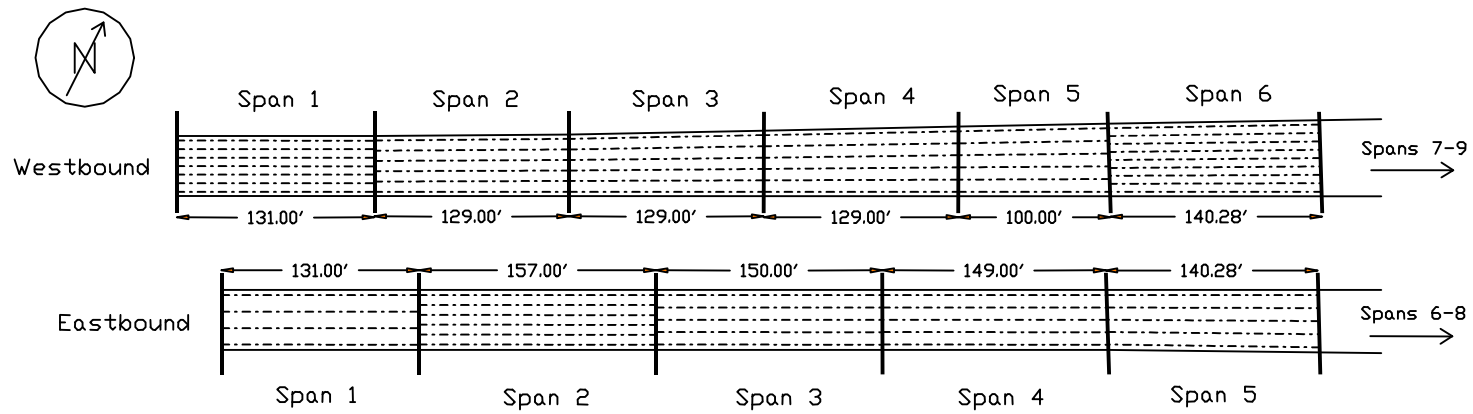
3.4.1 General Description

The North Concho River/US 87/South Orient Railroad Overpass on US 67 is centrally located in San Angelo, Texas. The US 67 bridges are adjacent multispan bridges. The bridges are shown in Figure 3.5. The eastbound bridge is eight spans and the westbound bridge is nine spans. Span lengths as well as beam spacings vary in both bridges. These dimensions are shown in the plan view of the San Angelo bridges in Figure 3.6. The bridge decks are made of prestressed, precast panels with a cast-in-place topping. AASHTO Type IV beams support the deck. The

beams are simply supported on bent caps, which are carried by single open-faced piers. These piers can be seen in Figure 3.5.



Figure 3.5: North Concho River/US 87/South Orient Railroad Overpass [10]



NORTH CONCHO RIVER/U. S. 87/S. O. R. R. OVERPASS (San Angelo)
(Only Main Spans Shown)

Figure 3.6: Plan View of North Concho River/US 87/South Orient Railroad Overpass [10]

All components, including the cast-in-place deck, prestressed panels, and girders of the eastbound bridge are made with HPC. The cast-in-place deck in spans 1-5 of the westbound bridge is HPC. The cast-in-place deck in spans 6-9 and all prestressed panels and girders are normal concrete. The design compressive strengths of the components of the two San Angelo bridges are given in Table 3.2.

Table 3.2: Design Compressive Strengths for San Angelo Bridges

Element	Compressive Strength (psi)	
	Eastbound	Westbound
I-Beams		
At Transfer	8,900 - 10,800	4,020 - 6,560
At 56 Days	10,900 - 14,700	5,000 - 8,920
Piers	6,000	3,600
Pier Cap	8,000	8,000
CIP Deck	6,000	4,000
Prestressed Panels	6,000	5,000

3.4.2 AASHTO Type IV I-Beam

AASHTO Type IV prestressed concrete I-beams are predominately used in the San Angelo bridges. Texas Type B prestressed concrete I-beams are used in the eighth span of the eastbound bridge. However, none of these beams were instrumented. The Type IV beams are 54 in. deep, 26 in. across the bottom flange, and 20 in. across the top flange. The web is 8 in. thick. The dimensions of the AASHTO Type IV I-beam are shown in Figure 3.2. The beams utilize both straight, pretensioned strands and draped, post-tensioned strands. The pretensioned strands are 0.6 in. in diameter and spaced on a 2 in. grid. The post-tensioned strands are carried in two ducts. The pretensioned strand pattern is shown in Figure 3.4. Note that this is a possible strand pattern and not necessarily indicative of all of the beams in this project. These beams are described in detail by Gross and Burns [10].

3.5 Original Data Acquisition System

An essential part of any research project is the Data Acquisition System (DAS). The DAS is responsible for collecting and storing data. The DAS in this research program collected strains and temperatures in the beams, prestressed precast panels, and cast-in-place decks.

3.5.1 Introduction

A brief description of the original DAS is described in this section. A more detailed description can be found in Gross and Burns [10], including a description of the gauge numbering system, drawings detailing the location of every gauge in the project, schematics of a typical DAS, and a description of the installation procedures used.

Five DAS systems were custom built by Gross. A typical system consists of embedded gauges run through multiplexers, which are connected to a datalogger. The datalogger was connected to a 12-volt power supply. Two systems are located at the Louetta Road Overpass, one each for the northbound and southbound bridges. The other three systems are located at the San

Angelo bridges. Two are located on the eastbound HPC bridge and the other is on the westbound non-HPC bridge. A total of 518 gauges are embedded in various beams, precast panels, and cast-in-place concrete in the two bridge sites. Table 3.3 summarizes the location and type of gauge in each of the bridges.

Table 3.3: Summary of Gauge Location

Gauge Location	Gauge Type			Total
	ERSG	VW / TR	TC	
Louetta Northbound HPC				
Beams	59	14	12	85
CIP Deck	24	2	4	30
Louetta Southbound HPC				
Beams	49	27	24	100
Panels	0	6	4	10
CIP Deck	4	17	10	31
San Angelo Eastbound HPC				
Beams	50	35	30	115
Panels	8	4	14	26
CIP Deck	11	9	20	40
San Angelo Westbound Non-HPC				
Beams	18	14	12	44
Panels	0	4	4	8
CIP Deck	7	14	8	29
Total	230	146	142	518

Twenty-four beams were instrumented. Five beams in both the northbound and southbound Louetta Road Overpass were equipped with gauges. The eastbound and westbound San Angelo bridges have ten and four beams, respectively, equipped with gauges. The instrumented areas for the Louetta Road Overpass and the San Angelo Bridges are shown in Chapter 4's Figures 4.1 and 4.2, respectively.

3.5.2 Gauge Types

As shown in Table 3.3, there were three types of gauges used in the DAS. A brief description of each gauge is given. Details on how the gauges were used are described in Chapter 4: Test Program.

Electrical resistance strain gauges (ERSG) were used to measure strains. These Model FLA-6-350-11-3LT strain gauges were purchased from Texas Measurements, Inc. The change in resistance of the gauge was caused by a change in length of the wire. This change in resistance was exactly proportional to the strain. These gauges have a nominal resistance of 350 ohms and were inexpensive compared to vibrating wire gauges.

Vibrating wire strain gauges (VW) were also used to measure strains. These gauges also have built-in thermistors (TR) to record temperatures. The Model EM-5 IRAD GAGE Vibrating Wire Embedment Strain Gage manufactured by Roctest, Inc. was used. These gauges work on the principle that measuring the natural frequency of a wire tensioned between two points inside

concrete can be correlated to the strains in that concrete. This VW has a nominal range of 3,300 microstrain. Vibrating wire gauges are very expensive compared to other strain gauges, but they last much longer to record concrete strains. The thermistor has a temperature range of -40°F to 160°F with an accuracy of 0.5°F .

Thermocouples (TC) were used to measure temperatures. The thermocouples used in the project were manufactured by Omega Scientific, Inc., with a reported accuracy of $\pm 1.8^{\circ}\text{F}$. Specifically, a twisted Type T (copper-constantan) 20-gauge wire was used. Thermocouples measure the voltage drop between the two metals. This voltage drop can then be converted into temperatures. Thermocouples were relatively inexpensive.

3.5.3 Programming, Data Retrieval, and Data Manipulation

Programming the DAS was accomplished using PC208W [6] software provided by Campbell Scientific, Inc. The datalogger itself can be programmed directly using PC208W, via a SC12 cable connected to a COM port on a personal computer. Another option commonly used during this research project was to upload a program from a storage module into the datalogger. Programs created on a personal computer using PC208W can be saved on a SM716 storage module. Storage modules communicated with a personal computer using an optically isolated RS232 interface. The storage modules were then taken into the field where the appropriate program was uploaded onto the datalogger using a CR10KD Keypad, also provided by Campbell Scientific, Inc. The storage module was left at the site to store data collected by the datalogger. Once the storage module was full, it was replaced with another storage module and the cycle was repeated. This process is shown schematically in Figure 3.7.

The data contained in a storage module was transferred to a comma-separated text file using PC208W. However, the raw data from the storage modules were not in useful engineering units. Therefore, a data manipulation program, SORTDTA1 [13], was written by Gross to convert the voltages and frequencies recorded by strain gauges into units of strain. The program also sorts the data into an organized format.

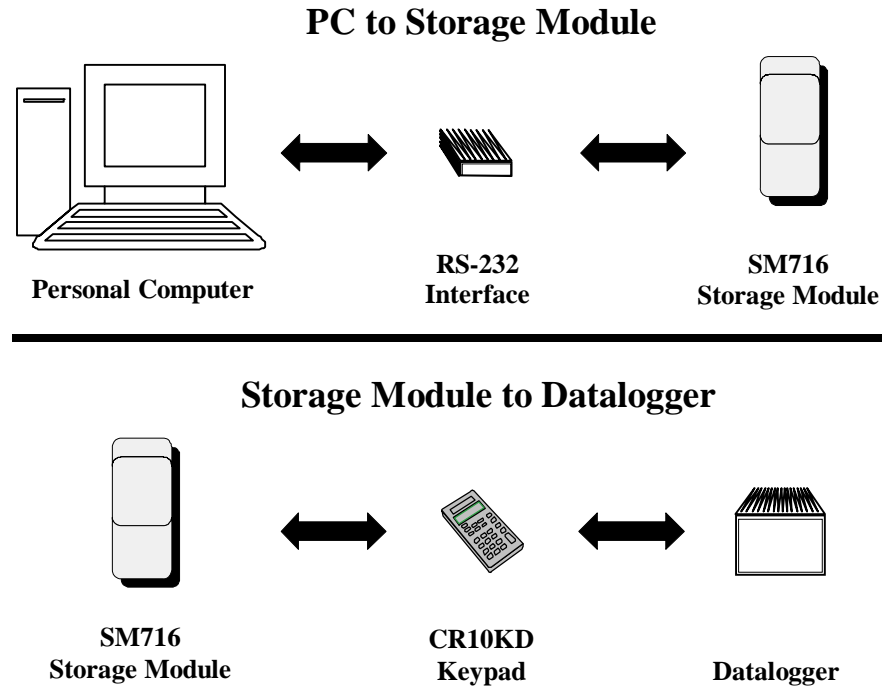


Figure 3.7: Schematic of Original Data Transfer Setup [10]

3.6 Modifications to Data Acquisition System

One of the major problems encountered by researchers during the research project was the amount of time and travel involved in making site visits to the two bridge sites. Therefore, establishing a remote-monitoring DAS was an important aspect of the research project.

3.6.1 Travel

Most travel consisted of day trips, although the annual visual inspections required overnight trips for both bridge sights. Day trips were favored for two reasons. They avoided the cost of an overnight stay in a hotel and were less likely to interfere with coursework members of the research team were taking. Day trips generally involved leaving early in the morning and returning in the evening or leaving in the afternoon and returning late the same night. However, overnight trips were necessary for the annual inspections in order to start work as early in the morning as possible. Another factor for early morning starts was to accommodate the work schedule of TxDOT maintenance crews required for traffic control.

The approximate distance and travel time to the bridge sites from Austin are shown in Table 3.4. As discussed in the next section, the storage modules and batteries had to be replaced approximately every 3 months. These tasks could easily be performed in less than 2 hours. In most cases, the amount of time spent at the bridge site was far exceeded by the time spent traveling to and from the site. Based on the researchers' travel records and approximate calculations, over 75 percent of the time on each trip was spent traveling. It is evident that a remote monitoring system will pay for itself in a short period of time.

Table 3.4: Travel Summary

	Louetta	San Angelo	Totals
Number of Trips ¹	12	14	26
Avg. People Travelling	1.5	1.5	
Travel Distance (Round Trip)	300	410	
Total Mileage	3600	5740	9340
Total Man-Miles	5400	8610	
Travel Time (Round Trip)	5.5	7	
Total Travel Time (Hours)	66	98	
Total Travel Man-Hours	99	147	246
Trip Time (Travel & Site Time)	7	9	
Total Trip Time (Hours)	84	126	
Total Trip Man-Hours	126	189	315
Percent of Time Travelling	78%		
¹ Number of trips based on an estimate of one trip every three months after the bridge was open to traffic.			

3.6.2 New Equipment

New equipment was installed in summer 2001 to make remote monitoring possible. The equipment was purchased from Campbell Scientific, Inc. This equipment allowed the data retrieval method described in Section 3.5.3 to be updated. Equipment was purchased for all five of the DAS boxes, thus updating the DAS for the entire project.

3.6.3 Power Issues

Eight “D” cell alkaline batteries, providing 12-volts of power, powered the old DAS. These batteries had to be replaced approximately once every 3 months. A constant power supply of at least 9.6 volts had to be maintained; otherwise, the DAS could suffer permanent damage. The maximum time eight “D” cell batteries could provide the minimum voltage varied slightly based on several factors. The five DAS were not identical. Therefore, the power drain varied slightly from system to system. The voltage level was checked each time the batteries were replaced. Based on personal observation, the batteries lasted longer during moderate temperatures. The voltage never dropped below 10 volts as long as they were replaced within 3 months.

A solar panel, shown in Figure 3.8, and rechargeable battery was installed to replace the alkaline battery power supply. The MSX10 Solar Panel is 17 x 11 x 1 in. and weighs only 3.3 lbs. Therefore, it could be installed safely and easily on the side of a highway. The solar panel converts sunlight into direct current. A PS12A charging regulator, shown in the upper left corner of Figure 3.9, must be used to connect the solar panel to the sealed rechargeable battery. The battery was, in turn, connected to the DAS and provided a power supply to all data acquisition equipment.



Figure 3.8: Solar Panel Mounted on San Angelo Bent Cap



Figure 3.9: Remote-Monitoring Equipment in DAS Box

3.6.4 Data Retrieval

In the original DAS, data were stored in SM716 Storage Modules, which were brought back to the CMRG lab to complete the data retrieval process, as discussed in Section 3.5.3. An antenna, cell phone, and modem made remote data retrieval possible. The new equipment as it is installed in the field is shown in Figure 3.9. The cellular phone is in the upper right-hand corner of the DAS box and the modem is in the lower left-hand corner. A personal computer running PC208W software could directly communicate with the DAS in the field. A Hayes-Compatible modem could dial up the cell phone and download the data via the field modem. A schematic of the new data retrieval system is shown in Figure 3.10. A Yagi antenna, COM100 Cellular Phone Package, and COM200 Telephone Modem were purchased from Campbell Scientific, Inc. for each DAS.

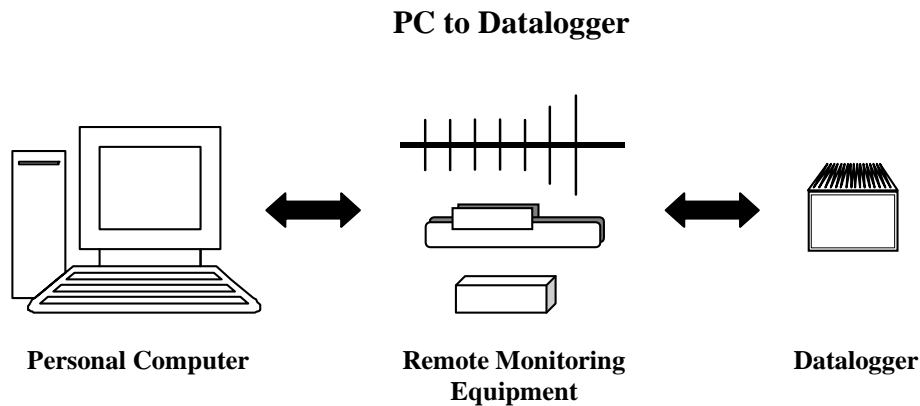


Figure 3.10: Schematic of New Data Transfer Setup

3.7 Gauge Durability

3.7.1 Introduction

Part of the long-term monitoring of these two bridges was measuring the performance of the different gauge types over the life of the bridge. A gauge durability survey was performed approximately once every year. The most recent survey was done during June 2001.

A gauge durability survey was achieved by manually looking through the data spreadsheets to determine if each of the 518 embedded gauges was still properly recording data. A gauge was deemed no longer functional when it was no longer reading any values, reading values of $-69,999$ or $-99,999$, or the readings were erratic. It was important to keep in mind what typical values should be for the different gauge types. Temperature readings have been known to be as low as 20°F during the winter and reach as high as 131°F in the summer. Readings from strain gauges were not as intuitive as temperature readings, but typically varied between $-2,000$ and $2,000$ microstrain. A VW/TR was considered malfunctioning if either component was no longer providing data. In most cases, the vibrating wire failed, while the thermistor recorded accurate temperatures. In a few cases, both failed or the thermistor alone failed, while the vibrating wire recorded strains.

Even using these guidelines, there was some subjectivity in determining the performance of a gauge. Gauges typically did not abruptly stop working. There was often a gradual decay, where the gauge occasionally read a value that did not make sense. When this occurred, a subjective decision had to be made to determine if the gauge was still producing usable data.

3.7.2 Results

Tables 3.5 and 3.6 show both the number and percentage of gauges working in the Louetta Road Overpass and San Angelo bridges, respectively. The gauges are broken into groups by their location in the bridges. Results are given for gauges embedded in the beams, precast panels, and cast-in-place deck. Surveys were performed after casting; after 60 days; after 1 year; and as of March 1998, June 1999, September 2000, and June 2001. Note that the tables first list the number of gauges still working and then the percentage of gauges still working.

Figure 3.11 graphically depicts the percentage of each gauge type still working. Also shown is the combined performance of three types of gauges. The performance for electric resistance strain gauges (ERSG), vibrating wire/thermistor (VW/TR) gauges, and thermocouples (TC) are shown in Figures 3.12, 3.13, and 3.14, respectively. The performance of each gauge is broken down by bridge. The percentage of gauges working in the northbound and southbound Louetta Road Overpass and in the eastbound and westbound San Angelo Bridge is shown.

3.7.3 Discussion

Electronic resistance strain gauges had the worst performance during long-term monitoring. VW/TR gauges performed moderately well, while thermocouples performed the best. It should be pointed out that some gauges were intentionally disconnected during the research project. This, in effect, skewed the results shown. Twenty-one electronic resistance strain gauges were disconnected in northbound Louetta. In southbound Louetta, forty-three electronic resistance strain gauges, two VW/TR gauges, and six thermocouples were disconnected. Seven electronic resistance strain gauges were disconnected in San Angelo eastbound. No gauges were intentionally disconnected in the westbound San Angelo Bridge. Many of the gauges that were intentionally disconnected were no longer working. Other gauges were accidentally disconnected during construction.

3.7.4 Conclusions

ERSGs have not performed well during long-term monitoring. As of June 2001, only 10 percent of these gauges were still working. Even if the disconnected gauges are not included, only 17 percent of the remaining gauges operated correctly. Therefore, ERSGs are not recommended for long-term monitoring.

VW/TR gauges have performed adequately. Sixty percent of these gauges remain in operation. Vibrating wire gauges are superior to ERSGs for long-term monitoring. Very few thermistors have failed. Approximately 95 percent of the thermistors still work. Therefore, the VW/TR gauge works well when measuring both strains and temperatures.

Thermocouples performed well during long-term monitoring. Seventy-five percent of the thermocouples were operative. The thermocouples on the San Angelo Bridge eastbound did not perform as well as the other three bridges. Only eight of the thermocouples in the other three bridges are no longer working, and six of those were intentionally disconnected. It is unclear why the San Angelo Bridge eastbound did not perform as well as the other structures.

Despite the fact some gauges no longer work, enough data were still being gathered to gain useful information about the Texas HPC bridges.

Table 3.5: Gauge Durability Summary for Louetta Road Overpass

	ERSG									VW/TR									TC									Total								
	Total	Initial Hookup	After Casting	After 60 Days	After 1 Year	As of 3/98	As of 6/99	As of 9/00	As of 6/01	Total	Initial Hookup	After Casting	After 60 Days	After 1 Year	As of 3/98	As of 6/99	As of 9/00	As of 6/01	Total	Initial Hookup	After Casting	After 60 Days	After 1 Year	As of 3/98	As of 6/99	As of 9/00	As of 6/01	Total	Initial Hookup	After Casting	After 60 Days	After 1 Year	As of 3/98	As of 6/99	As of 9/00	As of 6/01
Number of Guages																																				
Louetta NB Beams	59	49	47	31	18	6	2	2	1	14	14	13	12	7	7	5	5	3	12	11	11	11	11	12	12	12	12	85	74	71	54	36	25	19	19	16
Louetta NB CIP Deck	24	23	22	22	0	0	0	0	0	2	2	2	2	2	2	2	2	2	4	4	4	4	4	4	4	4	4	30	29	28	28	6	6	6	6	6
Louetta SB Beams	49	39	36	32	24	5	5	5	5	27	27	27	25	23	16	16	16	16	24	22	22	22	22	17	17	17	17	100	88	85	79	69	38	38	38	38
Louetta SB Panels	0	0	0	0	0	0	0	0	0	6	6	6	6	6	6	6	6	6	4	4	4	4	4	4	4	4	4	10	10	10	10	10	10	10	10	10
Louetta SB CIP Deck	4	3	3	3	0	0	0	0	0	17	15	14	14	14	14	14	14	14	10	10	10	10	10	10	10	10	9	31	28	27	27	24	24	24	24	23
Louetta NB	83	72	69	53	18	6	2	2	1	16	16	15	14	9	9	7	7	5	16	15	15	15	15	16	16	16	16	115	103	99	82	42	31	25	25	22
Louetta SB	53	42	39	35	24	5	5	5	5	50	48	47	45	43	36	36	36	36	38	36	36	36	36	31	31	31	30	141	126	122	116	103	72	72	72	71
Total	136	114	108	88	42	11	7	7	6	66	64	62	59	52	45	43	43	41	54	51	51	51	51	47	47	47	46	256	229	221	198	145	103	97	97	93
Percentages																																				
Louetta NB Beams		83	80	53	31	10	3	3	2		100	93	86	50	50	36	36	21		92	92	92	92	100	100	100	100		87	84	64	42	29	22	22	19
Louetta NB CIP Deck		96	92	92	0	0	0	0	0		100	100	100	100	100	100	100	100		100	100	100	100	100	100	100	100		97	93	93	20	20	20	20	20
Louetta SB Beams		80	73	65	49	10	10	10	10		100	100	93	85	59	59	59	59		92	92	92	92	71	71	71	71		88	85	79	69	38	38	38	38
Louetta SB Panels											100	100	100	100	100	100	100	100		100	100	100	100	100	100	100	100		100	100	100	100	100	100	100	100
Louetta SB CIP Deck		75	75	75	0	0	0	0	0		88	82	82	82	82	82	82	82		100	100	100	100	100	100	100	90		90	87	87	77	77	77	77	74
Louetta NB		87	83	64	22	7	2	2	1		100	94	88	56	56	44	44	31		94	94	94	94	100	100	100	100		90	86	71	37	27	22	22	19
Louetta SB		79	74	66	45	9	9	9	9		96	94	90	86	72	72	72	72		95	95	95	95	82	82	82	79		89	87	82	73	51	51	51	50
Total	84	79	65	31	8	5	5	4		97	94	89	79	68	65	65	62		94	94	94	94	87	87	87	85	89	86	77	57	40	38	38	36		

Table 3.6: Gauge Durability Summary for San Angelo Bridges

	ERSG									VW/TR									TC									Total								
	Total	Initial Hookup	After Casting	After 60 Days	After 1 Year	As of 3/98	As of 6/99	As of 9/00	As of 6/01	Total	Initial Hookup	After Casting	After 60 Days	After 1 Year	As of 3/98	As of 6/99	As of 9/00	As of 6/01	Total	Initial Hookup	After Casting	After 60 Days	After 1 Year	As of 3/98	As of 6/99	As of 9/00	As of 6/01	Total	Initial Hookup	After Casting	After 60 Days	After 1 Year	As of 3/98	As of 6/99	As of 9/00	As of 6/01
Number of Gauges																																				
San Angelo EB Beams	50	43	42	34	21	19	11	10	10	35	33	30	29	27	25	14	14	14	30	30	30	30	25	22	18	17	16	115	106	102	93	73	66	43	41	40
San Angelo EB Panels	8	8	0	0	0	0	0	0	0	4	4	4	4	4	4	4	4	4	14	12	12	12	11	11	7	7	6	26	24	16	16	15	15	11	11	10
San Angelo EB CIP Deck	11	11	11	11	11	11	4	3	0	9	8	8	8	8	8	8	7	7	20	19	19	19	19	17	17	16	15	40	38	38	38	38	36	29	26	22
San Angelo WB Beams	18	14	14	12	9	7	7	7	7	14	14	13	13	12	12	10	10	10	12	12	12	12	12	12	12	12	12	44	40	39	37	33	31	29	29	29
San Angelo WB Panels	0	0	0	0	0	0	0	0	0	4	4	4	4	4	4	4	4	4	4	4	4	4	4	4	4	4	4	8	8	8	8	8	8	8	8	8
San Angelo WB CIP Deck	7	7	6	6	0	0	0	0	0	14	9	8	8	8	8	8	8	8	8	8	8	8	8	8	8	8	8	29	24	22	22	16	16	16	16	16
San Angelo EB	69	62	53	45	32	30	15	13	10	48	45	42	41	39	37	26	25	25	64	61	61	61	55	50	42	40	37	181	168	156	147	126	117	83	78	72
San Angelo WB	25	21	20	18	9	7	7	7	7	32	27	25	25	24	24	22	22	22	24	24	24	24	24	24	24	24	24	81	72	69	67	57	55	53	53	53
TOTAL	94	83	73	63	41	37	22	20	17	80	72	67	66	63	61	48	47	47	88	85	85	85	79	74	66	64	61	262	240	225	214	183	172	136	131	125
Percentages																																				
San Angelo EB Beams		86	84	68	42	38	22	20	20		94	86	83	77	71	40	40	40		100	100	100	83	73	60	57	53		92	89	81	63	57	37	36	35
San Angelo EB Panels		100	0	0	0	0	0	0	0		100	100	100	100	100	100	100	100		86	86	86	79	79	50	50	43		92	62	62	58	58	42	42	38
San Angelo EB CIP Deck		100	100	100	100	100	36	27	0		89	89	89	89	89	89	78	78		95	95	95	95	85	85	80	75		95	95	95	95	90	73	65	55
San Angelo WB Beams		78	78	67	50	39	39	39	39		100	93	93	86	86	71	71	71		100	100	100	100	100	100	100	100		91	89	84	75	70	66	66	66
San Angelo WB Panels											100	100	100	100	100	100	100	100		100	100	100	100	100	100	100	100		100	100	100	100	100	100	100	100
San Angelo WB CIP Deck		100	86	86	0	0	0	0	0		64	57	57	57	57	57	57	57		100	100	100	100	100	100	100	100		83	76	76	55	55	55	55	55
San Angelo EB		90	77	65	46	43	22	19	14		94	88	85	81	77	54	52	52		95	95	95	86	78	66	63	58		93	86	81	70	65	46	43	40
San Angelo WB		84	80	72	36	28	28	28	28		84	78	78	75	75	69	69	69		100	100	100	100	100	100	100	100		89	85	83	70	68	65	65	65
TOTAL		88	78	67	44	39	23	21	18		90	84	83	79	76	60	59	59		97	97	97	90	84	75	73	69		92	86	82	70	66	52	50	48

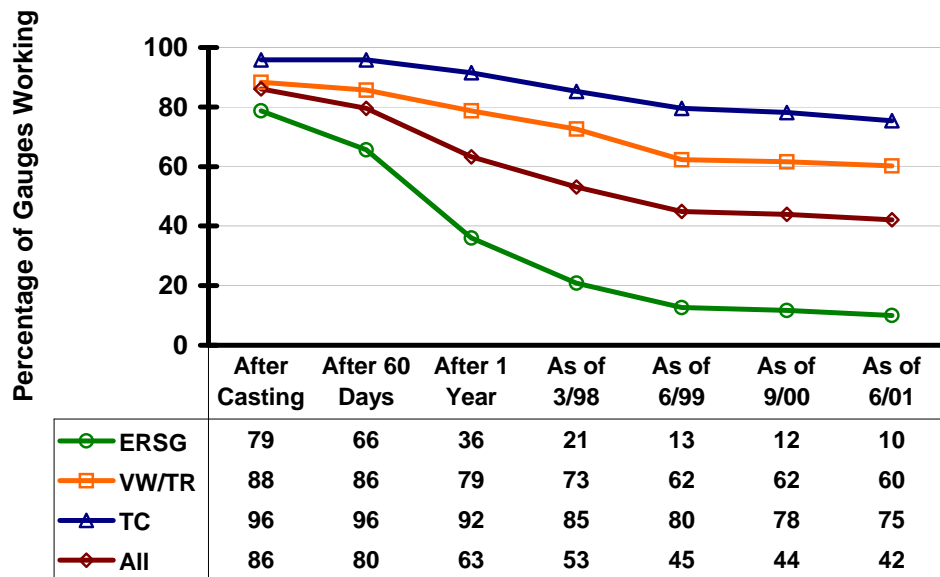


Figure 3.11: Percentage of Gauges Working

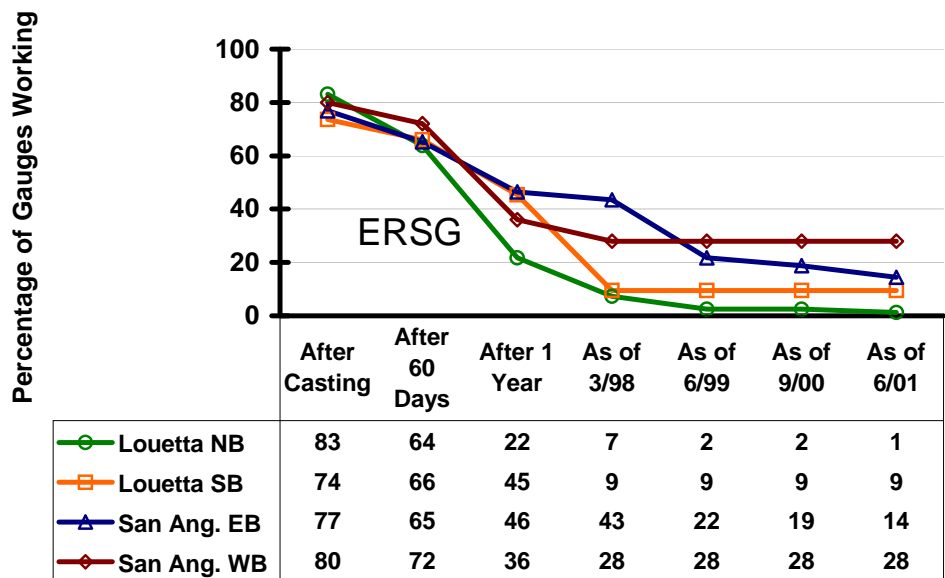


Figure 3.12: Percentage of ERS Gauges Working

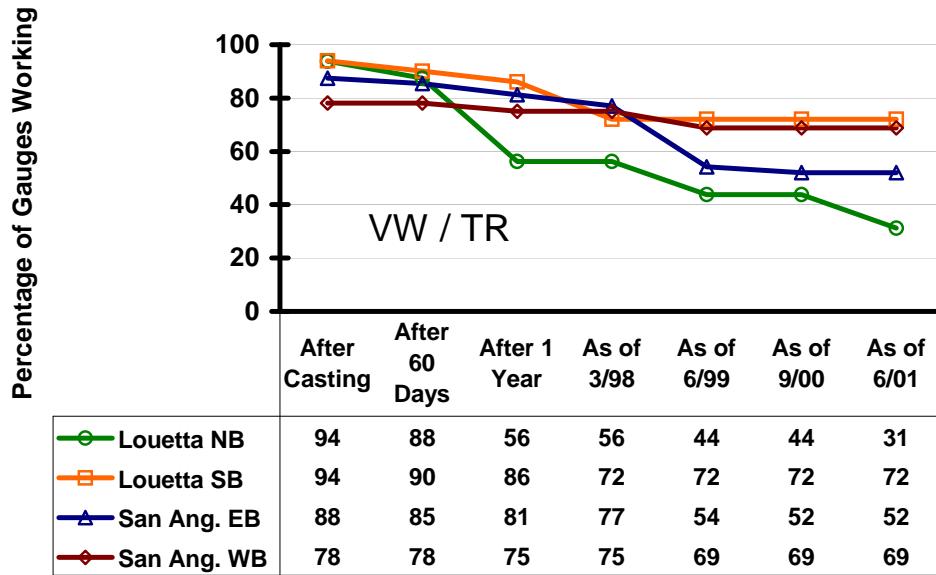


Figure 3.13: Percentage of VW/TR Gauges Working

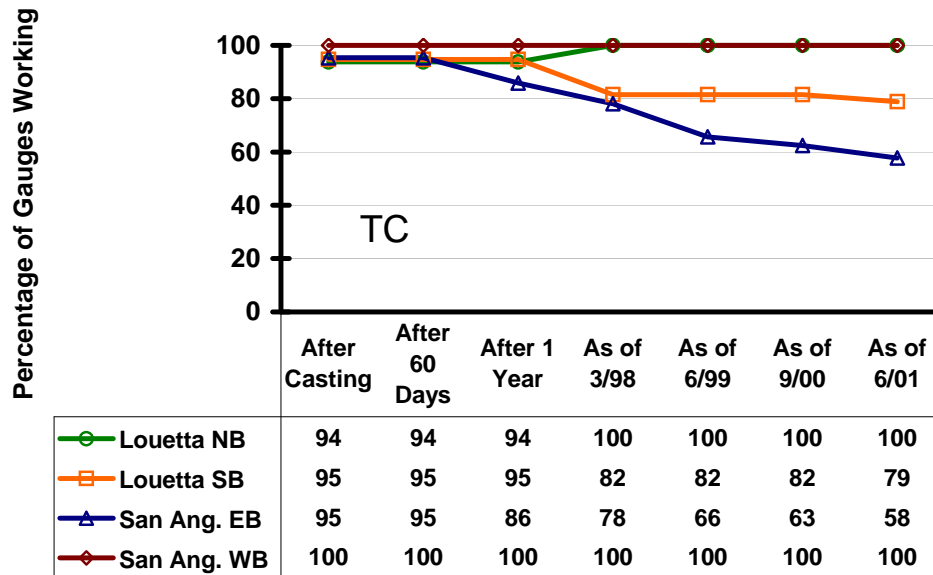


Figure 3.14: Percentage of TC Gauges Working

Chapter 4. Monitoring Program

4.1 Introduction

This chapter presents the monitoring program. It is divided into sections pertaining to durability and structural performance. The durability section describes the review of TxDOT Bridge Inspection reports and the methods used during visual inspections of the structures. It also describes the method used to test for chloride ion penetration in the concrete decks. The structural sections present details on how the instrumentation was used to acquire information about prestress losses and camber. The precise surveying method used to monitor changes in beam camber is also described.

4.2 Durability Monitoring

One of the expected advantages of HPC was improved durability when compared to normal concrete. These bridge sites provided a unique opportunity to make performance comparisons between different concrete mixes. As mentioned in Chapter 3, various aspects of each bridge were made with different concrete mixes. All aspects of the Louetta Road Overpass were considered HPC. However, the cast-in-place deck was normal strength (4000 psi) and high strength (8000 psi) in the northbound and southbound directions, respectively. The westbound San Angelo bridge was normal concrete, while the eastbound bridge utilized HPC. The sites in Lubbock and Amarillo, however, did not have different mixture designs within their respective CIP decks. The different locations differed from each other in mixture designs, though, based on the time of year and the construction project-specific sources of aggregates, cement, SCMs, and admixtures.

4.2.1 Bridge Inspection Review

Before the on-site inspections were carried out, the most recent Bridge Inspection report for each of the bridges was reviewed. TxDOT developed the Bridge Inventory, Inspection, and Appraisal Program to monitor the condition of the 48,000 bridges in Texas. As part of the report, various parts of the structure were given ratings based on their condition. The rating system is summarized in Table 4.1. The Bridge Inspection review was an important tool for the researchers. It aided preparations for the visual inspection by indicating problems the bridges were experiencing.

Table 4.1: Summary of the Bridge Inspection Rating System

Rating	Condition	Comments
9	Excellent	-
8	Very good	-
7	Good	Some minor problems
6	Satisfactory	Minor deterioration of structural elements (limited)
5	Fair	Minor deterioration of structural elements (extensive)
4	Poor	Deterioration significantly affects structural capacity
3	Serious	Deterioration seriously affects structural capacity
2	Critical	Bridge should be closed until repaired
1	Failing	Bridge closed but repairable
0	Failed	Bridge closed but beyond repair

4.2.2 Visual Inspection

A formal visual inspection was made at each bridge site during the course of this research program. However, less formal inspections were made during each DAS maintenance trip as well. The purpose of the visual inspection was to identify any defects in the structure, which may indicate a more serious problem with the structure. Surface defects such as cracking, spalling, delamination, and efflorescence are common symptoms of concrete deterioration.

The deck was investigated for surface defects with the naked eye. A visual inspection could easily be made by walking along the bridge deck when traffic control was provided by TxDOT. Deck overhangs could be inspected from below the bridge by the naked eye or by using binoculars for a closer view. Defects were photographed and recorded. Cracking was measured for length using a tape measure and for width using a crack comparator.

The superstructure (prestressed beams and precast panels) and substructure (piers, columns, and bent caps) were investigated from below the bridges. At Louetta, the substructure could be viewed up close from the ground and the superstructure could easily be inspected with a pair of binoculars. Due to the height of the San Angelo Bridge, a snooper truck was used to get a closer look at the underside of the structure. The tall San Angelo piers were inspected from below the deck and from the snooper truck. Photographs and measurements were taken of any surface defects.

In July and August 2003, after five years of service, the Federal Highway Administration contracted with PSI to officially inspect and report on the conditions of the Louetta and San Angelo bridges. CTR researchers assisted PSI personnel in mapping the extensive cracking in the HPC decks. The inspectors' markings along the cracks clearly showed "streets" of cracking patterns in the CIP surface that outlined each of the underlying precast panels. These PSI reports are included in Appendix C.

In 2002 researchers began the regular inspection and monitoring of TxDOT-identified new HPC bridge decks in the Lubbock and Amarillo Districts. These decks were part of the followings structures:

- A. The first in Lubbock was the 82nd Street overpass on US 82/62, and it was already showing evidence of significant early cracking. This bridge was constructed in 1999. It was constructed of a 4-inch cast-in-place deck over precast deck panels. Standard Class S concrete was used with epoxy coated reinforcing steel. In addition to minor

surface stretch cracking from over-working and tining the drying surface, large transverse cracks had already developed.

- B. The second Lubbock Bridge was US 82/62 at FM 179. It used the older metal deck forms to make nominal 8-inch cast-in-place decks. This bridge was constructed in 2000. Standard Class S concrete was used with epoxy coated reinforcing steel. The cracking here was minimal, though, and due to misplaced zip strips or to continuing to try to tine the surface after it had already begun to dry.
- C. The third Lubbock Bridge was on Loop 289 at Frankford Street. This bridge was constructed in 2001. It was constructed of a 4-inch cast-in-place deck over precast panels. Standard Class S concrete was used, which included 25% Class F fly ash. Epoxy coated reinforcing steel was used. No early indications of cracking were visible on the first inspection.
- D. The fourth Lubbock structure was on IH 27 at New Deal. This bridge was constructed in 2002. The 5-inch deck was cast on prestressed concrete box beams. The concrete was identified as HPC which included 35% Class F fly ash. Epoxy coated reinforcing steel was used. Although we saw no obvious cracking during the first inspection, several early cracks developed in this bridge deck.
- E. The Amarillo Loop 335 at RM 1061 was constructed in 1999. The concrete was identified as HPC which included 20% Class C fly ash. In addition, 2 gallons per cubic yard of a calcium nitrite corrosion inhibitor was used in the concrete. Epoxy coated reinforcing steel was used. The bridge showed an area of transverse cracking and even intersecting longitudinal cracks early in its life.
- F. The last structure is in Amarillo on Loop 335 over Amarillo Creek. This bridge was constructed in 1997. The concrete was Class S concrete which did not include fly ash. In addition, 2 gallons per cubic yard of a calcium nitrite corrosion inhibitor was used in the concrete. Epoxy coated reinforcing steel was used. Longitudinal cracking patterns in the thickened CIP sections over bents were already exhibited in this deck.

4.2.3 Chloride Testing

Chloride content was determined using the CL-500 test equipment purchased from James Instrumentation. A hammer drill was used to pulverize the concrete. Samples were collected at various depths in the bridge deck. This process created a vertical profile to determine the penetration of chloride ions into the deck. The samples were stored in plastic bags and taken back to the lab for analysis.

To conduct the test, 1.5 grams of the concrete dust were combined with 10 mL of 15 percent acetic acid. The solution was shaken for 15 seconds and then allowed to stabilize for at least two hours. A reference electrode connected to an electrometer was used to determine the mV produced by the solution. Before the chloride ion content was determined, a calibration graph had to be made from the provided calibration liquids. This graph converted mV readings to percent chloride. The reference electrode was submerged in the sample solution and the mV reading was taken once it had stabilized. Lower chloride contents yield higher mV readings.

4.3 Prestress Loss Measurements

Long-term prestress loss measurements were successfully made for eleven of the twenty beams that were instrumented for such measurements. Four Louetta HPC beams, three San Angelo eastbound HPC beams, and four San Angelo westbound non-HPC beams, were measured for prestress loss. These beams are shown in the highlighted regions of Figures 4.1 and 4.2.

Prestress loss measurements were taken using vibrating wire gauges placed at the center of gravity of the prestressing steel. The gauges were actually measuring the strain in the concrete. Stress was determined by multiplying the strain times the modulus of elasticity as shown in Equation 4.1. This equation assumed strain compatibility between the concrete and steel.

$$\Delta f_{ps} = E_{ps} \epsilon_{cgs} \quad 4.1$$

where Δf_{ps} = change in stress of prestressing steel

E_{ps} = prestressing steel modulus of elasticity (28,000 psi)

ϵ_{cgs} = measured concrete strain at center of gravity of prestressing steel

However, Equation 4.1 does not account for losses due to relaxation, pre-release losses, and thermal effects. The relaxation loss occurred in the steel, and therefore was not measured by the gauge in the concrete. The first measurement made on each beam was taken just prior to transfer [10]. Early time-dependent prestress loss was not measured and therefore this analytical value must be added to the measured quantity. Temperature effects caused a change in stress due to thermal gradients and the gauges' coefficient of thermal expansion. Thermal gradient effects were reduced by taking all measurements at 8:00 AM, when the gradient was typically small. The change in strain due to thermal expansion of the gauge was corrected by using temperature measurements taken at the location of the strain gauge. Therefore, the actual measured prestress loss was determined using Equation 4.2 [10]:

$$\Delta f_{ps,total} = E_{ps} \epsilon_{cgs} + \Delta f_{ps,relaxation} + \Delta f_{ps,pre-release} \quad 4.2$$

where $\Delta f_{ps,total}$ = total measured prestress loss

$\Delta f_{ps,relaxation}$ = prestress loss due to steel relaxation

$\Delta f_{ps,pre-release}$ = prestress loss due to pre-release factors

Note that losses due to thermal effects were accounted for in the pre-release term.

The strain and temperature data were inputted into spreadsheets developed by Gross [12]. These spreadsheets made the necessary corrections to the measured strain and converted them to measured prestress loss.

4.4 Camber Measurements

Camber and deflection measurements were made on a number of beams in both structures. The fourteen measured Louetta beams are labeled in Figure 4.1. Twelve of the beams, boxed in Figure 4.1, were instrumented and measurements were made from casting through long-term behavior. The two non-instrumented beams in northbound span 3 were measured since erection at the bridge site. These beams were added so camber could be observed across an entire span [10].

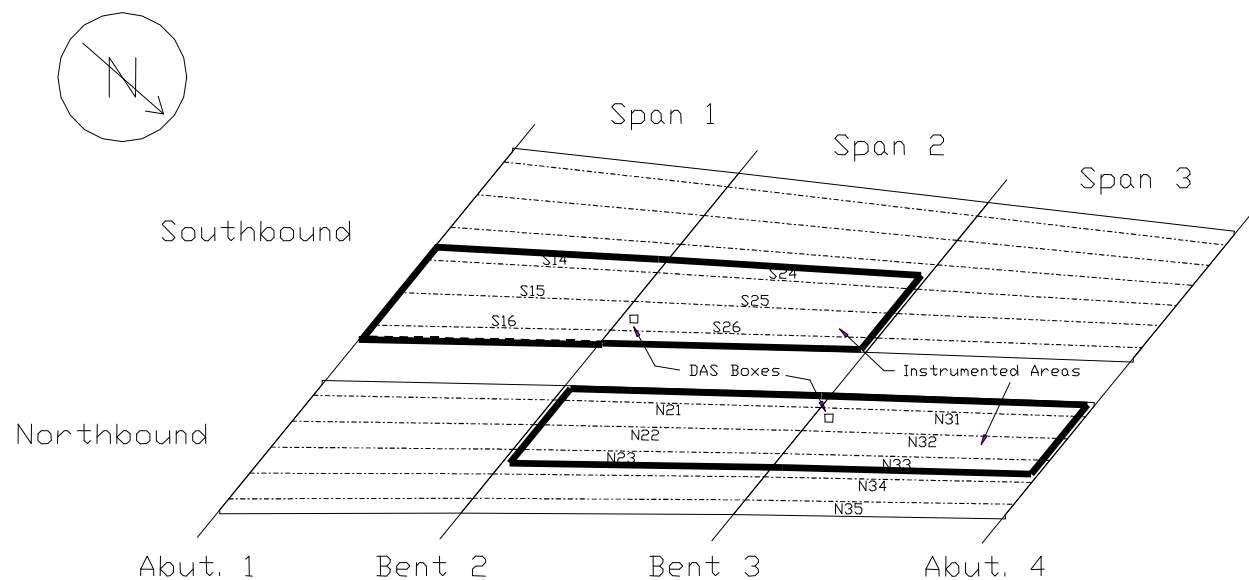
The measured San Angelo beams are labeled in Figure 4.2. All twenty-seven beams in eastbound spans 1 through 4 and westbound span 1 were measured since the bridge decks were completed. However, only the fourteen instrumented San Angelo beams were measured since casting. These beams are in the highlighted region of Figure 4.2.

The beam notation should be described at this point. All beams are described using a letter and two numbers. The letter identifies which bridge the beam belongs to: N for Louetta northbound, S for Louetta southbound, E for San Angelo eastbound, and W for San Angelo westbound. The first number identifies the span and the second identifies the beam in the span.

4.4.1 Precise Surveying System

All camber measurements were taken using the relative method of the precise surveying system. The system was used successfully in the past on both bridges to take camber and deflection measurements. It was recommended by researchers because of its flexibility and ease of use [5, 10, 12]. The system required a minimum of two people. One person was needed to hold the rod, while the other read beam elevations using the level and recorded them. However, it was desirable to have a third person when using the precise surveying system. Holding the rod in place could quickly become quite tiring for a single person and was even more difficult during windy conditions. Alternatively, the third person could be responsible for recording measurements. A recorder both reduces the chance for recording error and speeds up the process.

The precise surveying system is a modified simple rod and level surveying system. The surveying system was made *precise* by employing three modifications to increase the accuracy of the system. A post level was used to ensure the rod was kept vertical. In addition, precision scales were attached to the rod. Readings were made using the 0.02 in. divisions on the scales. Finally, sight distances were limited to 40 feet so that the precision scales may be read using a more magnified view. The rod, with close-up views of the precision scales and post level, is shown in Figure 4.3.



LOUETTA ROAD OVERPASS (prior to widening)

Figure 4.1: Instrumented Areas of Louetta Road Overpass [10]

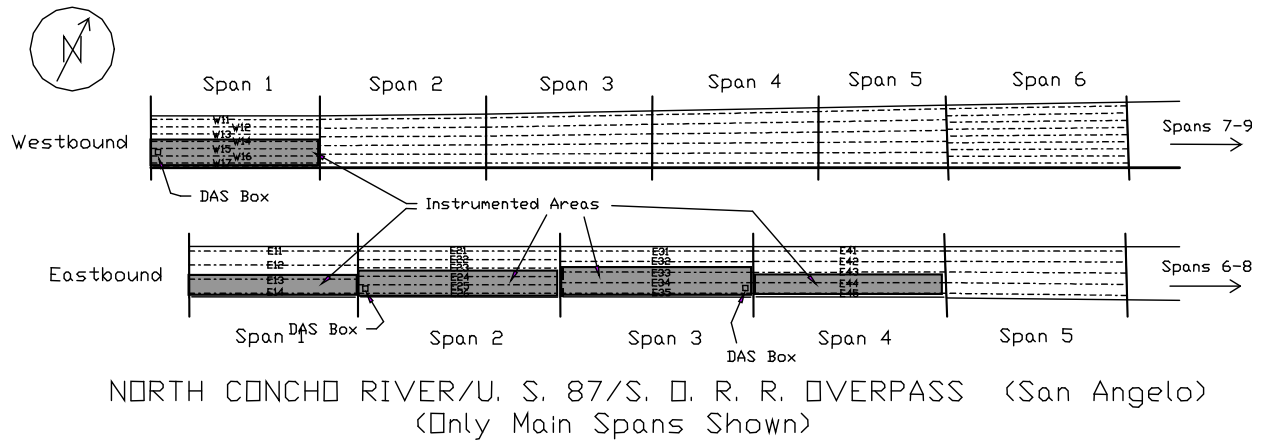


Figure 4.2: Instrumented Areas of San Angelo Bridges [10]



Figure 4.3: Precise Surveying System Equipment

The relative method did not determine the actual beam elevation. Instead, the *relative* change in elevation between points was used to determine the camber or deflection. Beam elevations were taken at the bearing points of the beams and at the beam midspan using the relative method. The surveying points had been painted on the bottom of the Louetta Road Overpass beams. The surveying points were mapped out on the deck of the San Angelo bridges using the known bridge geometry.

Measurements were taken from below the bridge at the Louetta Road Overpass. The survey rod could be extended, so that it reached the painted survey points on the beams. Survey points were located on both sides of the U-beam, such that six measurements were taken for each beam as illustrated in Figure 4.4. Each pair was averaged to obtain a single camber value for the beam. Measurements could not be taken at the true bearing point because the pier blocked its location. Therefore, a correction had to be made to the field measurement. This correction is discussed in Section 4.4.2.2.

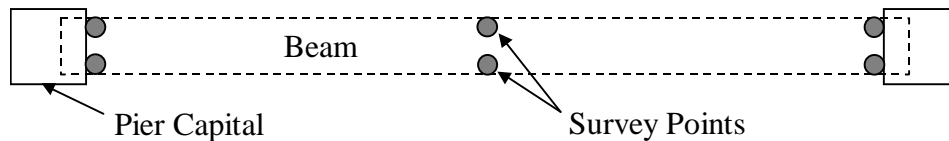


Figure 4.4: Location of Survey Points on a Louetta Beam

At the San Angelo bridge sites, measurements were made on top of the bridge deck. Taking camber measurements using the bottom of the beams was more desirable, but was impossible due to the bridge layout. Difficulties arose because of the fact that the bridges are located well above grade and multiple spans are over the North Concho River. A correction to the raw field measurements must be made due to the varying thickness of the cast-in-place concrete deck. This correction is discussed in Section 4.4.2.3. Figure 4.5 shows the relative method of the precise surveying system used to measure beam camber from the deck of the westbound San Angelo Bridge.



Figure 4.5: Camber Measurements at San Angelo

4.4.2 Corrections to the Precise Surveying System

The precise surveying system provided a value of the beam camber or deflection as measured on top of the deck or bottom of the beam, for the San Angelo and Louetta beams,

respectively. Several corrections had to be made to the field measurements before an accurate beam camber or deflection was obtained. The camber or deflection caused by thermal gradients must be removed from the field measurements. Two types of *offset* corrections must be made. The Louetta Road Overpass measurements must be offset to account for the difference between the bearing point of the beam and the actual survey point. The San Angelo bridge measurements must be offset to account for the variation in the depth of the cast-in-place deck.

Thermal Gradient Correction

A thermal gradient is the measured vertical variation in temperature throughout the bridge cross section. A thermal gradient was produced because the deck was directly exposed to sunlight while the underside of the bridge was shaded. A thermal gradient may also be produced at night when the deck cools faster than the rest of the bridge. The thermal gradient caused changes in strain in the bridge, resulting in a variation of camber or deflection. A detailed discussion of thermal gradients in the Texas HPC bridges can be found in Byle, Burns, and Carrasquillo [5] and Gross and Burns [10].

Thermal gradients were measured using the embedded gauges described in Section 3.4.2. Thermocouples and thermistors measured temperatures in the cast-in-place decks, precast prestressed panels, and beams. Measurements were made at the bottom flange, the center of gravity of the prestressed strands, the center of gravity of the noncomposite beam, the center of gravity of the composite beam, the top of the web, the top of the flange, and in the panel and deck. The temperature gradient at the time of the precise surveying system measurements was found using the data recorded by the DAS. The temperatures of thermal gradient were entered into spreadsheets developed by Gross [12], which calculated the thermally induced camber in the beams.

Bearing Point Correction

In the Louetta beams, a correction to field measurements had to be made to account for the difference between the actual bearing point of the beam ends and the survey point. The actual bearing point could not be reached because of the arrangement of the pier and beam. This fact is illustrated in Figure 4.4 and can be seen in the photograph in Figure 4.6. The offset between the bearing point and survey point is significant because the bridge was built on a slight super elevation. The north side of the bridge is actually higher than the south side. An analytical correction was applied to the measurements taken on the instrumented beams. This correction tended to be small, with the largest value of 0.31 in. occurring on Beam N21 [10].



Figure 4.6: Bearing Point versus Survey Point

Deck Offset Correction

As described in Section 4.4.1, camber measurements for San Angelo beams were made from the deck surface. In order to obtain a camber measurement for the beams and not the deck, the variation in the deck cast-in-place concrete depth had to be accounted for. Deck offsets were determined by comparing measurements taken from the bottom of the beams and from the deck. Gross determined the offset corrections [12]. Note that offsets were not determined for all of the beams. Offsets were only determined for the 19 beams in which measurements were recorded on the bottom of the beam prior to completion of the bridge. The deck offsets were less than 0.5 in. for most beams, but exceeded 2.0 in. in all eastbound span 1 beams.

Chapter 5. Monitoring Results

5.1 Introduction

The results of the monitoring program are presented in this chapter. First, the results of the durability testing are presented and a summary of the Bridge Inspection reports, the results of the visual inspections, and findings from the chloride ion penetration tests are included. Next, the results of the structural performance evaluations are presented. The measured prestress loss and the measured camber and deflection are presented for the twenty-six instrumented beams. These measurements were discussed in Sections 4.3 and 4.4, respectively. The instrumented beams were shown in Figures 4.1 and 4.2. Graphs for the measured and predicted long-term prestress losses and camber are provided for every instrumented beam in Appendix A. Several beams that were not instrumented were measured for camber as well.

5.2 Durability Results

5.2.1 Bridge Inspection Summary

The Bridge Inspection report was described in Section 4.2.1. The results of the Bridge Inspection report review are presented in this section. A single report was done for the Louetta Road Overpass. D. Gary Pickett of Pickett, Kelm & Associates, Inc. performed the inspection on March 5, 1999. Separate reports were done for the San Angelo bridges. Bill Tankersley performed the inspections on September 6, 2000. A summary of these reports is shown in Table 5.1. Both bridges received high ratings, but minor problems were reported on all of the structures.

Table 5.1: Summary of Routine Bridge Safety Inspection Report Review

	Rating	Comments
<i>Louetta HPC</i>		
Deck	8	Minor spalls on concrete traffic barrier. Joint seals have minor build-up of dirt and sand.
Superstructure	7	Minor spalls on bottom of U-beams. Bearing pads have deflected slightly.
Substructure	9	
<i>San Angelo Eastbound HPC</i>		
Deck	7	Minor cracks and efflorescence on underside of deck overhangs.
Superstructure	8	
Substructure	8	
<i>San Angelo Westbound Non-HPC</i>		
Deck	7	Minor transverse cracks in surface concrete. Very minor cracking and efflorescence on underside of deck overhangs.
Superstructure	8	
Substructure	8	

When the Lubbock and Amarillo HPC bridge decks were added to project monitoring activities. Bridge Inspection was no longer used by TxDOT, and our deck monitoring was more thorough than the Texas Bridge Inspection Program, so no other records were reviewed for these decks. One of the last reports is included in Appendix B to describe the condition of the decks with respect to durability.

5.2.2 Results of Visual Inspection

During the visual inspection, any distress in the structure was noted and documented. Previous work by Sheppard and Burns [19] was discussed in Section 2.7. This section discusses the crack mapping of the Louetta Road Overpass deck, as well as general comments on the observed condition of the deck concrete at the HPC bridge sites.

The Louetta Road Overpass was inspected on January 31, 2001. The cracking in the deck was mapped for comparison with the previous measurements. Unfortunately, researchers were only able to gain access to the shoulder and one lane of the deck due to traffic concerns. The previous investigation had access to the entire bridge deck. It is the author's opinion that measuring cracks, especially from distances as great as 30 ft., is somewhat subjective. Therefore, comparisons between the results of Table 5.2 and the results of Sheppard and Burns in Table 2.1 are at best imperfect. The results of the crack mapping are shown in Table 5.2.

Table 5.2: Crack Mapping Summary

Span	Cracking (ft)	
	Longitudinal	Transverse
<i>Louetta Northbound Normal Strength</i>		
N1	106	26
N2	163	42
N3	190	27
Total	459	95
<i>Louetta Southbound High Strength</i>		
S1	155	61
S2	250	66
S3	328	24
Total	733	151

Both investigations found more longitudinal cracks in the southbound high strength HPC deck than in the northbound normal strength HPC deck. However, the ratio of longitudinal to transverse cracks was not the same for the two investigations. The previous investigation found the longitudinal to traverse crack ratios to be 2.5 and 8.1 for the northbound and southbound bridges, respectively. The recent investigation found the ratio for both bridges to be approximately 4.8. The suspected reasons for these discrepancies were described earlier.

Although cracks widths were large at the surface of the deck on the southbound bridge, the width of the cracks typically narrowed as the crack extended down into the slab. Crack depths were not recorded. Cracks on the northbound bridge were typically much smaller than those on the southbound. Figure 5.1 and 5.2 show some of the most severe cracks on the

southbound bridge. Note that the crack continued across the control joint, proving the joint did not prevent transverse cracking.



Figure 5.1: Close-Up of Crack in Louetta Southbound Deck



Figure 5.2: Severe Crack in Louetta Southbound Deck

The rest of the structure was in very good condition. The minor problems detected by Shepperd and Burns [19] were investigated. These problems were discussed in Section 2.7 and include minor spalling and cracking around the drain ports of the beams and cracks and efflorescence in the cast-in-place deck. None of these problems had become worse, and the drain ports had been repaired.

The San Angelo bridges were also in very good condition. As noted in the Bridge Inspection report, minor cracking and efflorescence was detected on the underside of the deck overhangs. This is a common problem and interested parties are not concerned with this development. No significant signs of distress were found in the piers, bent caps, or beams. The minor transverse cracks in the westbound deck that were reported in the Bridge Inspection report were difficult to find during the inspection of September 7, 2000 when high daytime temperatures resulted in expanded decks and tighter transverse cracks.

In 2003, the Federal Highway Administration had contracted with a consulting firm, Professional Services Industries, Inc. (PSI) from the Washington, DC area, to officially inspect and report on the condition of the Louetta and San Angelo HPC bridges. So at TxDOT's request in late summer of 2003, CTR researchers assisted PSI in mapping the extensive cracking patterns that had already developed in the decks. A draft of their inspection report to TxDOT is included in Appendix C.

Also included in the appendix are the last visual monitoring reports of the bridges in Lubbock and Amarillo. These sites included four HPC bridge decks in the Lubbock District; the 82nd Street overpass on US Highways 82/62, US highways 82/62 at FM 179, Loop 289 at Frankford Street, and the IH 27 New Deal bridge. Two HPC bridge decks were selected in Amarillo District, and they were RM 1061 overpass on Loop 335 and the Amarillo Creek bridge on Loop 335.

5.2.3 Chloride Penetration

Chloride ion testing was not performed for the Louetta Road Overpass. Researchers planned on taking samples during the January 31, 2001, deck inspection. However, because of equipment failure and time constraints, samples were not acquired. Researchers and TxDOT officials agree that deicing salts have seldom been used, if used at all, on the bridge. Therefore, it is believed that significant amounts of chloride ions are not likely to be found. Table 5.3 summarizes the results of the chloride ion testing performed on September 7, 2000, from the San Angelo bridge decks. The highest reading occurred on the edge of the eastbound bridge at a depth of 0.5 inches. This value of 0.0074 percent chloride ions is considered negligible. Gerry Fields, of the TxDOT San Angelo District Office, said deicing salt had not been used on the bridges within the past year. He also stated that sand would be used instead of salt in the event of freezing weather.

The samples taken from the eastbound bridge were 22 ft, 12.3 ft, and 2 ft north of the southern guardrail for the center of deck, tire path, and edge samples, respectively. The samples taken from the westbound bridge were 19.7 ft, 11.7 ft, and 2 ft south of the northern guardrail for the center of deck, tire path, and edge samples, respectively. All samples were taken 3 feet east of the westernmost construction joint.

Table 5.3: Results of Chloride Ion Penetration Tests

Sample	% CL	Sample	% CL
EE0.5	0.0073	WE0.5	0.0044
EE1.0	0.0021	WE1.0	0.0031
ET0.5	0.0027	WT0.5	0.0035
ET1.0	0.0017	WT1.0	0.0022
EC0.5	0.0023	WC0.5	0.0033
EC1.0	0.0023	WC1.0	0.0024
XYn = Sample Notation X = bridge E = Eastbound W = Westbound Y = position in span E = outer edge of deck T = tire path C = center of deck n = depth of sample (in.)			

5.3 Prestress Loss

The measured prestress loss for each instrumented beam was graphed with respect to the number of days after release. These plots can be found in Appendix A. The beam identification number is written below the key. Notice the vertical axes show prestress loss in ksi and as the percentage of the jacking force. Data points occurring after the second to last camber data point were measured during the current phase of the project. The other data points were measured during earlier work on the HPC bridges [5, 10].

Note that plots were included for all twenty-six instrumented beams even though prestress loss were measured on only eleven of those beams. Prestress loss measurements are no longer possible because some of the vibrating wire gauges have failed, or never worked to begin

with. In addition, prestress loss measurements were not taken for all of the beams that were measured for camber and deflection. Prestress loss measurements rely on a single gauge placed at the center of gravity of the strands. If budget allows, a backup gauge is recommended for prestress loss measurements due to the dependence on the reading of a single gauge.

A typical plot of the measured prestress loss is shown in Figure 5.3. The measurements generally show good correlation with the prestress loss predicted by the time-dependent model. Figure 5.4 shows the worst-case scenario, with regards to measured prestress loss compared to the time-dependent model.

Table 5.4 shows the components of the measured long-term prestress loss. These values were current as of March 2001. Results are given for eleven beams: four Louetta HPC U-beams, three San Angelo eastbound HPC beams, and four San Angelo westbound non-HPC beams. The total loss was made up of losses due to pre-release loss, elastic shortening, creep and shrinkage, and relaxation. Creep and shrinkage are listed as one component because they cannot be measured separately. The total loss is given in terms of ksi as well as the percentage of the jacking force. The strands were jacked to a stress of 202.5 ksi.

Table 5.4: Components of Measured Prestress Loss

Beam	Days After Release	Δ Time ¹ (days)	Loss Components (ksi)				Total Loss (ksi)	Δ Total Loss ³ (ksi)	Total Loss (% of f_{jack})
			PR	ES	CR+SH ²	RE			
Louetta HPC Beams									
N32	1865	1104	8.10	17.75	15.43	3.28	44.56	-1.45	22.00
S15	1854	1106	8.10	16.38	11.84	3.28	39.60	-1.74	19.55
S16	2368	1106	8.10	17.16	14.23	3.41	42.90	-2.64	21.19
S25	2327	1106	8.10	12.96	11.07	3.40	35.54	-1.73	17.55
Average			8.10	16.07	13.14	3.34	40.65	-1.89	20.07
San Angelo Eastbound HPC Beams									
E14	1495	1073	8.10	24.58	24.51	3.16	60.35	-3.11	29.80
E24	1477	1073	9.11	20.19	22.33	3.15	54.78	-3.27	27.05
E25	1819	1073	8.10	22.46	20.98	3.27	54.80	-2.85	27.06
Average			8.44	22.41	22.60	3.19	56.64	-3.07	27.97
San Angelo Westbound Non-HPC Beams									
W14	1844	1073	7.09	13.94	11.01	3.27	35.32	-0.65	17.44
W15	1844	1073	7.09	14.73	10.00	3.27	35.09	-0.68	17.33
W16	1844	1073	7.09	12.18	11.32	3.27	33.86	-1.18	16.72
W17	1839	1073	7.09	12.80	8.51	3.27	31.67	-1.16	15.64
Average			7.09	13.41	10.21	3.27	33.99	-0.92	16.78
1 ksi = 6.895 Mpa									
¹ Change in time between data shown in Table 5.4 and data shown in Table 7.8 of reference [10].									
² Includes compensation for measured elastic change in stress due to superimposed dead load.									
³ Change in total prestress loss between data shown in Table 5.4 and data shown in Table 7.8 reference [10].									
PR = Pre-release; ES = Elastic Shortening; CR = Creep; SH = Shrinkage; RE = Relaxation									

Four Louetta HPC beams were measured for long-term prestress loss. The average total loss was 40.7 ksi. The values ranged between 35.5 ksi and 44.6 ksi. In terms of percentage of the jacking force, the average prestress loss was 20.1 percent. These values ranged between 17.6 and 22.0 percent. Elastic shortening was the most significant component of the measured prestress loss. However, the creep and shrinkage component was nearly as large, as noted from Table 5.4.

The time-dependent creep and shrinkage component increased slightly, while the instantaneous loss from elastic shortening remained constant. The average prestress loss due to elastic shortening was 16.1 ksi, while the creep and shrinkage component was 13.1 ksi.

Three San Angelo eastbound HPC beams were successfully measured for long-term prestress loss. The average total loss was 56.6 ksi. The values ranged between 54.8 ksi and 60.4 ksi. In terms of percentage of the jacking force, the average prestress loss was 28.0 percent. These values ranged between 27.1 and 29.8 percent. Elastic shortening and creep and shrinkage were the most significant components of the total prestress loss, similar to the Louetta HPC beams. However, the elastic shortening term was smaller than the creep and shrinkage term in two of the beams. The average values for elastic shortening and creep and shrinkage were 22.4 and 22.6 ksi, respectively.

The average total loss of the four San Angelo westbound non-HPC beams that were successfully measured for long-term prestress loss was 34.0 ksi. These beams had a high value of 35.3 ksi and a low value of 31.7 ksi. The average loss, in terms of percentage of the jacking force, was 16.8 percent. The high and low percentages were 17.4 and 15.6, respectively. As with most of the beams measured, elastic shortening was the largest component of the measured prestress loss.

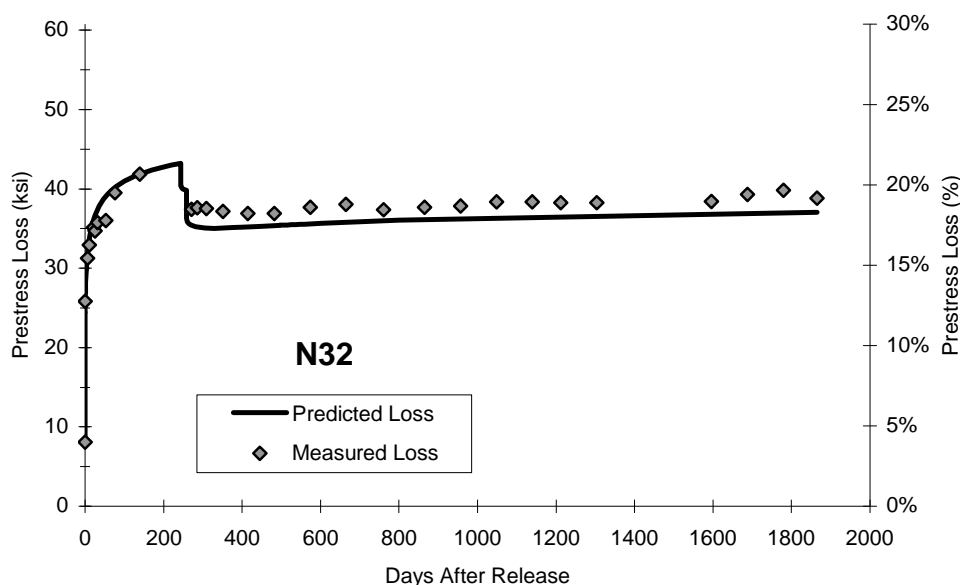


Figure 5.3: Measured Prestress Loss—Typical Case (Beam N32)

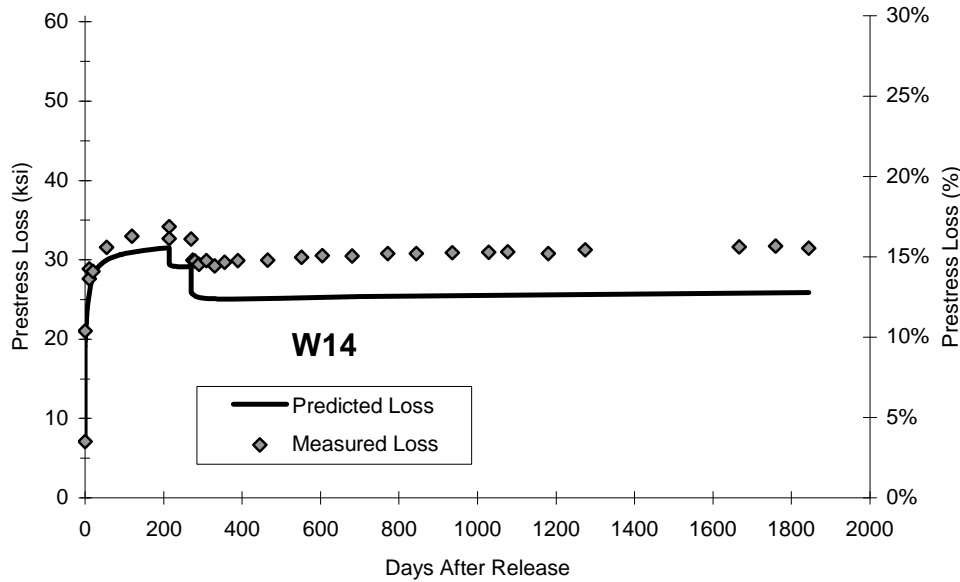


Figure 5.4: Measured Prestress Loss—Worst Case (Beam W14)

5.4 Camber

The graphical results of the camber and deflection measurements are found in Appendix A. The beam identification number is written above the key. The measurements were graphed as a function of upward camber versus the number of days after release. The plots also include the predicted camber calculated by the time-dependent model. Only the most recent data point was determined during the current phase of the project. The other data points were measured during earlier work on the HPC bridges [5, 10]. These data points were corrected using the methods described in Section 4.4.2.

A typical plot of the measured camber is shown in Figure 5.5. The measurements generally show good correlation with the camber predicted by the time-dependent model. Figure 5.6 shows the worst-case scenario, in terms of measured camber compared to the time-dependent model prediction.

Camber and deflection was measured in fourteen Louetta HPC beams, twenty San Angelo eastbound HPC beams, and seven San Angelo westbound non-HPC beams. Table 5.5 shows the results of the Louetta camber measurements and Table 5.6 shows the results of the San Angelo camber measurements. The final corrected measured camber is shown, along with the field measurement and the corrections applied to the field measurement. The correction factors were subtracted from the field measurement to determine the corrected measured camber. These corrections were discussed in Section 4.4.2. Note that an offset correction was not determined for every San Angelo beam.

Table 5.5: Louetta Camber Measurements

Beam	Camber (in.)			Final Corrected Measured Camber	Measured Camber After Deck Placement ¹
	Field Meas.	Offset Corr.	Thermal Corr.		
Louetta Northbound HPC Beams					
N21	2.61	-0.31	0.21	2.71	3.12
N22	0.45	-0.13	0.23	0.34	0.72
N23	0.29	-0.13	0.23	0.19	0.57
N31	2.13	-0.25	0.18	2.19	3.19
N32	1.22	-0.17	0.18	1.20	1.59
N33	0.97	-0.17	0.18	0.96	1.38
N34	1.53	-0.17	0.18	1.51	N/A
N35	1.08	-0.22	0.18	1.13	N/A
Louetta Southbound HPC Beams					
S14	1.56	-0.03	0.16	1.43	1.69
S15	1.52	-0.02	0.16	1.38	1.67
S16	1.93	-0.04	0.15	1.82	2.26
S24	-0.29	-0.13	0.18	-0.35	0.23
S25	-0.30	-0.12	0.18	-0.36	0.22
S26	1.72	-0.30	0.18	1.84	2.56
¹ Corrected measured camber after placement of precast panels and cast-in-place deck. [12]					

Table 5.6: San Angelo Camber Measurements

Beam	Camber (in.)			Final Corrected Measured Camber	Measured Camber After Deck Placement ²
	Field Meas.	Offset Corr. ¹	Thermal Corr.		
San Angelo Eastbound HPC Beams					
E11	-0.34	-2.73	0.35	2.04	N/A
E12	-0.49	-2.11	0.36	1.26	N/A
E13	-0.04	-2.24	0.36	1.84	2.95
E14	-0.55	-3.00	0.35	2.10	3.44
E21	1.76	N/A	0.57	1.19	N/A
E22	1.99	N/A	0.57	1.42	N/A
E23	2.24	N/A	0.57	1.67	N/A
E24	1.97	-0.35	0.57	1.75	2.67
E25	1.70	-0.01	0.57	1.14	2.14
E26	1.32	0.28	0.57	0.47	1.80
E31	1.37	N/A	0.34	1.03	N/A
E32	1.76	N/A	0.35	1.41	N/A
E33	1.84	-0.27	0.35	1.76	2.28
E34	1.81	0.19	0.35	1.27	1.78
E35	1.23	-1.19	0.34	2.08	2.90
E41	1.26	N/A	0.33	0.93	N/A
E42	1.66	N/A	0.34	1.32	N/A
E43	1.80	N/A	0.34	1.46	N/A
E44	1.66	-1.18	0.34	2.50	2.22
E45	1.21	-0.74	0.33	1.62	1.76
San Angelo Westbound Non-HPC Beams					
W11	-1.39	0.04	0.32	-1.75	N/A
W12	-1.49	-0.54	0.32	-1.27	N/A
W13	-1.55	0.12	0.32	-1.99	N/A
W14	-1.64	-0.36	0.32	-1.60	1.03
W15	-1.53	-0.28	0.32	-1.57	0.95
W16	-1.84	-0.42	0.32	-1.74	0.86
W17	-2.22	0.04	0.32	-2.58	0.77
¹ Deck offset corrections were not determined for all beams					
² Corrected measured camber after placement of precast panels and cast-in-place deck [12]					

The following trends were observed for all camber measurements, including those where the offset correction was not available. In general, there was agreement between camber measurements in each span of all of the bridges. Nearly all of the HPC beams exhibit the desired slight upward camber. The deck offset correction typically increased the measured camber. Therefore, it could be assumed that a beam, which clearly shows an upward camber before the offset correction was applied, would maintain an upward camber after the correction was made. Only two Louetta southbound beams show a slight downward deflection. All of the San Angelo westbound non-HPC beams displayed a downward deflection.

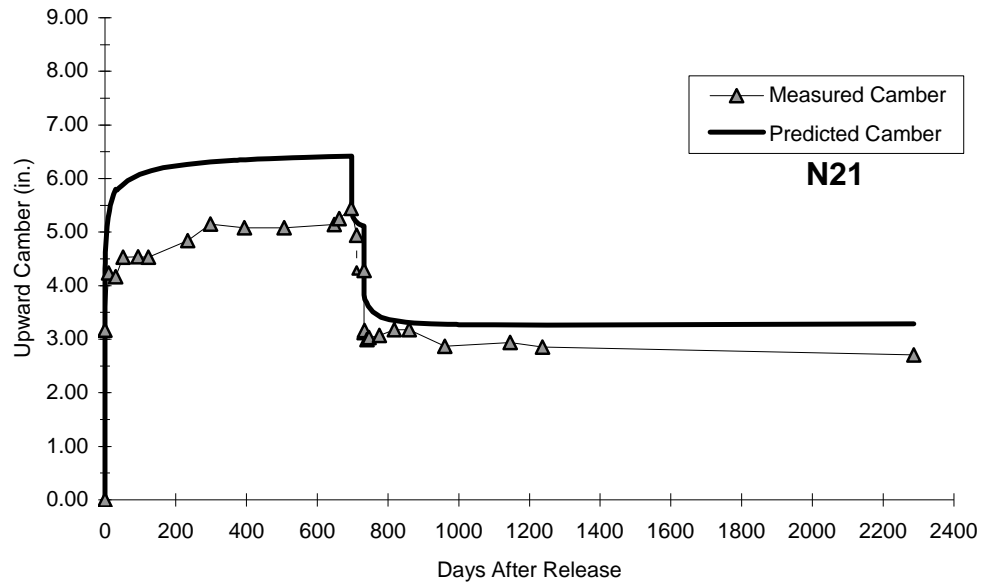


Figure 5.5: Measured Camber and Deflection—Typical Case (Beam N21)

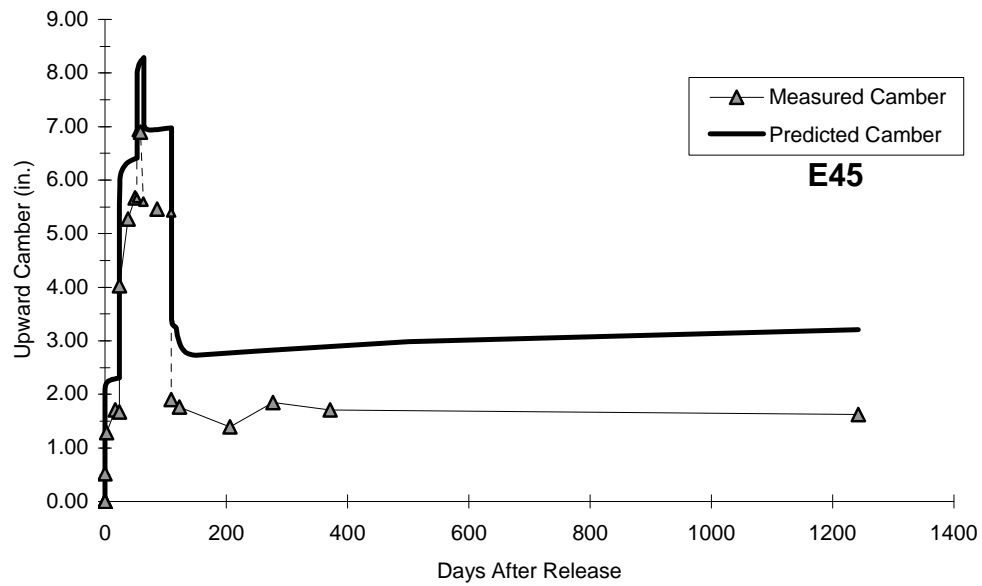


Figure 5.6: Measured Camber and Deflection—Worst Case (Beam E45)

Chapter 6. Discussion of Test Results and Field Inspections

6.1 Introduction

This chapter discusses the results of structural performance evaluations on the Louetta and San Angelo HPC structures that were presented in the previous chapter. The measured values for identical or similar beams are compared. The measured prestress loss is compared to the actual design predictions, as well as the predictions from the AASHTO and PCI methods. Prestress loss measurements are compared to the method suggested by Gross and Burns [10]. Measured camber is discussed and values for similar beams are compared. Finally, measured camber is compared to values predicted by the time-step model and the actual design.

6.2 Prestress Loss

Prestress loss was determined using several different methods, which were discussed in Section 2.4. Some methods utilized design parameters, while others used measured values. Design parameters were calculated from commonly used equations. Measured values were determined from tests performed on the actual mix design used in the HPC beams. The differences between the design and measured parameters are summarized in Table 6.1. Note that different design equations were used to predict the modulus of elasticity for non-HPC and HPC. These equations are shown here:

$$E_c = w_c^{1.5} 33 \sqrt{f'_c} \quad 6.1$$

where E_c = modulus of elasticity for concrete (psi)
 w_c = unit weight of concrete (90 to 155 pcf)
 f'_c = compressive strength of concrete (psi)

$$E_c = 40,000 \sqrt{f'_c} + 1,000,000 \quad 6.2$$

Equation 6.1 is suggested by both AASHTO [2] and ACI [4]. ACI points out the modulus of concrete is sensitive to the modulus of the aggregate. Therefore, measured values typically vary between 80 and 120 percent of results predicted by Equation 6.1. Carrasquillo, Nilson, and Slate [7] observed that Equation 6.1 overestimated the modulus of elasticity for high strength concrete. They proposed Equation 6.2, where E_c and f'_c are in psi.

Table 6.1: Comparison of Design versus Measured Parameters [10]

Parameters	Design Parameters	Measured Parameters
Section Properties	Gross section properties	Transformed section properties
Concrete Unit Weights & Dead Loads	Based on assumed deck dimensions and 150 pcf for all concrete.	Based on measured deck thickness and measured unit weights, with approximate weight of steel included for beams.
Concrete Strength	Nominal design concrete strength	Based on tests of companion specimens.
Modulus of Elasticity	Eq. 6.1 (non-HPC) or Eq.6.2 (HPC), using nominal design strengths.	Based on tests of companion specimens.

In general, for all of the beams in which long-term prestress loss measurements were made, the total prestress loss increased slightly. This increase was continued over a succession of measurements and was attributed to time-dependent sources of prestress loss. These sources were described in Section 2.3 and included creep, shrinkage, and relaxation.

Unfortunately, only the San Angelo bridges allow for a comparison between similar beams in the same span. There are two Louetta southbound span one beams with measured prestress loss. The number of days after release for the two beams varies by more than a year. It could be argued that this difference in age should no longer be significant, due to the expected flattening of the prestress loss curve. However, one beam is a U54A beam while the other is a U54B, making comparisons less significant.

San Angelo HPC beams E24 and E25 were both measured for long-term prestress loss. Although these beams vary in age by close to one year, that fact should be insignificant as discussed earlier. The beams have nearly identical measured prestress loss. The measured values differ by just 0.02 ksi. Beam E24 contains four additional pretensioned strands and six additional post-tensioned strands when compared to Beam E25.

All four of the San Angelo westbound beams that were instrumented for prestress loss measurements are successfully monitored for long-term prestress loss. These beams are identical except for the spacing of the exterior beam, W17. These beams have similar measured long-term prestress loss, especially the three interior beams.

Table 6.2 summarizes the prestress loss as determined using the previously discussed methods. These predictions were calculated using data current as of March of 2001. It should be pointed out that several of the methods listed are general long-term predictions and do not vary with time. Long-term prestress loss has been successfully measured on eleven beams. Four Louetta HPC U-beams, three San Angelo eastbound HPC I-beams, and four San Angelo westbound non-HPC I-beams are shown in Table 6.2. The first column of data lists the prestress loss as determined from strain measurements discussed in Section 4.3. The average prestress loss for each set of beams is given. Note that the methods vary in how they determine pre-release losses. The prediction methods suggested by AASHTO and PCI do not include all pre-release losses. Therefore, the values predicted by these methods should theoretically be less than the other methods. These methods were described in Section 2.4.

These methods produced a wide spectrum of results. Some methods were quite accurate compared to the measured prestress loss, while others were not. In general, most methods predicted the greatest prestress loss in the San Angelo eastbound HPC beams, followed by the Louetta HPC beams and then the San Angelo westbound non-HPC beams. This trend was in agreement with the measured results. The two components methods developed by AASHTO and PCI were used to predict long-term prestress loss using both design and measured parameters. As expected, the components methods produced estimates closer to the measured prestress loss when using measured parameters.

In general, the long-term prestress losses predicted by the incremental time-step analysis were in agreement with the measured value. The results were expected to be accurate, because they incorporated detailed information such as measured properties and construction schedules. The values predicted using this method was all within 10 percent of the measured prestress loss.

Table 6.2: Comparison of Total Prestress Losses

Beam	Total Prestress Losses (ksi)								
	Measured ¹	Incremental Time-Step (Measured Parameters) ¹	Actual Beam Designs (PSTRS14 or ADAPT-ABI) ¹	AASHTO LRFD Time- Dependent Lump-Sum (Design Parameters) ²	AASHTO LRFD Components (Design Parameters) ²	AASHTO LRFD Components (Design Parameters) ²	PCI Design Handbook Components (Design Parameters)	PCI Design Handbook Components (Measured Parameters)	Suggested Method (Measured Parameters) ¹
Louetta HPC Beams									
N32	44.56	43.40	57.79	38.72	67.05	57.71	50.57	38.79	40.02
S15	39.60	45.53	57.79	40.65	72.53	61.25	55.99	40.85	41.60
S16	42.90	47.03	52.99	38.29	69.92	59.88	55.78	41.64	41.65
S25	35.54	41.64	52.99	36.68	62.12	52.46	46.27	34.27	36.83
Avg.	40.65	44.40	55.39	38.59	67.91	57.83	52.15	38.89	40.03
San Angelo Eastbound HPC Beams									
E14	60.35	57.51	47.45	57.21	104.46	89.40	84.84	65.40	56.27
E24	54.78	56.94	52.16	56.43	103.96	89.09	83.02	65.16	55.67
E25	54.80	51.25	41.69	51.50	89.31	77.32	70.00	55.23	49.63
Avg.	56.64	55.23	47.10	55.05	99.24	85.27	79.29	61.93	53.86
San Angelo Westbound Non-HPC Beams									
W14	35.32	30.99	47.91	41.02	51.91	45.54	39.18	31.76	28.68
W15	35.09	30.99	47.91	41.02	51.91	45.54	39.18	31.76	28.68
W16	33.86	30.99	47.91	41.02	51.91	45.54	39.18	31.76	28.68
W17	31.67	30.87	47.91	41.02	51.71	43.98	38.87	29.55	28.15
Avg.	33.99	30.96	47.91	41.02	51.86	45.15	39.10	31.21	28.55
¹ Includes pre-release losses.									
² Includes pre-release relaxation losses only									

The values predicted by the programs used in the actual beam design were not as accurate. PSTRS14 [20], used in the Louetta HPC and San Angelo westbound non-HPC beam designs, overestimated the long-term prestress loss by a significant amount. The long-term prestress loss for the San Angelo eastbound HPC beams was significantly underestimated by ADAPT-ABI [1].

Surprisingly, the AASHTO LRFD Time-Dependent Lump Sum method was in agreement with the measured prestress loss values [10]. Its predictions were actually closer for the HPC beams than the non-HPC beams. The average predicted prestress loss was 95 and 97 percent of the average measured values for the Louetta HPC and San Angelo eastbound HPC beams, respectively. The San Angelo westbound non-HPC beams prestress losses were overestimated. The average predicted value was 121 percent of the measured value. However, this method tended to overestimate the elastic shortening component, while underestimating the time-dependent component for the HPC beams. Therefore, this method cannot be recommended for use with HPC beams.

The results of the AASHTO LRFD Time-Dependent Lump Sum method were even more surprising in light of the results produced by the AASHTO LRFD components method. The

components method was intended to be more accurate than the time-dependent lump sum method. However, the component method was not nearly as accurate. In fact, the AASHTO LRFD components method was the least accurate method investigated in the research project. Using design parameters, the predicted long-term prestress loss was nearly twice as large as the measured values in some instances. The average predicted long-term prestress loss using the AASHTO LRFD components method and design parameters was 167, 175, and 153 percent of the measured values for the Louetta HPC beams, San Angelo eastbound HPC beams, and San Angelo westbound non-HPC beams, respectively. This can be explained by the fact that creep and shrinkage of HPC are not appropriately modeled using conventional design equations. Farrington et al. [8] showed the HPC used in this project exhibits less creep and shrinkage than predicted by conventional methods. Also, Gross and Burns [10] showed Equations **Error! eference source not found.** and 6.22 underestimate the modulus of elasticity by as much as 25 percent. This causes an overestimation of the prestress loss owing to elastic shortening. Even using measured parameters, this method greatly overestimated the measured prestress loss. In the same order as established, these values were 142, 151, and 115 percent.

In general, the *PCI Design Handbook* components method produced more accurate results than the AASHTO LRFD components method. Similar to the AASHTO LRFD components method, the predictions using design parameters greatly overestimated the prestress loss. This overestimation is caused by the same reasons discussed in the previous paragraph. These values were 142, 151, and 133 percent of the measured prestress losses for the Louetta HPC beams, San Angelo eastbound HPC beams, and San Angelo westbound non-HPC beams, respectively. The *PCI Design Handbook* Components method using measured parameters produced values that were generally in agreement with the measured prestress loss. In fact, this method was nearly as accurate as the values predicted by the time-step analysis and the suggested method. The values predicted using measured parameters were 96, 109, and 92 percent of the measured prestress loss. However, this method does not include pre-release methods, thus effectively lowering its predicted prestress loss.

Gross and Burns [10] proposed a suggested components method similar to the components methods presented by AASHTO and PCI. The refinements made to this method, in addition to the use of measured parameters, make it very accurate. The use of components makes computations simpler than a time-step analysis. However, determining measured parameters make it more difficult compared to the conventional components methods.

Clearly, using measured parameters allows for a more accurate prediction of prestress losses. However, determining these parameters is more time and labor intensive than using the common design parameters. Unfortunately, current design equations do not adequately estimate the material properties of HPC such as the modulus of elasticity, creep, and shrinkage. Until a larger volume of information on HPC can be gathered, new empirical formulas that will better predict HPC behavior cannot be developed. Until this time, all future HPC bridges should be measured for material properties. This is especially true for new HPC mix designs.

6.3 Camber

Table 6.3 shows the measured camber results of the twenty-six instrumented beams. The measured camber is listed next to the camber predicted by the time-step analysis and the camber determined during the actual design. The design camber was calculated using one of the previously discussed programs. PSTRS14 [20] was used to determine the camber of the Louetta

HPC beams and the San Angelo westbound non-HPC beams. ADAPT-ABI [1] was used to determine camber in the San Angelo eastbound HPC beams.

Plots for the instrumented beams showing the measured camber and the time-step predicted camber are found in Appendix A. These plots reveal camber is expected to remain very stable at this point in the bridge's life. The measured camber values confirm this expectation. In general, camber measurements have remained relatively stable. Approximately three years had passed between the most recent and previous camber measurements. Despite this large change in time, most of the recent measurements are within 0.5 in. of the previous measurements. There is good agreement among measurements taken in the same span of each bridge. Most measurements in a single span remained relatively stable. If any variation between the last two readings was evident, a slight decrease in camber was observed. More long-term camber measurements would need to be taken to determine if this downward trend continued or if it was just an anomaly.

All but two of the Louetta HPC beams display the desired upward camber. The measured camber in the Louetta beams ranged from -0.36 to 2.71 in. The average measured camber is 1.11 in. In general, there was agreement between similar beams in the same span. The camber of beams N22 and N23 (both U54A beams) was very close. Beam N21 has a much larger camber, but it is a U54B beam with nineteen more pretensioned strands. Therefore, a larger camber was expected. This same trend was seen in the three beams of Louetta northbound span 3. The two U54A beams exhibit similar camber, while the U54B beam has a significantly larger camber.

Table 6.3: Long-Term Camber

Beam	Days After		Long-Term Service Camber (in.)		
	Release	CIP Deck	Measured	Predicted ¹	Actual Design ²
<i>Louetta HPC Beams</i>					
N21	2224	1491	2.71	3.29	5.05
N22	2252	1491	0.34	0.44	2.97
N23	2259	1491	0.19	-0.31	2.97
N31	2224	1491	2.19	3.33	4.54
N32	1749	1491	1.20	0.99	3.99
N33	1749	1491	0.96	0.94	3.99
S14	1738	1483	1.43	1.80	3.99
S15	1738	1483	1.38	1.60	3.99
S16	2252	1483	1.82	2.39	2.97
S24	2211	1483	-0.35	0.19	2.97
S25	2211	1483	-0.36	-0.09	2.97
S26	2239	1483	1.84	2.18	5.05
<i>San Angelo Eastbound HPC Beams</i>					
E13	1295	1183	1.84	2.90	0.43
E14	1295	1183	2.10	3.48	0.43
E24	1277	1170	1.75	2.38	-0.90
E25	1619	1170	1.14	0.58	-1.86
E26	1277	1170	0.47	1.69	-0.90
E33	1263	1156	1.76	2.69	-0.22
E34	1263	1156	1.27	2.69	-0.22
E35	1256	1156	2.08	2.82	-0.22
E44	1242	1132	2.50	2.70	-0.09
E45	1242	1132	1.62	3.21	-0.09
<i>San Angelo Westbound Non-HPC Beams</i>					
W14	1644	1374	-1.60	-1.49	1.15
W15	1644	1374	-1.57	-1.49	1.15
W16	1644	1374	-1.74	-1.49	1.15
W17	1639	1374	-2.58	-1.97	1.15
¹ Using incremental time-step analysis					
² Using PSTRS14 or ADAPT					

The three beams in southbound span one all have similar camber. Despite the fact that two of the beams are type U54A, while the other is type U54B, the number of strands is very similar. This explains why the camber is similar even though the beam types are different. The two beams with downward deflection are found in southbound span two. All of these beams are type U54B, but beam S26 (which has an upward camber) has 87 strands versus the 68 in the other two beams (which have a downward deflection). These are the longest instrumented beams measured for camber. An investigation of the mechanics equations used to determine camber reveals they are sensitive to beam length. Therefore, it becomes increasingly difficult to design for the desired upward camber as beam length increases. This difficulty in design is a likely

reason these beams have a downward deflection. It should be noted that the downward deflection is very small for both beam S24 and S25 at -0.35 and -0.36 in., respectively.

All of the San Angelo eastbound HPC beams exhibit the desired slight upward camber. The measured camber varied between 0.47 and 2.50 in. with an average of 1.65 in. There is reasonable agreement between beams in a single span. The beams in eastbound spans one, three, and four are identical and their measured camber were all within one inch of each other. The largest variation between beams in a similar span occurred in eastbound span two. Beam E26 exhibits the smallest upward camber of any eastbound beam. Beam E26 contains more pre and post-tensioned steel than beams E23 and E24. It is believed the measured value is an anomaly, because the time-step predicted camber is significantly higher for this beam. Further camber measurements need to be taken to confirm this belief.

All of the San Angelo westbound non-HPC beams exhibit a significant downward deflection. The measured deflection varies between -1.57 and -2.58 in. with an average of -1.87 in. There is reasonable agreement between the beams in this single span. This downward deflection has been attributed to the fact that these non-HPC beams in actuality possess similar material properties to the HPC beams [10]. These beams used a lower prestress force and therefore a downward deflection occurred.

Table 6.4 compares the measured camber to the other methods. The average, minimum, and maximum camber is presented for each bridge. The measured values are then compared to the values predicted by the time-step model and the actual design. The differences between the measured camber and the two predicted values were calculated. The average of the absolute value of these differences, as well as the maximum positive and negative values, are presented.

In general, all of the measured camber values are less than values predicted by the time-step analysis and the actual design, as shown in Table 6.4. The time-step analysis was closer to the measured values than the actual design values. The average time-step predicted value was within one inch of the measured value. This was a reasonable difference given the uncertainties involved in determining long-term camber. It is difficult to calculate long-term camber in any beam, especially one with the very long spans of these bridges. This calculation is further complicated due to the uncertainties involved with the material properties of HPC. On average, none of the design predictions was within two inches of the measured camber. Surprisingly, the values for the San Angelo westbound non-HPC beams were the least accurate compared to the measured camber. Although the San Angelo westbound beams are considered non-HPC, they do possess some properties that are similar to the HPC beams. For example, the compressive strength of the beams (8,920 psi) is considered HPC by some definitions. This could explain part of the over-prediction.

Table 6.4: Analysis of Long-Term Camber

	Long-Term Service Camber (in.)		
	Louetta HPC	SA EB HPC	SA WB Non-HPC
Measured Camber			
Average	1.11	1.65	-1.87
Minimum	-0.36	0.47	-2.58
Maximum	2.71	2.50	-1.57
Difference (Measured - Predicted)			
Avg. Absolute Difference ¹	0.41	0.97	0.26
Max. Negative Difference	-1.14	-1.59	-0.61
Max. Positive Difference	0.50	0.56	-0.08
Difference (Measured - Actual Design)			
Avg. Absolute Difference ¹	2.68	2.02	3.02
Max. Negative Difference	-3.33	1.37	-3.73
Max. Positive Difference	-1.15	3.00	-2.72
¹ Average of the absolute values of the differences.			

6.4 Findings in the Field Performance of HPC Decks

When it became clear that most of the early age structural events for the beams had already happened and that, barring accidents or natural disasters, no new changes would be likely for the next several years, the researchers were asked to change focus from beams and automated data acquisition to distress and performance on new HPC bridge decks. These new decks fell into the HPC category because, during the time of cement shortages, contractors wanted to take advantage of lower concrete costs associated with the use of less expensive supplemental cementitious materials (SCMs). SCMs such as fly ash and ground glass blast-furnace slag are typically substituted for 20 to 35 percent of the portland cement in the batch designs for decks. TxDOT was willing to allow this because these SCMs were known to add performance benefits to the concrete in addition to the economic considerations. These benefits include reduced permeability, lower maximum curing temperatures due to heat of hydration, slower modulus development, mitigation for internal expansion mechanisms like ASR and DEF, and less drying shrinkage.

TxDOT asked the research team to monitor the field performance of several new HPC bridge decks found in Amarillo and Lubbock in addition to the Houston Louetta and San Angelo Concho River Bridge decks. Figures in Appendix B show the locations of each bridge deck on maps of the two regions.

This sudden strong interest was based upon earlier observations, concerns, and discussions in Houston, where it became apparent on the first inspection visits that two patterns of early cracking were in evidence on both the decks. While anyone associated with large exterior concrete flatwork surfaces in Texas has become accustomed to some cracking in the surface, TxDOT and FHWA were not prepared for such extensive cracking to show up at such early ages.

Extensive cracking is a concern because cracks provide a direct conduit for oxygen, water and deicing salts (used to keep the wet sand piles in the maintenance yards from freezing hard) to corrode the steel reinforcement in the deck, resulting in surface spalling, delaminations, rougher ride quality, and punch-outs.

The irony in this cracking problem for the new decks is that TxDOT Bridge Division and the Districts tried to ensure a nominal two inches of concrete cover, and they worked very diligently to reduce the permeability of the mixture designs for the decks, so that deck deterioration due to corrosion of the reinforcement would be mitigated. The cracks in a cold, contracted slab can allow many times the water-borne chlorides to the steel than the permeable capillaries and pore structure in the sound concrete next to them. It is likely that efforts to reduce the permeability of the deck mixes may have backfired, resulting in a denser, more brittle deck that was likely to crack more extensively.

In addition to high strength concrete, additional blame could be attributed to the use of the precast panel stay in place forms. The sharp transitions between the deep cast-in-place regions that exists at the beam ends and directly above the beams and the shallow cast-in-place concrete on top of the panes give a location for shrinkage prone concrete to crack. Such rapid transitions often result in stress risers at the transition. This is evidenced by the fine cracks found above and progressing to the edges of some of the panels. The cracks can most easily be seen in the mornings whenever the moisture on the wetted deck evaporates more slowly out of the cracks than from the uncracked surface.

The second item relates to the intersection of cracks at every panel corner. Each longitudinal panel edge produces a crack that intersects with the transverse edges at the panel corner. These corner cracks are typically initiation sites for early spalling. The corner cracking is most apparent as wider stair-step cracks over skewed bents. It is at these corners that mid-span flexural deflections in the underlying beams and in the panels allow panel ends (longest corner projection) over the bent cap and opposite side of the bearing pad to strain upward from resulting lever actions.

A third item relating to cracking is associated with construction technology versus materials constraints, and it involves the forming of reduced sections to force cracking to occur as an oriented joint over the edges of skewed bent caps. This practice normally involves placing 1-inch deep zip strips into the surface of the fresh concrete over the edges of the bent caps. The concept can work, but the skewed bents seem to present alignment problems for construction teams on top of the deck, and timing of the joint forming is critical. For these reasons the first sign of either of these problems is often obvious surface cracking that is clearly not in alignment with the contractors' formed or sawed joints.

Chapter 7. Summary, Conclusions, and Recommendations

7.1 Summary

The long-term structural behavior of two high performance concrete bridges in Texas and the long-term performance with regard to distress in eight HPC bridge decks has been monitored in this study. Twelve Texas U54 beams in the Louetta Road Overpass in Houston, TX had been instrumented for strain and temperature readings. The U-beams varied in length from 117.9 to 136.4 ft and utilized 0.6 in. diameter low relaxation prestressing strands. All of the U-beams were made from high performance concrete. Fourteen AASHTO Type IV beams in the North Concho River/US 87/South Orient Railroad Overpass in San Angelo, TX had been instrumented for strain and temperature readings. Ten of these beams were high performance concrete, while four were considered non-HPC. These HPC beams varied in length from 129.0 to 153.3 ft, while the non-HPC beams were all 129.0 ft. The HPC beams utilized 0.6 in. diameter strands in a two stage tensioning process, involving both pretension and post-tension. The non-HPC beam utilized 0.5 in. diameter strands. Only pretension was applied to the non-HPC beams.

The original data acquisition system was updated to allow for remote monitoring of the bridges. The data gathered from the instrumentation was used to make field measurements of prestress loss and camber. The measured prestress losses were compared to values predicted by other methods. The methods included a time-step model, common methods suggested by AASHTO and PCI, as well as a suggested method for HPC beams. The measured prestress losses were also compared to values calculated during the actual beam design. The measured camber values were compared to values predicted by the time-step model and calculated during the actual beam design.

Limited durability testing was performed. The durability performance of these bridges was not the focus of this paper. The results of the durability testing are presented, but are not discussed in detail.

Field inspection monitoring of distress symptoms in bridge decks for several years has clearly shown that current bridge construction technology using stay-in-place precast concrete panels mounted on top of the beam edges and spanning the gap between the beams frequently resulted in repeating cracking patterns in the 4-inch-thick cast-in-place portion of the deck above and around panels. These cracks are typically quite tight for the first few years, but soon areas where longitudinal cracks intersect with transverse cracks (areas of the cast-in-place concrete over the corners of the precast panels) begin to spall. In cold weather the spalls retain non-compressible sand or debris to cause further spalling when warmer weather expands the concrete. The spalls also retain surface water for later damage due to freezing and thawing, and they serve as reservoirs to feed saltwater (from deicing salts or marine exposure) through the cracks to the steel reinforcement for eventual corrosion.

The dilemma at issue is that the precast panels are a way to economically construct bridge decks. The panels are faster and safer. If the service life is significantly shortened, however, due to the earlier presence of deep cracks, then the service life costs of the bridge deck are probably higher than with the older method using permanent metal deck forms and full depth cast-in-place concrete placements.

7.2 Conclusions

7.2.1 The following observations have been made with regards to long-term prestress loss in HPC beams:

1. The average measured prestress loss, taken after several years of bridge service, was 40.7, 56.6, and 34.0 ksi for the Louetta HPC beams, San Angelo eastbound HPC beams, and San Angelo westbound non-HPC beams, respectively. In terms of percentage of the jacking force, these values were 20.1, 28.0, and 16.8 percent, respectively.
2. The measured prestress loss values, taken several years after construction of the bridges was complete, remain stable for beams in a single span.
3. Predicted prestress loss calculated during the actual beam design generally does not agree well with the measured values. PSTRS14, used in the Louetta HPC and San Angelo Westbound Non-HPC Beam design, predicted prestress losses higher than the measured values. ADAPT-ABI, used in the design of San Angelo Eastbound HPC Beams, predicted prestress losses lower than the measured values.
4. The time-step model did a good job of predicting prestress loss. However, this model is based on information specific to the beams in this study and cannot be applied to other beams.
5. Prediction methods suggested by AASHTO and PCI significantly overestimated the prestress loss. The methods cannot be recommended for use with HPC beams. Using measured parameters versus design parameters, significantly improved the accuracy of these methods.
6. The method suggested by Gross and Burns [10] did a very good job of predicting prestress loss. This method requires measured parameters and is the method recommended by this report until further information can be gathered on HPC beams.

7.2.2 The following observations have been made with regards to long-term camber and deflection of HPC beams:

1. The average measured upward camber, taken after several years of bridge service, was 1.11, 1.65, and -1.87 in. for the Louetta HPC beams, San Angelo eastbound HPC beams, and San Angelo westbound non-HPC beams, respectively.
2. In general, the measured camber values, taken several years after construction of the bridges was complete, remain stable for beams in a single span.
3. All but two of the HPC beams exhibit the desired upward camber. The downward camber is attributed to large beam lengths and a smaller than typical (compared to other HPC beams) prestressing force.
4. All of the non-HPC beams exhibit a downward deflection. This has been attributed to these beams possessing properties similar to HPC beams combined with a smaller than typical (compared to other HPC beams) prestressing force.

5. Measured camber values are generally less than values predicted by the time-step analysis. Average differences between measured and predicted camber values were 0.41, 0.97, and 0.26 in. for the Louetta HPC beams, San Angelo eastbound HPC beams, and San Angelo westbound non-HPC beams, respectively.
6. Measured camber values are much less than values predicted by the actual beam design. Average differences between measured and actual beam design camber values were 2.68, 2.02, and 3.02 in. for the Louetta HPC beams, San Angelo eastbound HPC beams, and San Angelo westbound non-HPC beams, respectively.
7. Long-term camber is extremely difficult to predict for HPC beams. Measured properties should be used whenever possible until a larger database of information on HPC can be collected.

7.3 Recommendations

7.3.1 HPC Bridge Elements

A. HPC Beams

1. Creep and shrinkage were less than ACI 209 methods predicted. Updated prediction methods now make adequate predictions for HPC, too.
2. Prestress losses—Measured parameters worked better than design parameters for predicting prestress losses. AASHTO and PCI prediction methods from the mid 1990s did not work well for predicting prestress losses in HPC beams. Use the new AASHTO methods that have been developed since then to better address HPC considerations.
3. Deflections and camber—The precise surveying system used to monitor changes in camber and deflections proved impractical and inaccurate. When the structure is new and static changes are larger, high-tech surveying or laser levels work well enough, but small changes later in the life of the structure are not easily or reliably monitored.

B. HPC Beam Fabrications and Performance

1. Use HPC mixtures with high-range water reducers and well-graded, high strength crushed aggregates to design for adequate flow through congested areas of draped tendons, as well as rapid strength and modulus development, resulting in faster prestress release times in the fabrication yard and lower creep and shrinkage in the cured beams.
2. Use supplemental cementitious materials (SCMs) to replace some of the portland cement in the mixtures. This keeps temperatures in the larger mass sections below 158 degrees F, thereby mitigating the likelihood of delayed ettringite formation. At the same time the strategic use of SCMs mitigates potential alkali silica reactions exacerbated by hot Texas weather.

C. HPC Decks

1. Monitoring confirmed previous observations that cracks reflected through the cast-in-place concrete wearing surface of the deck immediately above underlying precast panel corners and above the joints between the panels. Fine cracking in the deck surface distinctly outlined precast panels underneath.
2. Cracking patterns resembling stair steps occurred over every skewed bent that was monitored. This pattern resulted from the square corners of the precast panels ending over the top of the bent in a diagonal pattern. Mid-span deflections due to loads on the beam caused slight rotation of the panel ends resting above the beam edge.
3. Cracking typically occurred in the thinner CIP sections immediately adjacent to the thickened sections over the bent caps.
4. The patterns described were nonexistent in the thicker CIP HPC decks constructed with the stay-in-place metal pan forms (without precast panels).

D. Recommendations for deck construction using precast panels

1. When using precast panels, additional emphasis on proper concrete placing procedures and rapid placement of curing mats is essential.
2. Fill the joints between precast panels and at areas over the bent caps until flush with panel tops. After the filled portion cures and cools to ambient temperature, place joint tape or anti-fracture membrane over all joints, and place a well designed lower modulus CIP wearing surface. Or...
3. When using precast panels, be aware that cracking may be more pronounced than traditional full depth construction. Toward the end of the construction contract, inspect the deck for cracking and fill the cracks with a gravity feed epoxy.

7.3.2 Data Acquisition Systems for Monitoring Field Performance

1. Sensors—Vibrating wire strain gages (VWG) with their own temperature sensing were more consistent and more durable than resistance-type electrical strain gages and simple thermocouples for monitoring. VWGs are recommended for any in-place monitoring.
2. Data Loggers—Campbell Scientific CR10 data loggers served without problems, other than power sources and remote data transfer, but peripheral equipment for these units has improved greatly since the project began.
3. Power—12-volt DC powers the logger and is available from many sources. These are recommended.
 - a. Transformers that convert 120 volt AC or 240 volts AC to 12 volts DC are recommended for the power source to the DAS. Most 12-volt battery systems required too much effort in battery maintenance and replacement.

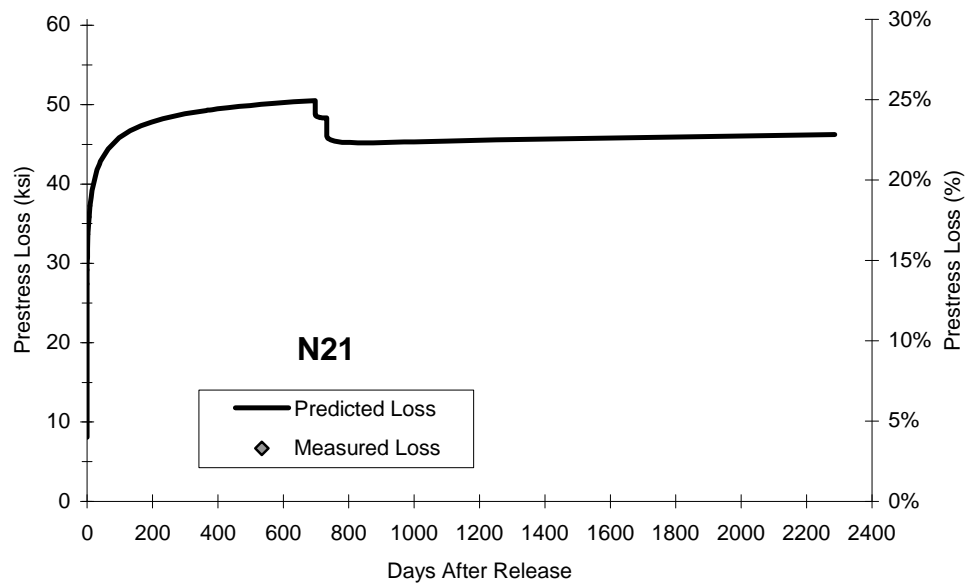
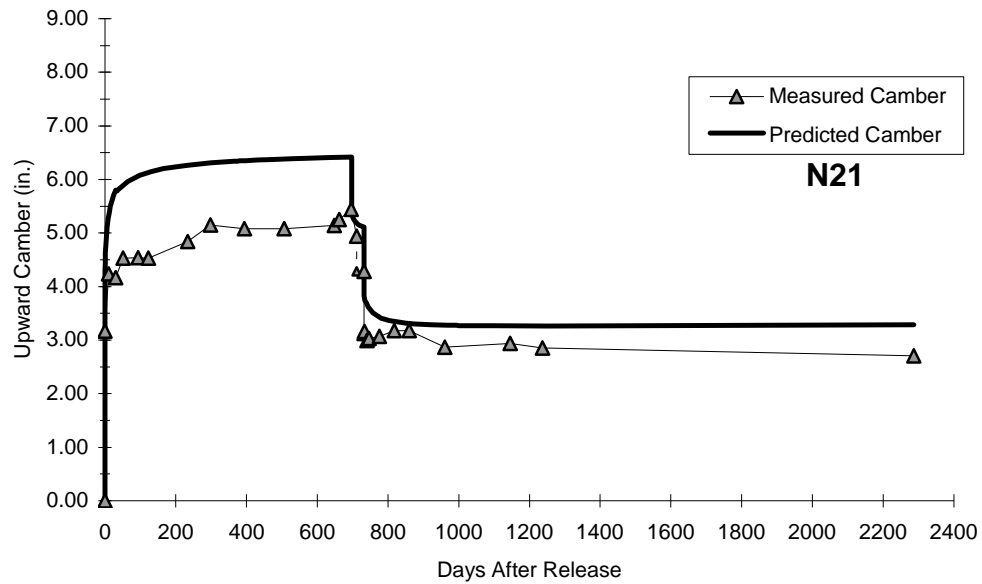
- b. Photo-voltaic (solar) cells to automatically maintain batteries' charges should be used where AC power is not easily available.
- 4. Data transfer—Two modes were used to transfer data from loggers to laptop computers for data reduction and analysis.
 - a. The most reliable was RS 232 port and cable connections to a laptop computer, but it required up to four trips per year to each bridge (depending on the number of data points collected each month).
 - b. New digital technology has produced reliable data modems that download data remotely to desktop computers.

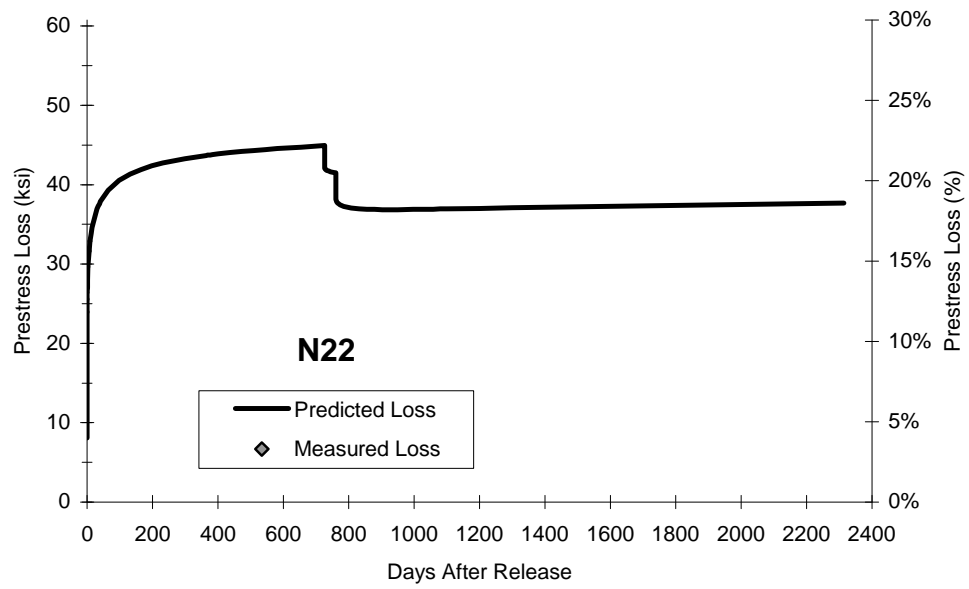
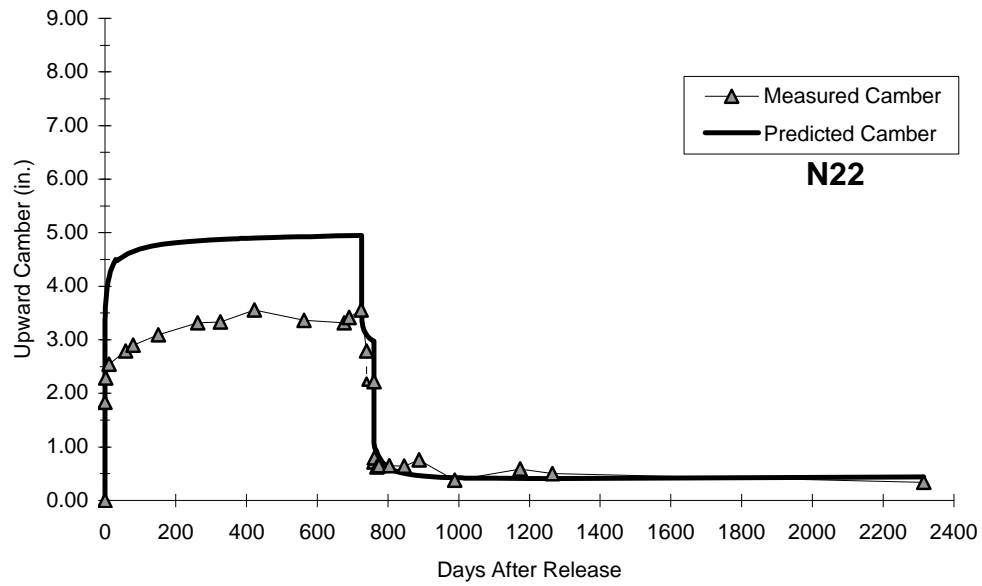
References

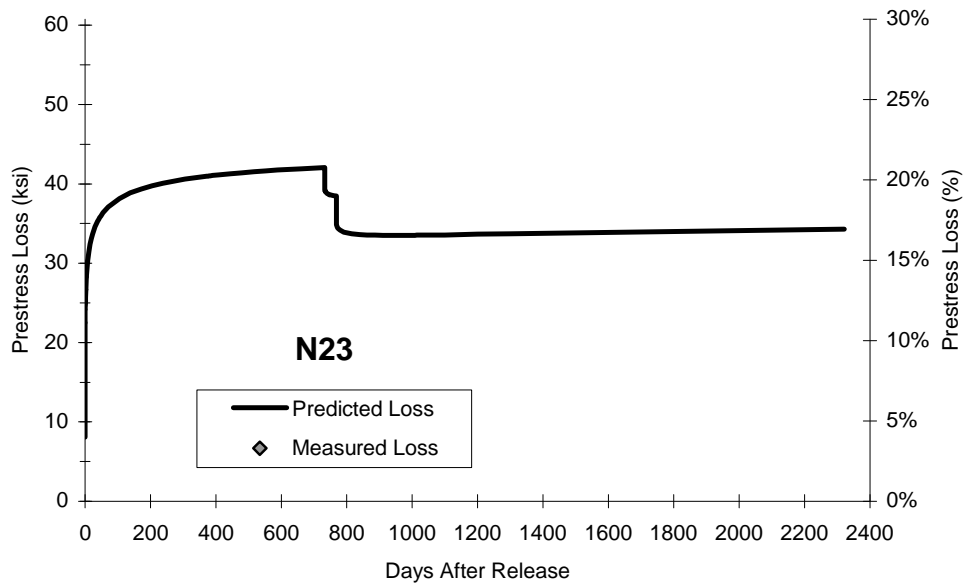
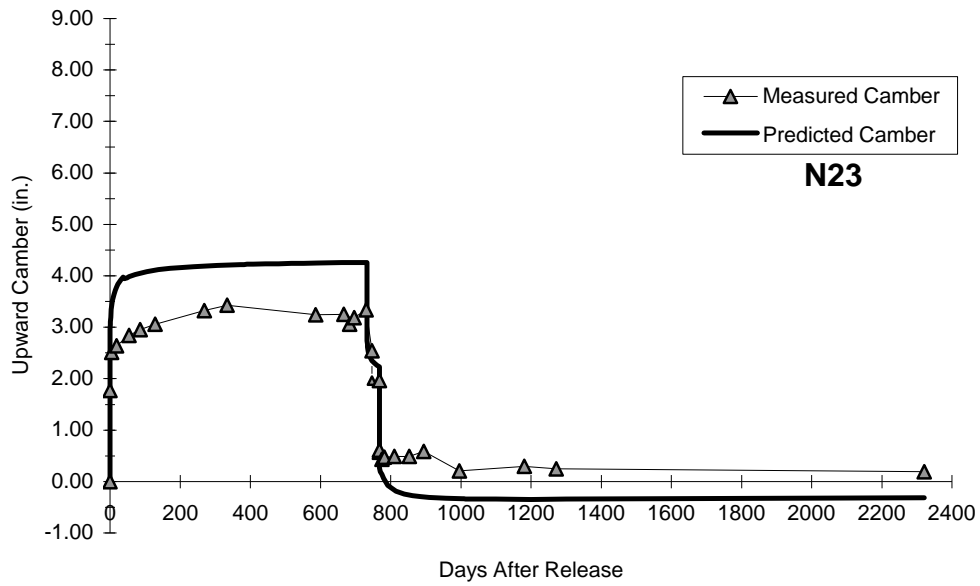
1. ADAPT Corporation, ADAPT-ABI, ADAPT-Bridge Incremental Structural Concrete Software System, Version 2.00, 1996.
2. American Association of State Highway and Transportation Officials, AASHTO LRFD Bridge Design Specifications, First Edition, Washington, D.C., 1994.
3. American Concrete Institute Committee 209, Prediction of Creep, Shrinkage, and Temperature Effects in Concrete Structures (ACI 209R-92), American Concrete Institute, Detroit, 1992.
4. American Concrete Institute Committee 318, Building Code Requirements for Structural Concrete (ACI 318-99) and Commentary (ACI 318R-99), American Concrete Institute, Detroit, 1999.
5. Byle, K. A., Burns, N. H. and Carrasquillo, R. L., Time-Dependent Deformation Behavior of Prestressed High Performance Concrete Bridge Beams, Research Report 580-6, Center for Transportation Research, The University of Texas at Austin, Austin, TX, 1997.
6. Campbell Scientific, Inc., PC208W, Software Package for Campbell Scientific Dataloggers, Version 3.01, 1992.
7. Carrasquillo, R. L., Nilson, A. H., and Slate, F. O., "Properties of High Strength Concrete Subject to Short-Term Loads," ACI Journal, May/June 1981, Vol. 78, No. 3, pp. 171-179.
8. Farrington, E. W., Burns, N. H., and Carrasquillo, R. L., Creep and Shrinkage of High Performance Concrete, Research Report 580-5, Center for Transportation Research, The University of Texas at Austin, Austin, TX, 1996.
9. Goodspeed, C. H., Vanikar, S., and Cook, R. A., "High Performance Concrete Defined for Highway Structures," Concrete International, February 1996, Vol. 18, No. 2, pp. 62-67.
10. Gross, S. P. and Burns, N. H., Field Performance of Prestressed High Performance Concrete Highway Bridges in Texas, Research Report 580/589-2, Center for Transportation Research, The University of Texas at Austin, Austin, TX, 1999.
11. Gross, S. P. and Burns, N. H., Transfer and Development Length of 15.2 mm (0.6 in.) Diameter Prestressing Strand in High Performance Concrete: Results of the Hoblitzell-Buckner Beam Tests, Research Report 580-2, Center for Transportation Research, The University of Texas at Austin, Austin, TX, 1995.
12. Gross, S. P., Collecting and Downloading Strain and Temperature Data from the Louetta Bridge and San Angelo HPC Bridge Data Loggers, 2001.

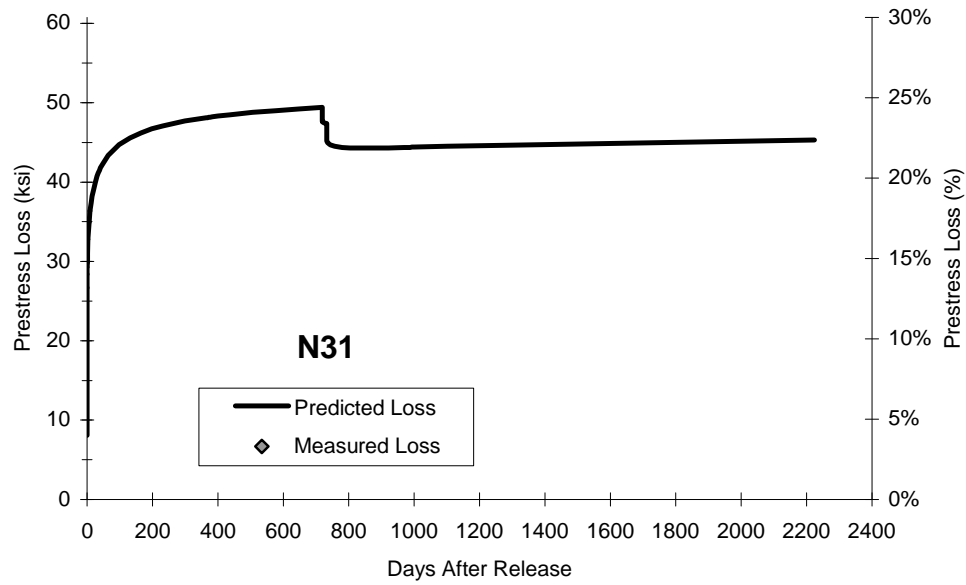
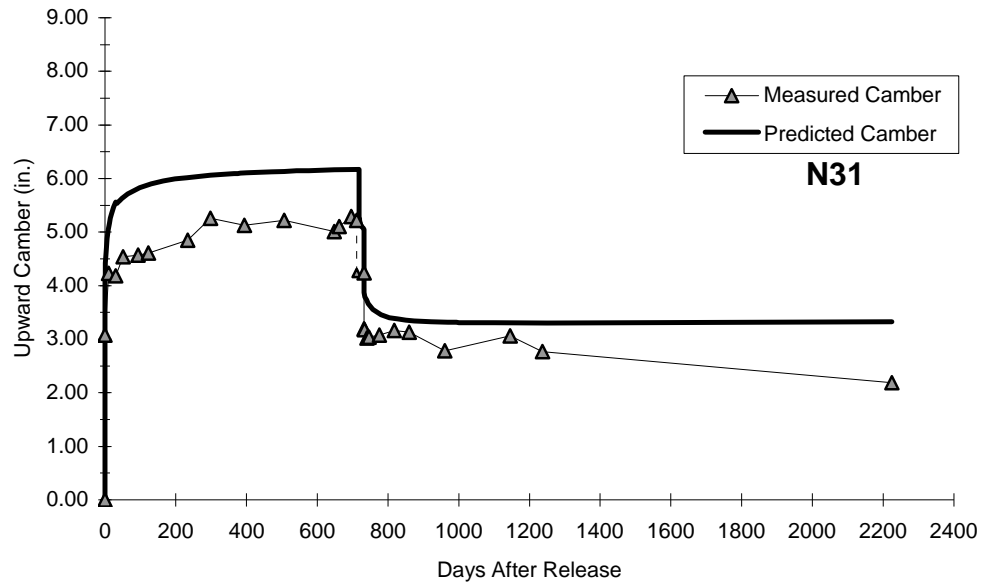
13. Gross, S. P., SORTDTA1, Data Manipulation and Reduction Program for Use With Custom Data Acquisition Systems in the Texas HPC Bridge Instrumentation Projects, Version 1.0, 1994.
14. Lin, T. Y. and Burns, N. H., Design of Prestressed Concrete Structures, John Wiley and Sons, New York, 1981.
15. Myers, J. J. and Carrasquillo, R. L., Production and Quality Control of High Performance Concrete in Texas Bridge Structures, Research Report 580/589-1, Center for Transportation Research, The University of Texas at Austin, Austin, TX, 1998.
16. Nilson, A. H., Design of Prestressed Concrete, John Wiley and Sons, New York, 1987.
17. Precast/Prestressed Concrete Institute, PCI Design Handbook, Fifth Edition, Chicago, 1999.
18. Prestressed Concrete Institute Committee on Prestress Losses, "Recommendations for Estimating Prestress Losses," Journal of the Prestressed Concrete Institute, July-August 1975, Vol., 20, No. 4. pp. 43-75.
19. Shepperd, G. A. and Burns, N. H., Long-Term Behavior of HPC Louetta Road Overpass, Research Report 7-3993, Center for Transportation Research, The University of Texas at Austin, Austin, TX, 2001 (under review).
20. Texas Department of Transportation, PSTRS14, Prestressed Concrete Beam Design/Analysis Program, Version 3.20, 1991.
21. Zia, P., Leming, M. L., and Ahmad, S. H., High Performance Concretes: A State of the Art Report, SHRP-C/FR-91-103, Strategic Research Highway Program, National Research Council, Washington, D.C., 1991.
22. Zia, P., Preston, H. K., Scott, N. L. and Workman, E. B., "Estimating Prestress Losses," Concrete International, June 1979, Vol. 1, No. 6, pp. 32-38.

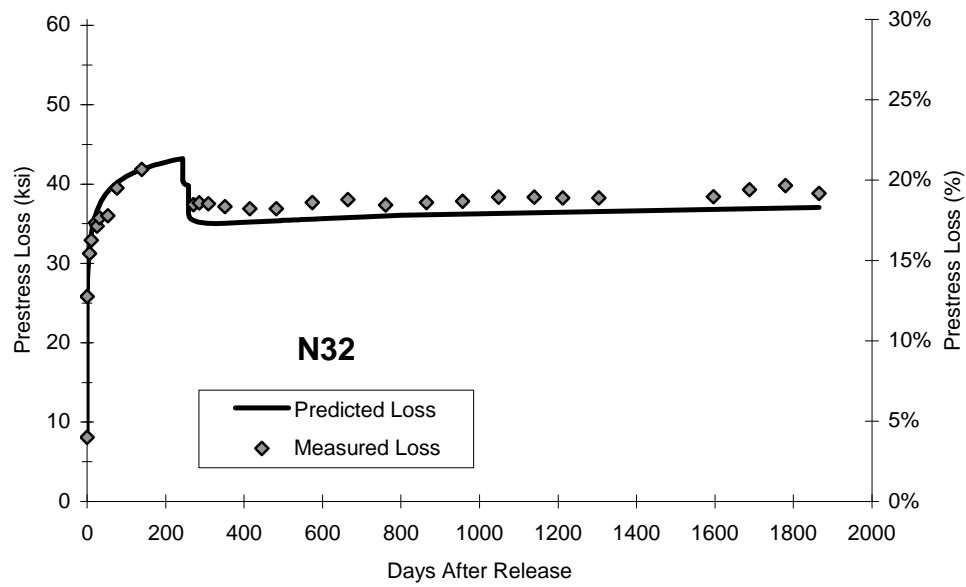
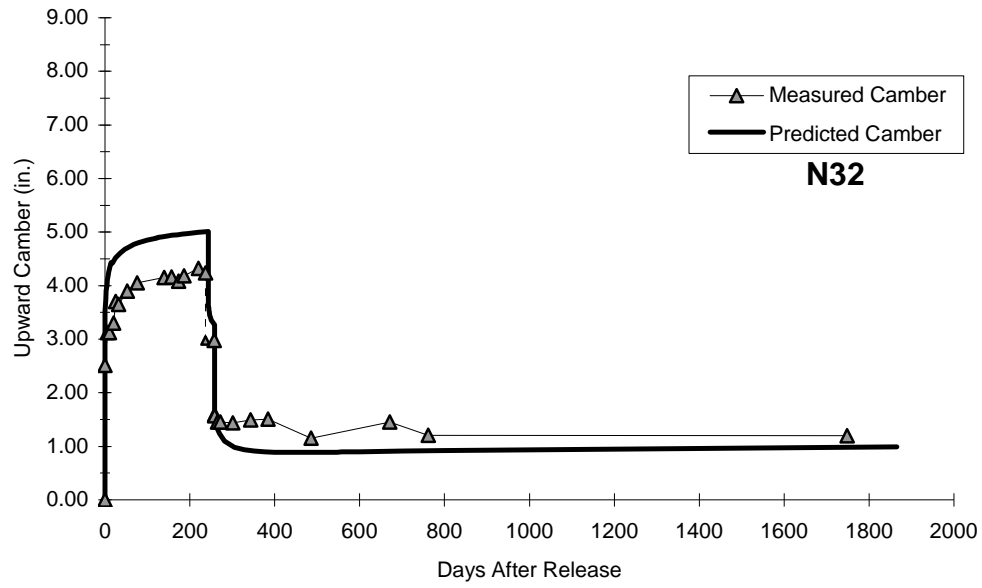
Appendix A: Camber and Prestress Losses

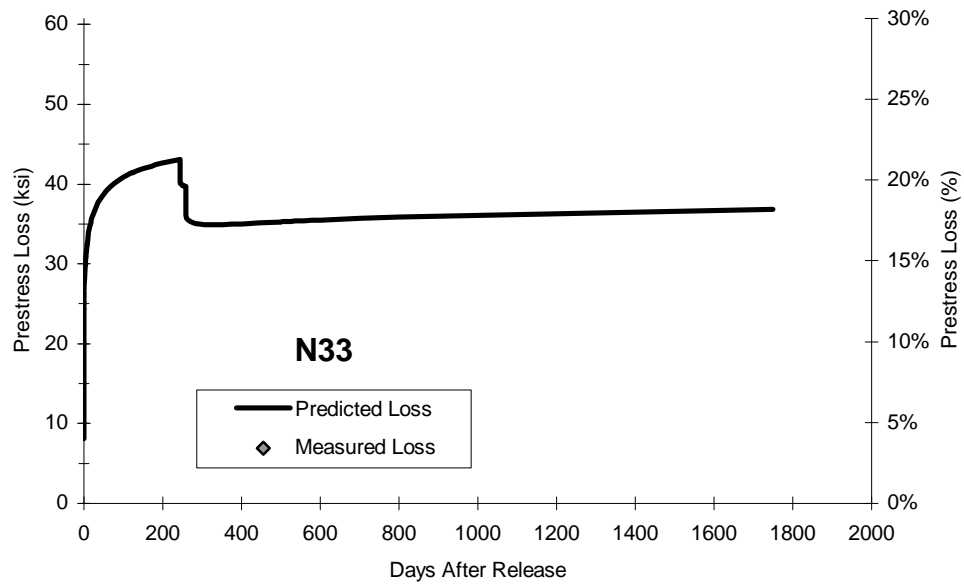
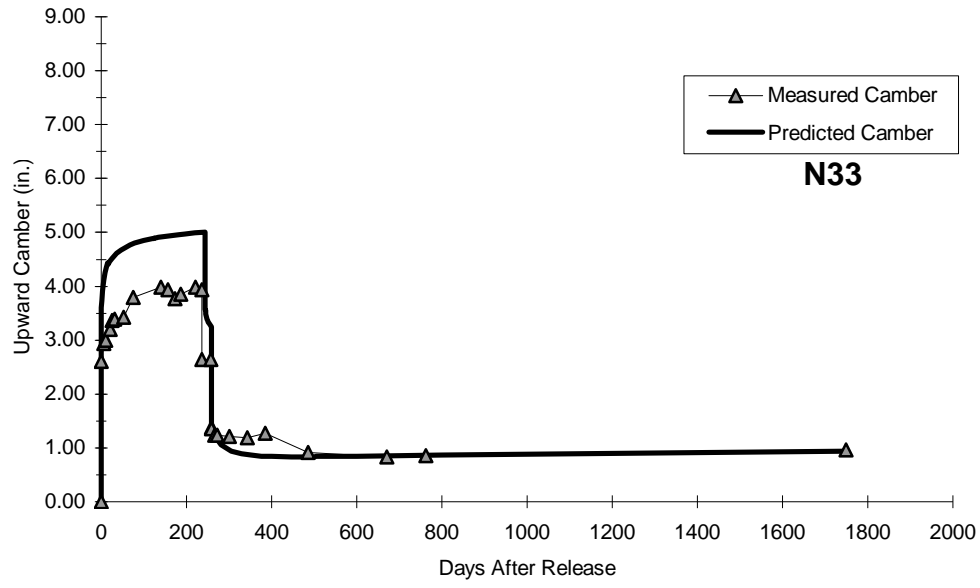


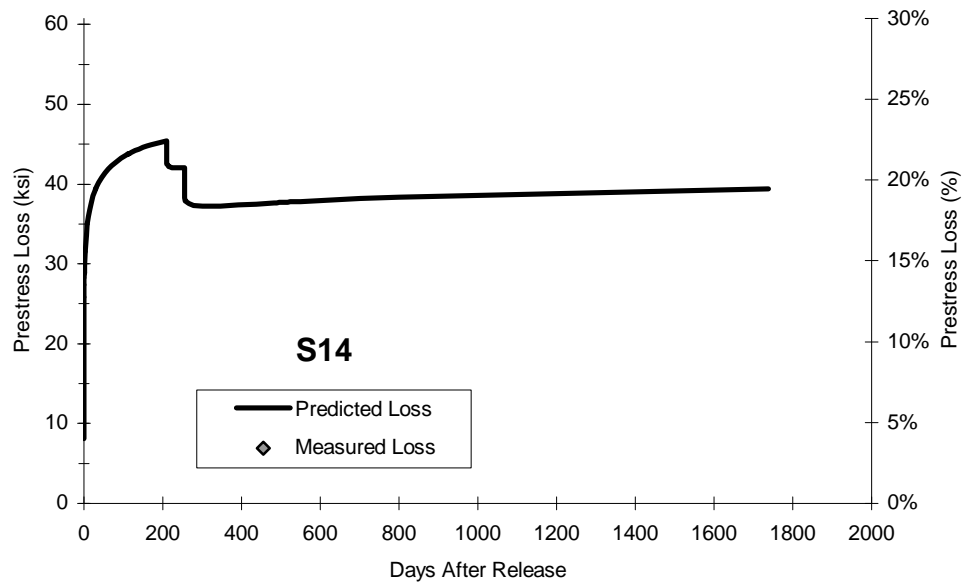
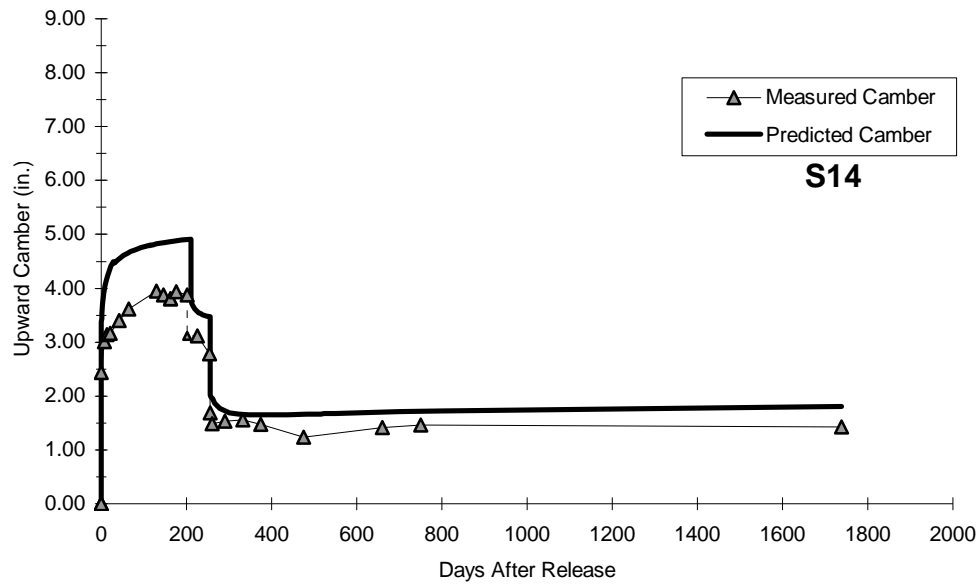


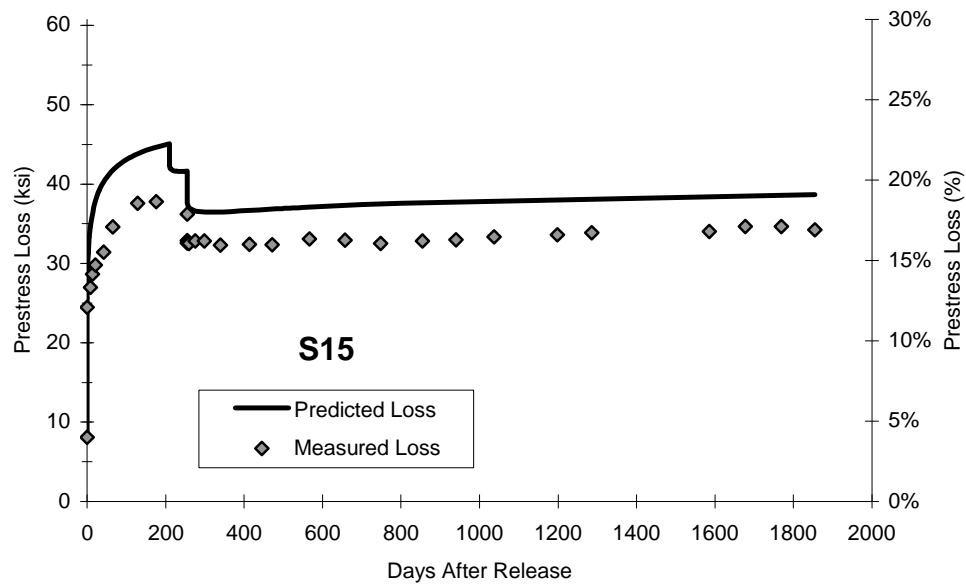
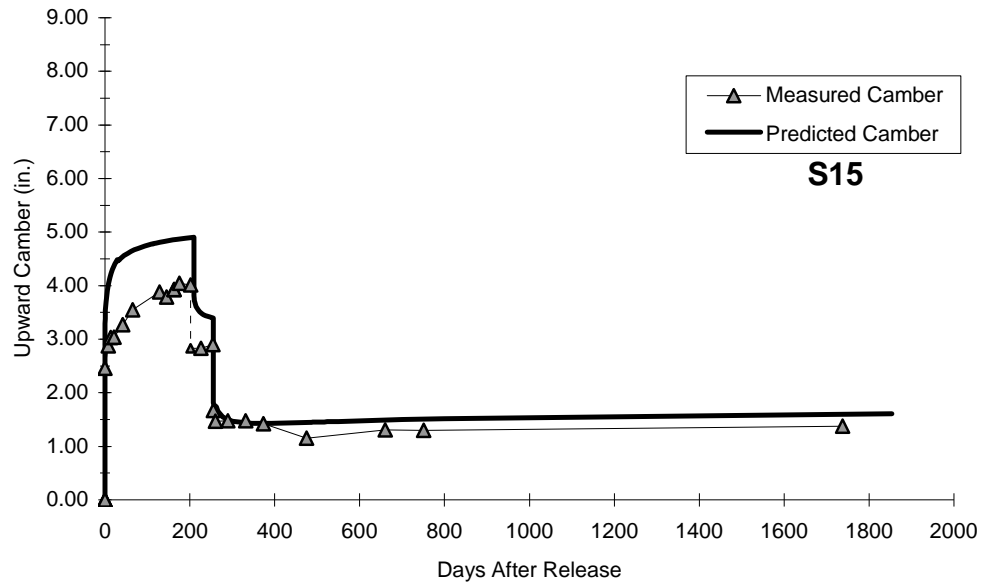


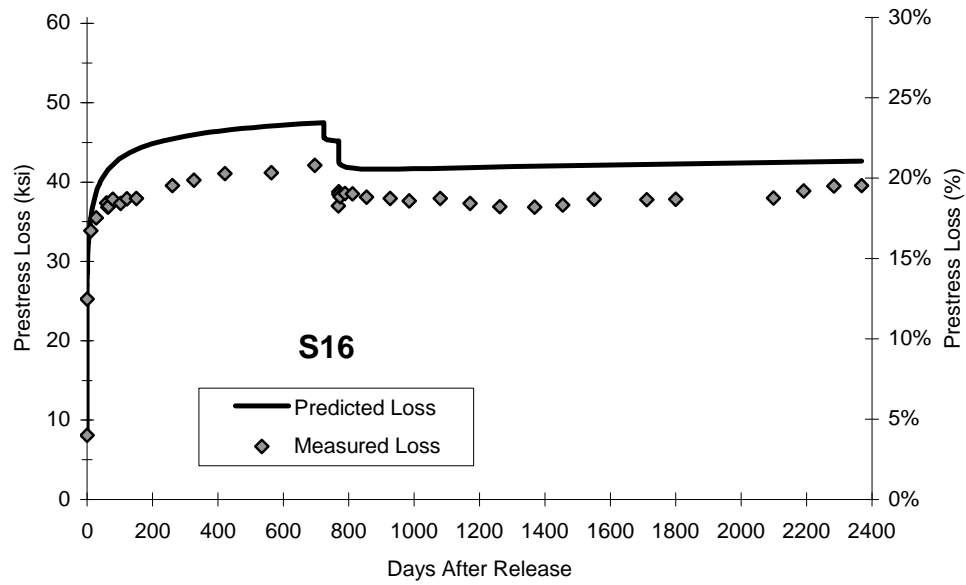
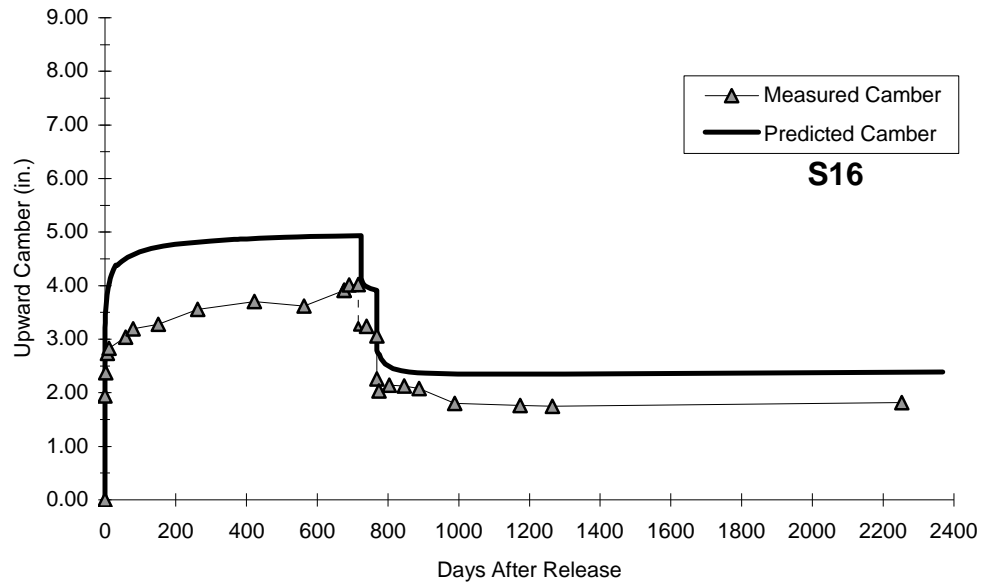


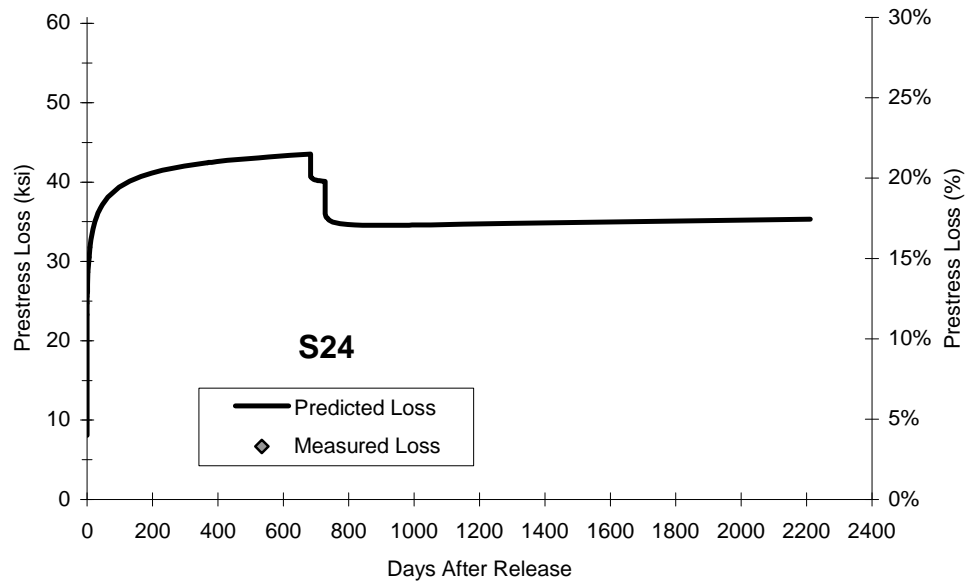
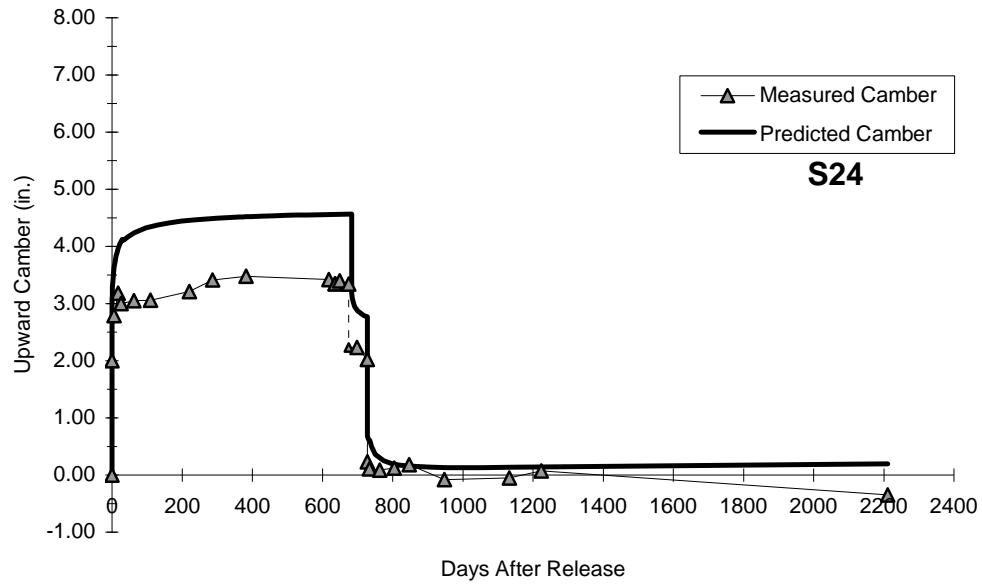


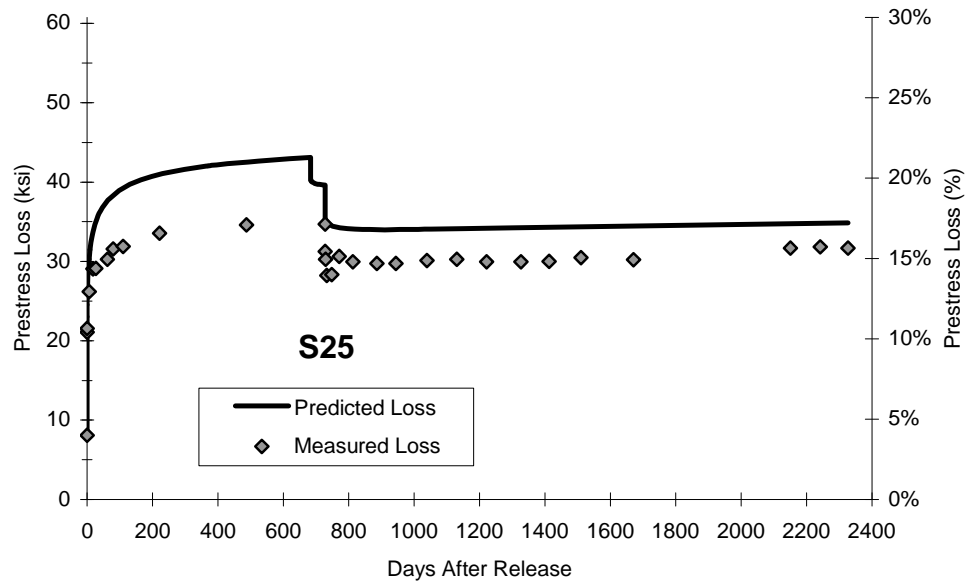
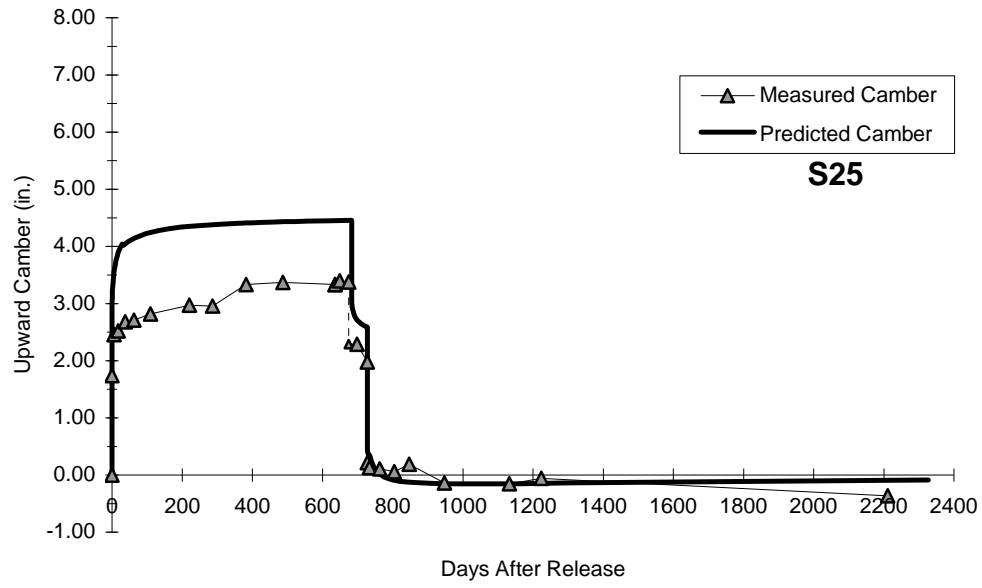


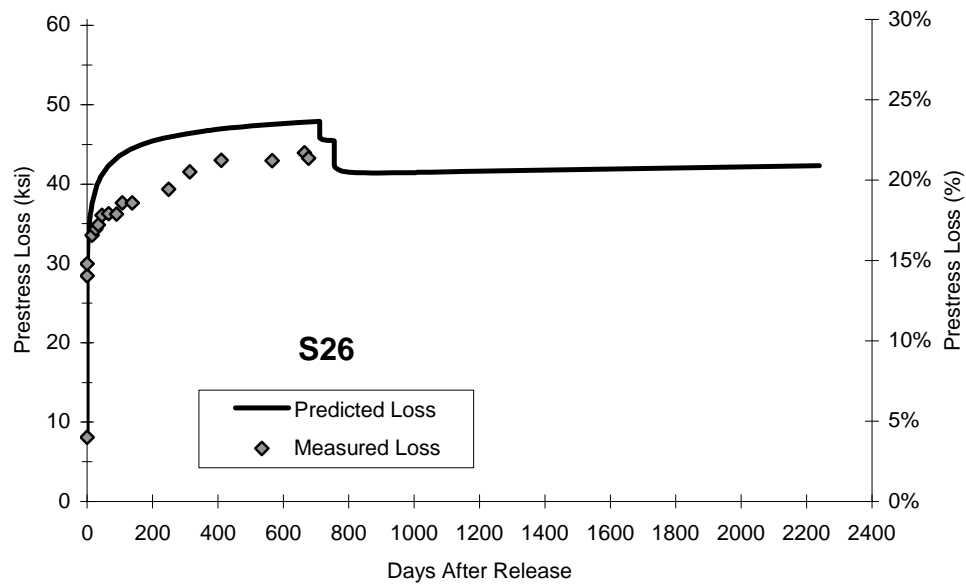
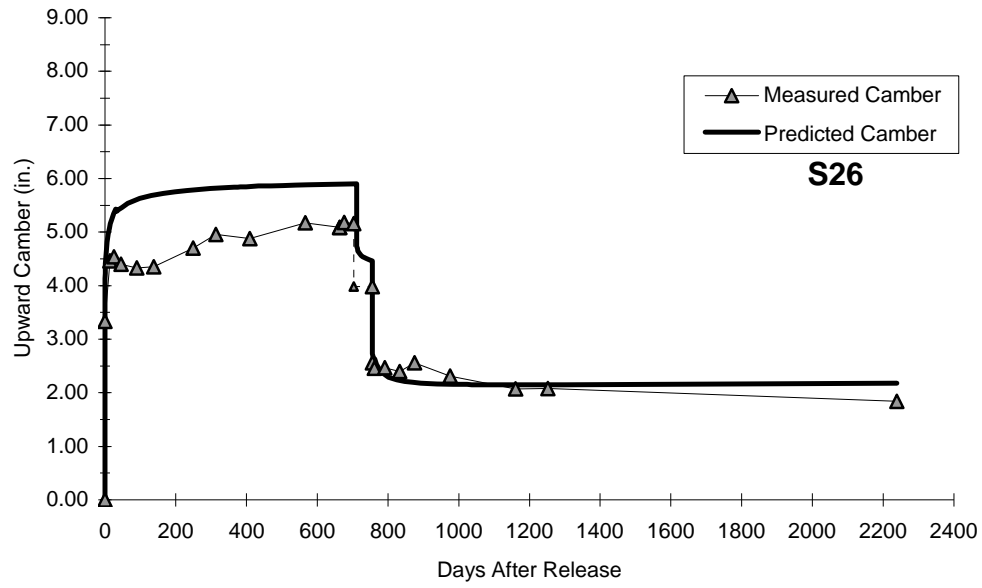


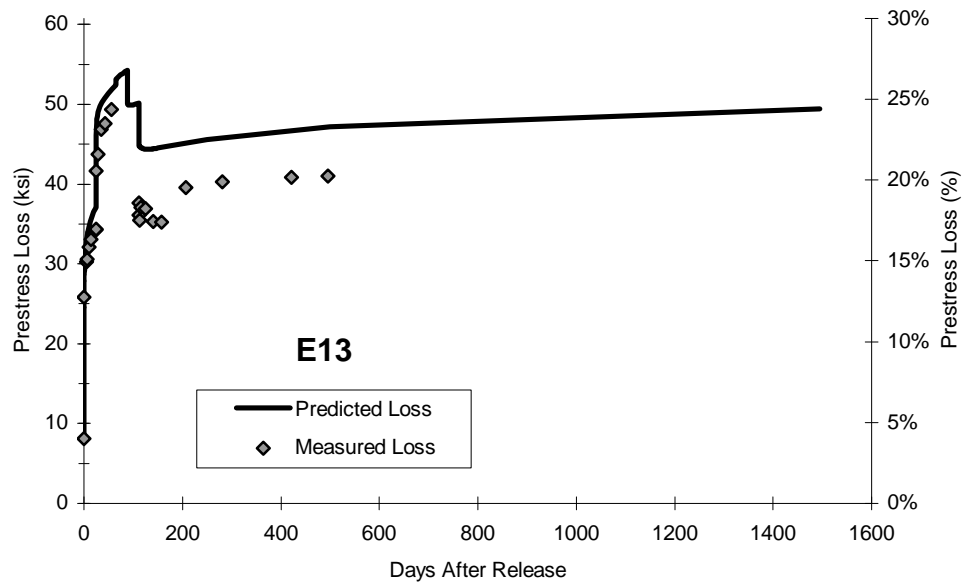
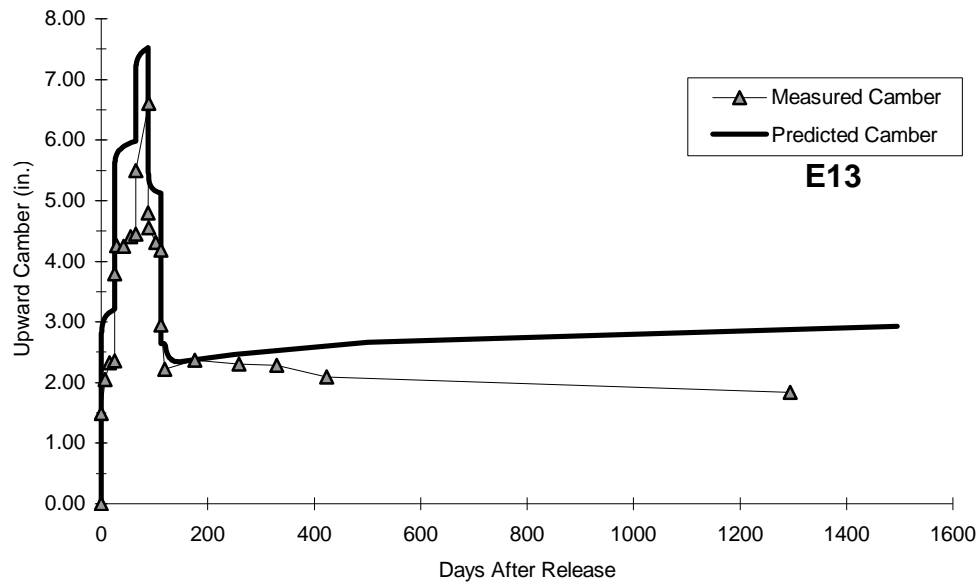


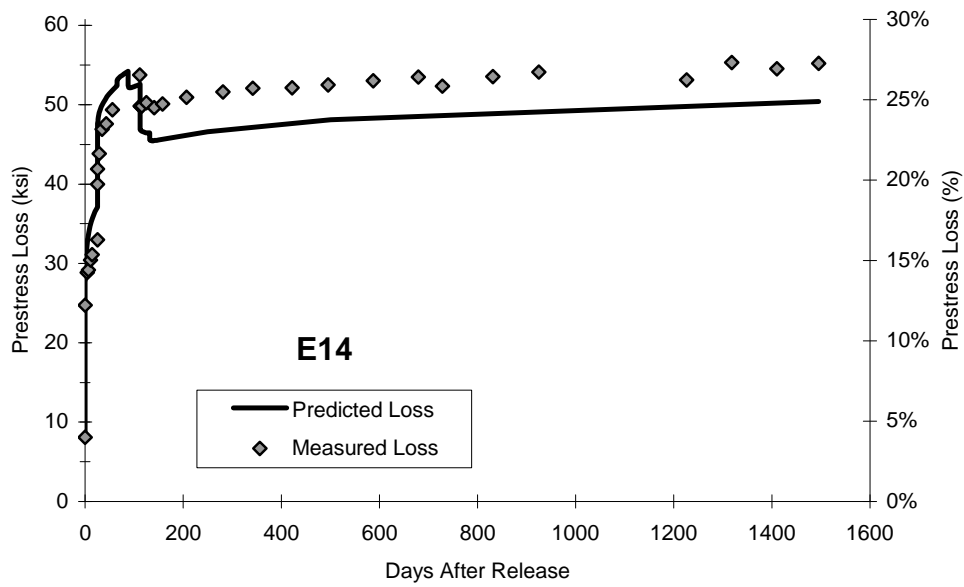
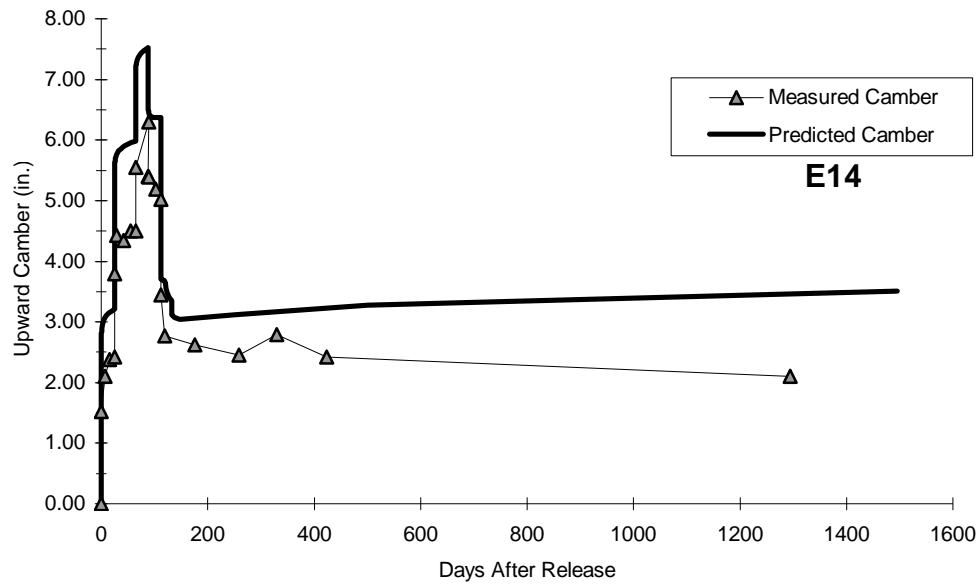


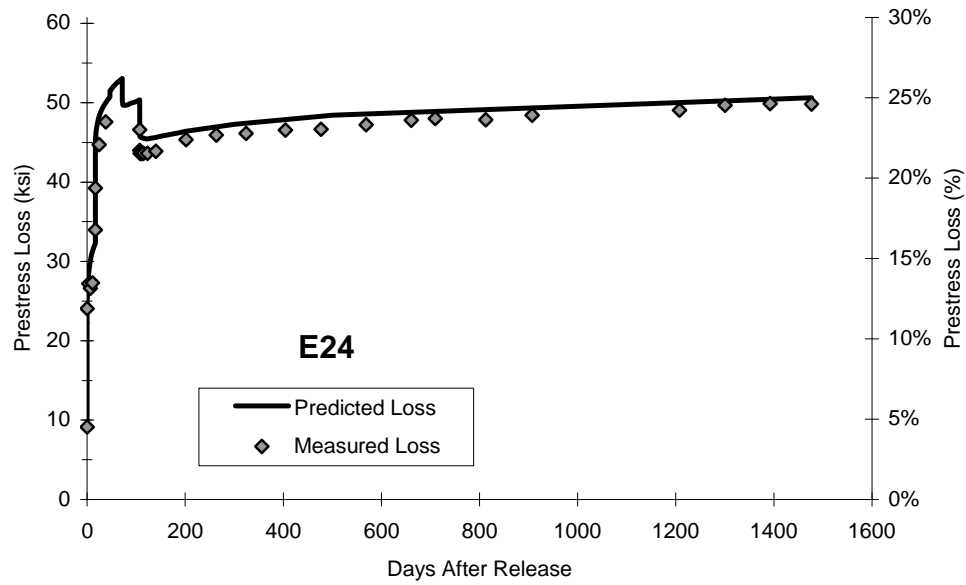
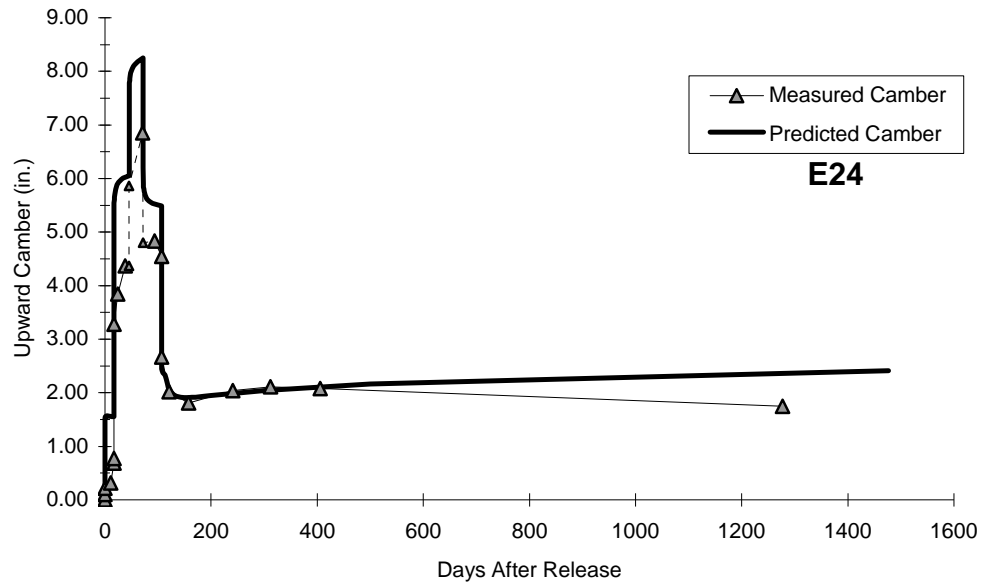


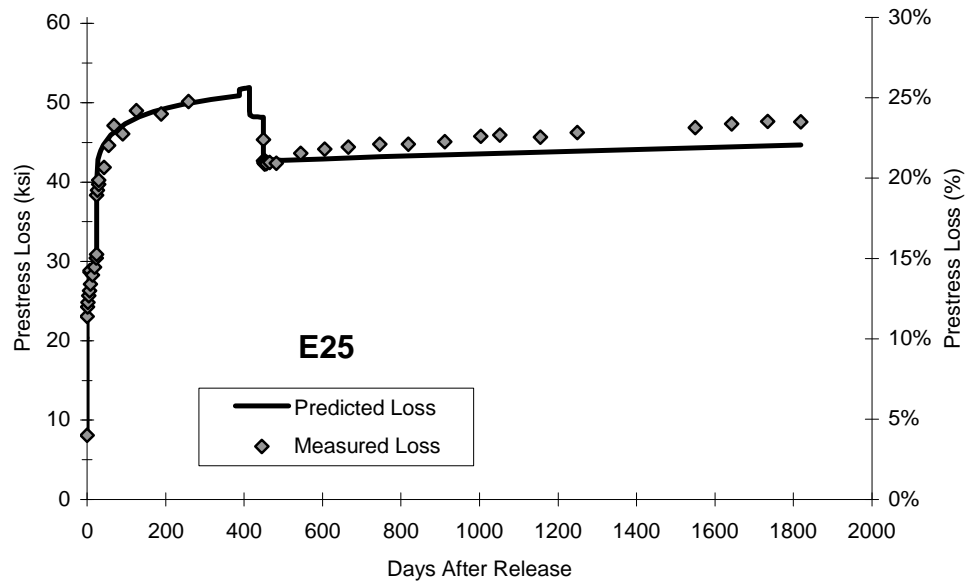
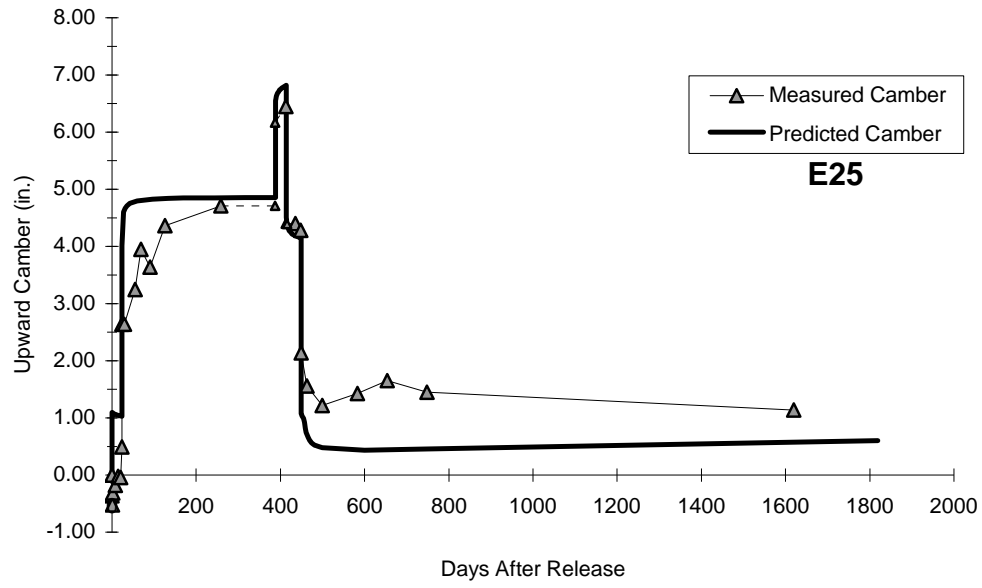


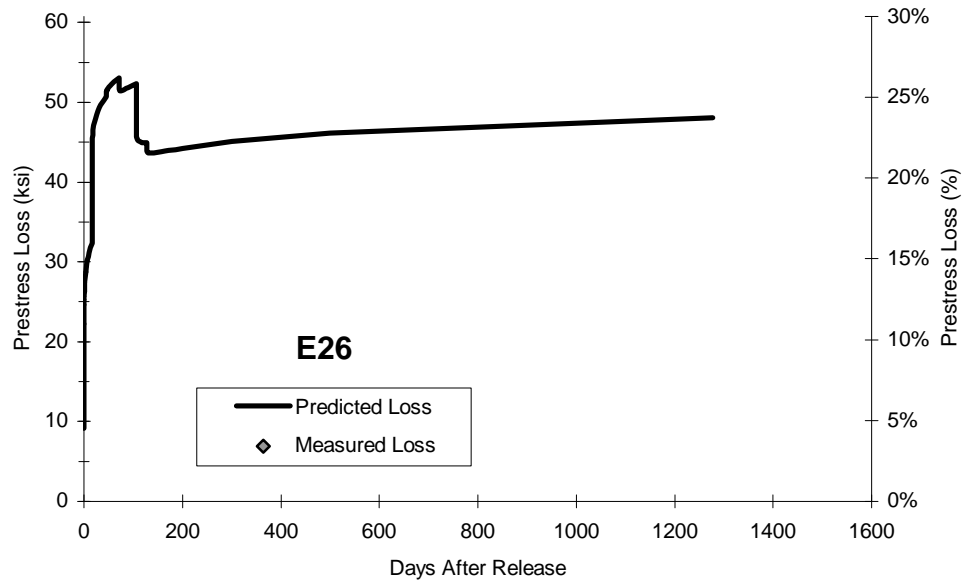
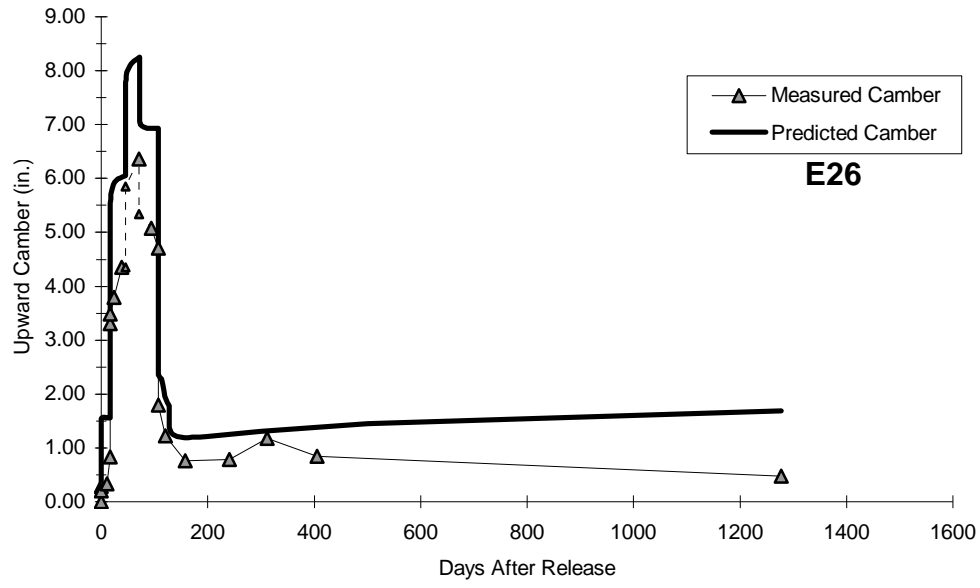


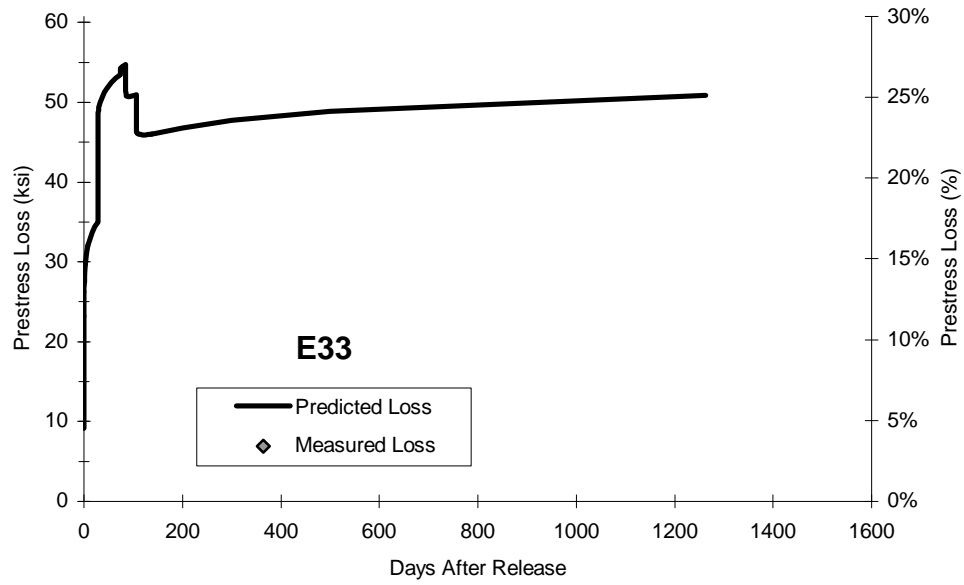
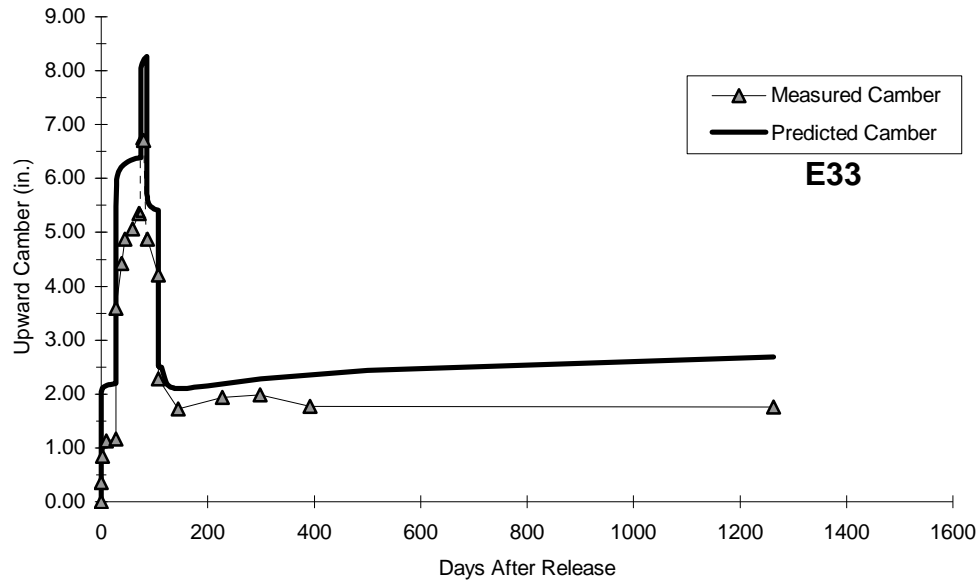


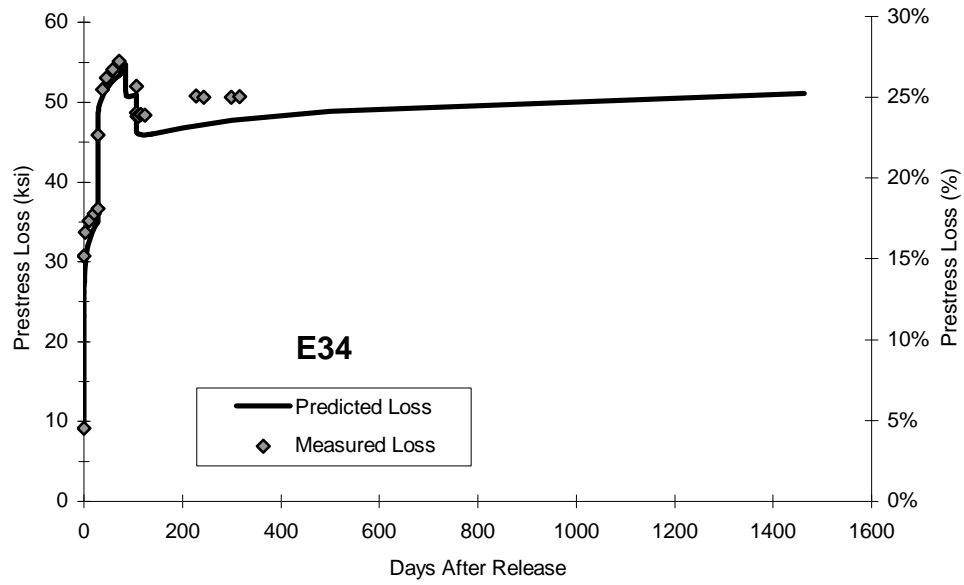
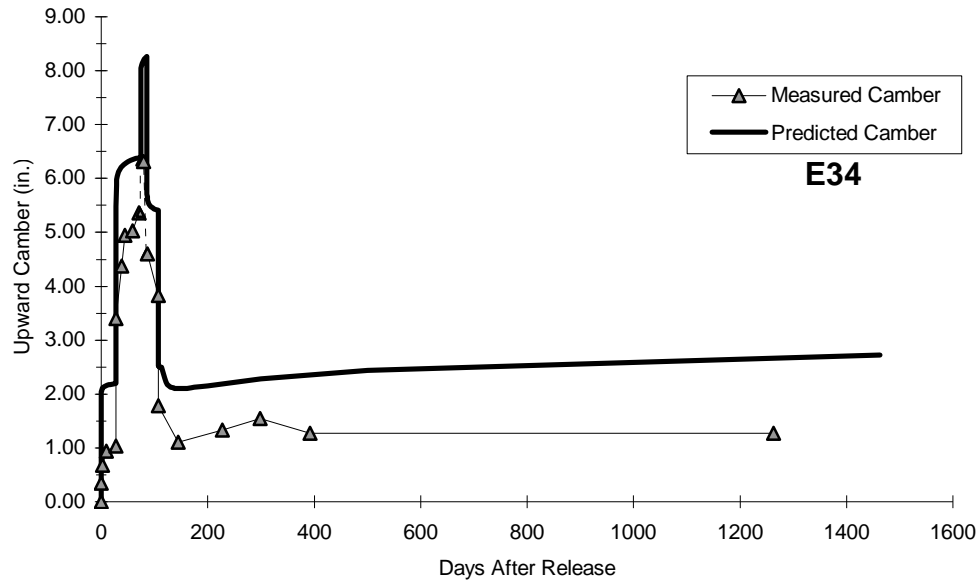


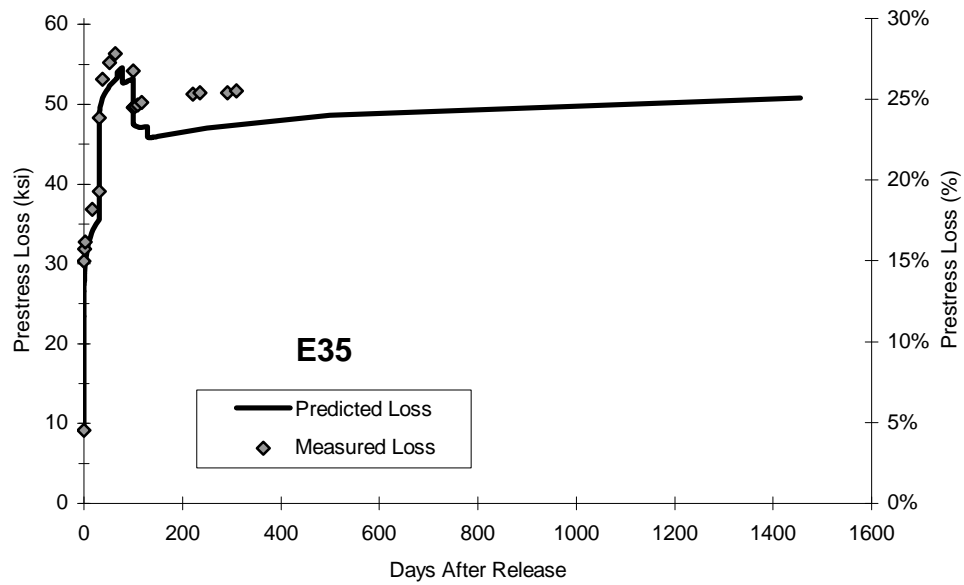
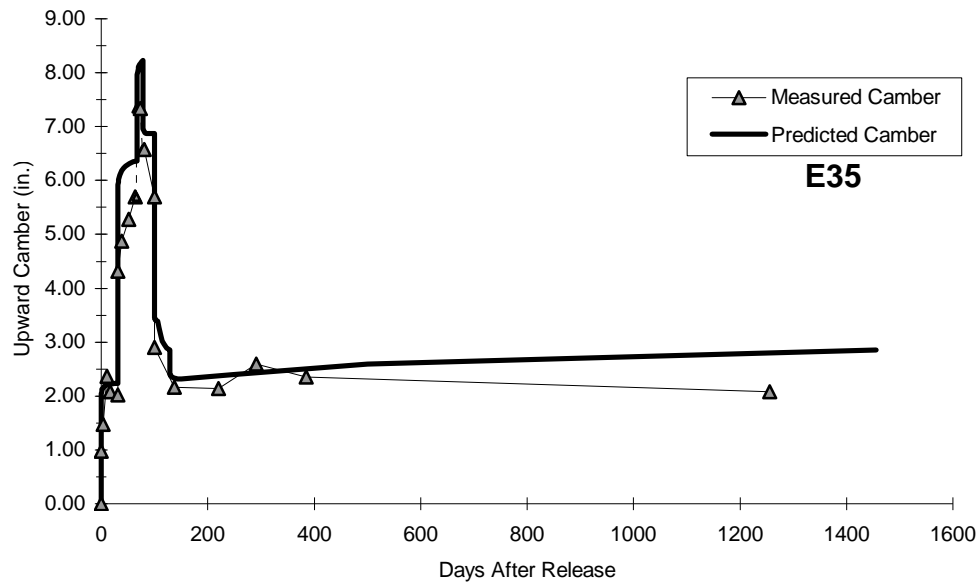


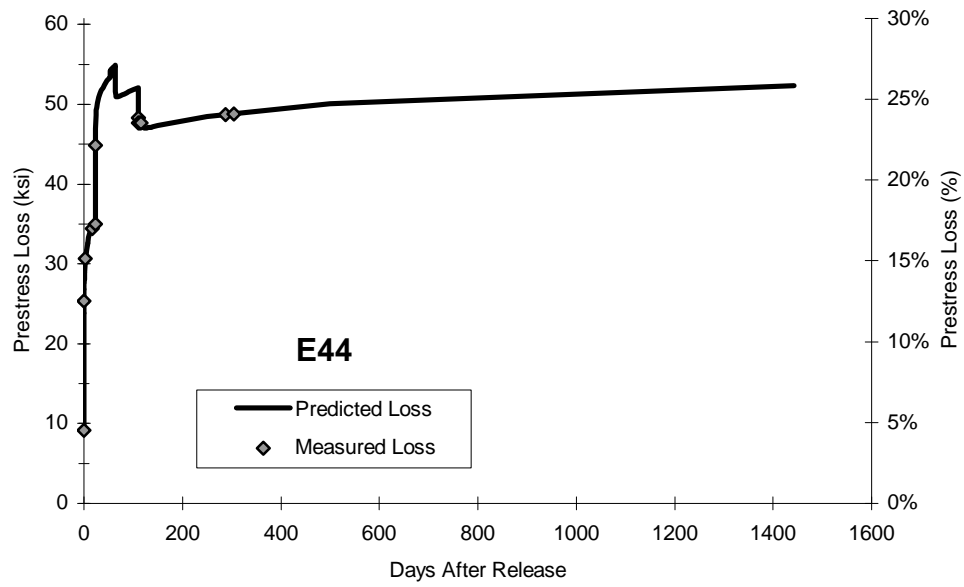
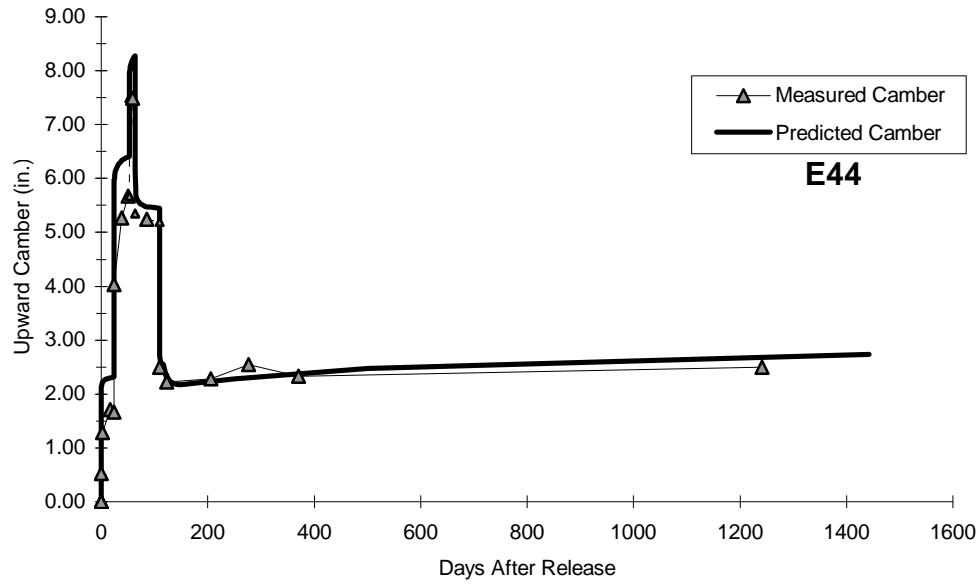


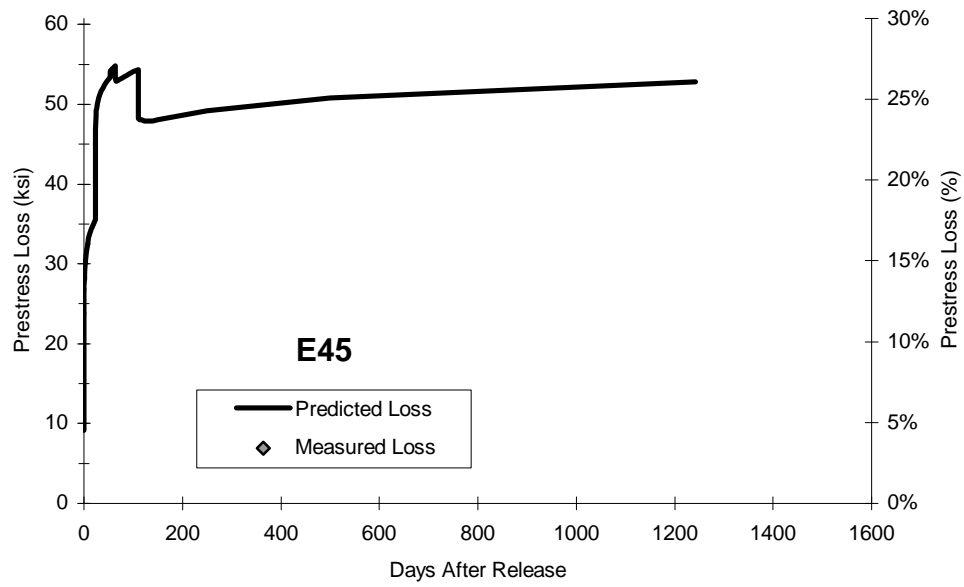
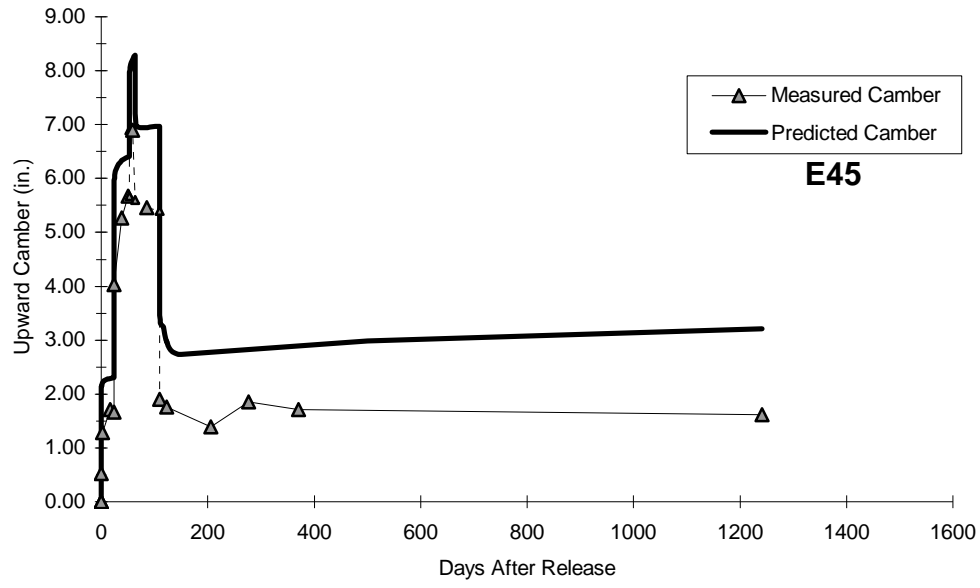


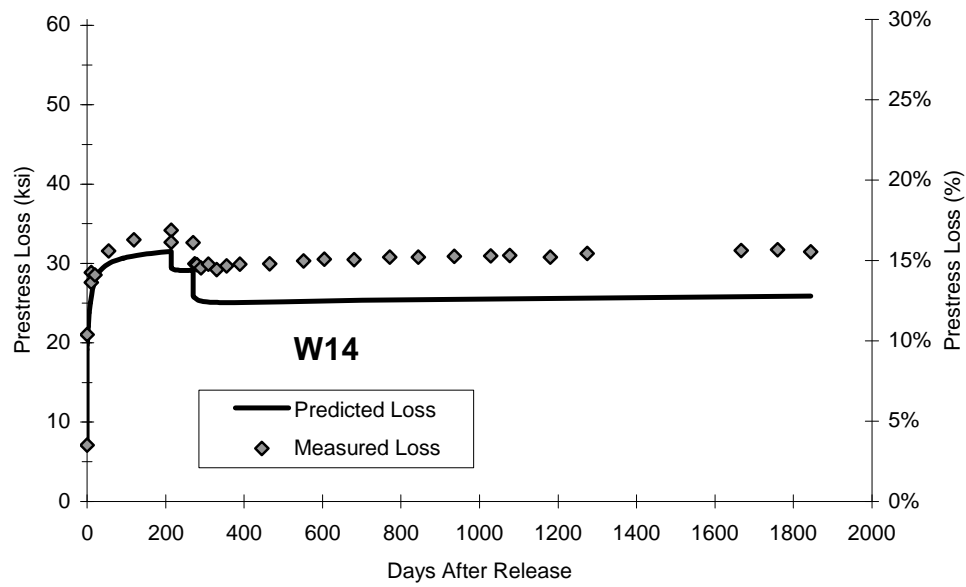
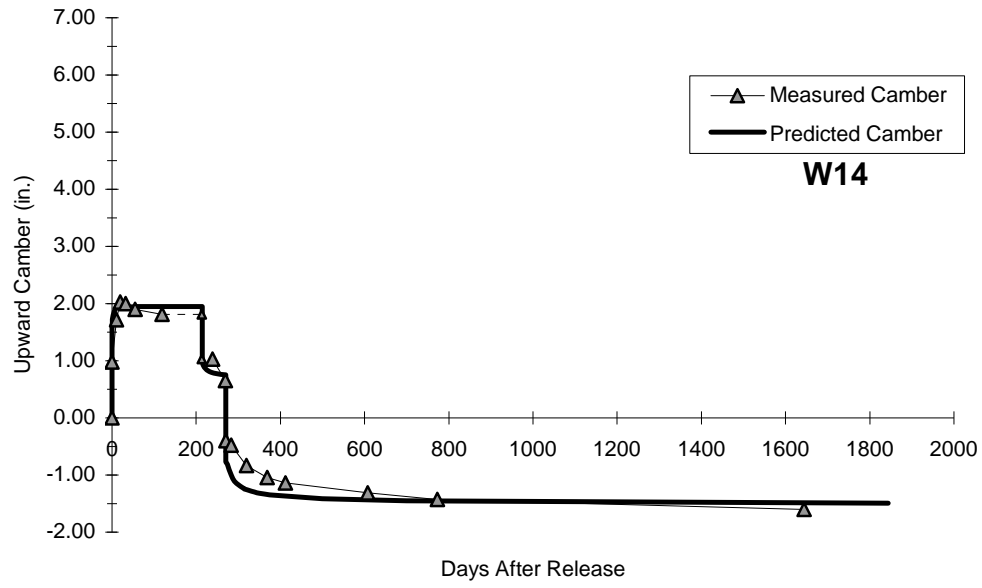


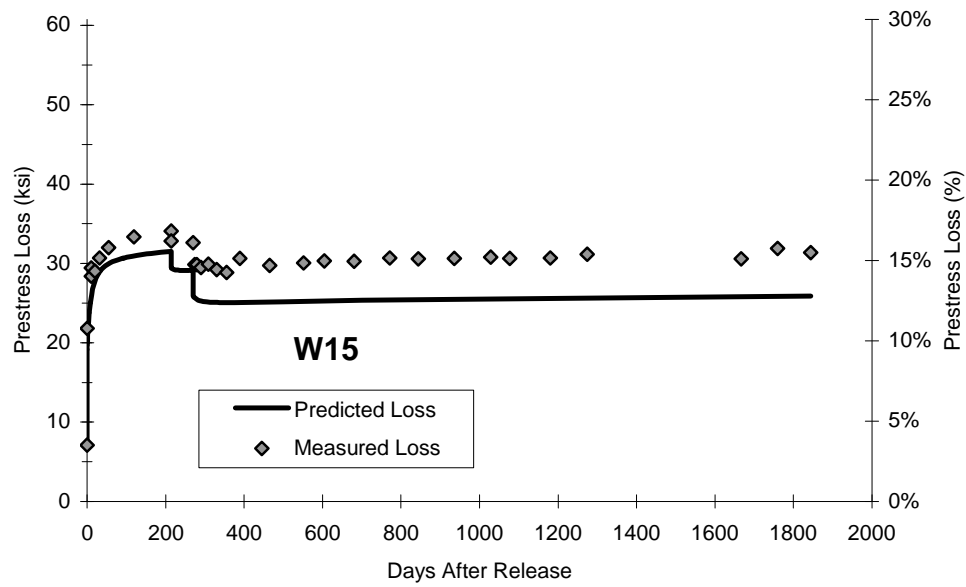
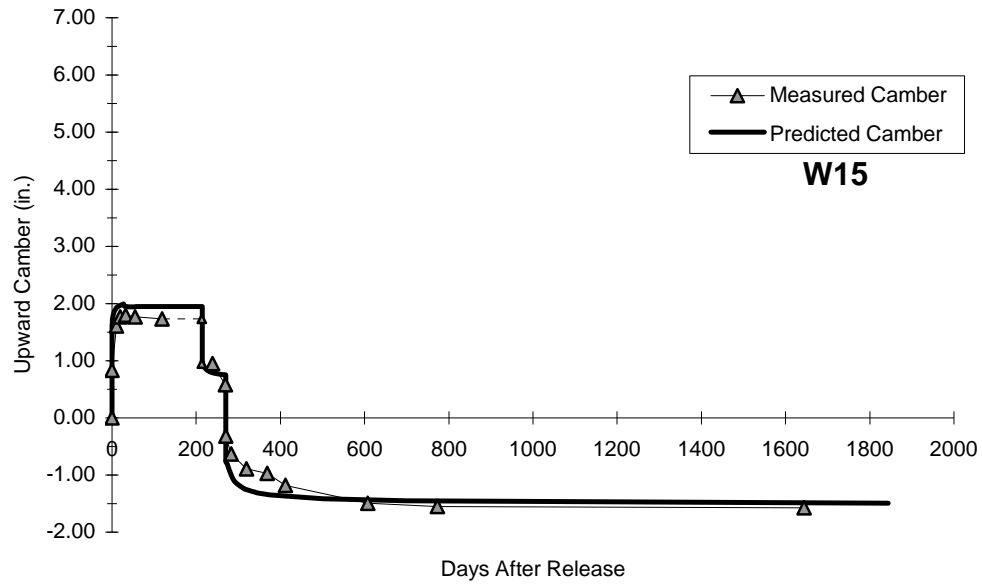


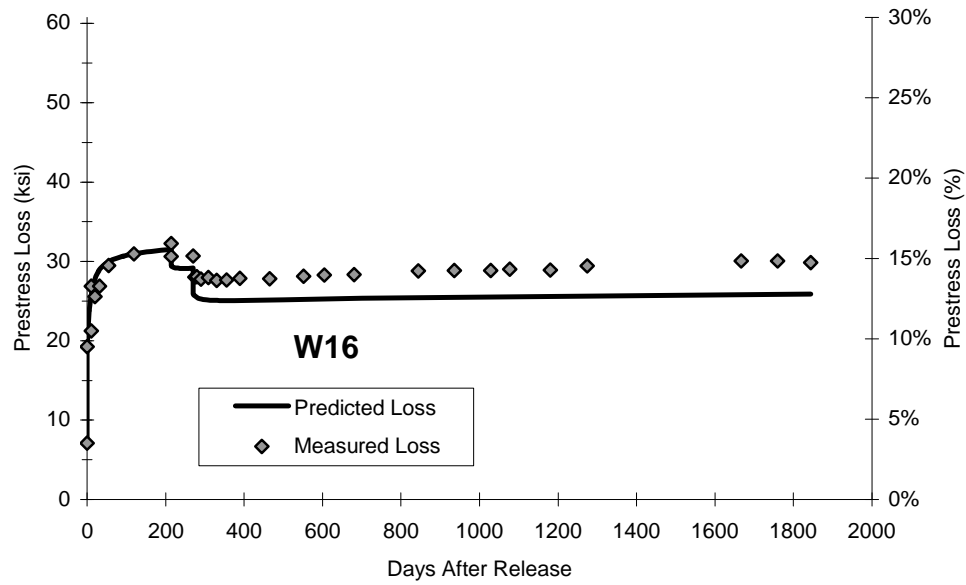
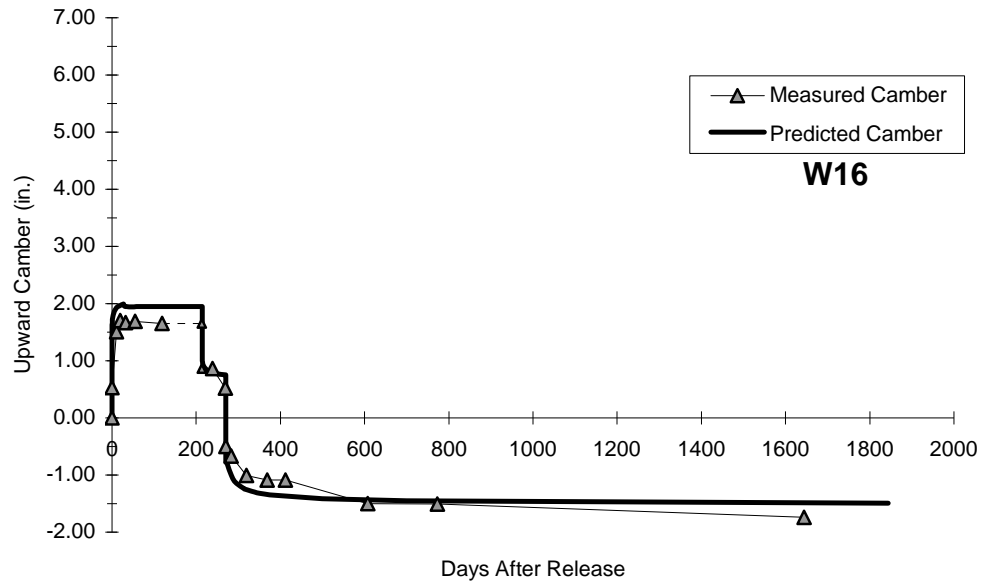


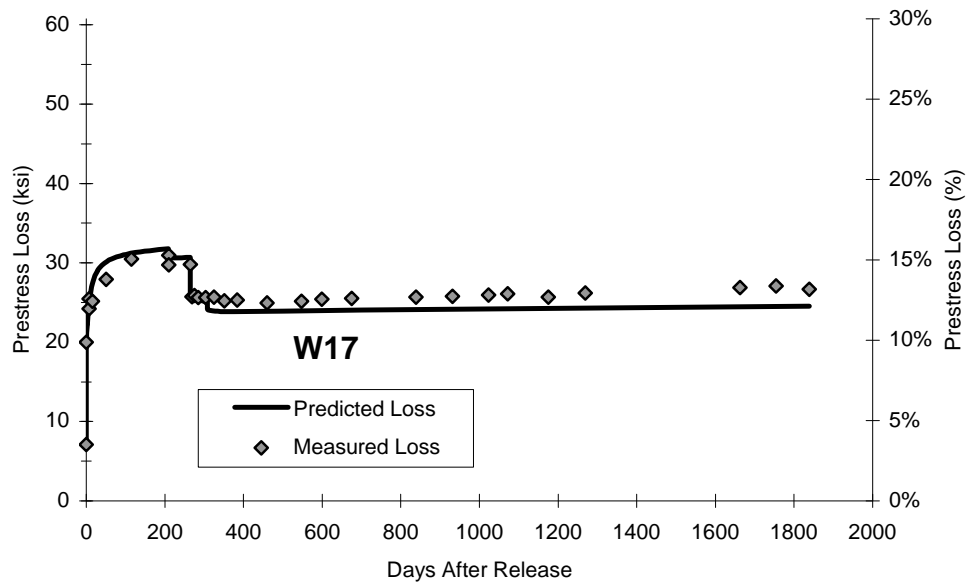
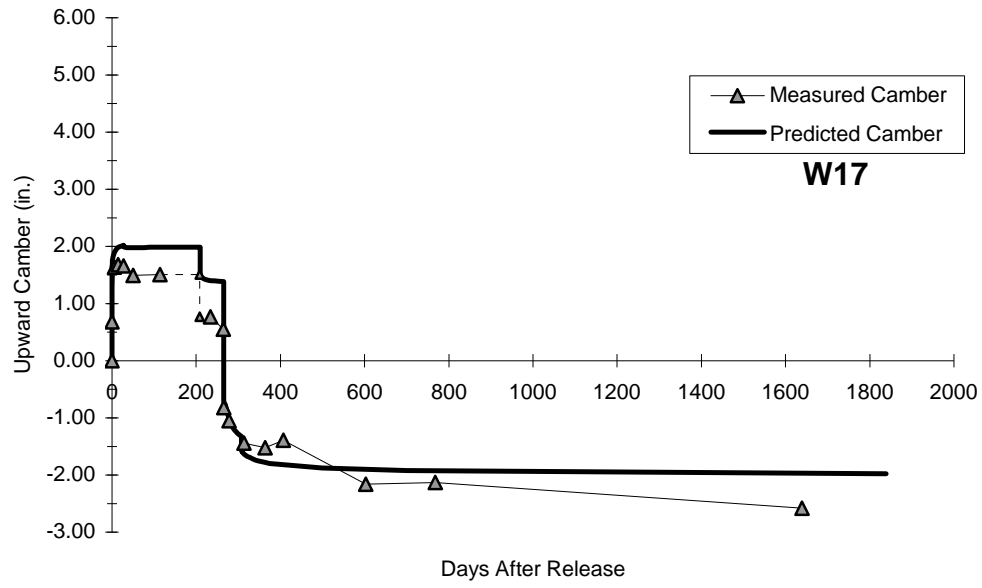












Appendix B: 2941-2 Report

Long-Term Behavior of High Performance Concrete Bridges in Texas

by

Brian Dahm

Chris Shoemaker

Ned Burns

Ramon Carrasquillo

David Whitney

Research Report Number (2941-2)

PRELIMINARY REVIEW COPY

Research Project (7-2941)

Long-Term Behavior of HPC Bridges

Conducted for the

TEXAS DEPARTMENT OF TRANSPORTATION

in cooperation with the

U.S. DEPARTMENT OF TRANSPORTATION

Federal Highway Administration

by the

CENTER FOR TRANSPORTATION RESEARCH

Bureau of Engineering Research

THE UNIVERSITY OF TEXAS AT AUSTIN

October 2001

DISCLAIMERS

The contents of this report reflect the views of the authors, who are responsible for the facts and the accuracy of the data presented herein. The contents do not necessarily reflect the official views or policies of the Federal Highway Administration or the Texas Department of Transportation. This report does not constitute a standard, specification, or regulation.

There was no invention or discovery conceived or first actually reduced to practice in the course of or under this contract, including any art, method, process, machine, manufacture, design or composition of matter, or any new and useful improvement thereof, or any variety of plant, which is or may be patentable under the patent laws of the United States of America or any foreign country.

IMPLEMENTATION RECOMMENDATIONS

NOT INTENDED FOR CONSTRUCTION,
BIDDING, OR PERMIT PURPOSES

David Whitney
Research Supervisor

ACKNOWLEDGMENTS

Throughout the course of this research project, numerous people have lent their support and help. Thanks are expressed to all of these people who have provided aid in one form or another. The author wishes to thank several people specifically:

All of the employees we dealt with from the Houston, San Angelo, Lubbock, and Amarillo Districts and the Bridge Division at the Texas Department of Transportation must be thanked, in particular Gerry Fields, Bobby Bridges, Lewis Gamboa, and Sam Harris. Without their work, assistance, and patience much of the work on this project would not have been possible.

The staff of the Construction Materials Research Group (CMRG), Kerry Rothenbach, Michael Rung, and Sherian Williams. Their dedication, suggestions, and assistance were essential in the coordination of this long-term project.

There were numerous structures and materials students from CTR and CMRG who assisted in the project, and who also made it that much more enjoyable. These individuals often spent long hours reading BRNSAP and Texas Bridge Inspection reports, loading toolboxes and equipment into vehicles, and traveling across Texas to closely inspect bridge elements and the authors thank them.

Faculty supervisors and consultants included Dr. Ned Burns, our reader and supervisor on the earlier associated projects' reports. His vast knowledge of prestressed concrete was greatly appreciated throughout this project. Dr. David Fowler, too, is appreciated for sharing so much of his time, effort, encouragement, suggestions, and support throughout this project.

Research performed in cooperation with the Texas Department of Transportation.

Table of Contents

CHAPTER 1: Introduction.....	1
1.1 Background.....	1
1.2 Research Objectives.....	2
1.3 Outline of This Report.....	2
CHAPTER 2: Literature Review	3
2.1 Introduction	3
2.2 Definition of High Performance Concrete.....	3
2.3 Sources of Long-Term Prestress Loss	3
2.4 Predicting Long-Term Prestress Loss.....	5
2.5 Sources of Long-Term Camber	9
2.6 Predicting Long-Term Camber.....	9
2.7 Previous Durability Monitoring.....	10
CHAPTER 3: Structural HPC Bridge Descriptions and Data Acquisition System	13
3.1 Introduction	13
3.2 Louetta Road Overpass.....	13
3.3 North Concho River/US 87/South Orient Railroad Overpass	18
3.4 Original Data Acquisition System.....	21
3.5 Modifications to Data Acquisition System.....	24
3.6 Gauge Durability	27
CHAPTER 4: Monitoring Program.....	33
4.1 Introduction	33
4.2 Durability Monitoring.....	33
4.3 Prestress Loss Measurements	35
4.4 Camber Measurements	36
CHAPTER 5: Monitoring Results.....	43
5.1 Introduction	43
5.2 Durability Results	43
5.3 Prestress Loss	47
5.4 Camber.....	50
CHAPTER 6: Discussion of Test Results and field inspections.....	53
6.1 Introduction	53

6.2 Prestress Loss	53
6.3 Camber.....	56
CHAPTER 7: Summary, Conclusions, and Recommendations	63
7.1 Summary.....	63
7.2 Conclusions	64
7.3 Recommendations	65
REFERENCES.....	67

List of Tables

Table 2.1 Crack Mapping Summary [19]	10
Table 3.1 Design Compressive Strengths for Louetta Road Overpass	16
Table 3.2 Design Compressive Strengths for San Angelo Bridges	21
Table 3.3 Summary of Gauge Location	22
Table 3.4 Travel Summary	25
Table 3.5 Gauge Durability Summary for Louetta Road Overpass	29
Table 3.6 Gauge Durability Summary for San Angelo Bridges	30
Table 4.1 Summary of the BRINSAP Rating System	34
Table 5.1 Summary of BRINSAP Report Review	43
Table 5.2 Crack Mapping Summary	44
Table 5.3 Results of Chloride Ion Penetration Tests	47
Table 5.4 Components of Measured Prestress Loss	50
Table 5.5 San Angelo Camber Measurements	51
Table 6.1 Comparison of Design versus Measured Parameters [10]	53
Table 6.2 Comparison of Total Prestress Losses	55
Table 6.3 Long-Term Camber	58
Table 6.4 Analysis of Long-Term Camber	60

List of Figures

Figure 3.1 Louetta Road Overpass.....	14
Figure 3.2 Plan View of Louetta Road Overpass [10].....	15
Figure 3.3 Cross-Section Dimensions of Texas HPC Beams [adapted from 10]	17
Figure 3.4 Strand Pattern of Texas HPC Beams [adapted from 10]	18
Figure 3.5 North Concho River/US 87/South Orient Railroad Overpass [10]	19
Figure 3.6 Plan View of North Concho River/US 87/South Orient Railroad Overpass [10]	20
Figure 3.7 Schematic of Original Data Transfer Setup [10]	24
Figure 3.8 Solar Panel Mounted on San Angelo Bent Cap.....	26
Figure 3.9 Remote-Monitoring Equipment in DAS Box.....	26
Figure 3.10 Schematic of New Data Transfer Setup	27
Figure 3.11 Percentage of Gauges Working	31
Figure 3.12 Percentage of ERSG Gauges Working.....	31
Figure 3.13 Percentage of VW/TR Gauges Working	32
Figure 3.14 Percentage of TC Gauges Working.....	32
Figure 4.1 Instrumented Areas of Louetta Road Overpass [10]	38
Figure 4.2 Instrumented Areas of San Angelo Bridges [10]	39
Figure 4.3 Precise Surveying System Equipment.....	40
Figure 4.4 Location of Survey Points on a Louetta Beam.....	40
Figure 4.5 Camber Measurements at San Angelo	41
Figure 4.6 Bearing Point versus Survey Point.....	42
Figure 5.1 Close-Up of Crack in Louetta Southbound Deck.....	45
Figure 5.2 Severe Crack in Louetta Southbound Deck.....	46
Figure 5.3 Measured Prestress Loss – Typical Case (Beam N32).....	49
Figure 5.4 Measured Prestress Loss – Worst Case (Beam W14)	49
Figure 5.5 Measured Camber and Deflection – Typical Case (Beam N21)	52
Figure 5.6 Measured Camber and Deflection – Worst Case (Beam E45)	52

CHAPTER 1: Introduction

1.1 BACKGROUND

In 1993 the Federal Highway Administration (FHWA) began a program to build high performance concrete (HPC) bridges in the United States. As part of this program two HPC bridges were built in Texas. The Louetta Road Overpass on Texas State Highway 249 near Houston, TX, commonly referred to as the Louetta Road Overpass or more simply the Louetta bridges, was opened to traffic in May 1998. The North Concho River/US 87/South Orient Railroad Overpass on US 67 in San Angelo, TX, commonly referred to as the San Angelo bridges, was opened to traffic in January 1998.

This report covers the continuation of performance monitoring done under three previous projects by the Center for Transportation Research (CTR) at The University of Texas at Austin. Two comprehensive reports detailing work completed under CTR Project 9-580, "Design and Construction of Extra-High Strength Concrete for Bridges," and 9-589, "High Performance Concrete for Bridges" discussed these bridges from their inception through construction and early structural performance until December 1998 [10, 15]. When Project 9-580 ended, the Louetta bridges were monitored under CTR Project 7-3993. Another report [19] covered the work done under CTR Project 7-3993, "Long-Term Behavior of HPC Louetta Road Overpass." CTR Project 7-2941, "Long-Term Behavior of HPC Bridges," began September 1, 1999 to continue monitoring efforts on both Texas HPC bridges. At that time Project 7-3993 was terminated, and its field information and database were incorporated into Project 7-2941. This report discusses the findings and refinements in methods for the early performance stages and long-term monitoring of the Texas HPC bridges, the Louetta Road Overpass, and San Angelo bridges, since 1999.

This research project continued monitoring these two HPC bridges in Texas for long-term performance and durability. Monitoring included collection and interpretation of data from the extensive network of gauges installed in the bridges. Early field evaluations in this project involved measuring the camber and deflection of specific beams, close inspections for cracking or signs of deterioration in the bridges, and determinations of chloride content in the decks.

Analysis of the collected data included calculating prestress losses and camber and deflection on specific beams. This analysis included data collected from April 1998 to September 1999 during CTR Project 7-3993, as well as data collected from January 2000 to August 2001. Data were only collected during CTR Project 7-3993 and not analyzed as part of that research project. A final status report of the Louetta and San Angelo data acquisition systems (DAS) was also performed.

It is important to note that even during the construction of the Louetta and San Angelo bridges, the accepted definition of HPC rapidly evolved from meaning very high strength or high-early strength to mean an engineered material enhanced to optimize properties associated with durability in the specified applications. Transportation structures, especially in Texas, have increasingly used this HPC concept to construct concrete decks with improved abrasion resistance, reduced chloride penetrability, and improved resistance to freezing and thawing damage. Although benefits from these properties improvements are apparent, it can be difficult to predict how much specific target properties result solely from concrete constituents, and how much those properties are influenced by other construction circumstances. Consequently, successful efforts to minimize permeability in bridge decks with high substitutions of

supplemental cementitious materials such as fly ash, silica fume, or slag resulted in a denser concrete matrix. Unfortunately, as the density increased, so did the modulus of elasticity, and early cracking of the brittle deck rapidly became apparent.

Thus it was that TxDOT became interested in adding several new HPC decks to be regularly monitored for distress as part of this HPC-bridge-monitoring project. Later as early structural changes became minimal and stabilized on the Louetta and San Angelo bridges, the focus of the project shifted entirely to monitoring and reporting the deteriorating conditions of their decks and of the newly specified bridge decks in the Lubbock and Amarillo Districts.

1.2 RESEARCH OBJECTIVES

The primary objectives of this research project were to monitor the long-term structural behavior of the pretensioned HPC beams and the durability of the HPC decks, as well as to evaluate the performance of the DAS.

The structural advantages of the HPC beams used in these bridges allowed for longer spans and fewer beams per span. By monitoring prestress loss and camber in the beams, a better understanding of the behavior of HPC beams can be achieved. This information can lead to more appropriate specifications in design codes with respect to HPC. The HPC eastbound bridge and non-HPC westbound bridge in San Angelo allow the unique opportunity to compare their long-term durability and structural performance side by side.

One of the expected advantages of HPC is improved durability. In order to monitor the durability of the bridges, a review of the most recent Texas Department of Transportation (TxDOT) Bridge Inventory, Inspection and Appraisal Program (BRINSAP) reports (and later Texas Bridge Inspection Reports, which replaced BRINSAP) was made before every annual inspection of the bridges. As part of this inspection, visual observations of the concrete were made and documented with photographs and drawings. The deck concrete was also tested for chloride penetration.

The data acquisition evaluations included recording readings from embedded gauges and monitoring the status of all gauges and the condition of the DAS. In this report, an evaluation of the status of the DAS is made and possible improvements are recommended. By observing the performance of the DAS, field-tried recommendations can be implemented for future long-term monitoring projects.

It should be noted that the emphasis of this report on the structural performance and data acquisition occurred earlier in the project, since most of the structural changes occurred in the early ages of the bridges. Existing durability issues are discussed in this report, but many durability issues cannot be addressed completely since important symptoms may have not yet be manifested and will hopefully only occur much later in the life of these structures. The data acquisition and method of deflection measurement are emphasized because they provide the data by which the research team analyzed the structural performance.

1.3 OUTLINE OF THIS REPORT

This chapter has introduced the material covered in this report. Chapter 2 provides a literature review of relevant material. Chapter 3 describes the Texas HPC bridges monitored in this project. Chapter 4 describes the test program, and its results are presented in Chapter 5. Chapter 6 discusses the results from the test program. Chapter 7 offers a summary of the findings and conclusions from the research. **[Note: see Appendices A, C, and D in 7-2941-5 for additional, finalized information.]**

CHAPTER 2: Literature Review

2.1 INTRODUCTION

The literature was reviewed to determine appropriate definitions for high performance concrete. Over the years, numerous definitions have been proposed and refined, but only the most relevant have been included in Section 2.2. Section 2.3 reviews research regarding prestress loss and camber. Codes and specifications are reviewed, and several methods for predicting prestress loss and camber are presented in Section 2.4. The literature reviewed in this chapter is not exhaustive given the wealth of information on some of the topics, but serves as an introduction to the work performed in this study.

2.2 DEFINITION OF HIGH PERFORMANCE CONCRETE

Today high performance concrete (HPC) is most simply described as a concrete possessing some characteristic that distinguishes it as superior to normal concrete in a given application. Normal concrete can be defined as any concrete made using local materials, without the benefit of high range water reducers or other admixtures. In recent years, many definitions have been proposed. This section discusses some of those definitions.

The Strategic Highway Research Program (SHRP) developed one of the earlier definitions of high performance concrete in their 1991 state-of-the-art report by Zia, Leming, and Ahmad [21]. They defined HPC based on three criteria: (1) maximum water/cement ratio of 0.35, (2) minimum durability factor of 80 percent, and (3) minimum strength criteria of either: (a) 3,000 psi within 4 hours, (b) 5,000 psi within 24 hours, or (c) 10,000 psi within 28 days. The three strength criteria are described as very early strength (VES), high early strength (HES), and very high strength (VHS), respectively.

In 1996, the Federal Highway Administration (FHWA) defined HPC for highway structures. The proposed definition consists of four durability characteristics (freeze-thaw durability, scaling resistance, abrasion resistance, and chloride penetration) and four strength characteristics (compressive strength, modulus of elasticity, shrinkage, and creep). Goodspeed, Vankikar, and Cook [9] provide details on performance criteria, standard tests to evaluate performance, and recommended relationships between performance and exposure conditions for each of the eight characteristics.

Gross and Burns [10] proposed a broad and general definition of HPC in 1998, incorporating many of ideas proposed by the previously mentioned definitions. They defined HPC as follows:

HPC is an engineered concrete whose components are carefully selected and proportioned to produce a material with beneficial properties suitable for a specific application. Beneficial properties may be related to any number of strength and/or durability characteristics, dependent upon the given application.

2.3 SOURCES OF LONG-TERM PRESTRESS LOSS

Prestress losses occur due to a number of phenomena. Sources of prestress loss can be divided into two categories. Instantaneous losses, such as elastic shortening, anchorage set, and friction occur immediately after the prestressing strands have been cut. The time at which the strands are cut may be referred to as transfer. Time-dependent losses, such as creep and

shrinkage of concrete and relaxation of steel, vary during the life of the structure. All of these phenomena are discussed in detail by several texts [14, 16], and are summarized in this section.

2.3.1 Instantaneous Losses

Instantaneous losses include elastic shortening of the concrete, anchorage set, and friction. All of these losses occur when the tension carried by the strands is transferred to the concrete member.

Once the prestressing strands have been cut, the tension in the strands is transferred to the concrete. This causes a compressive force to act on the member. Due to the typical eccentricity of the strands, a compression force forms in the bottom of the beam and a tension force in the top. *Elastic shortening* occurs due to the compressive force. The change in stress of the strands, or prestress loss due to elastic shortening, can be determined by the calculation shown in Equation 2.1:

$$\Delta f_{ps,ES} = \frac{E_{ps}}{E_{ci}} f_{cgp} \quad 2.1$$

where $\Delta f_{ps,ES}$ = prestress loss due to elastic shortening

E_{ps} = modulus of elasticity of prestressing steel

E_{ci} = modulus of elasticity of concrete at time prestress is applied

f_{cgp} = stress in concrete at the center of gravity of the prestressing steel
due to self-weight and prestress force

A detailed analysis can be carried out to determine the exact theoretical loss, using the transformed section and the jacking force. However, it is commonly accepted to use gross section properties and estimate the prestress force after transfer, P_0 [14]. The stress in the concrete at the center of gravity of the prestressing strands is:

$$f_{cgp} = \frac{P_0}{A_g} + \frac{P_0 e^2}{I_g} - \frac{M_{sw} e}{I_g} \quad 2.2$$

where P_0 = prestress force after release

e = eccentricity of the prestressing steel

A_g = area of the beam based on gross section properties

I_g = moment of inertia base on gross section properties

M_{sw} = moment due to the self-weight of the beam

As Equation 2.2 shows, this stress is the result of the prestress force and the self-weight of the beam.

Instantaneous losses due to *friction* and *anchorage set* are most significant in post-tensioned members. They are typically compensated for by overstressing the strands. Friction loss is the sum of two components, caused by the wobble factor of the duct and the intentional curvature of draped strands. Coefficients accounting for these effects have been developed and can be found in the ACI Building Code Commentary [4]. The loss in prestress due to friction can be expressed as:

$$\Delta f_{ps,FR} = f_{pj} (1 - e^{-(KL + \mu\alpha)}) \quad 2.3$$

where $\Delta f_{ps,FR}$ = prestress loss due to friction

f_{pj} = stress in the strands due to jacking

K = wobble coefficient

L = distance of strand from jack

- μ = curvature coefficient
 α = total angle change of the strand path from jacking end

The derivation of Equation 2.3 is carried out in the texts [14, 16]

Anchorage set, also referred to as anchorage slip or take-up, is caused by the sudden application of the jacking force to the selected anchorage type holding the strands. This loss can be calculated using Equation 2.4.

$$\Delta f_{ps,AN} = \frac{\Delta L}{L} E_{ps} \quad 2.4$$

where $\Delta f_{ps,FR}$ = prestress loss due to friction
 ΔL = amount of slip
 L = length of the prestressing steel

The significance of anchorage slip decreases with long members, because the amount of slip, ΔL , is independent of the strand length, L .

2.3.2 Time-Dependent Losses

Time-dependent losses include losses due to creep and shrinkage of concrete, and relaxation of the prestressing steel. These losses are difficult to calculate because they vary with time and are interdependent.

Shrinkage is defined as the decrease in volume of concrete with time. The loss in volume is caused by loss of moisture and chemical changes in the concrete. A large amount of shrinkage occurs early, and the total shrinkage is approached asymptotically. As the concrete member shortens due to the decrease in volume, the prestressed steel decreases in length as well. This causes a reduction in the prestress force.

Creep is defined as the time-dependent increase in strain of concrete under a sustained stress or load. The rate of creep rapidly increases initially, but eventually reaches a constant asymptotically. Creep need only be considered for prestress loss beginning with transfer for pretensioned beams, and after tensioning in post-tensioned beams. Stress changes due to creep can be measured by comparing the stress in the concrete before and after a load has been applied. This change in stress can be used to determine the prestress loss due to creep.

Farrington, Burns, and Carrasquillo [8] investigated creep and shrinkage of the HPC mixes used in the Texas HPC Bridges. The measured data were compared to the prediction methods suggested by ACI Committee 209 [3]. The study found the ultimate shrinkage strain and the ultimate creep coefficient of HPC were 55% and 60% lower, respectively, than the amount suggested by the ACI Committee 209 report.

Relaxation is defined as the gradual reduction of stress in the prestressing steel with time due to sustained strain. Strain change in the prestressing steel is caused by a reduction in length due to creep and shrinkage. Here the interdependence of the time-dependent factors can be seen. The prestress loss due to relaxation depends on the strength of the strands and amount of initial stressing as well as the type of strand.

2.4 PREDICTING LONG-TERM PRESTRESS LOSS

Knowing prestress loss is seldom important with regards to design strengths. However, prestress loss does play an important role in service conditions, such as camber, deflection, and cracking. The amount of prestress must be properly balanced with loads, in order to achieve the

desired slight upward camber. An upward camber is largely desired for its aesthetic appeal. It is typical to think an overestimation is conservative. This is not true for prestress loss. A high estimate may result in tensile forces in the member at service load and cracking may occur. In addition, excessive camber in a series of simply supported beams can lead to an uncomfortable and bumpy ride for vehicular traffic.

Many methods for predicting prestress loss have been suggested. Methods suggested by the *AASHTO LRFD Bridge Design Specifications* [2] and the *PCI Design Handbook* [17] are described in Sections 2.4.3, 2.4.4, and 2.4.5. These methods are for pretensioned members and cannot be applied to the pretensioned/post-tensioned San Angelo eastbound HPC beams without modification. The loss due to post-tensioning was incorporated in the elastic shortening component [10]. This simplification allows prestress losses in these complex beams to be compared to the simple prediction methods presented in the *AASHTO LRFD Bridge Design Specifications* [2] and the *PCI Design Handbook* [17]. Variable names may have been altered from their appearance in the literature in order to make comparison of the methods simpler. In addition, numerical values for constants may have been substituted in cases where the value was constant for all beams studied in this program.

2.4.1 Incremental Time-Step Method

Time-step methods calculate prestress loss at time intervals throughout the life of the member. The prestressing force for each step is taken as the end result of the previous step. The number and length of the steps depends on the desired accuracy. Typical time steps include: at the time of prestressing, the time when a member is subjected to new loads, at an age of one year, and at the end of service life [18]. Computer programs are often employed when high accuracy and therefore a large number of time-steps are required. Gross has developed a time-step program capable of analyzing both the AASHTO Type IV I-beams and TxDOT U54 U-beams [10, 12].

2.4.2 Actual Beam Designs

Prestress loss was calculated during the actual beam design by TxDOT engineers. Two programs were used to predict long-term prestress losses. ADAPT-ABI [1] was used to predict losses in the San Angelo eastbound I-beams. ADAPT-ABI is a commercial program developed by the ADAPT Corporation that employs a time-step process to determine prestress loss. PSTRS14 [20] was used to predict losses in the San Angelo westbound I-beams and the Louetta U-beams. PSTRS14 is a design and analysis program developed by TxDOT.

2.4.3 AASHTO LRFD Time-Dependent Lump Sum Method

The AASHTO LRFD Time-Dependent Lump Sum Method [2] is the sum of two components. It is the combination of losses due to elastic shortening and a lump sum estimate for time-dependent losses, as shown in Equation 2.5:

$$\Delta f_{ps,total} = \Delta f_{ps,ES} + \Delta f_{ps,TD} \quad 2.5$$

where $\Delta f_{ps,total}$ = total prestress loss

$\Delta f_{ps,TD}$ = time-dependent prestress loss

Elastic shortening losses are predicted using Equation 2.1. As discussed in Section 2.3.1, the prestress force in equation 2.2 is often calculated using an assumed value. The AASHTO LRFD Time-Dependent Lump Sum Method recommends the prestress force may be calculated

using an assumed prestressing steel stress of seventy percent of the ultimate strength of prestressing steel, $0.70 f_{pu}$, for low relaxation strands.

Time-dependent losses are predicted using a single equation, depending on the type of beam section. These lump sum estimates have been developed from trends observed in a time-step computer analysis for a large number of bridges [2]. For members with no mild steel reinforcement using 270 ksi low relaxation strands, such as those in the Texas HPC Bridges, the time-dependent losses in ksi are predicted as:

$$\Delta f_{ps,TD} = 33.0 \left[1.0 - 0.15 \frac{f'_c - 6.0}{6.0} \right] \quad 2.6$$

and

$$\Delta f_{ps,TD} = 19 \quad 2.7$$

for I-beams and U-beams, respectively. The 28-day compressive strength of the concrete is given as f'_c .

2.4.4 AASHTO LRFD Component Method

The AASHTO LRFD Component method [2] is the sum of four components and is intended to lead to a better estimate of time-dependent losses than the lump sum used in the AASHTO LRFD Time-Dependent Lump Sum method. Total prestress loss is given by Equation 2.8:

$$\Delta f_{ps,total} = \Delta f_{ps,ES} + \Delta f_{ps,SH} + \Delta f_{ps,CR} + \Delta f_{ps,RE} \quad 2.8$$

where $\Delta f_{ps,SH}$ = prestress loss due to shrinkage

$\Delta f_{ps,CR}$ = prestress loss due to creep

$\Delta f_{ps,RE}$ = prestress loss due to relaxation

Note that the three time-dependent terms (shrinkage, creep, and relaxation) are now calculated separately, as opposed to a single lump sum.

Loss due to elastic shortening of the concrete is calculated as described in Section 2.4.3. Shrinkage loss is based on the average annual ambient relative humidity RH, which can be obtained from local weather statistics or from figures in the *AASHTO LRFD Bridge Design Specifications* [2].

$$\Delta f_{ps,SH} = 17.0 - 0.015 RH \quad 2.9$$

Prestress loss due to creep is estimated as

$$\Delta f_{ps,CR} = 12.0 f_{cgp} - 7.0 \Delta f_{cdp} \quad 2.10$$

where f_{cdp} = the stress in concrete at the center of gravity of pretensioned strands due to applied loads not acting at release

The two stresses in Equation 2.10 are calculated at the same section. Note that at this point the beam and deck are acting compositely to resist loads carried by the bridge.

Loss due to the relaxation of steel is estimated as the sum of losses at transfer and after transfer:

$$\Delta f_{ps,RE1} = \frac{\log(24.0t)}{40.0} \left[\frac{f_{pj}}{f_{py}} - 0.55 \right] f_{pj} \quad 2.11$$

$$\Delta f_{ps,RE2} = 20.0 - 0.4 \Delta f_{ps,ES} - 0.2 (\Delta f_{ps,SH} + \Delta f_{ps,CR}) \quad 2.12$$

where t = time in days between stressing and transfer

f_{pj} = stress in the prestressing strand at the end of stressing

f_{py} = yield strength of the prestressing strand

The stress at the end of stressing may be taken as $0.80 f_{pu}$.

2.4.5 PCI Design Handbook Method

The PCI Design Handbook method [17] is based on the work of a task group sponsored by ACI-ASCE Committee 423, Prestressed Concrete [22]. The PCI Design Handbook method estimates prestress loss as the sum of the same four components in the AASHTO LRFD Component method shown in Equation 2.8. However, the components are calculated using a different set of equations. The *PCI Design Handbook* points out this method is intended for common design conditions, and therefore may be insufficient for HPC beams. A more detailed analysis is suggested for unusual designs or structures.

Elastic shortening is the same as Equation 2.1. However, it indirectly recommends taking the prestress force after transfer as 90 percent of the initial prestress force after anchorage losses ($P_0 = 0.90 P_i$).

Loss due shrinkage incorporates the volume to surface ratio, V/S , in addition to the average ambient relative humidity as shown in Equation 2.13.

$$\Delta f_{ps,SH} = (8.2 \times 10^{-6}) E_{ps} \left(1 - 0.06 \frac{V}{S} \right) (100 - RH) \quad 2.13$$

Creep prestress loss for normal weight concrete is:

$$\Delta f_{ps,CR} = 2.0 \frac{E_{ps}}{E_c} (f_{cgp} - f_{cdp}) \quad 2.14$$

where the calculation of f_{cdp} is based on gross section properties.

Similar to the AASHTO LRFD Component method, prestress loss from relaxation is calculated using the other components. Equation 2.15 gives the loss due to relaxation using 270 ksi low relaxation strands initially stressed to $0.75 f_{pu}$.

$$\Delta f_{ps,RE} = 5.0 - 0.040 (\Delta f_{ps,ES} + \Delta f_{ps,SH} + \Delta f_{ps,CR}) \quad 2.15$$

2.4.6 Suggested Method

A suggested method for calculating long-term prestress loss was presented by Gross and Burns [10], and a thorough discussion of the shortcomings of other prediction methods is presented by the authors. Their suggested method is a component method similar to the AASHTO LRFD Component and *PCI Design Handbook* methods. However, refinements have been made and the suggested method uses measured material properties. It predicts prestress loss as the sum of five components.

$$\Delta f_{ps,total} = \Delta f_{ps,ES} + \Delta f_{ps,SH} + \Delta f_{ps,CR} + \Delta f_{ps,RE} + \Delta f_{ps,PR} \quad (2.16)$$

The fifth term accounts for losses that occur before release of the strands due to relaxation and thermal effects.

Elastic shortening loss should be calculated according to Equation 2.1, where the prestressing force is calculated using f_{po} equal to $0.90 f_{pj}$.

Prestress loss caused by creep takes the following form:

$$\Delta f_{ps,CR} = K_{cr} \frac{E_{ps}}{E_c} (f_{cgp} - f_{cdp}) \quad (2.17)$$

K_{cr} is a constant, which can be adjusted by any common method based on the volume-to-surface ratio of the beam and the average ambient relative humidity.

The suggested method uses the same equation for relaxation loss as the *PCI Design Handbook* [17].

The fifth term is a combination of relaxation loss before transfer and losses due to thermal effects. These losses are expressed in Equation (2.18).

$$\Delta f_{ps,PR} = \frac{\log(24t)}{45} \left[\frac{f_{pj}}{f_{py}} - 0.55 \right] f_{pj} + \frac{1}{3} E_{ps} \alpha_{ps} \Delta T \quad (2.18)$$

where α_{ps} = coefficient of thermal expansion of prestressing strands

ΔT = change in temperature between peak hydration and stressing

It is suggested that the change in temperature should be estimated based on past experience. The reported change in temperature for beams in this project was about 60° F.

2.5 SOURCES OF LONG-TERM CAMBER

Camber is essentially a function of the upward deflection caused by the eccentricity of the prestressing force, and the downward deflection caused by loads. Initial camber is easily calculated using moment-area theory. The initial camber is simply a function of the deflection owing to prestressing force and the deflection due to self-weight of the member. Instantaneous deflections caused by additional loads, such as the weight of the slab and parapets, can be determined using classical methods of mechanics.

Determining long-term camber becomes far more difficult. As discussed in Section 0, prestress losses are time-dependent. Camber is highly dependent on the prestress force; therefore, camber is time-dependent as well. Another difficulty is caused by the increased strength concrete gains with time.

2.6 PREDICTING LONG-TERM CAMBER

The literature provides few procedures for predicting long-term camber. The *AASHTO LRFD Bridge Design Specifications* [2] mentions calculating camber, but no guidelines are given. ACI 318 [4] provides an estimate of long-term deflection for non-prestressed, reinforced concrete members based on multiplying the initial camber by a factor. No multiplier is provided for prestressed concrete. The *PCI Design Handbook* [17] suggests a set of multipliers as a guide to estimate long-term camber. This estimate of long-term camber is determined by multiplying the instantaneous elastic deformations caused by the prestress force and loads by a set of constants. Equation (2.19) presents the *PCI Design Handbook* calculation of long-term camber:

$$\Delta_{long-term} = 2.20\Delta_{ps} - 2.40\Delta_{sw} - 3.00\Delta_{sdl} - 2.30\Delta_{ct} \quad (2.19)$$

where Δ_{ps} = deflection due to the prestressing force,

Δ_{sw} = deflection due to the self-weight of the member at transfer,

Δ_{sdl} = deflection due to the superimposed dead load, and

Δ_{ct} = deflection due to the composite topping

Numerous computer programs have been developed to determine long-term camber. The use of a computer makes the complex calculations of time-dependent behavior much easier. The two programs used in the TxDOT design of the Texas HPC beams, ADAPT-ABI [1] and

PSRTS14 [20], were both used to predict long-term prestress. These programs were discussed in Section 0. Gross and Burns [10] developed a time-dependent program capable of predicting long-term camber of the Texas HPC beams. This program was based on the work of Byle and Burns [5].

2.7 PREVIOUS DURABILITY MONITORING

Shepperd and Burns [19] reported on the early results of long-term monitoring of the Louetta Road Overpass, as mentioned in Chapter 1. Their report focused on the durability aspects of the bridge. The report discusses visual inspections, testing on core drilled cylinders, petrographic examinations, and chloride content evaluations. Testing of the cylinders included carbonation, compressive strengths, and chloride ion permeability. Only the results that are related to the limited durability testing performed during this project are summarized below.

The deck cracking was first discovered during an annual inspection performed by researchers in July 1998 [19]. At that time, the cracking patterns were recorded and transferred to AutoCAD for analysis. Cracks were measured in the longitudinal and transverse directions in terms of linear feet. Table 2.1 lists the result of the crack mapping. The crack lengths for longitudinal and transverse cracking are shown for the northbound and southbound bridges. Both cast-in-place decks are considered HPC, but the compressive strengths are 4,000 and 8,000 psi for the northbound and southbound decks, respectively. Compressive strengths for all portions of the bridges can be found in Table 3.1.

Shepperd and Burns [19] found that cracking in the longitudinal and transverse directions corresponded to the flanges and ends, respectively, of the U-beams. A suggested cause of the longitudinal cracking was inadequate bearing conditions of the precast panels. The transverse cracks were attributed to improper installation of control joints. The skew of the control joints did not properly align with the skew of the bridge. The largest crack width was reported as 0.01 in. This width was observed in numerous locations.

Table 2.1 Crack Mapping Summary [19]

Span	Cracking (ft)	
	Longitudinal	Transverse
<i>Louetta Northbound Normal Strength</i>		
N1	65	25
N2	280	95
N3	190	95
Total	535	215
<i>Louetta Southbound High Strength</i>		
S1	185	65
S2	1005	90
S3	510	55
Total	1700	210

The visual inspection of the underside of the bridge revealed some minor problems. Cracking and spalling were detected around the drain ports in the beams. Hairline cracks were

detected in the flanges of six beams. The precast panels were observed to be in good shape. Cracking and efflorescence was detected along the column line in the cast-in-place deck.

Chloride penetration testing was performed on the northbound and southbound decks. This testing method is described in Section 4.2.3. The chloride content was negligible at all levels.

CHAPTER 3: Structural HPC Bridge Descriptions and Data Acquisition System

3.1 INTRODUCTION

This chapter provides a description of the two HPC earliest bridges studied in this project. They were uniquely constructed, because of their specially designed HPC beams, and, due to structural interests, they were the original focus of the monitoring activities. Later bridges in Lubbock and Amarillo were monitored only for HPC deck durability, and a description of each of these bridge locations is presented in the appendix in report 7-2941-5.

The Louetta Road Overpass is discussed first. A description of the bridge layout is presented as well as information on the TxDOT U54 Beam.

The description of the North Concho River/US 67/ South Orient Railroad Overpass is next. Details on AASHTO Type IV I-beams are given.

A description of the instrumentation and data acquisition system (DAS) used on these two bridges is presented. Adjustments made to the DAS to allow for remote monitoring are discussed. A discussion of the long-term durability of the different gauges used in DAS concludes the chapter. Details on how the instrumentation was used are presented in Chapter 4.

3.2 LOUETTA ROAD OVERPASS

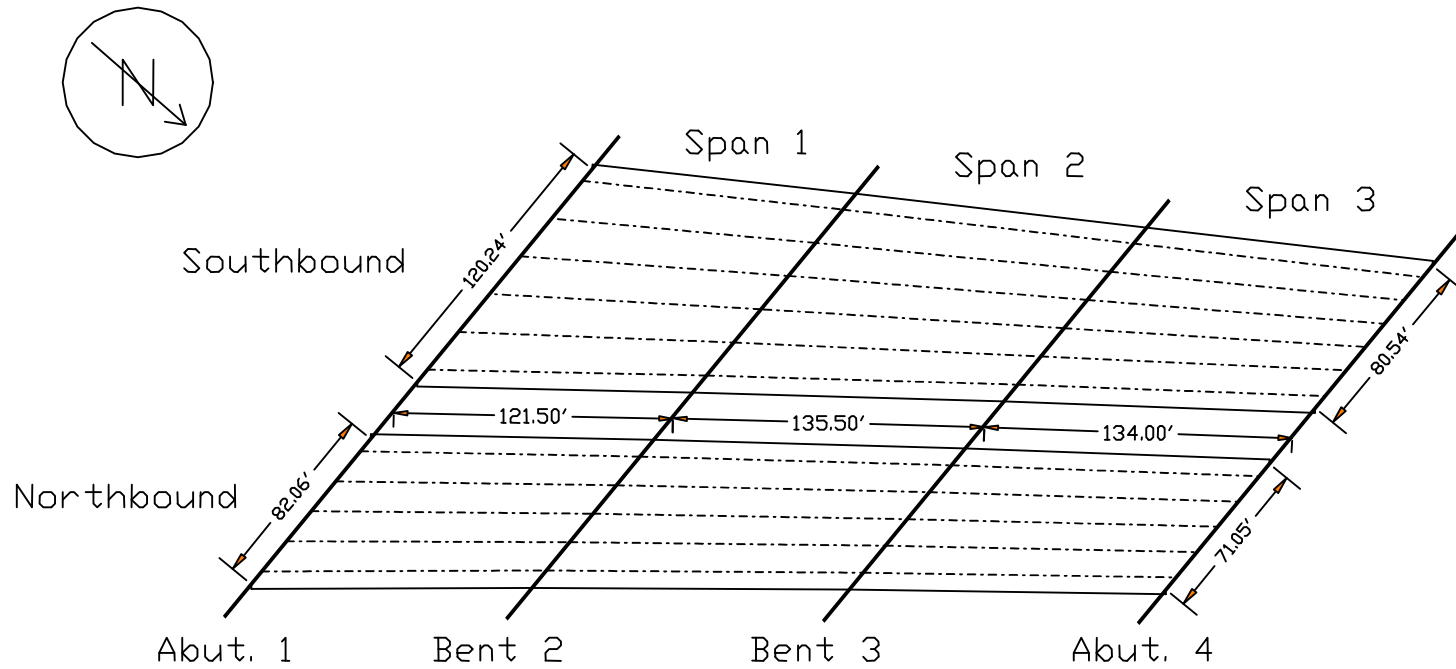
3.2.1 General Description

The Louetta Road Overpass on State Highway 249 is located on the northwest side of Houston, Texas. The overpass is shown in Figure 3.1. The construction of the overpass was part of a 3.0 mile highway improvement project upgrading SH 249 from a four-lane roadway at grade road to an eight-lane freeway. The overpass is 391 ft long, consisting of adjacent northbound and southbound bridges, each with three spans measuring 121.5 ft, 135.5 ft, and 134.0 ft along the centerline of the structure. The overpass was originally planned to carry three lanes of traffic in each direction, northbound and southbound. Before the bridge was open to traffic, both directions were expanded by one lane. The final bridge layout has seven beams in the southbound direction and six beams in the northbound direction. The southbound bridge was built to accommodate an exit ramp, which accounts for the extra beam and larger clear width. The clear width was measured prior to the widening. A plan view of the Louetta Road Overpass is shown in Figure 3.2. Note that the bridge was built with a skew resulting in varying beam lengths.



Figure 3.1 Louetta Road Overpass

The bridge decks are made up of prestressed panels with a cast-in-place topping. The deck is supported by prestressed Texas U-beams, which in turn are simply supported by single piers. The U-beam and pier combination was considered a more aesthetically pleasing option than the typical I-beam, bent cap, and column system. All components of the Louetta Road Overpass are HPC. Table 3.1 lists the design compressive strengths of the different components of the northbound and southbound Louetta Road Overpass bridges. The northbound deck is normal strength HPC.



LOUETTA ROAD OVERPASS (prior to widening)

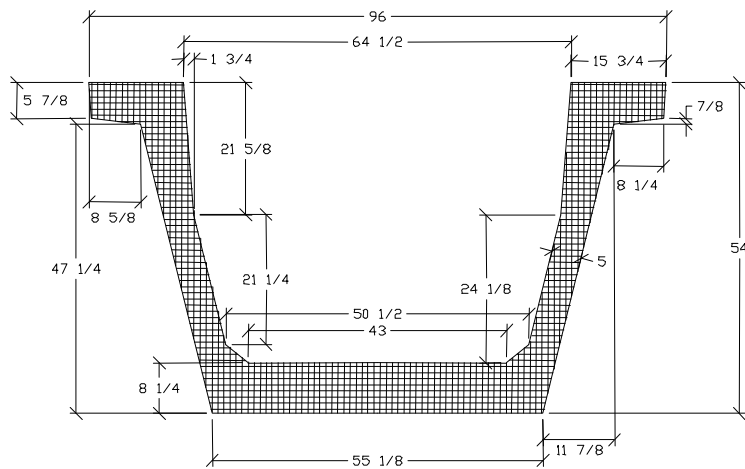
Figure 3.2 Plan View of Louetta Road Overpass [10]

Table 3.1 Design Compressive Strengths for Louetta Road Overpass

Element	Compressive Strength (psi)	
	Northbound	Southbound
U-Beams		
At Transfer	6,900 - 8,800	6,900 - 8,800
At 56 Days	9,800 - 13,100	9,800 - 13,100
Piers	10,000	10,000
CIP Deck	4,000	8,000
Prestressed Panels	8,000	8,000

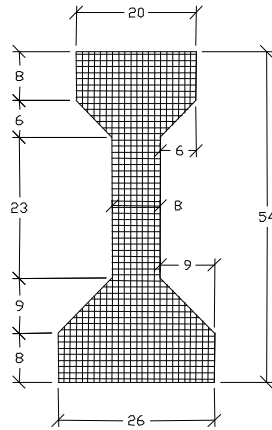
3.2.2 TxDOT U54 Beam

The pretensioned beam used throughout the Louetta Road Overpass was the newly developed TxDOT U54 Beam. The beam is trapezoidal in cross section with an open top. The beam is 54 in. deep, 8 ft across the top, and 4.59 ft across the bottom. The webs are 5 in. thick and the bottom flange is 6.25 in or 8.25 in. thick for the U54A and U54B beams, respectively. The only difference between the two U54 beams is the thickness of the bottom flange, with the U54A allowing for another row of prestressing strands. The beam and its complete dimensions are shown in Figure 3.3. The strand patterns are shown in Figure 3.4. Note that this is a possible strand pattern and not necessarily indicative of all of the beams in this project. Transfer and development length tests were performed to gain approval to use 0.6 in. diameter prestressing strands at 2 in. spacing [11]. A more extensive description of the TxDOT U-beam can be found in Byle and Burns [5] and Gross and Burns [10]. These reports provide such details as strength, strand pattern, and debonding length for each beam in the bridge.



Texas U54B

Note: Texas U54A Beam is same as above, except for 6 1/4 in. bottom flange.



AASHTO Type IV

All units in inches. (1 in. = 25.4 mm)

Figure 3.3 Cross-Section Dimensions of Texas HPC Beams [adapted from 10]

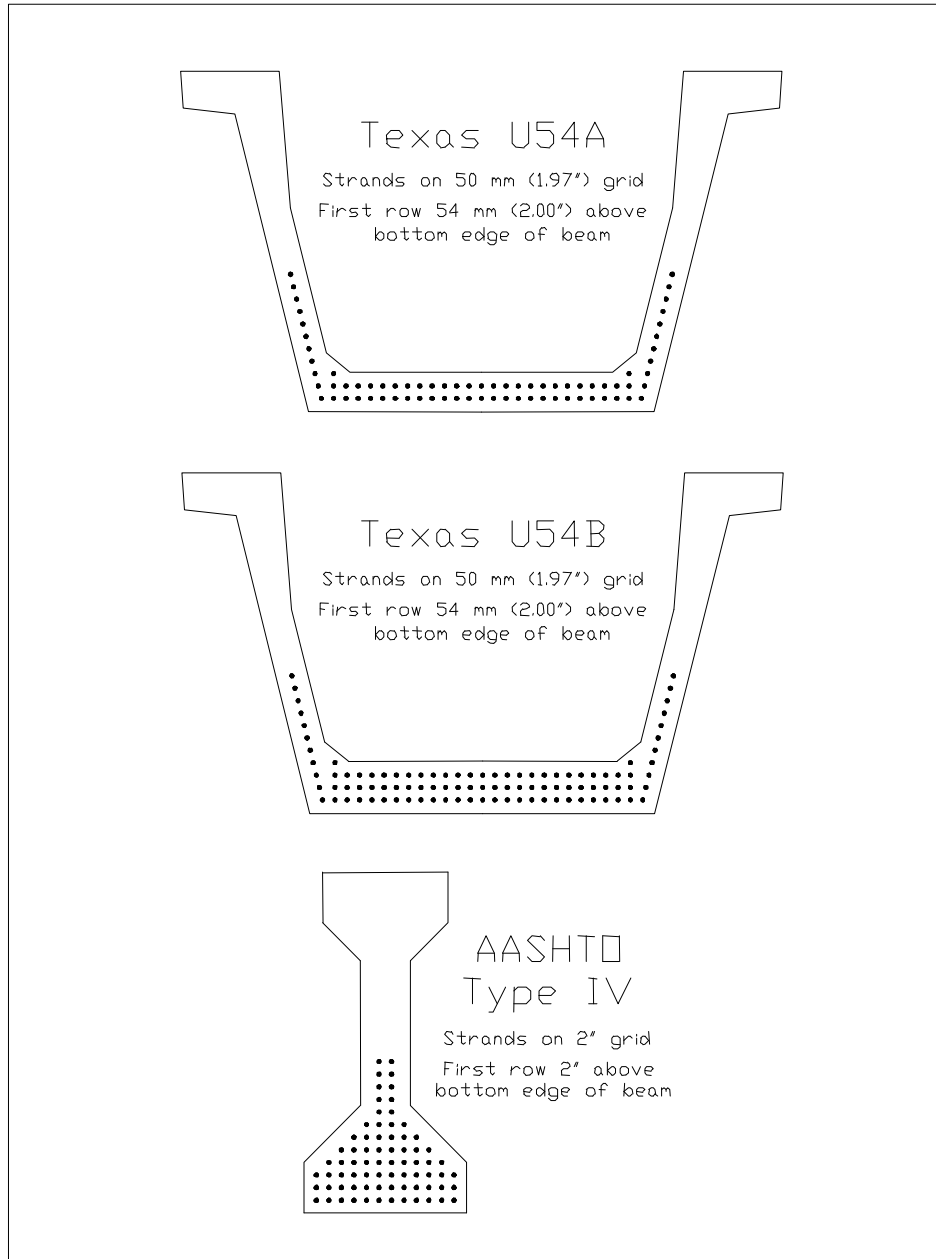


Figure 3.4 Strand Pattern of Texas HPC Beams [adapted from 10]

3.3 NORTH CONCHO RIVER/US 87/SOUTH ORIENT RAILROAD OVERPASS

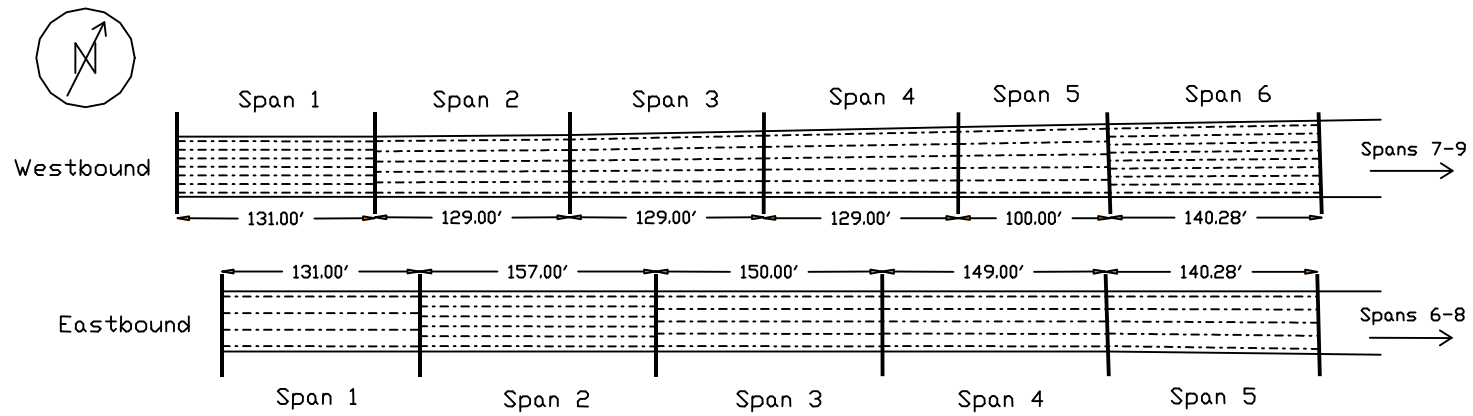
3.3.1 General Description

The North Concho River/US 87/South Orient Railroad Overpass on US 67 is centrally located in San Angelo, Texas. The US 67 bridges are adjacent multispan bridges. The bridges are shown in Figure 3.5. The eastbound bridge is eight spans and the westbound bridge is nine spans. Span lengths as well as beam spacings vary in both bridges. These dimensions are shown in the plan view of the San Angelo bridges in Figure 3.6. The bridge decks are made of prestressed, precast panels with a cast-in-place topping. AASHTO Type IV beams support the deck. The

beams are simply supported on bent caps, which are carried by single open-faced piers. These piers can be seen in Figure 3.5.



Figure 3.5 North Concho River/US 87/South Orient Railroad Overpass [10]



NORTH CONCHO RIVER/U. S. 87/S. O. R. R. OVERPASS (San Angelo)
(Only Main Spans Shown)

Figure 3.6 Plan View of North Concho River/US 87/South Orient Railroad Overpass [10]

All components, including the cast-in-place deck, prestressed panels, and girders of the eastbound bridge are made with HPC. The cast-in-place deck in spans 1-5 of the westbound bridge is HPC. The cast-in-place deck in spans 6-9 and all prestressed panels and girders are normal concrete. The design compressive strengths of the components of the two San Angelo bridges are given in Table 3.2.

Table 3.2 Design Compressive Strengths for San Angelo Bridges

Element	Compressive Strength (psi)	
	Eastbound	Westbound
I-Beams		
At Transfer	8,900 - 10,800	4,020 - 6,560
At 56 Days	10,900 - 14,700	5,000 - 8,920
Piers	6,000	3,600
Pier Cap	8,000	8,000
CIP Deck	6,000	4,000
Prestressed Panels	6,000	5,000

3.3.2 AASHTO Type IV I-Beam

AASHTO Type IV prestressed concrete I-beams are predominately used in the San Angelo bridges. Texas Type B prestressed concrete I-beams are used in the eighth span of the eastbound bridge. However, none of these beams were instrumented. The Type IV beams are 54 in. deep, 26 in. across the bottom flange, and 20 in. across the top flange. The web is 8 in. thick. The dimensions of the AASHTO Type IV I-beam are shown in Figure 3.3. The beams utilize both straight, pretensioned strands and draped, post-tensioned strands. The pretensioned strands are 0.6 in. in diameter and spaced on a 2 in. grid. The post-tensioned strands are carried in two ducts. The pretensioned strand pattern is shown in Figure 3.4. Note that this is a possible strand pattern and not necessarily indicative of all of the beams in this project. These beams are described in detail by Gross and Burns [10].

3.4 ORIGINAL DATA ACQUISITION SYSTEM

An essential part of any research project is the DAS. The DAS is responsible for collecting and storing data. The DAS in this research program collected strains and temperatures in the beams; prestressed precast panels; and cast-in-place decks.

3.4.1 Introduction

A brief description of the original DAS is described in this section. A more detailed description can be found in Gross and Burns [10], including a description of the gauge numbering system, drawings detailing the location of every gauge in the project, schematics of a typical DAS, and a description of the installation procedures used.

Five DAS systems were custom built by Gross. A typical system consists of embedded gauges run through multiplexers, which are connected to a datalogger. The datalogger was connected to a 12-volt power supply. Two systems are located at the Louetta Road Overpass, one each for the northbound and southbound bridges. The other three systems are located at the San Angelo bridges. Two are located on the eastbound HPC bridge and the other is on the westbound

non-HPC bridge. A total of 518 gauges are embedded in various beams, precast panels, and cast-in-place concrete in the two bridge sites. Table 3.3 summarizes the location and type of gauge in each of the bridges.

Table 3.3 Summary of Gauge Location

Gauge Location	Gauge Type			Total
	ERSG	VW / TR	TC	
Louetta Northbound HPC				
Beams	59	14	12	85
CIP Deck	24	2	4	30
Louetta Southbound HPC				
Beams	49	27	24	100
Panels	0	6	4	10
CIP Deck	4	17	10	31
San Angelo Eastbound HPC				
Beams	50	35	30	115
Panels	8	4	14	26
CIP Deck	11	9	20	40
San Angelo Westbound Non-HPC				
Beams	18	14	12	44
Panels	0	4	4	8
CIP Deck	7	14	8	29
Total	230	146	142	518

Twenty-four beams were instrumented. Five beams in both the northbound and southbound Louetta Road Overpass were equipped with gauges. The eastbound and westbound San Angelo bridges have ten and four beams, respectively, equipped with gauges. The instrumented areas for the Louetta Road Overpass and the San Angelo Bridges are shown in Figures 4.1 and 4.2, respectively.

3.4.2 Gauge Types

As shown in Table 3.3, there were three types of gauges used in the DAS. A brief description of each gauge is given. Details on how the gauges were used are described in Chapter 4: Test Program.

Electrical resistance strain gauges (ERSG) were used to measure strains. These Model FLA-6-350-11-3LT strain gauges were purchased from Texas Measurements, Inc. The change in resistance of the gauge was caused by a change in length of the wire. This change in resistance was exactly proportional to the strain. These gauges have a nominal resistance of 350 ohms and were inexpensive compared to vibrating wire gauges.

Vibrating wire strain gauges (VW) were also used to measure strains. These gauges also have built-in thermistors (TR) to record temperatures. The Model EM-5 IRAD GAGE Vibrating Wire Embedment Strain Gage manufactured by Roctest, Inc. was used. These gauges work on the principle that measuring the natural frequency of a wire tensioned between two points inside concrete can be correlated to the strains in that concrete. This VW has a nominal range of 3,300

microstrain. Vibrating wire gauges are very expensive compared to other strain gauges, but they last much longer to record concrete strains. The thermistor has a temperature range of -40°F to 160°F with an accuracy of 0.5°F .

Thermocouples (TC) were used to measure temperatures. The thermocouples used in the project were manufactured by Omega Scientific, Inc., with a reported accuracy of $\pm 1.8^{\circ}\text{F}$. Specifically, a twisted Type T (copper-constantan) 20-gauge wire was used. Thermocouples measure the voltage drop between the two metals. This voltage drop can then be converted into temperatures. Thermocouples were relatively inexpensive.

3.4.3 Programming, Data Retrieval, and Data Manipulation

Programming the DAS was accomplished using PC208W [6] software provided by Campbell Scientific, Inc. The datalogger itself can be programmed directly using PC208W, via a SC12 cable connected to a COM port on a personal computer. Another option commonly used during this research project, was to upload a program from a storage module into the datalogger. Programs created on a personal computer using PC208W can be saved on a SM716 storage module. Storage modules communicated with a personal computer using an optically isolated RS232 interface. The storage modules were then taken into the field where the appropriate program was uploaded onto the datalogger using a CR10KD Keypad, also provided by Campbell Scientific, Inc. The storage module was left at the site to store data collected by the datalogger. Once the storage module was full, it was replaced with another storage module and the cycle was repeated. This process is shown schematically in Figure 3.7.

The data contained in a storage module was transferred to a comma-separated text file using PC208W. However, the raw data from the storage modules were not in useful engineering units. Therefore, a data manipulation program, SORTDTA1 [13], was written by Gross to convert the voltages and frequencies recorded by strain gauges into units of strain. The program also sorts the data into an organized format.

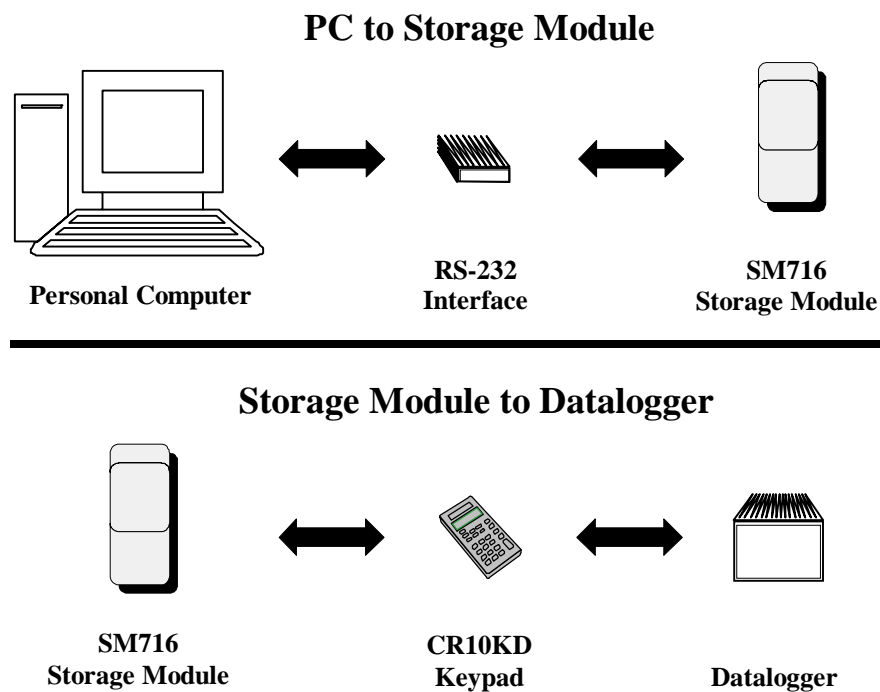


Figure 3.7 Schematic of Original Data Transfer Setup [10]

3.5 MODIFICATIONS TO DATA ACQUISITION SYSTEM

One of the major problems encountered by researchers during the research project was the amount of time and travel involved in making site visits to the two bridge sites. Therefore, establishing a remote-monitoring DAS was an important aspect of the research project.

3.5.1 Travel

Most travel consisted of day trips, although the annual visual inspections required overnight trips for both bridge sights. Day trips were favored for two reasons. They avoided the cost of an overnight stay in a hotel and were less likely to interfere with coursework members of the research team were taking. Day trips generally involved leaving early in the morning and returning in the evening or leaving in the afternoon and returning late the same night. However, overnight trips were necessary for the annual inspections in order to start work as early in the morning as possible. Another factor for early morning starts was to accommodate the work schedule of TxDOT maintenance crews required for traffic control.

Table 3.4 Travel Summary

	Louetta	San Angelo	Totals
Number of Trips ¹	12	14	26
Avg. People Travelling	1.5	1.5	
Travel Distance (Round Trip)	300	410	
Total Mileage	3600	5740	9340
Total Man-Miles	5400	8610	
Travel Time (Round Trip)	5.5	7	
Total Travel Time (Hours)	66	98	
Total Travel Man-Hours	99	147	246
Trip Time (Travel & Site Time)	7	9	
Total Trip Time (Hours)	84	126	
Total Trip Man-Hours	126	189	315
Percent of Time Travelling			78%
¹ Number of trips based on an estimate of one trip every three months after the bridge was open to traffic.			

The approximate distance and travel time to the bridge sites from Austin are shown in Table 3.4. As discussed in the next section, the storage modules and batteries had to be replaced approximately every 3 months. These tasks could easily be performed in less than 2 hours. In most cases, the amount of time spent at the bridge site was far exceeded by the time spent traveling to and from the site. Based on researchers travel records and approximate calculations, over 75 percent of the time on each trip was spent traveling. It is evident that a remote monitoring system will pay for itself in a short period of time.

3.5.2 New Equipment

New equipment was installed in summer 2001 to make remote monitoring possible. The equipment was purchased from Campbell Scientific, Inc. This equipment allowed the data retrieval method described in Section 3.4.3 to be updated. Equipment was purchased for all five of the DAS boxes, thus updating the DAS for the entire project.

3.5.2.1 Power Issues

Eight “D” cell alkaline batteries, providing 12-volts of power, powered the old DAS. These batteries had to be replaced approximately once every 3 months. A constant power supply of at least 9.6 volts had to be maintained; otherwise the DAS could suffer permanent damage. The maximum time eight “D” cell batteries could provide the minimum voltage varied slightly based on several factors. The five DAS were not identical. Therefore, the power drain varied slightly from system to system. The voltage level was checked each time the batteries were replaced. Based on personal observation, the batteries lasted longer during moderate temperatures. The voltage never dropped below 10 volts as long as they were replaced within 3 months.

A solar panel, shown in Figure 3.8, and rechargeable battery was installed to replace the alkaline battery power supply. The MSX10 Solar Panel is 17 x 11 x 1 in. and weighs only 3.3 lbs. Therefore, it could be installed safely and easily on the side of a highway. The solar panel converts sunlight into direct current. A PS12A charging regulator, shown in the upper left corner

of Figure 3.9, must be used to connect the solar panel to the sealed rechargeable battery. The battery was, in turn, connected to the DAS and provided a power supply to all data acquisition equipment.



Figure 3.8 Solar Panel Mounted on San Angelo Bent Cap



Figure 3.9 Remote-Monitoring Equipment in DAS Box

3.5.2.2 Data Retrieval

In the original DAS, data were stored in SM716 Storage Modules, which were brought back to the CMRG lab to complete the data retrieval process, as discussed in Section 3.4.3. An antenna, cell phone, and modem made remote data retrieval possible. The new equipment as it is installed in the field is shown in Figure 3.9. The cellular phone is in the upper right-hand corner of the DAS box and the modem is in the lower left-hand corner. A personal computer running PC208W software could directly communicate with the DAS in the field. A Hayes-Compatible modem could dial up the cell phone and download the data via the field modem. A schematic of the new data retrieval system is shown in Figure 3.10. A Yagi antenna, COM100 Cellular Phone

Package, and COM200 Telephone Modem were purchased from Campbell Scientific, Inc. for each DAS.

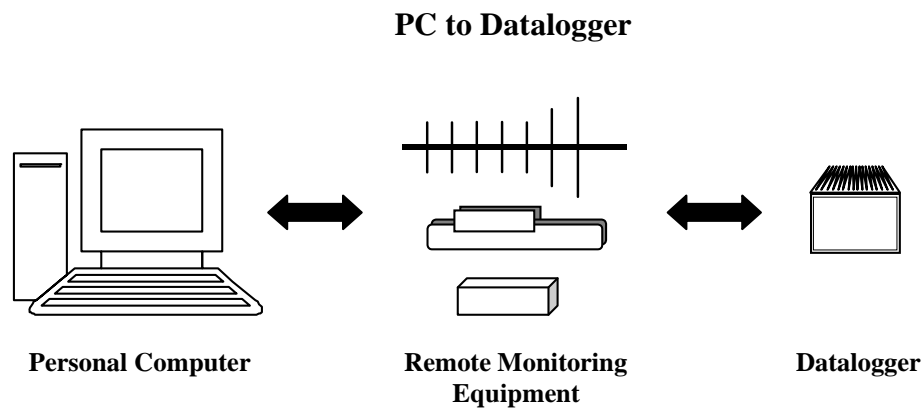


Figure 3.10 Schematic of New Data Transfer Setup

3.6 GAUGE DURABILITY

3.6.1 Introduction

Part of the long-term monitoring of these two bridges was measuring the performance of the different gauge types over the life of the bridge. A gauge durability survey was performed approximately once every year. The most recent survey was done during June 2001.

A gauge durability survey was achieved by manually looking through the data spreadsheets to determine if each of the 518 embedded gauges was still properly recording data. A gauge was deemed no longer functional, when it was no longer reading any values, reading values of -69,999 or -99,999, or the readings were erratic. It was important to keep in mind what typical values should be for the different gauge types. Temperature readings have been known to be as low as 20° F during the winter and reach as high as 131° F in the summer. Readings from strain gauges were not as intuitive as temperature readings, but typically varied between -2,000 and 2,000 microstrain. A VW/TR was considered malfunctioning if either component was no longer providing data. In most cases, the vibrating wire failed, while the thermistor continued to record accurate temperatures. In a few cases, both failed or the thermistor alone failed, while the vibrating wire continued to record strains.

Even using these guidelines, there was some subjectivity in determining the performance of a gauge. Gauges typically did not abruptly stop working. There was often a gradual decay, where the gauge occasionally read a value that did not make sense. When this occurred, a subjective decision had to be made to determine if the gauge was still producing usable data.

3.6.2 Results

Table 3.5 and Table 3.6 show both the number and percentage of gauges working in the Louetta Road Overpass and San Angelo bridges, respectively. The gauges are broken into groups by their location in the bridges. Results are given for gauges embedded in the beams, precast panels, and cast in place deck. Surveys were performed after casting; after 60 days; after 1 year;

and as of March 1998, June 1999, September 2000, and June 2001. Note that the tables first list the number of gauges still working and then the percentage of gauges still working.

Figure 3.11 graphically depicts the percentage of each gauge type still working. Also shown is the combined performance of three types of gauges. The performance for electric resistance strain gauges (ERSG), vibrating wire/thermistor (VW/TR) gauges, and thermocouples (TC) are shown in Figures 3.10, 3.11, and 3.12, respectively. The performance of each gauge is broken down by bridge. The percentage of gauges working in the northbound and southbound Louetta Road Overpass and in the eastbound and westbound San Angelo Bridge is shown.

3.6.3 Discussion

Electronic resistance strain gauges had the worst performance during long-term monitoring. VW/TR gauges performed moderately well, while thermocouples performed the best. It should be pointed out that some gauges were intentionally disconnected during the research project. This, in effect, skewed the results shown above. Twenty-one electronic resistance strain gauges were disconnected in northbound Louetta. In southbound Louetta, forty-three electronic resistance strain gauges, two VW/TR gauges, and six thermocouples were disconnected. Seven electronic resistance strain gauges were disconnected in San Angelo eastbound. No gauges were intentionally disconnected in the westbound San Angelo Bridge. Many of the gauges that were intentionally disconnected were no longer working. Other gauges were accidentally disconnected during construction.

3.6.4 Conclusions

ERSGs have not performed well during long-term monitoring. As of June 2001, only 10 percent of these gauges were still working. Even if the disconnected gauges are not included, only 17 percent of the remaining gauges continue to operate correctly. Therefore, ERSGs are not recommended for long-term monitoring.

VW/TR gauges have performed adequately. Sixty percent of these gauges remain in operation. Vibrating wire gauges are superior to ERSGs for long-term monitoring. Very few thermistors have failed. Approximately 95 percent of the thermistors still work. Therefore, the VW/TR gauge works well when measuring both strains and temperatures.

Thermocouples continue to perform well during long-term monitoring. Seventy-five percent of the thermocouples continue to operate. The thermocouples on the San Angelo Bridge eastbound did not perform as well as the other three bridges. Only eight of the thermocouples in the other three bridges are no longer working, and six of those were intentionally disconnected. It is unclear why the San Angelo Bridge eastbound did not perform as well as the other structures.

Despite the fact some gauges no longer work, enough data were still being gathered to gain useful information about the Texas HPC bridges.

Table 3.5 Gauge Durability Summary for Louetta Road Overpass

	ERSG									VW/TR									TC									Total								
	Total	Initial Hookup	After Casting	After 60 Days	After 1 Year	As of 3/98	As of 6/99	As of 9/00	As of 6/01	Total	Initial Hookup	After Casting	After 60 Days	After 1 Year	As of 3/98	As of 6/99	As of 9/00	As of 6/01	Total	Initial Hookup	After Casting	After 60 Days	After 1 Year	As of 3/98	As of 6/99	As of 9/00	As of 6/01	Total	Initial Hookup	After Casting	After 60 Days	After 1 Year	As of 3/98	As of 6/99	As of 9/00	As of 6/01
Number of Gauges																																				
Louetta NB Beams	59	49	47	31	18	6	2	2	1	14	14	13	12	7	7	5	5	3	12	11	11	11	11	12	12	12	12	85	74	71	54	36	25	19	19	16
Louetta NB CIP Deck	24	23	22	22	0	0	0	0	0	2	2	2	2	2	2	2	2	2	4	4	4	4	4	4	4	4	4	30	29	28	28	6	6	6	6	6
Louetta SB Beams	49	39	36	32	24	5	5	5	5	27	27	27	25	23	16	16	16	16	24	22	22	22	22	17	17	17	17	100	88	85	79	69	38	38	38	38
Louetta SB Panels	0	0	0	0	0	0	0	0	0	6	6	6	6	6	6	6	6	6	4	4	4	4	4	4	4	4	4	10	10	10	10	10	10	10	10	10
Louetta SB CIP Deck	4	3	3	3	0	0	0	0	0	17	15	14	14	14	14	14	14	14	10	10	10	10	10	10	10	10	9	31	28	27	27	24	24	24	24	23
Louetta NB	83	72	69	53	18	6	2	2	1	16	16	15	14	9	9	7	7	5	16	15	15	15	15	16	16	16	16	115	103	99	82	42	31	25	25	22
Louetta SB	53	42	39	35	24	5	5	5	5	50	48	47	45	43	36	36	36	36	38	36	36	36	36	31	31	31	30	141	126	122	116	103	72	72	72	71
Total	136	114	108	88	42	11	7	7	6	66	64	62	59	52	45	43	43	41	54	51	51	51	51	47	47	47	46	256	229	221	198	145	103	97	97	93
Percentages																																				
Louetta NB Beams		83	80	53	31	10	3	3	2		100	93	86	50	50	36	36	21		92	92	92	92	100	100	100	100		87	84	64	42	29	22	22	19
Louetta NB CIP Deck		96	92	92	0	0	0	0	0		100	100	100	100	100	100	100	100		100	100	100	100	100	100	100	100		97	93	93	20	20	20	20	20
Louetta SB Beams		80	73	65	49	10	10	10	10		100	100	93	85	59	59	59	59		92	92	92	92	71	71	71	71		88	85	79	69	38	38	38	38
Louetta SB Panels											100	100	100	100	100	100	100	100		100	100	100	100	100	100	100	100		100	100	100	100	100	100	100	100
Louetta SB CIP Deck		75	75	75	0	0	0	0	0		88	82	82	82	82	82	82	82		100	100	100	100	100	100	100	90		90	87	87	77	77	77	77	74
Louetta NB		87	83	64	22	7	2	2	1		100	94	88	56	56	44	44	31		94	94	94	94	100	100	100	100		90	86	71	37	27	22	22	19
Louetta SB		79	74	66	45	9	9	9	9		96	94	90	86	72	72	72	72		95	95	95	95	82	82	82	79		89	87	82	73	51	51	51	50
Total		84	79	65	31	8	5	5	4		97	94	89	79	68	65	65	62		94	94	94	94	87	87	87	85		89	86	77	57	40	38	38	36

Table 3.6 Gauge Durability Summary for San Angelo Bridges

	ERSG									VW/TR									TC									Total								
	Total	Initial Hookup	After Casting	After 60 Days	After 1 Year	As of 3/98	As of 6/99	As of 9/00	As of 6/01	Total	Initial Hookup	After Casting	After 60 Days	After 1 Year	As of 3/98	As of 6/99	As of 9/00	As of 6/01	Total	Initial Hookup	After Casting	After 60 Days	After 1 Year	As of 3/98	As of 6/99	As of 9/00	As of 6/01	Total	Initial Hookup	After Casting	After 60 Days	After 1 Year	As of 3/98	As of 6/99	As of 9/00	As of 6/01
Number of Guages																																				
San Angelo EB Beams	50	43	42	34	21	19	11	10	10	35	33	30	29	27	25	14	14	14	30	30	30	30	25	22	18	17	16	115	106	102	93	73	66	43	41	40
San Angelo EB Panels	8	8	0	0	0	0	0	0	0	4	4	4	4	4	4	4	4	4	14	12	12	12	11	11	7	7	6	26	24	16	16	15	15	11	11	10
San Angelo EB CIP Deck	11	11	11	11	11	11	4	3	0	9	8	8	8	8	8	8	7	7	20	19	19	19	19	17	17	16	15	40	38	38	38	38	36	29	26	22
San Angelo WB Beams	18	14	14	12	9	7	7	7	7	14	14	13	13	12	12	10	10	10	12	12	12	12	12	12	12	12	12	44	40	39	37	33	31	29	29	29
San Angelo WB Panels	0	0	0	0	0	0	0	0	0	4	4	4	4	4	4	4	4	4	4	4	4	4	4	4	4	4	4	8	8	8	8	8	8	8	8	8
San Angelo WB CIP Deck	7	7	6	6	0	0	0	0	0	14	9	8	8	8	8	8	8	8	8	8	8	8	8	8	8	8	8	29	24	22	22	16	16	16	16	16
San Angelo EB	69	62	53	45	32	30	15	13	10	48	45	42	41	39	37	26	25	25	64	61	61	61	55	50	42	40	37	181	168	156	147	126	117	83	78	72
San Angelo WB	25	21	20	18	9	7	7	7	7	32	27	25	25	24	24	22	22	22	24	24	24	24	24	24	24	24	24	81	72	69	67	57	55	53	53	53
TOTAL	94	83	73	63	41	37	22	20	17	80	72	67	66	63	61	48	47	47	88	85	85	85	79	74	66	64	61	262	240	225	214	183	172	136	131	125
Percentages																																				
San Angelo EB Beams		86	84	68	42	38	22	20	20		94	86	83	77	71	40	40	40		100	100	100	83	73	60	57	53		92	89	81	63	57	37	36	35
San Angelo EB Panels		100	0	0	0	0	0	0	0		100	100	100	100	100	100	100	100		86	86	86	79	79	50	50	43		92	62	62	58	58	42	42	38
San Angelo EB CIP Deck		100	100	100	100	100	36	27	0		89	89	89	89	89	89	78	78		95	95	95	95	85	85	80	75		95	95	95	95	90	73	65	55
San Angelo WB Beams		78	78	67	50	39	39	39	39		100	93	93	86	86	71	71	71		100	100	100	100	100	100	100	100		91	89	84	75	70	66	66	66
San Angelo WB Panels											100	100	100	100	100	100	100	100		100	100	100	100	100	100	100	100		100	100	100	100	100	100	100	100
San Angelo WB CIP Deck		100	86	86	0	0	0	0	0		64	57	57	57	57	57	57	57		100	100	100	100	100	100	100	100		83	76	76	55	55	55	55	55
San Angelo EB		90	77	65	46	43	22	19	14		94	88	85	81	77	54	52	52		95	95	95	86	78	66	63	58		93	86	81	70	65	46	43	40
San Angelo WB		84	80	72	36	28	28	28	28		84	78	78	75	75	69	69	69		100	100	100	100	100	100	100	100		89	85	83	70	68	65	65	65
TOTAL		88	78	67	44	39	23	21	18		90	84	83	79	76	60	59	59		97	97	97	90	84	75	73	69		92	86	82	70	66	52	50	48

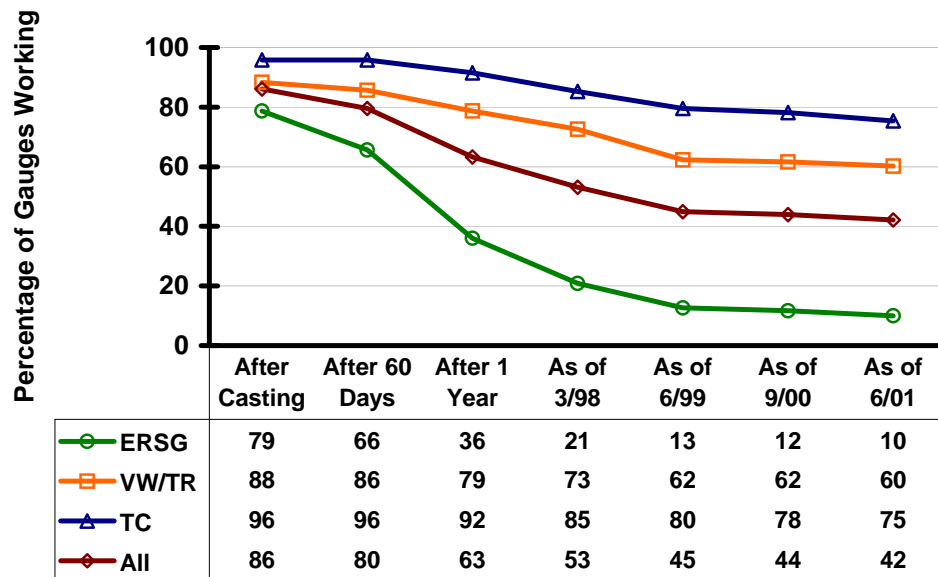


Figure 3.11 Percentage of Gauges Working

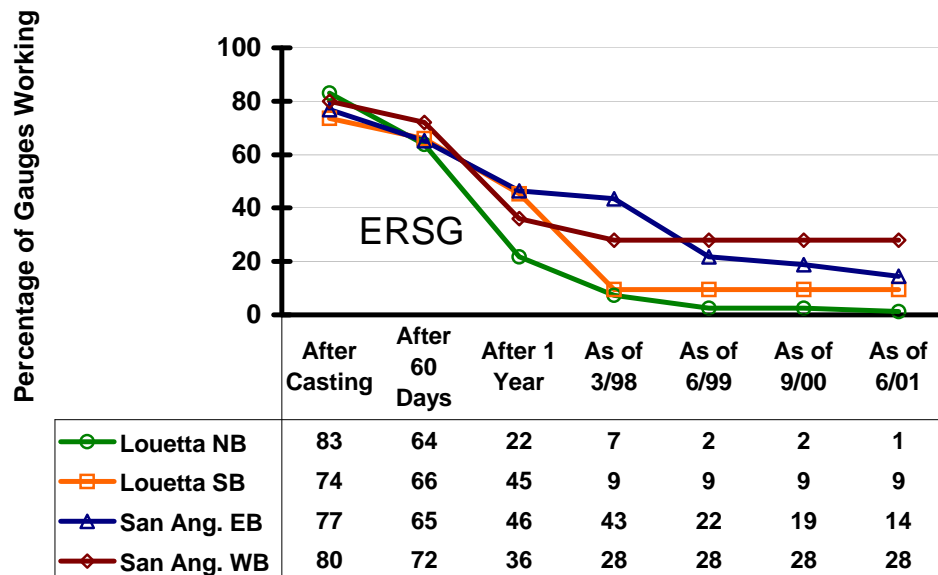


Figure 3.12 Percentage of ERSG Gauges Working

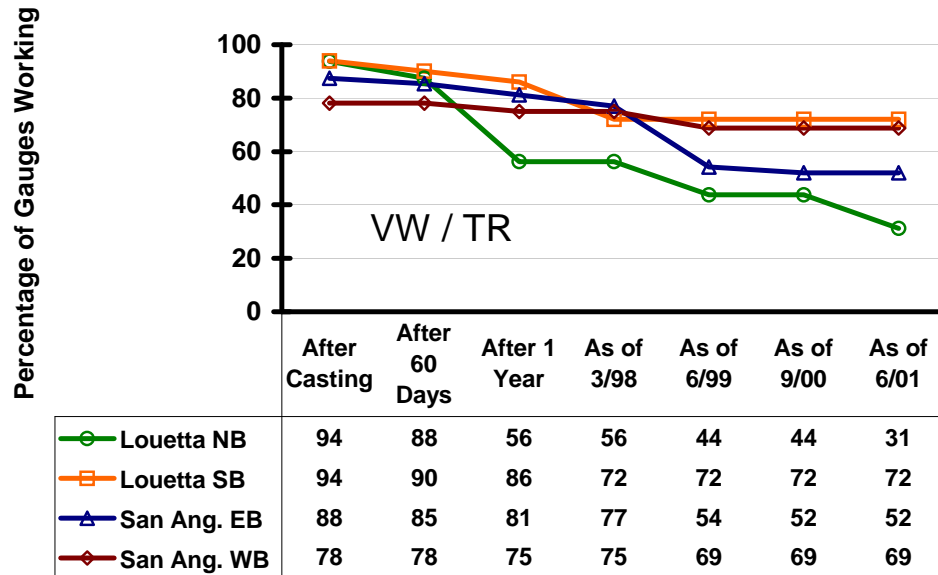


Figure 3.13 Percentage of VW/TR Gauges Working

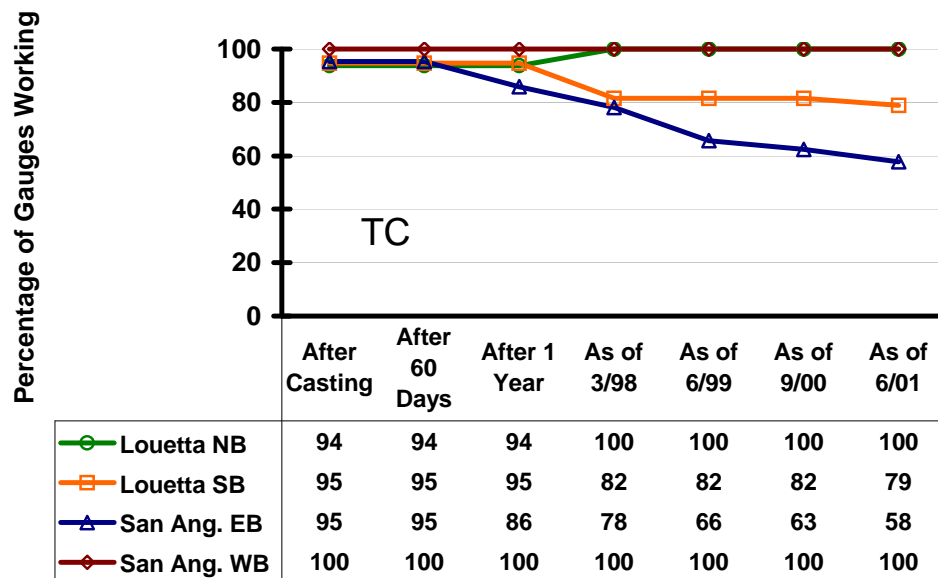


Figure 3.14 Percentage of TC Gauges Working

CHAPTER 4: Monitoring Program

4.1 INTRODUCTION

This chapter presents the monitoring program. It is divided into sections pertaining to durability and structural performance. The durability section describes the review of TxDOT BRINSAP reports and the methods used during visual inspections of the structures. It also describes the method used to test for chloride ion penetration in the concrete decks. The structural sections present details on how the instrumentation was used to acquire information about prestress losses and camber. The precise surveying method used to monitor changes in beam camber is also described.

4.2 DURABILITY MONITORING

One of the expected advantages of HPC was improved durability when compared to normal concrete. These bridge sites provided a unique opportunity to make performance comparisons between different concrete mixes. As mentioned in Chapter 3, various aspects of each bridge were made with different concrete mixes. All aspects of the Louetta Road Overpass were considered HPC. However, the cast-in-place deck was normal strength (4000 psi) and high strength (8000 psi) in the northbound and southbound directions, respectively. The westbound San Angelo bridge was normal concrete, while the eastbound bridge utilized HPC. The sites in Lubbock and Amarillo, however, did not have different mixture designs within their respective CIP decks. The different locations differed from each other in mixture designs, though, based on the time of year and the construction project-specific sources of aggregates, cement, SCMs, and admixtures.

4.2.1 BRINSAP Review

Before the on-site inspections were carried out, the most recent BRINSAP report for each of the bridges was reviewed. TxDOT developed the Bridge Inventory, Inspection, and Appraisal Program to monitor the condition of the 48,000 bridges in Texas. As part of the report, various parts of the structure were given ratings based on their condition. The rating system is summarized in Table 4.1. The BRINSAP review was an important tool for the researchers. It aided preparations for the visual inspection by indicating problems the bridges were experiencing.

Table 4.1 Summary of the BRINSAP Rating System

Rating	Condition	Comments
9	Excellent	-
8	Very good	-
7	Good	Some minor problems
6	Satisfactory	Minor deterioration of structural elements (limited)
5	Fair	Minor deterioration of structural elements (extensive)
4	Poor	Deterioration significantly affects structural capacity
3	Serious	Deterioration seriously affects structural capacity
2	Critical	Bridge should be closed until repaired
1	Failing	Bridge closed but repairable
0	Failed	Bridge closed but beyond repair

4.2.2 Visual Inspection

A formal visual inspection was made at each bridge site during the course of this research program. However, less formal inspections were made during each DAS maintenance trip as well. The purpose of the visual inspection was to identify any defects in the structure that may indicate a more serious problem with the structure. Surface defects such as cracking, spalling, delamination, and efflorescence are common symptoms of concrete deterioration.

The deck was investigated for surface defects with the naked eye. A visual inspection could easily be made by walking along the bridge deck when traffic control was provided by TxDOT. Deck overhangs could be inspected from below the bridge by the naked eye or by using binoculars for a closer view. Defects were photographed and recorded. Cracking was measured for length using a tape measure and for width using a crack comparator.

The superstructure (prestressed beams and precast panels) and substructure (piers, columns, and bent caps) were investigated from below the bridges. At Louetta, the substructure could be viewed up close from the ground and the superstructure could easily be inspected with a pair of binoculars. Due to the height of the San Angelo Bridge, a snooper truck was used to get a closer look at the underside of the structure. The tall San Angelo piers were inspected from below the deck and from the snooper truck. Photographs and measurements were taken of any surface defects.

In July and August 2003 after five years of service the Federal Highway Administration contracted with PSI to officially inspect and report on the conditions of the Louetta and San Angelo bridges. CTR researchers assisted PSI personnel in mapping the extensive cracking in the HPC decks. The inspectors' markings along the cracks clearly showed "streets" of cracking patterns in the CIP surface that outlined each of the underlying precast panels. These PSI reports are included in the appendix in report 7-2941-5.

In 2002 researchers began the regular inspection and monitoring of TxDOT-identified new HPC bridge decks in the Lubbock and Amarillo Districts. These decks were part of the followings structures:

- A. The first in Lubbock was the 82nd street overpass on US 82/62, and it was already showing evidence of significant early cracking. It was constructed of a 4-inch cast-in-place deck over precast deck panels. In addition to minor surface stretch cracking from over-working and tining the drying surface, large transverse cracks had already developed.

- B. The second Lubbock bridge was US 82/62 at FM 179. It used the older permanent metal deck forms to make nominal 8-inch cast in place decks. The cracking here was minimal, though, and due to misplaced zip strips or to continuing to try to fine the surface after it had already begun to dry.
- C. The third Lubbock bridge was on Loop 289 at Frankford Street. No early indications of cracking were visible on the first inspection.
- D. The fourth Lubbock structure was on IH 27 at New Deal. Although we saw no obvious cracking during the first inspection, several early cracks developed in this bridge deck.
- E. The Amarillo Loop 335 at RM 1061 showed an area of transverse cracking and even intersecting longitudinal cracks early in its life.
- F. The last structure was in Amarillo On Loop 335 over Amarillo Creek. Longitudinal cracking patterns in the thickened CIP sections over bents were already exhibited in this deck.

4.2.3 Chloride Testing

Chloride content was determined using the CL-500 test equipment purchased from James Instrumentation. A hammer drill was used to pulverize the concrete. Samples were collected at various depths in the bridge deck. This process created a vertical profile to determine the penetration of chloride ions into the deck. The samples were stored in plastic bags and taken back to the lab for analysis.

To conduct the test, 1.5 grams of the concrete dust were combined with 10 mL of 15 percent acetic acid. The solution was shaken for 15 seconds and then allowed to stabilize for at least two hours. A reference electrode connected to an electrometer was used to determine the mV produced by the solution. Before the chloride ion content was determined, a calibration graph had to be made from the provided calibration liquids. This graph converted mV readings to percent chloride. The reference electrode was submerged in the sample solution and the mV reading was taken once it had stabilized. Lower chloride contents yield higher mV readings.

4.3 PRESTRESS LOSS MEASUREMENTS

Long-term prestress loss measurements were successfully made for eleven of the twenty beams that were instrumented for such measurements. Four Louetta HPC beams, three San Angelo eastbound HPC beams, and four San Angelo westbound non-HPC beams, were measured for prestress loss. These beams are shown in the highlighted regions of Figures 4.1 and 4.2.

Prestress loss measurements were taken using vibrating wire gauges placed at the center of gravity of the prestressing steel. The gauges were actually measuring the strain in the concrete. Stress was determined by multiplying the strain times the modulus of elasticity as shown in Equation 4.1. This equation assumed strain compatibility between the concrete and steel.

$$\Delta f_{ps} = E_{ps} \epsilon_{cgs} \quad 4.1$$

where Δf_{ps} = change in stress of prestressing steel

E_{ps} = prestressing steel modulus of elasticity (28,000 psi)

ϵ_{cgs} = measured concrete strain at center of gravity of prestressing steel

However, Equation 4.1 does not account for losses due to relaxation, pre-release losses, and thermal effects. The relaxation loss occurred in the steel, and therefore was not measured by the gauge in the concrete. The first measurement made on each beam was taken just prior to

transfer [10]. Early time-dependent prestress loss was not measured and therefore this analytical value must be added to the measured quantity. Temperature effects caused a change in stress due to thermal gradients and the gauges' coefficient of thermal expansion. Thermal gradient effects were reduced by taking all measurements at 8:00 AM, when the gradient was typically small. The change in strain due to thermal expansion of the gauge was corrected by using temperature measurements taken at the location of the strain gauge. Therefore, the actual measured prestress loss was determined using Equation 4.2 [10]:

$$\Delta f_{ps,total} = E_{ps} \epsilon_{cgs} + \Delta f_{ps,relaxation} + \Delta f_{ps,pre-release} \quad 4.2$$

where $\Delta f_{ps,total}$ = total measured prestress loss

$\Delta f_{ps,relaxation}$ = prestress loss due to steel relaxation

$\Delta f_{ps,pre-release}$ = prestress loss due to pre-release factors

Note that losses due to thermal effects were accounted for in the pre-release term.

The strain and temperature data were inputted into spreadsheets developed by Gross [12]. These spreadsheets made the necessary corrections to the measured strain and converted them to measured prestress loss.

4.4 CAMBER MEASUREMENTS

Camber and deflection measurements were made on a number of beams in both structures. The fourteen measured Louetta beams are labeled in Figure 4.1. Twelve of the beams, boxed in Figure 4.1, were instrumented and measurements were made from casting through long-term behavior. The two non-instrumented beams in northbound span 3 were measured since erection at the bridge site. These beams were added so camber could be observed across an entire span [10].

The measured San Angelo beams are labeled in Figure 4.2. All twenty-seven beams in eastbound spans 1 through 4 and westbound span 1 were measured since the bridge decks were completed. However, only the fourteen instrumented San Angelo beams were measured since casting. These beams are in the highlighted region of Figure 4.2.

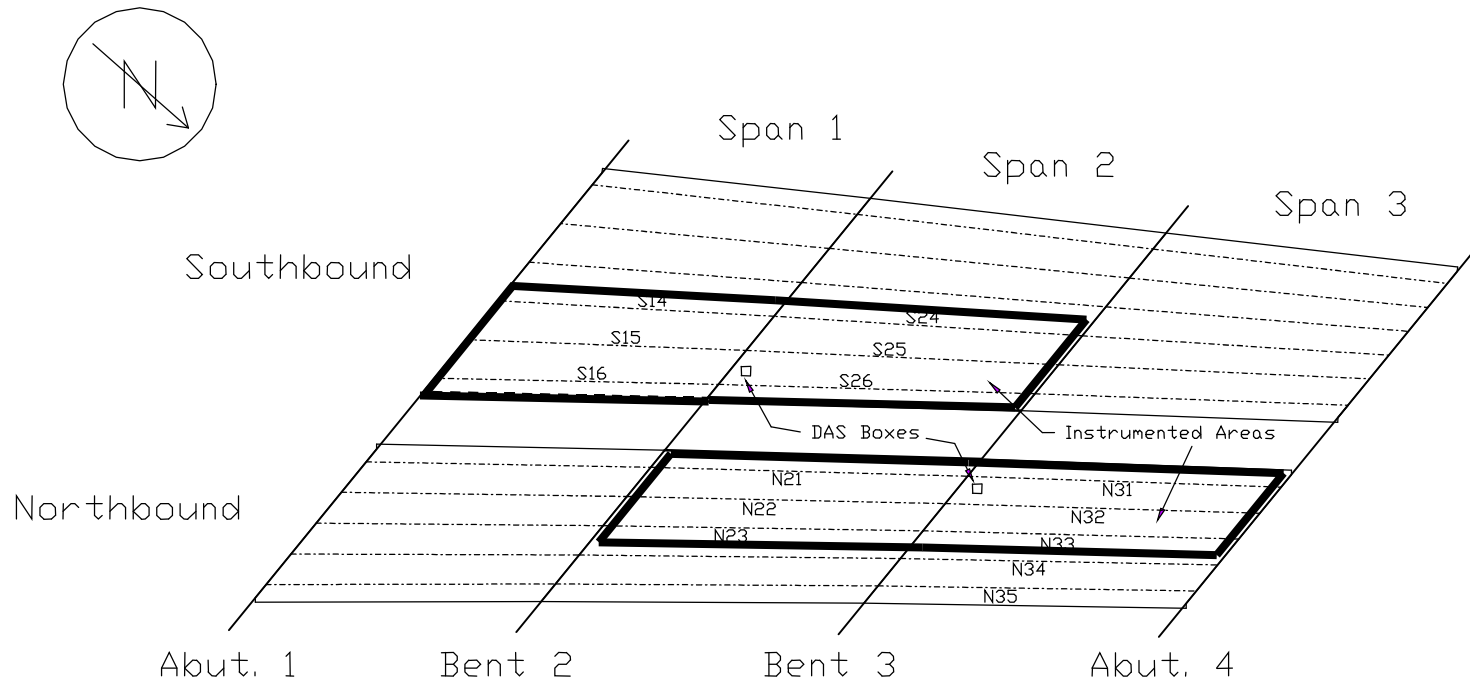
The beam notation should be described at this point. All beams are described using a letter and two numbers. The letter identifies which bridge the beam belongs to: N for Louetta northbound, S for Louetta southbound, E for San Angelo eastbound, and W for San Angelo westbound. The first number identifies the span and the second identifies the beam in the span.

4.4.1 Precise Surveying System

All camber measurements were taken using the relative method of the precise surveying system. The system was used successfully in the past on both bridges to take camber and deflection measurements. It was recommended by researchers because of its flexibility and ease of use [5, 10, 12]. The system required a minimum of two people. One person was needed to hold the rod, while the other read beam elevations using the level and recorded them. However, it was desirable to have a third person when using the precise surveying system. Holding the rod in place could quickly become quite tiring for a single person and was even more difficult during windy conditions. Alternatively, the third person could be responsible for recording measurements. A recorder both reduces the chance for recording error and speeds up the process.

The precise surveying system is a modified simple rod and level surveying system. The surveying system was made *precise* by employing three modifications to increase the accuracy of the system. A post level was used to ensure the rod was kept vertical. In addition, precision

scales were attached to the rod. Readings were made using the 0.02 in. divisions on the scales. Finally, sight distances were limited to 40 feet so that the precision scales may be read using a more magnified view. The rod, with close-up views of the precision scales and post level, is shown in Figure 4.3.



LOUETTA ROAD OVERPASS (prior to widening)

Figure 4.1 Instrumented Areas of Louetta Road Overpass [10]

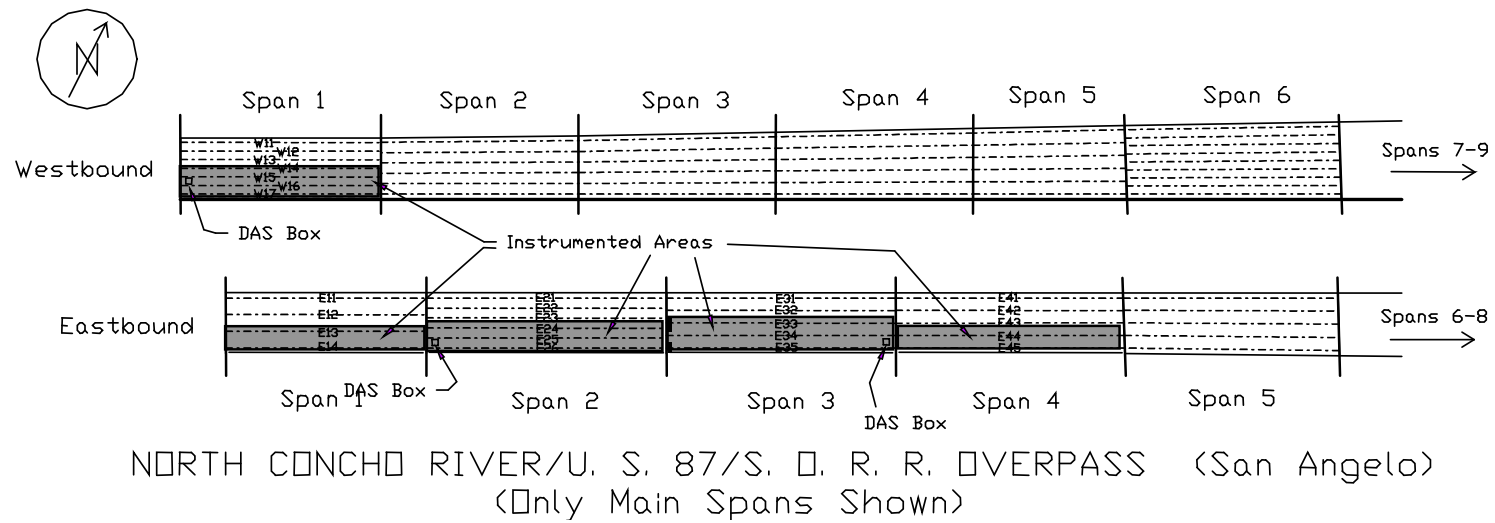


Figure 4.2 Instrumented Areas of San Angelo Bridges [10]

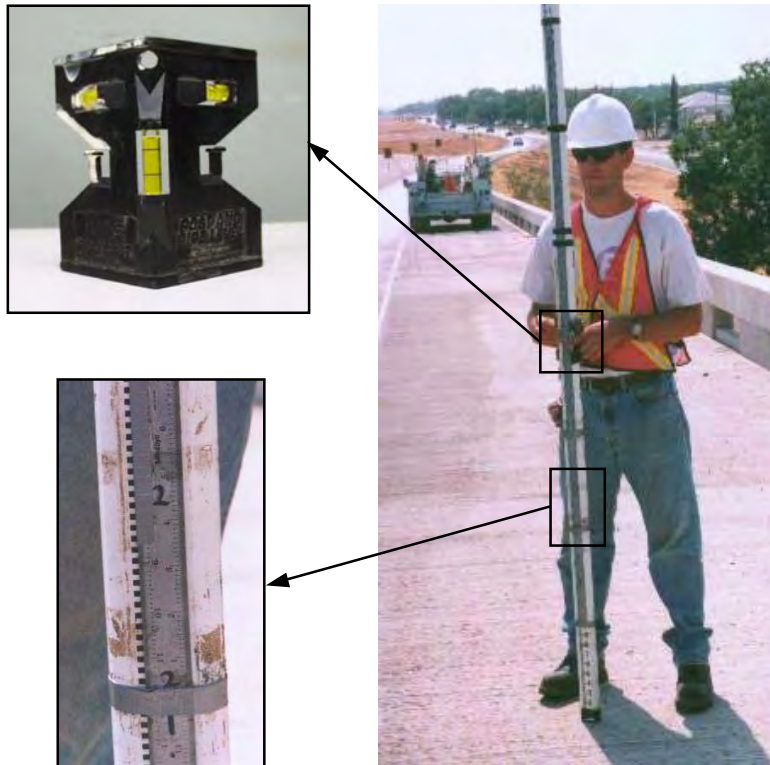


Figure 4.3 Precise Surveying System Equipment

The relative method did not determine the actual beam elevation. Instead, the *relative* change in elevation between points was used to determine the camber or deflection. Beam elevations were taken at the bearing points of the beams and at the beam midspan using the relative method. The surveying points had been painted on the bottom of the Louetta Road Overpass beams. The surveying points were mapped out on the deck of the San Angelo bridges using the known bridge geometry.

Measurements were taken from below the bridge at the Louetta Road Overpass. The survey rod could be extended, so that it reached the painted survey points on the beams. Survey points were located on both sides of the U-beam, such that six measurements were taken for each beam as illustrated in Figure 4.4. Each pair was averaged to obtain a single camber value for the beam. Measurements could not be taken at the true bearing point because the pier blocked its location. Therefore, a correction had to be made to the field measurement. This correction is discussed in Section 4.4.2.2.

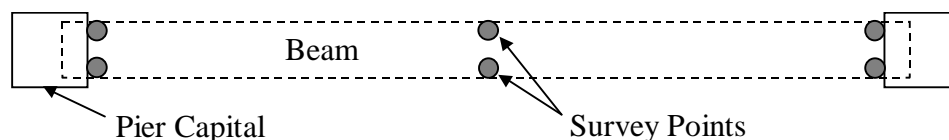


Figure 4.4 Location of Survey Points on a Louetta Beam

At the San Angelo bridge sites, measurements were made on top of the bridge deck. Taking camber measurements using the bottom of the beams was more desirable, but was

impossible due to the bridge layout. Difficulties arose because of the fact that the bridges are located well above grade and multiple spans are over the North Concho River. A correction to the raw field measurements must be made due to the varying thickness of the cast-in-place concrete deck. This correction is discussed in Section 4.4.2.3. Figure 4.5 shows the relative method of the precise surveying system used to measure beam camber from the deck of the westbound San Angelo Bridge.



Figure 4.5 Camber Measurements at San Angelo

4.4.2 Corrections to the Precise Surveying System

The precise surveying system provided a value of the beam camber or deflection as measured on top of the deck or bottom of the beam, for the San Angelo and Louetta beams, respectively. Several corrections had to be made to the field measurements before an accurate beam camber or deflection was obtained. The camber or deflection caused by thermal gradients must be removed from the field measurements. Two types of *offset* corrections must be made. The Louetta Road Overpass measurements must be offset to account for the difference between the bearing point of the beam and the actual survey point. The San Angelo bridge measurements must be offset to account for the variation in the depth of the cast-in-place deck.

4.4.2.1 Thermal Gradient Correction

A thermal gradient is the measured vertical variation in temperature throughout the bridge cross section. A thermal gradient was produced because the deck was directly exposed to sunlight while the underside of the bridge was shaded. A thermal gradient may also be produced at night when the deck cools faster than the rest of the bridge. The thermal gradient caused changes in strain in the bridge, resulting in a variation of camber or deflection. A detailed discussion of thermal gradients in the Texas HPC bridges can be found in Byle, Burns, and Carrasquillo [5] and Gross and Burns [10].

Thermal gradients were measured using the embedded gauges described in Section 3.4.2. Thermocouples and thermistors measured temperatures in the cast-in-place decks, precast prestressed panels, and beams. Measurements were made at the bottom flange, the center of gravity of the prestressed strands, the center of gravity of the noncomposite beam, the center of gravity of the composite beam, the top of the web, the top of the flange, and in the panel and deck. The temperature gradient at the time of the precise surveying system measurements was found using the data recorded by the DAS. The temperatures of thermal gradient were entered into spreadsheets developed by Gross [12], which calculated the thermally induced camber in the beams.

4.4.2.2 Bearing Point Correction

In the Louetta beams, a correction to field measurements had to be made to account for the difference between the actual bearing point of the beam ends and the survey point. The actual bearing point could not be reached because of the arrangement of the pier and beam. This fact is illustrated in Figure 4.4 and can be seen in the photograph in Figure 4.6. The offset between the bearing point and survey point is significant because the bridge was built on a slight superelevation. The north side of the bridge is actually higher than the south side. An analytical correction was applied to the measurements taken on the instrumented beams. This correction tended to be small, with the largest value of 0.31 in. occurring on Beam N21 [10].



Figure 4.6 Bearing Point versus Survey Point

4.4.2.3 Deck Offset Correction

As described in Section 4.4.1, camber measurements for San Angelo beams were made from the deck surface. In order to obtain a camber measurement for the beams and not the deck, the variation in the deck cast-in-place concrete depth had to be accounted for. Deck offsets were determined by comparing measurements taken from the bottom of the beams and from the deck. Gross determined the offset corrections [12]. Note that offsets were not determined for all of the beams. Offsets were only determined for the 19 beams in which measurements were recorded on the bottom of the beam prior to completion of the bridge. The deck offsets were less than 0.5 in. for most beams, but exceeded 2.0 in. in all eastbound span 1 beams.

CHAPTER 5: Monitoring Results

5.1 INTRODUCTION

The results of the monitoring program are presented in this chapter. First, the results of the durability testing are presented and a summary of the BRINSAP reports, the results of the visual inspections, and findings from the chloride ion penetration tests are included. Next, the results of the structural performance evaluations are presented. The measured prestress loss and the measured camber and deflection are presented for the twenty-six instrumented beams. These measurements were discussed in Sections 4.3 and 4.4, respectively. The instrumented beams were shown in Figures 4.1 and 4.2. Graphs for the measured and predicted long-term prestress losses and camber are provided for every instrumented beam in the appendix in report 7-2941-5. Several beams that were not instrumented were measured for camber as well.

5.2 DURABILITY RESULTS

5.2.1 BRINSAP Summary

The BRINSAP report was described in Section 4.2.1. The results of the BRINSAP report review are presented in this section. A single report was done for the Louetta Road Overpass. D. Gary Pickett of Pickett, Kelm & Associates, Inc. performed the inspection on March 5, 1999. Separate reports were done for the San Angelo bridges. Bill Tankersley performed the inspections on September 6, 2000. A summary of these reports is shown in Table 5.1. Both bridges received high ratings, but minor problems were reported on all of the structures.

Table 5.1 Summary of BRINSAP Report Review

	Rating	Comments
<i>Louetta HPC</i>		
Deck	8	Minor spalls on concrete traffic barrier. Joint seals have minor build-up of dirt and sand.
Superstructure	7	Minor spalls on bottom of U-beams. Bearing pads have deflected slightly.
Substructure	9	
<i>San Angelo Eastbound HPC</i>		
Deck	7	Minor cracks and efflorescence on underside of deck overhangs.
Superstructure	8	
Substructure	8	
<i>San Angelo Westbound Non-HPC</i>		
Deck	7	Minor transverse cracks in surface concrete. Very minor cracking and efflorescence on underside of deck overhangs.
Superstructure	8	
Substructure	8	

When the Lubbock and Amarillo HPC bridge decks were added to project monitoring activities BRINSAP was no longer used by TxDOT, and our deck monitoring was more thorough than the Texas Bridge Inspection Program, so no other records were reviewed for these decks. One of the last reports is included in the appendix in report 7-2941-5 to describe the condition of the decks with respect to durability.

5.2.2 Results of Visual Inspection

During the visual inspection, any distress in the structure was noted and documented. Previous work by Shepperd and Burns [19] was discussed in Section 2.7. This section discusses the crack mapping of the Louetta Road Overpass deck, as well as general comments on the observed condition of the deck concrete at the HPC bridge sites.

The Louetta Road Overpass was inspected on January 31, 2001. The cracking in the deck was mapped for comparison with the previous measurements. Unfortunately, researchers were only able to gain access to the shoulder and one lane of the deck due to traffic concerns. The previous investigation had access to the entire bridge deck. It is the author's opinion that measuring cracks, especially from distances as great as 30 ft., is somewhat subjective. Therefore, comparisons between the results of Table 5.2 and the results of Sheppard and Burns in Table 2.1 are at best imperfect. The results of the crack mapping are shown in Table 5.2.

Table 5.2 Crack Mapping Summary

Span	Cracking (ft)	
	Longitudinal	Transverse
<i>Louetta Northbound Normal Strength</i>		
N1	106	26
N2	163	42
N3	190	27
Total	459	95
<i>Louetta Southbound High Strength</i>		
S1	155	61
S2	250	66
S3	328	24
Total	733	151

Both investigations found more longitudinal cracks in the southbound high strength HPC deck than in the northbound normal strength HPC deck. However, the ratio of longitudinal to transverse cracks was not the same for the two investigations. The previous investigation found the longitudinal to traverse crack ratios to be 2.5 and 8.1 for the northbound and southbound bridges, respectively. The recent investigation found the ratio for both bridges to be approximately 4.8. The suspected reasons for these discrepancies were described above.

Cracks widths were measured as large as 0.25 in. at the surface of the deck on the southbound bridge. The width of the cracks typically narrowed as the crack extended down into the slab. Crack depths were not recorded. Cracks on the northbound bridge were typically much smaller. Figure 5.1 and 5.2 show some of the most severe cracks on the southbound bridge. Note

that the crack continues across the control joint, proving the joint did not prevent transverse cracking.



Figure 5.1 Close-Up of Crack in Louetta Southbound Deck



Figure 5.2 Severe Crack in Louetta Southbound Deck

The rest of the structure was in very good condition. The minor problems detected by Shepperd and Burns [19] were investigated. These problems were discussed in Section 2.7 and include minor spalling and cracking around the drain ports of the beams and cracks and efflorescence in the cast-in-place deck. None of these problems had become worse, and the drain ports had been repaired.

The San Angelo bridges were also in very good condition. As noted in the BRINSAP report, minor cracking and efflorescence was detected on the underside of the deck overhangs. This is a common problem and interested parties are not concerned with this development. No significant signs of distress were found in the piers, bent caps, or beams. The minor transverse cracks in the westbound deck that were reported in the BRINSAP report were difficult to find during the inspection of September 7, 2000 when high daytime temperatures resulted in expanded decks and tighter transverse cracks.

In 2003 the Federal Highway Administration had contracted with a consulting firm, Professional Services Industries, Inc. (PSI) from the Washington, DC area, to officially inspect and report on the condition of the Louetta and San Angelo HPC bridges. So at TxDOT's request in late summer of 2003 CTR researchers assisted PSI in mapping the extensive cracking patterns that had already developed in the decks. A draft of their inspection report to TxDOT is included in the appendix in report 7-2941-5.

Also included in the appendix in report 7-2941-5 are the last visual monitoring reports of the bridges in Lubbock and Amarillo. These sites included four HPC bridge decks in the Lubbock District; the 82nd street overpass on US Highways 82/62, US highways 82/62 at FM 179, Loop 289 at Frankford Street, and the IH 27 New Deal bridge. Two HPC bridge decks were selected in Amarillo District, and they were RM 1061 overpass on Loop 335 and the Amarillo Creek bridge on Loop 335.

5.2.3 Chloride Penetration

Chloride ion testing was not performed for the Louetta Road Overpass. Researchers planned on taking samples during the January 31, 2001, deck inspection. However, because of equipment failure and time constraints, samples were not acquired. Researchers and TxDOT officials agree that deicing salts have seldom been used, if used at all, on the bridge. Therefore, it is believed that significant amounts of chloride ions are not likely to be found. Testing for chloride ions will not be performed again until the next annual inspection.

Table 5.3 summarizes the results of the chloride ion testing performed on September 7, 2000, from the San Angelo bridge decks. The highest reading occurred on the edge of the eastbound bridge at a depth of 0.5 inches. This value of 0.0074 percent chloride ions is considered negligible. Gerry Fields, of the TxDOT San Angelo District Office, said deicing salt had not been used on the bridges within the past year. He also stated that sand would be used instead of salt in the event of freezing weather.

The samples taken from the eastbound bridge were 22 ft, 12.3 ft, and 2 ft north of the southern guardrail for the center of deck, tire path, and edge samples, respectively. The samples taken from the westbound bridge were 19.7 ft, 11.7 ft, and 2 ft south of the northern guardrail for the center of deck, tire path, and edge samples, respectively. All samples were taken 3-feet east of the westernmost construction joint.

Table 5.3 Results of Chloride Ion Penetration Tests

Sample	% CL	Sample	% CL
EE0.5	0.0073	WE0.5	0.0044
EE1.0	0.0021	WE1.0	0.0031
ET0.5	0.0027	WT0.5	0.0035
ET1.0	0.0017	WT1.0	0.0022
EC0.5	0.0023	WC0.5	0.0033
EC1.0	0.0023	WC1.0	0.0024
XYn = Sample Notation X = bridge E = Eastbound W = Westbound Y = position in span E = outer edge of deck T = tire path C = center of deck n = depth of sample (in.)			

5.3 PRESTRESS LOSS

The measured prestress loss for each instrumented beam was graphed with respect to the number of days after release. These plots can be found in the appendix in report 7-2941-5. The beam identification number is written below the key. Notice the vertical axes show prestress loss in ksi and as the percentage of the jacking force. Data points occurring after the second to last camber data point were measured during the current phase of the project. The other data points were measured during earlier work on the HPC bridges [5, 10].

Note that plots were included for all twenty-six instrumented beams even though prestress loss only continues to be measured on eleven of those beams. Prestress loss measurements are no longer possible because some of the vibrating wire gauges have failed, or never worked to begin with. In addition, prestress loss measurements were not taken for all of the beams that were measured for camber and deflection. Prestress loss measurements rely on a single gauge placed at the center of gravity of the strands. If budget allows, a backup gauge is recommended for prestress loss measurements due to the dependence on the reading of a single gauge.

A typical plot of the measured prestress loss is shown in Figure 5.3. The measurements generally show good correlation with the prestress loss predicted by the time-dependent model. Figure 5.4 shows the worst-case scenario, with regards to measured prestress loss compared to the time-dependent model.

Table 5.4 shows the components of the measured long-term prestress loss. These values were current as of March 2001. Results are given for eleven beams: four Louetta HPC U-beams, three San Angelo eastbound HPC beams, and four San Angelo westbound non-HPC beams. The total loss was made up of losses due to pre-release loss, elastic shortening, creep and shrinkage, and relaxation. Creep and shrinkage are listed as one component because they cannot be measured separately. The total loss is given in terms of ksi as well as the percentage of the jacking force. The strands were jacked to a stress of 202.5 ksi.

Four Louetta HPC beams continue to be measured for long-term prestress loss. The average total loss was 40.7 ksi. The values ranged between 35.5 ksi and 44.6 ksi. In terms of percentage of the jacking force, the average prestress loss was 20.1 percent. These values ranged between 17.6 and 22.0 percent. Elastic shortening was the most significant component of the measured prestress loss. However, the creep and shrinkage component was nearly as large, as noted from Table 5.4. The time-dependent creep and shrinkage component continued to increase slightly, while the instantaneous loss from elastic shortening remained constant. The average prestress loss due to elastic shortening was 16.1 ksi, while the creep and shrinkage component was 13.1 ksi.

Three San Angelo eastbound HPC beams were successfully measured for long-term prestress loss. The average total loss was 56.6 ksi. The values ranged between 54.8 ksi and 60.4 ksi. In terms of percentage of the jacking force, the average prestress loss was 28.0 percent. These values ranged between 27.1 and 29.8 percent. Elastic shortening and creep and shrinkage were the most significant components of the total prestress loss, similar to the Louetta HPC beams. However, the elastic shortening term was smaller than the creep and shrinkage term in two of the beams. The average values for elastic shortening and creep and shrinkage were 22.4 and 22.6 ksi, respectively.

The average total loss of the four San Angelo westbound non-HPC beams that were successfully measured for long-term prestress loss was 34.0 ksi. These beams had a high value of 35.3 ksi and a low value of 31.7 ksi. The average loss, in terms of percentage of the jacking force, was 16.8 percent. The high and low percentages were 17.4 and 15.6, respectively. As with most of the beams measured, elastic shortening was the largest component of the measured prestress loss.

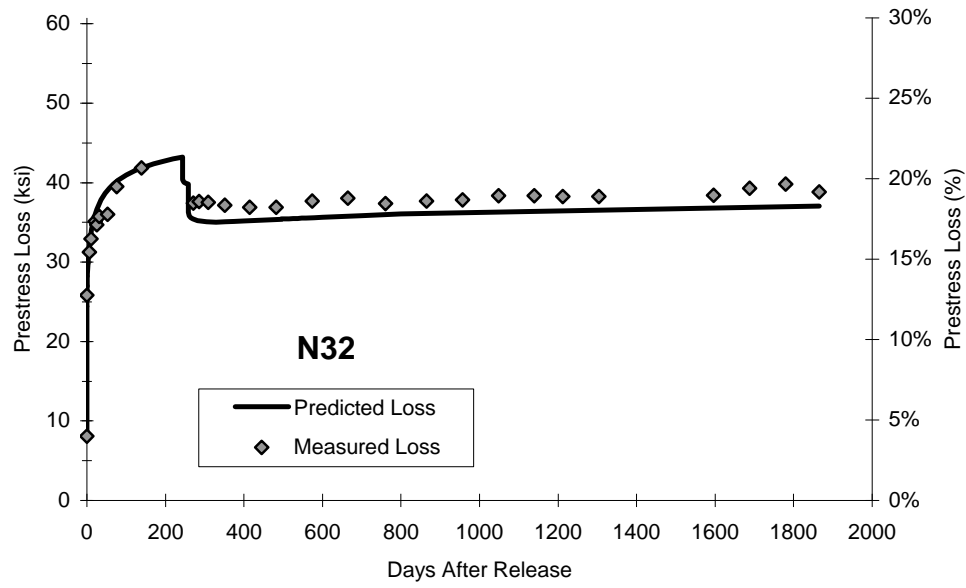


Figure 5.3 Measured Prestress Loss – Typical Case (Beam N32)

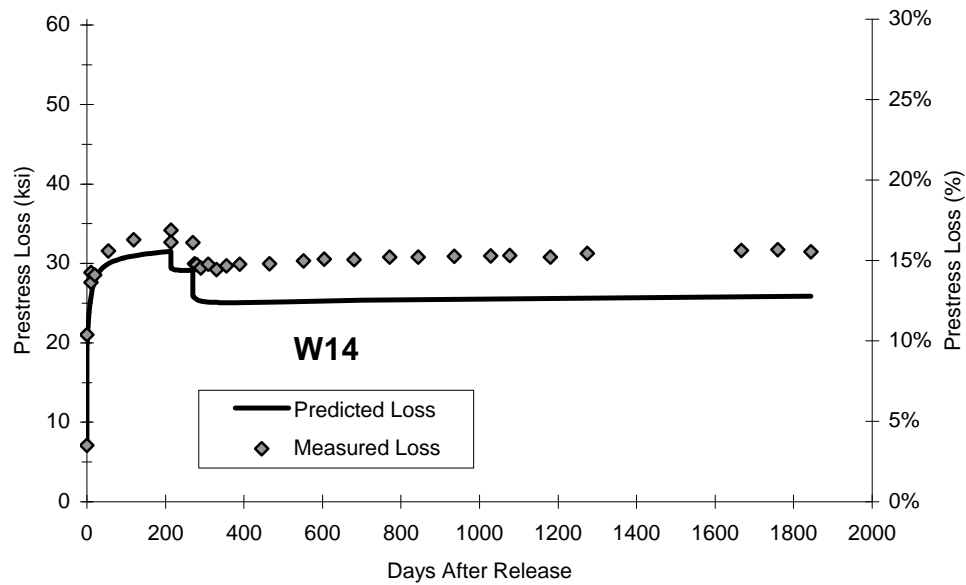


Figure 5.4 Measured Prestress Loss – Worst Case (Beam W14)

Table 5.4 Components of Measured Prestress Loss

Beam	Days After Release	Δ Time ¹ (days)	Loss Components (ksi)				Total Loss (ksi)	Δ Total Loss ³ (ksi)	Total Loss (% of f_{jack})
			PR	ES	CR+SH ²	RE			
Louetta HPC Beams									
N32	1865	1104	8.10	17.75	15.43	3.28	44.56	-1.45	22.00
S15	1854	1106	8.10	16.38	11.84	3.28	39.60	-1.74	19.55
S16	2368	1106	8.10	17.16	14.23	3.41	42.90	-2.64	21.19
S25	2327	1106	8.10	12.96	11.07	3.40	35.54	-1.73	17.55
Average			8.10	16.07	13.14	3.34	40.65	-1.89	20.07
San Angelo Eastbound HPC Beams									
E14	1495	1073	8.10	24.58	24.51	3.16	60.35	-3.11	29.80
E24	1477	1073	9.11	20.19	22.33	3.15	54.78	-3.27	27.05
E25	1819	1073	8.10	22.46	20.98	3.27	54.80	-2.85	27.06
Average			8.44	22.41	22.60	3.19	56.64	-3.07	27.97
San Angelo Westbound Non-HPC Beams									
W14	1844	1073	7.09	13.94	11.01	3.27	35.32	-0.65	17.44
W15	1844	1073	7.09	14.73	10.00	3.27	35.09	-0.68	17.33
W16	1844	1073	7.09	12.18	11.32	3.27	33.86	-1.18	16.72
W17	1839	1073	7.09	12.80	8.51	3.27	31.67	-1.16	15.64
Average			7.09	13.41	10.21	3.27	33.99	-0.92	16.78
1 ksi = 6.895 Mpa									
¹ Change in time between data shown in Table 5.4 and data shown in Table 7.8 of reference [10].									
² Includes compensation for measured elastic change in stress due to superimposed dead load.									
³ Change in total prestress loss between data shown in Table 5.4 and data shown in Table 7.8 reference [10].									
PR = Pre-release; ES = Elastic Shortening; CR = Creep; SH = Shrinkage; RE = Relaxation									

5.4 CAMBER

The graphical results of the camber and deflection measurements are found in the appendix in report 7-2941-5. The beam identification number is written above the key. The measurements were graphed as a function of upward camber versus the number of days after release. The plots also include the predicted camber calculated by the time-dependent model. Only the most recent data point was determined during the current phase of the project. The other data points were measured during earlier work on the HPC bridges [5, 10]. These data points were corrected using the methods described in Section 4.4.2.

A typical plot of the measured camber is shown in Figure 5.5. The measurements generally show good correlation with the camber predicted by the time-dependent model. Figure 5.6 shows the worst-case scenario, in terms of measured camber compared to the time-dependent model prediction.

Camber and deflection was measured in fourteen Louetta HPC beams, twenty San Angelo eastbound HPC beams, and seven San Angelo westbound non-HPC beams. Table 5.5 shows the results of the Louetta camber measurements and Table 5.5 shows the results of the San Angelo camber measurements. The final corrected measured camber is shown, along with the field measurement and the corrections applied to the field measurement. The correction factors were subtracted from the field measurement to determine the corrected measured camber. These corrections were discussed in Section 4.4.2. Note that an offset correction was not determined for every San Angelo beam.

The following trends were observed for all camber measurements, including those where the offset correction was not available. In general, there was agreement between camber measurements in each span of all of the bridges. Nearly all of the HPC beams exhibit the desired slight upward camber. The deck offset correction typically increased the measured camber. Therefore, it could be assumed that a beam, which clearly shows an upward camber before the offset correction was applied, would maintain an upward camber after the correction was made. Only two Louetta southbound beams show a slight downward deflection. All of the San Angelo westbound non-HPC beams displayed a downward deflection.

Table 5.5 San Angelo Camber Measurements

	Camber (in.)			Final Corrected Measured Camber	Measured Camber After Deck Placement ²
Beam	Field Meas.	Offset Corr. ¹	Thermal Corr.		
San Angelo Eastbound HPC Beams					
E11	-0.34	-2.73	0.35	2.04	N/A
E12	-0.49	-2.11	0.36	1.26	N/A
E13	-0.04	-2.24	0.36	1.84	2.95
E14	-0.55	-3.00	0.35	2.10	3.44
E21	1.76	N/A	0.57	1.19	N/A
E22	1.99	N/A	0.57	1.42	N/A
E23	2.24	N/A	0.57	1.67	N/A
E24	1.97	-0.35	0.57	1.75	2.67
E25	1.70	-0.01	0.57	1.14	2.14
E26	1.32	0.28	0.57	0.47	1.80
E31	1.37	N/A	0.34	1.03	N/A
E32	1.76	N/A	0.35	1.41	N/A
E33	1.84	-0.27	0.35	1.76	2.28
E34	1.81	0.19	0.35	1.27	1.78
E35	1.23	-1.19	0.34	2.08	2.90
E41	1.26	N/A	0.33	0.93	N/A
E42	1.66	N/A	0.34	1.32	N/A
E43	1.80	N/A	0.34	1.46	N/A
E44	1.66	-1.18	0.34	2.50	2.22
E45	1.21	-0.74	0.33	1.62	1.76
San Angelo Westbound Non-HPC Beams					
W11	-1.39	0.04	0.32	-1.75	N/A
W12	-1.49	-0.54	0.32	-1.27	N/A
W13	-1.55	0.12	0.32	-1.99	N/A
W14	-1.64	-0.36	0.32	-1.60	1.03
W15	-1.53	-0.28	0.32	-1.57	0.95
W16	-1.84	-0.42	0.32	-1.74	0.86
W17	-2.22	0.04	0.32	-2.58	0.77
¹ Deck offset corrections were not determined for all beams					
² Corrected measured camber after placement of precast panels and cast-in-place deck [12]					

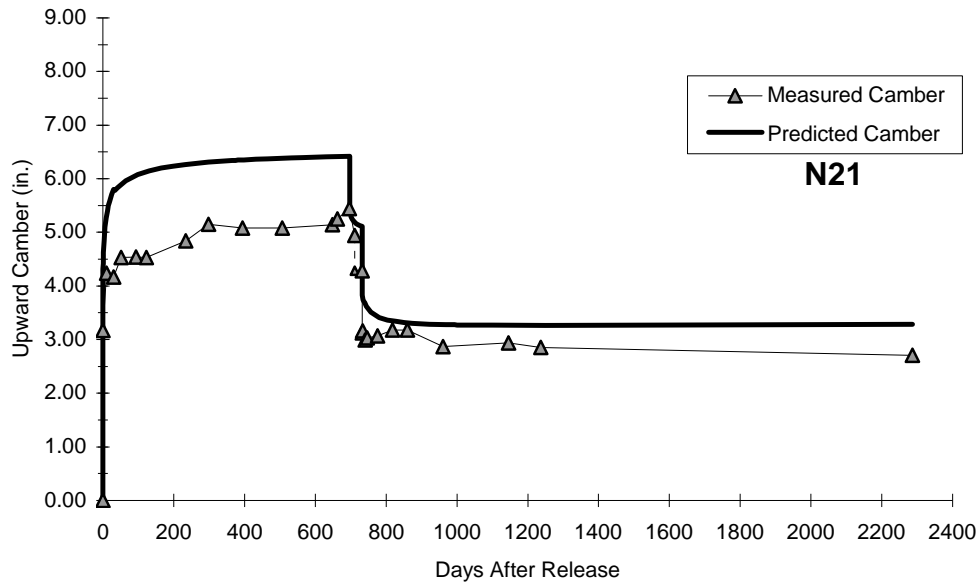


Figure 5.5 Measured Camber and Deflection – Typical Case (Beam N21)

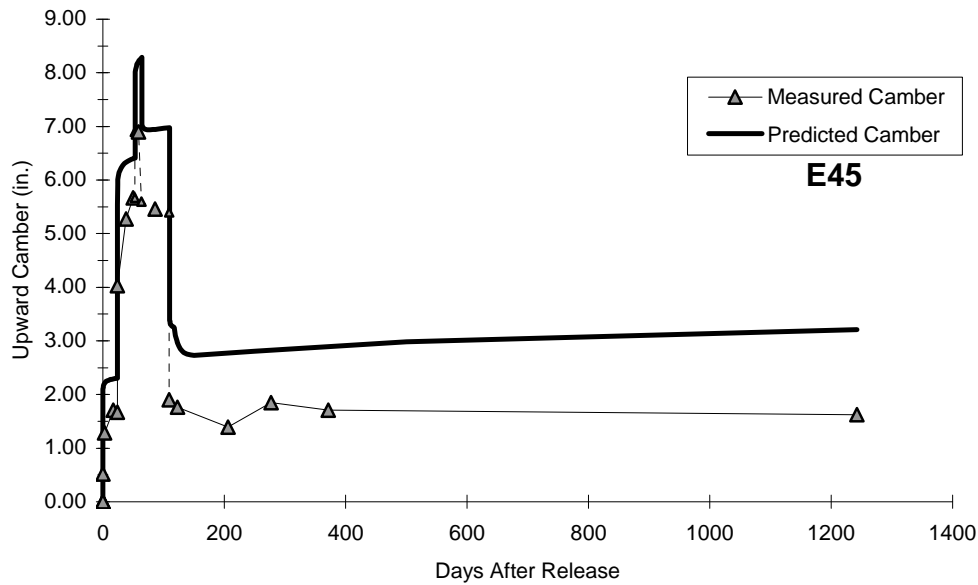


Figure 5.6 Measured Camber and Deflection – Worst Case (Beam E45)

CHAPTER 6: Discussion of Test Results and Field Inspections

6.1 INTRODUCTION

This chapter discusses the results of structural performance evaluations on the Louetta and San Angelo HPC structures that were presented in the previous chapter. The measured values for identical or similar beams are compared. The measured prestress loss is compared to the actual design predictions, as well as the predictions from the AASHTO and PCI methods. Prestress loss measurements are compared to the method suggested by Gross and Burns [10]. Measured camber is discussed and values for similar beams are compared. Finally, measured camber is compared to values predicted by the time-step model and the actual design.

6.2 PRESTRESS LOSS

Prestress loss was determined using several different methods, which were discussed in Section 2.4. Some methods utilized design parameters, while others used measured values. Design parameters were calculated from commonly used equations. Measured values were determined from tests performed on the actual mix design used in the HPC beams. The differences between the design and measured parameters are summarized in Table 6.1. Note that different design equations were used to predict the modulus of elasticity for non-HPC and HPC. These equations are shown below:

$$E_c = w_c^{1.5} 33 \sqrt{f'_c} \quad 6.1$$

where E_c = modulus of elasticity for concrete (psi)

w_c = unit weight of concrete (90 to 155 pcf)

f'_c = compressive strength of concrete (psi)

$$E_c = 40,000 \sqrt{f'_c} + 1,000,000 \quad 6.2$$

Equation 6.1 is suggested by both AASHTO [2] and ACI [4]. ACI points out the modulus of the concrete is sensitive to the modulus of the aggregate. Therefore, measured values typically vary between 80 and 120 percent of results predicted by Equation 6.1. Carrasquillo, Nilson, and Slate [7] observed that Equation 6.1 overestimated the modulus of elasticity for high strength concrete. They proposed Equation 6.2, where E_c and f'_c are in psi.

Table 6.1 Comparison of Design versus Measured Parameters [10]

Parameters	Design Parameters	Measured Parameters
Section Properties	Gross section properties	Transformed section properties
Concrete Unit Weights & Dead Loads	Based on assumed deck dimensions and 150 pcf for all concrete.	Based on measured deck thickness and measured unit weights, with approximate weight of steel included for beams.
Concrete Strength	Nominal design concrete strength	Based on tests of companion specimens.
Modulus of Elasticity	Eq. 6.1 (non-HPC) or Eq.6.2 (HPC), using nominal design strengths.	Based on tests of companion specimens.

In general, for all of the beams in which long-term prestress loss measurements were made the total prestress loss continues to increase slightly. This increase was continued over a succession of measurements and was attributed to time-dependent sources of prestress loss. These sources were described in Section 2.3 and included creep, shrinkage, and relaxation.

Unfortunately, only the San Angelo bridges allow for a comparison between similar beams in the same span. There are two Louetta southbound span one beams with measured prestress loss. The number of days after release for the two beams varies by more than a year. It could be argued that this difference in age should no longer be significant, due to the expected flattening of the prestress loss curve. However, one beam is a U54A beam while the other is a U54B, making comparisons less significant.

San Angelo HPC beams E24 and E25 were both measured for long-term prestress loss. Although, these beams vary in age by close to one year that fact should be insignificant as discussed above. The beams have nearly identical measured prestress loss. The measured values differ by just 0.02 ksi. Beam E24 contains four additional pretensioned strands and six additional post-tensioned strands when compared to Beam E25.

All four of the San Angelo westbound beams that were instrumented for prestress loss measurements continue to successfully monitor long-term prestress loss. These beams are identical except for the spacing of the exterior beam, W17. These beams have similar measured long-term prestress loss, especially the three interior beams.

Table 6.2 summarizes the prestress loss as determined using the previously discussed methods. These predictions were calculated using data current as of March of 2001. It should be pointed out that several of the methods listed are general long-term predictions and do not vary with time. Long-term prestress loss has been successfully measured on eleven beams. Four Louetta HPC U-beams, three San Angelo eastbound HPC I-beams, and four San Angelo westbound non-HPC I-beams are shown in Table 6.2. The first column of data lists the prestress loss as determined from strain measurements discussed in Section 4.3. The average prestress loss for each set of beams is given. Note that the methods vary in how they determine pre-release losses. The prediction methods suggested by AASHTO and PCI do not include all pre-release losses. Therefore, the values predicted by these methods should theoretically be less than the other methods. These methods were described in Section 2.4.

These methods produced a wide spectrum of results. Some methods were quite accurate compared to the measured prestress loss, while others were not. In general, most methods predicted the greatest prestress loss in the San Angelo eastbound HPC beams, followed by the Louetta HPC beams and then the San Angelo westbound non-HPC beams. This trend was in agreement with the measured results. The two components methods developed by AASHTO and PCI were used to predict long-term prestress loss using both design and measured parameters. As expected, the components methods produced estimates closer to the measured prestress loss when using measured parameters.

In general, the long-term prestress losses predicted by the incremental time-step analysis were in agreement with the measured value. The results were expected to be accurate, because they incorporated detailed information such as measured properties and construction schedules. The values predicted using this method were all within 10 percent of the measured prestress loss.

Table 6.2 Comparison of Total Prestress Losses

Beam	Total Prestress Losses (ksi)								
	Measured ¹	Incremental Time-Step (Measured Parameters) ¹	Actual Beam Designs (PSTRS14 or ADAPT-ABI) ¹	AASHTO LRFD Time- Dependent Lump-Sum (Design Parameters) ²	AASHTO LRFD Components (Design Parameters) ²	AASHTO LRFD Components (Design Parameters) ²	PCI Design Handbook Components (Design Parameters)	PCI Design Handbook Components (Measured Parameters)	Suggested Method (Measured Parameters) ¹
Louetta HPC Beams									
N32	44.56	43.40	57.79	38.72	67.05	57.71	50.57	38.79	40.02
S15	39.60	45.53	57.79	40.65	72.53	61.25	55.99	40.85	41.60
S16	42.90	47.03	52.99	38.29	69.92	59.88	55.78	41.64	41.65
S25	35.54	41.64	52.99	36.68	62.12	52.46	46.27	34.27	36.83
Avg.	40.65	44.40	55.39	38.59	67.91	57.83	52.15	38.89	40.03
San Angelo Eastbound HPC Beams									
E14	60.35	57.51	47.45	57.21	104.46	89.40	84.84	65.40	56.27
E24	54.78	56.94	52.16	56.43	103.96	89.09	83.02	65.16	55.67
E25	54.80	51.25	41.69	51.50	89.31	77.32	70.00	55.23	49.63
Avg.	56.64	55.23	47.10	55.05	99.24	85.27	79.29	61.93	53.86
San Angelo Westbound Non-HPC Beams									
W14	35.32	30.99	47.91	41.02	51.91	45.54	39.18	31.76	28.68
W15	35.09	30.99	47.91	41.02	51.91	45.54	39.18	31.76	28.68
W16	33.86	30.99	47.91	41.02	51.91	45.54	39.18	31.76	28.68
W17	31.67	30.87	47.91	41.02	51.71	43.98	38.87	29.55	28.15
Avg.	33.99	30.96	47.91	41.02	51.86	45.15	39.10	31.21	28.55
¹ Includes pre-release losses.									
² Includes pre-release relaxation losses only									

The values predicted by the programs used in the actual beam design were not as accurate. PSTRS14 [20], used in the Louetta HPC and San Angelo westbound non-HPC beam designs, overestimated the long-term prestress loss by a significant amount. The long-term prestress loss for the San Angelo eastbound HPC beams was significantly underestimated by ADAPT-ABI [1].

Surprisingly, the AASHTO LRFD Time-Dependent Lump Sum method was in agreement with the measured prestress loss values [10]. Its predictions were actually closer for the HPC beams than the non-HPC beams. The average predicted prestress loss was 95 and 97 percent of the average measured values for the Louetta HPC and San Angelo eastbound HPC beams, respectively. The San Angelo westbound non-HPC beams prestress losses were overestimated. The average predicted value was 121 percent of the measured value. However, this method tended to overestimate the elastic shortening component, while underestimating the time-dependent component for the HPC beams. Therefore, this method cannot be recommended for use with HPC beams.

The results of the AASHTO LRFD Time-Dependent Lump Sum method were even more surprising in light of the results produced by the AASHTO LRFD components method. The components method was intended to be more accurate than the time-dependent lump sum method. However, the component method was not nearly as accurate. In fact, the AASHTO LRFD components method was the least accurate method investigated in the research project. Using design parameters, the predicted long-term prestress loss was nearly twice as large as the measured values in some instances. The average predicted long-term prestress loss using the AASHTO LRFD components method and design parameters was 167, 175, and 153 percent of the measured values for the Louetta HPC beams, San Angelo eastbound HPC beams, and San Angelo westbound non-HPC beams, respectively. This can be explained by the fact that creep and shrinkage of HPC are not appropriately modeled using conventional design equations. Farrington et al. [8] showed the HPC used in this project exhibits less creep and shrinkage than predicted by conventional methods. Also, Gross and Burns [10] showed Equations 6.1 and 6.2 underestimate the modulus of elasticity by as much as 25 percent. This causes an overestimation of the prestress loss owing to elastic shortening. Even using measured parameters, this method greatly overestimated the measured prestress loss. In the same order as above, these values were 142, 151, and 115 percent.

In general, the *PCI Design Handbook* components method produced more accurate results than the AASHTO LRFD components method. Similar to the AASHTO LRFD components method, the predictions using design parameters greatly overestimated the prestress loss. This overestimation is caused by the same reasons discussed in the previous paragraph. These values were 142, 151, and 133 percent of the measured prestress losses for the Louetta HPC beams, San Angelo eastbound HPC beams, and San Angelo westbound non-HPC beams, respectively. The *PCI Design Handbook* Components method using measured parameters produced values that were generally in agreement with the measured prestress loss. In fact, this method was nearly as accurate as the values predicted by the time-step analysis and the suggested method. The values predicted using measured parameters were 96, 109, and 92 percent of the measured prestress loss. However, this method does not include pre-release methods, thus effectively lowering its predicted prestress loss.

Gross and Burns [10] proposed a suggested components method similar to the components methods presented by AASHTO and PCI. The refinements made to this method, in addition to the use of measured parameters, make it very accurate. The use of components makes computations simpler than a time-step analysis. However, determining measured parameters make it more difficult compared to the conventional components methods.

Clearly, using measured parameters allows for a more accurate prediction of prestress losses. However, determining these parameters is more time and labor intensive than using the common design parameters. Unfortunately, current design equations do not adequately estimate the material properties of HPC such as the modulus of elasticity, creep, and shrinkage. Until a larger volume of information on HPC can be gathered, new empirical formulas that will better predict HPC behavior cannot be developed. Until this time, all future HPC bridges should be measured for material properties. This is especially true for new HPC mix designs.

6.3 CAMBER

Table 6.3 shows the measured camber results of the twenty-six instrumented beams. The measured camber is listed next to the camber predicted by the time-step analysis and the camber determined during the actual design. The design camber was calculated using one of the

previously discussed programs. PSTRS14 [20] was used to determine the camber of the Louetta HPC beams and the San Angelo westbound non-HPC beams. ADAPT-ABI [1] was used to determine camber in the San Angelo eastbound HPC beams.

Plots for the instrumented beams showing the measured camber and the time-step predicted camber are found in the appendix in report 7-2941-5. These plots reveal camber is expected to remain very stable at this point in the bridge's life. The measured camber values confirm this expectation. In general, camber measurements have remained relatively stable. Approximately three years had passed between the most recent and previous camber measurements. Despite this large change in time, most of the recent measurements are within 0.5 in. of the previous measurements. There is good agreement among measurements taken in the same span of each bridge. Most measurements in a single span remained relatively stable. If any variation between the last two readings was evident, a slight decrease in camber was observed. More long-term camber measurements need to be taken to determine if this downward trend will continue or if it is just an anomaly.

All but two of the Louetta HPC beams display the desired upward camber. The measured camber in the Louetta beams ranged from -0.36 to 2.71 in. The average measured camber is 1.11 in. In general, there was agreement between similar beams in the same span. The camber of beams N22 and N23 (both U54A beams) was very close. Beam N21 has a much larger camber, but it is a U54B beam with nineteen more pretensioned strands. Therefore, a larger camber was expected. This same trend was seen in the three beams of Louetta northbound span 3. The two U54A beams exhibit similar camber, while the U54B beam has a significantly larger camber.

Table 6.3 Long-Term Camber

Beam	Days After		Long-Term Service Camber (in.)		
	Release	CIP Deck	Measured	Predicted ¹	Actual Design ²
<i>Louetta HPC Beams</i>					
N21	2224	1491	2.71	3.29	5.05
N22	2252	1491	0.34	0.44	2.97
N23	2259	1491	0.19	-0.31	2.97
N31	2224	1491	2.19	3.33	4.54
N32	1749	1491	1.20	0.99	3.99
N33	1749	1491	0.96	0.94	3.99
S14	1738	1483	1.43	1.80	3.99
S15	1738	1483	1.38	1.60	3.99
S16	2252	1483	1.82	2.39	2.97
S24	2211	1483	-0.35	0.19	2.97
S25	2211	1483	-0.36	-0.09	2.97
S26	2239	1483	1.84	2.18	5.05
<i>San Angelo Eastbound HPC Beams</i>					
E13	1295	1183	1.84	2.90	0.43
E14	1295	1183	2.10	3.48	0.43
E24	1277	1170	1.75	2.38	-0.90
E25	1619	1170	1.14	0.58	-1.86
E26	1277	1170	0.47	1.69	-0.90
E33	1263	1156	1.76	2.69	-0.22
E34	1263	1156	1.27	2.69	-0.22
E35	1256	1156	2.08	2.82	-0.22
E44	1242	1132	2.50	2.70	-0.09
E45	1242	1132	1.62	3.21	-0.09
<i>San Angelo Westbound Non-HPC Beams</i>					
W14	1644	1374	-1.60	-1.49	1.15
W15	1644	1374	-1.57	-1.49	1.15
W16	1644	1374	-1.74	-1.49	1.15
W17	1639	1374	-2.58	-1.97	1.15
¹ Using incremental time-step analysis					
² Using PSTRS14 or ADAPT					

The three beams in southbound span one all have similar camber. Despite the fact that two of the beams are type U54A, while the other is type U54B, the number of strands is very similar. This explains why the camber is similar even though the beam types are different. The two beams with downward deflection are found in southbound span two. All of these beams are type U54B, but beam S26 (which has an upward camber) has 87 strands versus the 68 in the other two beams (which have a downward deflection). These are the longest instrumented beams measured for camber. An investigation of the mechanics equations used to determine camber reveals they are sensitive to beam length. Therefore, it becomes increasingly difficult to design for the desired upward camber as beam length increases. This difficulty in design is a likely

reason these beams have a downward deflection. It should be noted that the downward deflection is very small for both beam S24 and S25 at -0.35 and -0.36 in., respectively.

All of the San Angelo eastbound HPC beams exhibit the desired slight upward camber. The measured camber varied between 0.47 and 2.50 in. with an average of 1.65 in. There is reasonable agreement between beams in a single span. The beams in eastbound spans one, three, and four are identical and their measured camber was all within one inch of each other. The largest variation between beams in a similar span occurred in eastbound span two. Beam E26 exhibits the smallest upward camber of any eastbound beam. Beam E26 contains more pre and post-tensioned steel than beams E23 and E24. It is believed the measured value is an anomaly, because the time-step predicted camber is significantly higher for this beam. Further camber measurements need to be taken to confirm this belief.

All of the San Angelo westbound non-HPC beams exhibit a significant downward deflection. The measured deflection varies between -1.57 and -2.58 in. with an average of -1.87 in. There is reasonable agreement between the beams in this single span. This downward deflection has been attributed to the fact that these non-HPC beams in actuality possess similar material properties to the HPC beams [10]. These beams used a lower prestress force and therefore a downward deflection occurred.

Table 6.4 compares the measured camber to the other methods. The average, minimum, and maximum camber is presented for each bridge. The measured values are then compared to the values predicted by the time-step model and the actual design. The differences between the measured camber and the two predicted values were calculated. The average of the absolute value of these differences, as well as the maximum positive and negative values, are presented.

In general, all of the measured camber values are less than values predicted by the time-step analysis and the actual design, as shown in Table 6.4. The time-step analysis was closer to the measured values than the actual design values. The average time-step predicted value was within one inch of the measured value. This was a reasonable difference given the uncertainties involved in determining long-term camber. It is difficult to calculate long-term camber in any beam, especially one with the very long spans of these bridges. This calculation is further complicated due to the uncertainties involved with the material properties of HPC. On average, none of the design predictions was within two inches of the measured camber. Surprisingly, the values for the San Angelo westbound non-HPC beams were the least accurate compared to the measured camber. Although the San Angelo westbound beams are considered non-HPC, they do possess some properties that are similar to the HPC beams. For example, the compressive strength of the beams (8,920 psi) is considered HPC by some definitions. This could explain part of the over prediction.

Table 6.4 Analysis of Long-Term Camber

	Long-Term Service Camber (in.)		
	Louetta HPC	SA EB HPC	SA WB Non-HPC
Measured Camber			
Average	1.11	1.65	-1.87
Minimum	-0.36	0.47	-2.58
Maximum	2.71	2.50	-1.57
Difference (Measured - Predicted)			
Avg. Absolute Difference ¹	0.41	0.97	0.26
Max. Negative Difference	-1.14	-1.59	-0.61
Max. Positive Difference	0.50	0.56	-0.08
Difference (Measured - Actual Design)			
Avg. Absolute Difference ¹	2.68	2.02	3.02
Max. Negative Difference	-3.33	1.37	-3.73
Max. Positive Difference	-1.15	3.00	-2.72
¹ Average of the absolute values of the differences.			

6.4 FINDINGS IN THE FIELD PERFORMANCE OF HPC DECKS

When it became clear that most of the early age structural events for the beams had already happened and that, barring accidents or natural disasters, no new changes would be likely for the next several years, the researchers were asked to change focus from beams and automated data acquisition to distress and performance on new HPC bridge decks. These new decks fell into the HPC category, because during the time of cement shortages contractors wanted to take advantage of lower concrete costs associated with the use of less expensive supplemental cementitious materials (SCMs). SCMs such as fly ash and ground glass blast-furnace slag are typically substituted for 20 to 35 per cent of the portland cement in the batch designs for decks. TxDOT was willing to allow this since these SCMs were known to add performance benefits to the concrete in addition to the economic considerations. These benefits include reduced permeability, lower maximum curing temperatures due to heat of hydration, slower modulus development, mitigation for internal expansion mechanisms like ASR and DEF, and less drying shrinkage.

TxDOT asked the research team to monitor the field performance of several new HPC bridge decks found in Amarillo and Lubbock in addition to the Houston Louetta and San Angelo Concho River Bridge decks. Table ??? lists the locations of each bridge deck and Figures ?? through ??? show the locations on an aerial map of the region.

This sudden strong interest was based upon earlier observations, concerns, and discussions in Houston, where it became apparent on the first inspection visits that two patterns of early cracking were in evidence on both the decks. While anyone associated with large exterior concrete flatwork surfaces in Texas has become accustomed to some cracking in the surface, TxDOT and FHWA were not prepared for such extensive cracking to show up at such early ages.

Extensive cracking is a concern because cracks provide a direct conduit for oxygen, water and deicing salts (used to keep the wet sand piles in the maintenance yards from freezing hard) to corrode the steel reinforcement in the deck, resulting in surface spalling, delaminations, rougher ride quality, and punch-outs.

The irony in this cracking problem for the new decks is that TxDOT Bridge Division and the Districts tried to ensure a nominal two inches of concrete cover, and they worked very diligently to reduce the permeability of the mixture designs for the decks, so that deck deterioration due to corrosion of the reinforcement would be mitigated. The cracks in a cold, contracted slab can allow many times the water-borne chlorides to the steel than the permeable capillaries and pore structure in the sound concrete next to them. It is likely that efforts to reduce the permeability of the deck mixes may have backfired, resulting in a denser, more brittle deck that was more likely to crack extensively.

The excessive cracking in these decks can be blamed primarily on two items that are directly related to the use of precast panels in constructing the deck. The first item is associated with sudden transitions from the deeper portions of cast-in-place deck (over the beams and between the panels) to the shallow cast in place concrete on top of the panels. Such rapid transitions often result in stress risers at the transition. This is evidenced by the fine cracks found above and progressing to the edges of virtually every panel. They can be most easily be seen on mornings whenever the moisture on the wetted deck evaporates more slowly out of the cracks than from the uncracked surface.

The second item relates to the intersection of cracks at every panel corner. Each longitudinal panel edge produces a crack that intersects with the transverse edges at the panel corner. These corner cracks are typically initiation sites for early spalling. The corner cracking is most apparent as wider stair-step cracks over skewed bents. It is at these corners that mid-span flexural deflections in the underlying beams and in the panels allow panel ends (longest corner projection) over the bent cap and opposite side of the bearing pad to strain upward from resulting lever actions.

A third item relating to cracking is associated with construction technology versus materials constraints, and it involves the forming of reduced sections to force cracking to occur as an oriented joint over the edges of skewed bent caps. This practice normally involves the use of saw-cutting a hardened deck immediately after set or placing removable plastic 1-inch deep zip strips temporarily placed into the surface of the fresh concrete over the edges of the bent caps. The concept can work, but the skewed bents seem to present alignment problems for construction teams on top of the deck, and timing of the joint forming is critical. For these reasons the first sign of either of these problems is often obvious surface cracking that is clearly not in alignment with the contractors' formed or sawed joints.

CHAPTER 7: Summary, Conclusions, and Recommendations

7.1 SUMMARY

The long-term structural behavior of two high performance concrete bridges in Texas and the long-term performance with regard to distress in eight HPC bridge decks has been monitored in this study. Twelve Texas U54 beams in the Louetta Road Overpass in Houston, TX had been instrumented for strain and temperature readings. The U-beams varied in length from 117.9 to 136.4 ft and utilized 0.6 in. diameter low relaxation prestressing strands. All of the U-beams were made from high performance concrete. Fourteen AASHTO Type IV beams in the North Concho River/US 87/South Orient Railroad Overpass in San Angelo, TX had been instrumented for strain and temperature readings. Ten of these beams were high performance concrete, while four were considered non-HPC. These HPC beams varied in length from 129.0 to 153.3 ft, while the non-HPC beams were all 129.0 ft. The HPC beams utilized 0.6 in. diameter strands in a two stage tensioning process, involving both pretension and post-tension. The non-HPC beam utilized 0.5 in. diameter strands. Only pretension was applied to the non-HPC beams.

The original data acquisition system was updated to allow for remote monitoring of the bridges. The data gathered from the instrumentation was used to make field measurements of prestress loss and camber. The measured prestress losses were compared to values predicted by other methods. The methods included a time-step model, common methods suggested by AASHTO and PCI, as well as a suggested method for HPC beams. The measured prestress losses were also compared to values calculated during the actual beam design. The measured camber values were compared to values predicted by the time-step model and calculated during the actual beam design.

Limited durability testing was performed. The durability performance of these bridges was not the focus of this paper. The results of the durability testing are presented, but are not discussed in detail.

Field inspection monitoring of distress symptoms in bridge decks for several years has clearly shown that current bridge construction technology using stay-in-place precast concrete panels mounted on top of the beam edges and spanning the gap between the beams almost always results in repeating cracking patterns in the 4-inch thick cast-in-place portion of the deck above and around every panel. These cracks are typically quite tight for the first few years, but soon areas where longitudinal cracks intersect with transverse cracks (areas of the cast-in-place concrete over the corners of the precast panels) begin to spall. In cold weather the spalls retain non-compressible sand or debris to cause further spalling when warmer weather expands the concrete. The spalls also retain surface water for later damage due to freezing and thawing, and they serve as reservoirs to feed saltwater (from deicing salts or marine exposure) through the cracks to the steel reinforcement for eventual corrosion.

The dilemma at issue is that the precast panels are a way to lower the cost of the bridge deck construction, since the panels are basically contributed by ????. If the service life is significantly shortened, however, due to the earlier presence of deep cracks, then the service life costs of the bridge deck are probably higher than with the older method using permanent metal deck forms and full depth cast-in-place concrete placements.

7.2 CONCLUSIONS

The following observations have been made with regards to long-term prestress loss in HPC beams:

1. The average measured prestress loss, taken after several years of bridge service, was 40.7, 56.6, and 34.0 ksi for the Louetta HPC beams, San Angelo eastbound HPC beams, and San Angelo westbound non-HPC beams, respectively. In terms of percentage of the jacking force, these values were 20.1, 28.0, and 16.8 percent, respectively.
2. The measured prestress loss values, taken several years after construction of the bridges was complete, remain stable for beams in a single span.
3. Predicted prestress loss calculated during the actual beam design generally does not agree well with the measured values. PSTRS14, used in the Louetta HPC and San Angelo Westbound Non-HPC Beam design, predicted prestress losses higher than the measured values. ADAPT-ABI, used in the design of San Angelo Eastbound HPC Beams, predicted prestress losses lower than the measured values.
4. The time-step model did a good job of predicting prestress loss. However, this model is based on information specific to the beams in this study and cannot be applied to other beams.
5. Prediction methods suggested by AASHTO and PCI significantly overestimated the prestress loss. The methods cannot be recommended for use with HPC beams. Using measured parameters versus design parameters, significantly improved the accuracy of these methods.
6. The method suggested by Gross and Burns [10] did a very good job of predicting prestress loss. This method requires measured parameters and is the method recommended by this report until further information can be gathered on HPC beams.

The following observations have been made with regards to long-term camber and deflection of HPC beams:

1. The average measured upward camber, taken after several years of bridge service, was 1.11, 1.65, and -1.87 in. for the Louetta HPC beams, San Angelo eastbound HPC beams, and San Angelo westbound non-HPC beams, respectively.
2. In general, the measured camber values, taken several years after construction of the bridges was complete, remain stable for beams in a single span.
3. All but two of the HPC beams exhibit the desired upward camber. The downward camber is attributed to large beam lengths and a smaller than typical (compared to other HPC beams) prestressing force.
4. All of the non-HPC beams exhibit a downward deflection. This has been attributed to these beams possessing properties similar to HPC beams combined with a smaller than typical (compared to other HPC beams) prestressing force.
5. Measured camber values are generally less than values predicted by the time-step analysis. Average differences between measured and predicted camber values were 0.41, 0.97, and 0.26 in. for the Louetta HPC beams, San Angelo eastbound HPC beams, and San Angelo westbound non-HPC beams, respectively.
6. Measured camber values are much less than values predicted by the actual beam design. Average differences between measured and actual beam design camber values were 2.68, 2.02, and 3.02 in. for the Louetta HPC beams, San Angelo eastbound HPC beams, and San Angelo westbound non-HPC beams, respectively.

7. Long-term camber is extremely difficult to predict for HPC beams. Measured properties should be used whenever possible until a larger database of information on HPC can be collected.

These observations were made concerning HPC Bridge Decks:

Field inspection monitoring of distress symptoms in bridge decks for several years has clearly shown that current bridge construction technology using stay-in-place precast concrete panels mounted on top of the beam edges and spanning the gap between the beams almost always results in repeating cracking patterns in the 4-inch thick cast-in-place portion of the deck above and around every panel. These cracks are typically quite tight for the first few years, but soon areas where longitudinal cracks intersect with transverse cracks (areas of the cast-in-place concrete over the corners of the precast panels) begin to spall. In cold weather the spalls retain non-compressible sand or debris to cause further spalling when warmer weather expands the concrete. The spalls also retain surface water for later damage due to freezing and thawing, and they serve as reservoirs to feed saltwater (from deicing salts or marine exposure) through the cracks to the steel reinforcement for eventual corrosion.

The dilemma at issue is that the precast panels are a way to economically construct the bridge deck; the panel construction method is faster and safer. If the service life is significantly shortened, however, due to the earlier presence of deep cracks, then the service life costs of the bridge deck are probably higher than with the older method using permanent metal deck forms and full depth cast-in-place concrete placements.

7.3 RECOMMENDATIONS

7.3.1 HPC Bridge Elements

A. HPC Beams

1. Creep and shrinkage were less than ACI 209 methods predicted. Updated prediction methods now make adequate predictions for HPC, too.
2. Prestress losses- Measured parameters worked better than design parameters for predicting prestress losses. AASHTO and PCI prediction methods from the mid 1990s did not work well for predicting prestress losses in HPC beams. Use the new AASHTO methods that have been developed since then to better address HPC considerations.
3. Deflections and camber- The precise surveying system used to monitor changes in camber and deflections proved impractical and inaccurate. When the structure is new and static changes are larger, high-tech surveying or laser levels work well enough, but small changes later in the life of the structure are not easily or reliably monitored.

B. HPC Beam Fabrications and Performance

1. Use HPC mixtures with high-range water reducers and well-graded, high strength crushed aggregates to design for adequate flow through congested areas of draped tendons, as well as rapid strength and modulus development, resulting in faster prestress release times in the fabrication yard and lower creep and shrinkage in the cured beams.
2. Use supplemental cementitious materials (SCMs) to replace some of the portland cement in the mixtures. This keeps temperatures in the larger mass sections below 158 degrees F, thereby mitigating the likelihood of delayed ettringite formation. At

the same time the strategic use of SCMs mitigates for potential alkali silica reactions exacerbated by hot Texas weather.

C. HPC Decks

1. Monitoring confirmed previous observations that cracks reflected through the cast-in-place concrete wearing surface of the deck immediately above underlying precast panel corners and above the joints between the panels. Fine cracking in the deck surface distinctly outlined precast panels underneath.
2. Cracking patterns resembling stair steps occurred over every skewed bent that was monitored. This pattern resulted from the square corners of the precast panels ending over the top of the bent in a diagonal pattern. Mid-span deflections due to loads on the beam caused slight rotation of the panel ends resting above the beam edge.
3. Cracking always occurred in the thinner CIP sections immediately adjacent to the thickened sections over the bent caps.
4. The above patterns were nonexistent in the thicker CIP HPC decks constructed with the stay-in-place metal pan forms (without precast panels).

D. Recommendations for deck construction-

1. Abandon the use of precast panel in favor of the older technology using the stay-in-place metal pan forms. Costs are approximately the same for either method. Or...
2. Use precast panels, but fill the joints between precast panels and at areas over the bent caps until flush with panel tops. After the filled portion cures and cools to ambient temperature place joint **tape or anti-fracture membrane** over all joints, and place a well designed lower modulus CIP wearing surface. Or...
3. Use precast panels and place CIP as currently done, but place durable elastomeric polymer concrete overlay over CIP to bridge cracks and improve wearing surface.

7.3.2 Data Acquisition Systems for Monitoring Field Performance

1. Sensors - Vibrating wire strain gages (VWG) with their own temperature sensing were more consistent and more durable than resistance-type electrical strain gages and simple thermocouples for monitoring. VWGs are recommended for any in-place monitoring.
2. Data Loggers – Campbell Scientific CR10 data loggers served without problems, other than power sources and remote data transfer, but peripheral equipment for these units has improved greatly since the project began.
3. Power – 12-volts DC powers the logger and is available from many sources. These are recommended.
 - a. Transformers that convert 120 volt AC or 240 volts AC to 12 volts DC are recommended for the power source to the DAS. Most 12-volt battery systems required too much effort in battery maintenance and replacement.
 - b. Photo-voltaic (solar) cells to automatically maintain batteries' charges should be used where AC power is not easily available.
4. Data transfer – two modes were used to transfer data from loggers to laptop computers for data reduction and analysis.
 - a. The most reliable was RS 232 port and cable connections to a laptop computer, but it required up to four trips per year to each bridge (depending on the number of data points collected each month).
 - b. New digital technology has produced reliable data modems that download data remotely to desktop computers.

References

1. ADAPT Corporation, ADAPT-ABI, *ADAPT-Bridge Incremental Structural Concrete Software System*, Version 2.00, 1996.
2. American Association of State Highway and Transportation Officials, *AASHTO LRFD Bridge Design Specifications*, First Edition, Washington, D.C., 1994.
3. American Concrete Institute Committee 209, *Prediction of Creep, Shrinkage, and Temperature Effects in Concrete Structures (ACI 209R-92)*, American Concrete Institute, Detroit, 1992.
4. American Concrete Institute Committee 318, *Building Code Requirements for Structural Concrete (ACI 318-99) and Commentary (ACI 318R-99)*, American Concrete Institute, Detroit, 1999.
5. Byle, K. A., Burns, N. H. and Carrasquillo, R. L., *Time-Dependent Deformation Behavior of Prestressed High Performance Concrete Bridge Beams*, Research Report 580-6, Center for Transportation Research, The University of Texas at Austin, Austin, TX, 1997.
6. Campbell Scientific, Inc., PC208W, *Software Package for Campbell Scientific Dataloggers*, Version 3.01, 1992.
7. Carrasquillo, R. L., Nilson, A. H., and Slate, F. O., "Properties of High Strength Concrete Subject to Short-Term Loads," *ACI Journal*, May/June 1981, Vol. 78, No. 3, pp. 171-179.
8. Farrington, E. W., Burns, N. H., and Carrasquillo, R. L., *Creep and Shrinkage of High Performance Concrete*, Research Report 580-5, Center for Transportation Research, The University of Texas at Austin, Austin, TX, 1996.
9. Goodspeed, C. H., Vanikar, S., and Cook, R. A., "High Performance Concrete Defined for Highway Structures," *Concrete International*, February 1996, Vol. 18, No. 2, pp. 62-67.
10. Gross, S. P. and Burns, N. H., *Field Performance of Prestressed High Performance Concrete Highway Bridges in Texas*, Research Report 580/589-2, Center for Transportation Research, The University of Texas at Austin, Austin, TX, 1999.
11. Gross, S. P. and Burns, N. H., *Transfer and Development Length of 15.2 mm (0.6 in.) Diameter Prestressing Strand in High Performance Concrete: Results of the Hoblitzell-Buckner Beam Tests*, Research Report 580-2, Center for Transportation Research, The University of Texas at Austin, Austin, TX, 1995.
12. Gross, S. P., *High Performance Concrete Monitoring Manual for Use In Monitoring Long-Term Behavior of Texas HPC Bridges*, 2001.
13. Gross, S. P., SORTDTA1, *Data Manipulation and Reduction Program for Use With Custom Data Acquisition Systems in the Texas HPC Bridge Instrumentation Projects*, Version 1.0, 1994.
14. Lin, T. Y. and Burns, N. H., *Design of Prestressed Concrete Structures*, John Wiley and Sons, New York, 1981.

15. Myers, J. J. and Carrasquillo, R. L., *Production and Quality Control of High Performance Concrete in Texas Bridge Structures*, Research Report 580/589-1, Center for Transportation Research, The University of Texas at Austin, Austin, TX, 1998.
16. Nilson, A. H., *Design of Prestressed Concrete*, John Wiley and Sons, New York, 1987.
17. Precast/Prestressed Concrete Institute, *PCI Design Handbook*, Fifth Edition, Chicago, 1999.
18. Prestressed Concrete Institute Committee on Prestress Losses, "Recommendations for Estimating Prestress Losses," *Journal of the Prestressed Concrete Institute*, July-August 1975, Vol., 20, No. 4. pp. 43-75.
19. Shepperd, G. A. and Burns, N. H., Long-Term Behavior of HPC Louetta Road Overpass, Research Report 7-3993, Center for Transportation Research, The University of Texas at Austin, Austin, TX, 2001 (under review).
20. Texas Department of Transportation, PSTRS14, *Prestressed Concrete Beam Design/Analysis Program*, Version 3.20, 1991.
21. Zia, P., Leming, M. L., and Ahmad, S. H., High Performance Concretes: A State of the Art Report, SHRP-C/FR-91-103, Strategic Research Highway Program, National Research Council, Washington, D.C., 1991.
22. Zia, P., Preston, H. K., Scott, N. L. and Workman, E. B., "Estimating Prestress Losses," *Concrete International*, June 1979, Vol. 1, No. 6, pp. 32-38.

Appendix C: Last Bridge Deck Inspection Report

NOTE:

Although annual inspections were made in 2003 and 2004, no new deterioration and no obvious growth in existing deterioration were evident. This information was discussed with the Project Director over the phone at the time, but no formal written report was submitted.

Development of a Comprehensive Database of High Performance Concrete Bridge Decks

Chris Shoemaker
Graduate Research
Assistant
University of Texas
at Austin

David Whitney
Res Engr/Sci Assoc
Center for Transportation
Research

November 13, 2002

Introduction

High Performance Concrete (HPC) is an engineered material enhanced to optimize properties associated with durability for the specified applications. Transportation structures have increasingly used this HPC concept to construct concrete decks with improved surface abrasion resistance, reduced chloride penetrability, and improved resistance to freezing and thawing damage. Although the benefits of these properties are apparent, it can be difficult to predict how much specific target properties result solely from concrete constituents, and how much those properties will be affected by other construction circumstances.

This report summarizes the research conducted during the past year as specified in the Center for Transportation Research Project 7-2941, "Long-Term Behavior of High Performance Concrete Bridges." In addition to the ongoing monitoring of sites at the Louetta Road Overpass on State Highway 249 in Houston, TX, and the North Concho River/US 87/South Orient Railroad (S.O.R.R.) Overpass on US 67 in San Angelo, TX, several new HPC bridges were examined for inclusion in this study.

These additional sites will serve as monitoring points to build a HPC bridge database in which the behavior can be catalogued for study and comparison. It is the intent of this project to establish and maintain a database of HPC bridge sites throughout the state so the specific long-term effects of various HPC mix designs and strategies can be evaluated and improved.

Background

The new bridges selected for study include several locations in Lubbock and Amarillo, TX. In Lubbock, particular attention will be focused on the 82nd St. overpass on US 82/62 (Figure 1) which has immediate evidence of cracking. Also, two recently constructed bridges which may be considered for future monitoring include Loop 289 & Frankford St. and the IH 27 New Deal bridge. In Amarillo, the bridges of primary interest are shown in Figure 2 and include the RM 1061 overpass on Loop 335 (3.4 mi. north of IH 40) and the Amarillo Creek Bridge on Loop 335 (1.8 mi. north of IH 40).



Figure 1: Map of US 82/62 Bridge in Lubbock, TX

Annual Inspection

Lubbock - July 10, 2002

US HW 82/62 & FM 179

Currently, this bridge has no significant cracking that would warrant its inclusion in this study. A few observations of note include the use permanent metal deck forms, and irregular zip strips which appear to be misaligned with the joints in the deck, and some slight stretch-cracking on the east side of the east-bound bridge. Stretch cracking is a series of shallow longitudinal tears running orthogonally to the tie grooves. The cracks are thought to be the result of surface tears from the tining process after the surface of the concrete has begun to dry and lose its plasticity. The surface tears are exacerbated by plastic drying and shrinkage.

US HW 82/62 & 82nd St.

This structure presented the most visual evidence of cracking and merits its inclusion in this HPC deck study. Cores were drilled from the deck upon a subsequent visit to further examine the chloride content and permeability. The cast-in-place (CIP) deck is supported with precast deck panels and has a slight negative camber. There is minor stretch cracking which appears to be induced by tining and plastic shrinkage. The most serious problem with



Figure 2: Map of Bridges in Amarillo, TX

this deck is several large transverse cracks in areas located over the supports. Figure 3 shows a cracked region of the deck that was cored for determining the chloride content along the crack surface.

LP 289 & Frankford St.

We visited this newly constructed bridge to see if there were any early signs that would suggest including this HPC deck in our study. However, at this early point in time in the bridge's service life, there are no distress symptoms such as visible signs of cracking that indicate any potential problems.

New Deal

During our first inspection of this structure, the north-bound direction had been completed and was carrying both directions of traffic while the south-bound bridge was being constructed. At the time, we did not observe any serious cracking in the completed deck. However, there have been recent reports of cracking since our last visit and researchers will check again to see if this bridge should be included in the database.



Figure 3: Region of Cracked HPC Deck Used for Chloride Determination

Amarillo - July 11, 2002

LP 335 & RM 1061 - 3.4 Mi. N. of IH 40

There are several regions of this deck with a moderate amount of transverse cracks and would therefore warrant its inclusion within the database. Approximately 51 ft. from the southern end is an area with several significant cracks. A typical representation of the transverse cracks is shown in Figure 4. Also in this area are a few longitudinal cracks located midspan.

LP 335 & Amarillo Creek - 1.8 Mi. N. of IH 40

The most significant cracking in this HPC deck appears to be longitudinal, located primarily in the thickened CIP sections over the bents. Figure 5 shows a crack typical of the longitudinal patterns observed in this deck. The cracking is not severe in this deck, but, due to the fact that the pattern is longitudinal rather than the transverse cracking seen in other HPC decks, this bridge will be included in the database for comparison.



Figure 4: Transverse Cracks in the LP 335 & FM 1061 Bridge in Amarillo



Figure 5: Longitudinal Cracks in the Amarillo Creek Bridge

Houston - September 26, 2002

SH 249 & Louetta Rd.

High traffic volume in both directions limited our inspection of the deck to visual observations from the outer shoulder lanes. There is a moderate concentration of cracks throughout the deck, particularly in the areas above the skewed bents. Some of the cracks appear to have been routed or sawed, and had accumulated in some of the wider cracks. Figures 6 and 7 show two of the larger cracks observed from the shoulder.

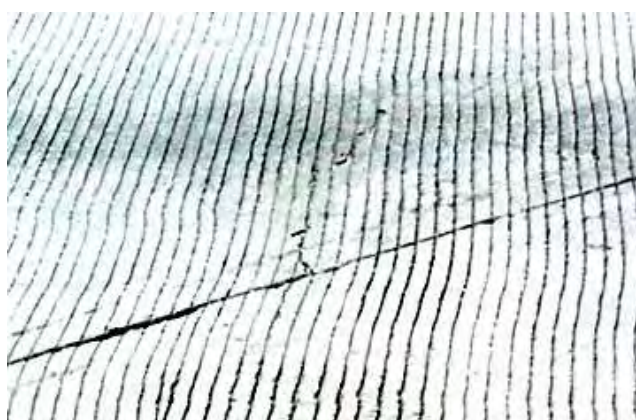


Figure 6: Large Transverse Cracking in the Louetta Bridge Deck (Contrast Raised to Highlight Crack)

The research team observed some minor cracking from below the bridge in a couple beams and panels. A few of the beams showed some structurally insignificant cracking, but the most noticeable instance is shown in Figure 8 where a large crack starts in the top flange and continues vertically through one of the web faces of the U-beam. Although this larger crack does not appear to present any structural implications at this time, it should be closely inspected and reported every year. Another non-structural beam anomaly was observed, where the underside had a "honeycombing" pattern of cracking, resulting from poor consolidation in the form bottom.

The deck panels with cracks seemed to be located in areas over the skewed bents. In these deck panels the cracks were oriented diagonally from the



Figure 7: Another Large Crack in Louetta Bridge Deck (Contrast Raised to Highlight Crack)

main axis of the roadway, an example of which is presented in Figure 9. Additionally, the soffits on both edges of the deck had several occurrences of very obvious cracking, presented in Figure 10.

San Angelo, September 24, 2002

US 87 & N. Concho River Bridge

At the time of our inspection, the east-bound bridge was shut down due to unrelated construction in the area. This facilitated our observation of that entire deck. However, due to the high volume of traffic passing over the west-bound bridge we were unable to observe this deck during this trip. TxDOT area engineers did not want to close down traffic on the one bridge not in the construction traffic control plan, so another inspection trip will be necessary in the future. There is some cracking located in the east-bound bridge deck over the bents. There are both transverse and longitudinal cracks, with a few regions of bisecting cracks. With the exception of this one moderately cracked region, the majority of the deck was problem free. The snoop truck provided a view of the underside of the bridge, and we did not observe any significant cracking or other problems in the beams or precast panels from our vantage point.



Figure 8: Large Crack in Flange and Web of Louetta U-Beam



Figure 9: Underside of Cracked Panel in Louetta Bridge



Figure 10: Cracked Soffit Section on Westbound Deck

Chloride Content and Permeability Evaluation

Core samples were collected in the Lubbock US 82/62 & 82nd St. bridge and the two Amarillo bridges on LP 335. At each site, two cores were selected with cracks for use in determining the chloride content along the crack face at varying depths. Two additional uncracked specimens were collected to evaluate the permeability of each HPC deck.

A 3/8-in. drill bit was used to extract the sampling material from the cracked cores. For each core, the chloride content was determined at depths of 0 - 1/4 in. and 1/4 - 1/2 in. Samples were drilled from the top surface of each core, and from the crack faces. A diagram is presented in Figure 11 showing the location of each sampling location for this test. Enough material was collected so that two separate 1.5-g samples could be tested at each location. Tests were conducted using a James Instruments CL-500 meter, according to ASTM C 1152, except for the smaller sample size specified by the manufacturer of this equipment.

The percent Cl values were determined using the CL-500 test calibration graphs and graphed in Figure 12. For clarification, the prefix for each group indicates the core from which the sample was retrieved, and the suffix lettering indicates the two samples collected at each core.

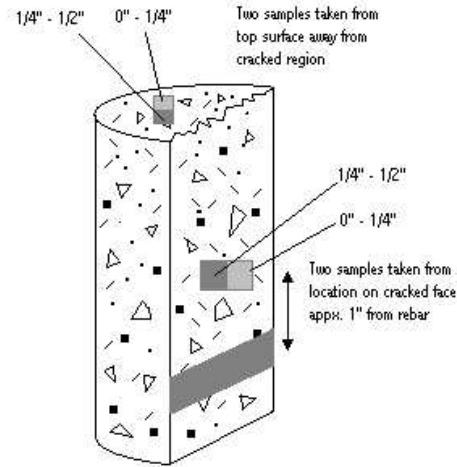


Figure 11: Drill Locations for Sampling Procedure 1

As should be expected, the highest chloride concentrations are found at the surface readings. For several of the samples the chloride content is higher at the locations along the crack face than the readings 1/4 - 1/2 in. at the surface. This is important to note, as it strengthens the hypothesis that the cracks serve as a more important vehicle to transporting the chloride ions than the permeability of the concrete matrix.

Later, it was determined that chloride content readings should also be recorded at depths closer to the rebar at the cracked section face, and compared with the equivalent depth in an uncracked portion of the deck. In this second procedure samples were collected 1/2 in. above the rebar depth both inside the cracked surface and the exterior circumference of the core. Furthermore, samples were collected 1/2 in. from the top surface inside the crack face as well as the exterior. A diagram showing the location of these tests are presented in 13 and the results can be found in 14.

It needs mentioning that the first sampling process with our limited number of specimens left the cores from the RM 1061 bridge too badly damaged to drill material with the required confidence of location and contamination to conduct the ASTM C 1152 chloride evaluation test procedure. The impact rotary drill disintegrated portions of these cores and made it impossible to say with certainty which locations were 1/2 in. above the rebar and 1/2

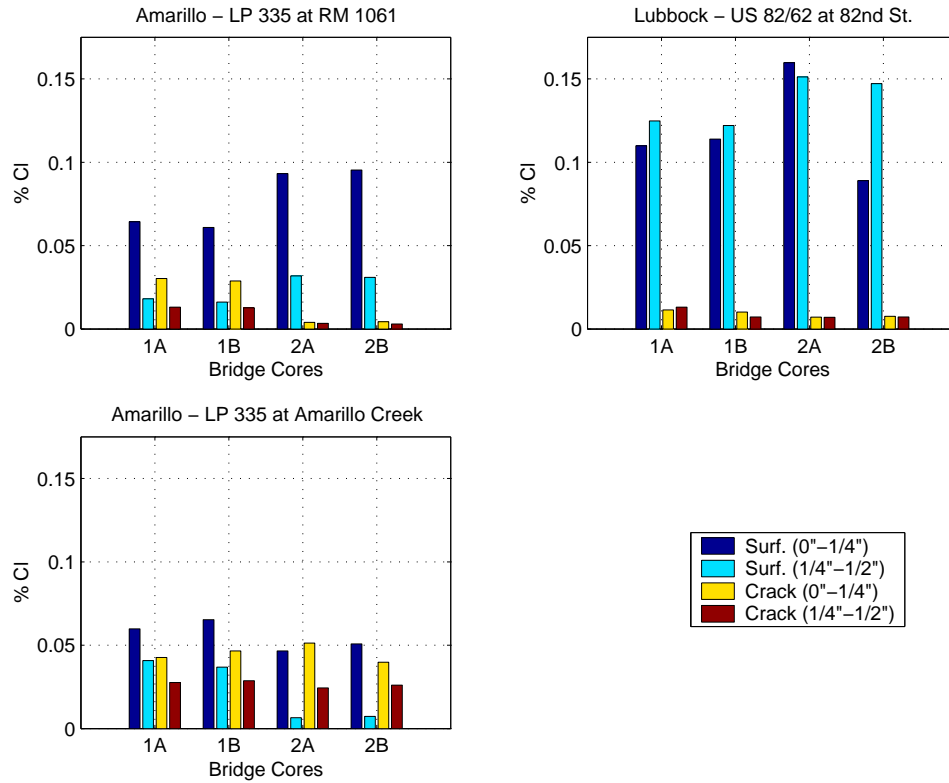


Figure 12: Chloride Content Evaluation Number 1

in. from the surface.

In order to evaluate the permeability of each HPC deck, the concrete cores were cut to provide 2-in. thick slices from the top of each core for testing. The circumferential surface of each slice was coated with rapid setting epoxy that was allowed to cure and then placed into a desiccator for three hours. Then, each specimen was placed in a plastic tray and filled with de-aerated water. The specimens were then soaked under vacuum pressure for an additional hour. After the pressure treatment, the samples soaked for 18 hours. Following the 18-hour period, silicone was applied around each end plated and fastened to the exposed surfaces of each core. One cell (-) was filled with 3% NaCl solution, and the other cell (+) was filled with 0.3-N NaOH solution. The lead wires were attached to banana posts, and automated scanning using a computer-integrated data logger was enabled

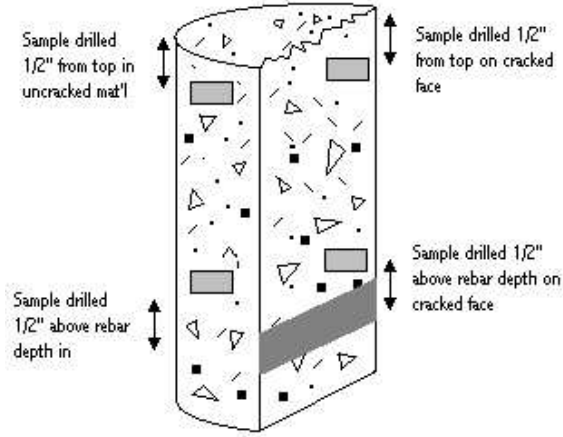


Figure 13: Drill Locations for Sampling Procedure 2

for 6 hours, with readings being taken every 30 minutes. This test was conducted according to AASHTO T 277-93 (ASTM C1202-91).

The results from the rapid-ion permeability test are presented in Table 1. Two of the test cylinders had to be stopped before the test period was scheduled to be completed, because these specimens reached the 190-degree maximum temperature. These cylinders are indicated with an (*) in the results shown in Table 1. According to the T 277-93 test standard, a charge passed greater than 4000 coulombs is categorized as being high, and charge between 2000-4000 is categorized as being moderate.

Monitoring Equipment

In addition to making visual observations on the condition of the HPC bridge decks and beams, one of the goals was to report on the status of the monitoring equipment being used at the San Angelo and Houston sites. The objective of this site visit was to access the data collection stations, examine the monitoring equipment for any problems, and reestablish a connection between the modem and the local computers in Austin.

The bridge in San Angelo has three data acquisition stations (DAS), indicated in the diagram in Figure 15. The DAS monitoring the westbound

Table 1: Results From Rapid-Ion Permeability Test

Time	Lubb 1	Lubb 2	Am 1061 1	Am 1061 2	Am Creek 1	Am Creek 2
1	0.00311	0.00329	0.00206	0.002	0.00129	0.00092
2	0.00403	0.00449	0.00247	0.00244	0.00144	0.00104
3	0.00514	0.00527	0.00261	0.00287	0.00146	0.00114
4	0.00611	0.00592	0.00273	0.0032	0.00153	0.00125
5	0.00701	0.00633	0.00294	0.00342	0.00158	0.00133
6	0.00773	0.00666	0.00307	0.00362	0.00165	0.00139
7	0.00827	0.00703	0.00317	0.00374	0.0017	0.00142
8	*	*	0.00318	0.00387	0.00175	0.00147
9	*	*	0.0032	0.00399	0.00178	0.0015
10	*	*	0.00316	0.00404	0.0018	0.00156
11	*	*	0.00312	0.00415	0.00184	0.00159
12	*	*	0.00297	0.00462	0.0018	0.00162
13	*	*	0.00288	0.00473	0.0018	0.00165
Charge Passed in Columbs						
	6430	6090	6320	7800	3580	2900

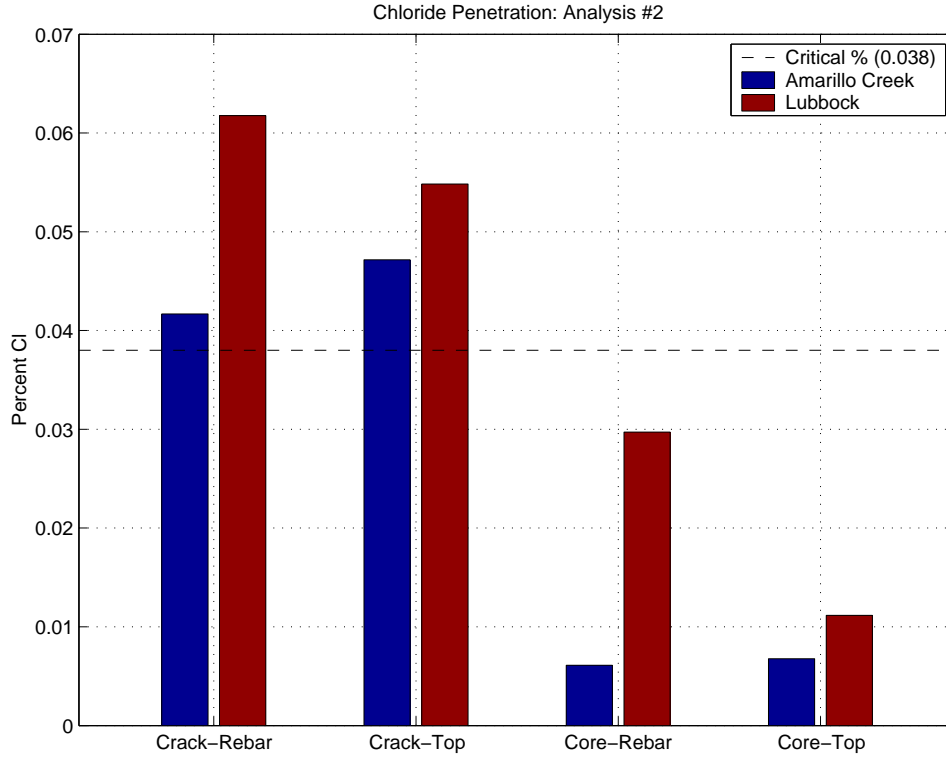


Figure 14: Chloride Content Evaluation Number 2

span had a connection problem between the data module and the solar panel source. After checking the solar panel source with a voltmeter it appeared no power was being transmitted to the module. The research team was unable to make a connection between the data module and the data logging software on the laptop computer in the field, so the module was removed and replaced for further examination in Austin.

The data acquisition stations located on the eastbound bridge (Figure 16) appeared to be functioning properly, in-so-far that there were audible indications of a periodic and regular timer sending data to the storage modules. However, there were similar difficulties achieving a connection between the module and the laptop in the field. The full modules were replaced with fresh ones and transported to Austin for data retrieval.

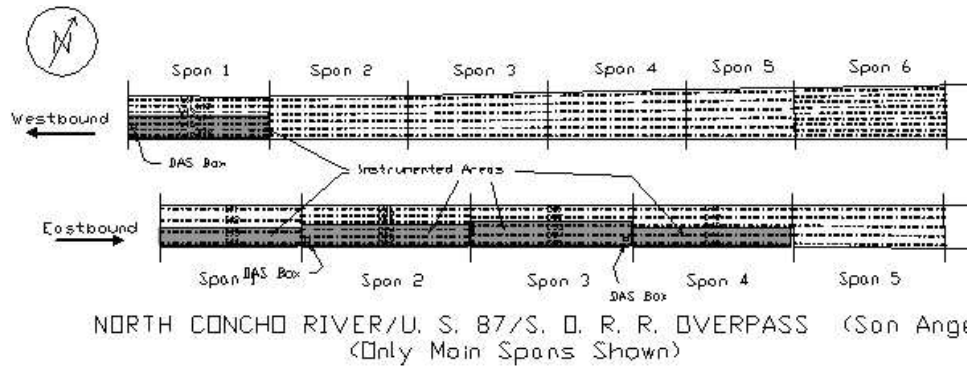


Figure 15: Diagram of Data Acquisition Stations on San Angelo N. Concho River Bridge

A few of the PVC pipes used to encase the exposed wires were originally connected with duct tape. Exposure to the elements has caused many of these fittings to separate, revealing the cables inside. The research team has noted that in a future trip more permanent means of sealing the PVC pipes will be considered.

In Houston, one of the noticeable problems with the DAS on the north-bound bridge was the absence of an antennae. This obviously will need to be replaced for any modem connection to be established. Similarly, the storage modules were swapped out for data retrieval at the lab in Austin.

Recommendations & Conclusions

Having identified the additional HPC bridges in Lubbock and Amarillo, the next step in preparing the database will include contacting each district for any and all relevant construction and materials data. Researchers will repair remote download problems in Houston and San Angelo and continue to annually monitor the selected HPC decks for further symptoms. More cores will be collected from each bridge every four or five years to monitor significant changes in the permeability and chloride content near the steel reinforcement.

With the data modules in the research team's possession at the lab, the next major step in evaluating the condition of the monitoring stations and



Figure 16: Eastbound, Westend Box

the ability to engage the remote access capability will be two-fold. First, verification needs to be made to see exactly what, if any, data is successfully being stored in each module. Second, confirm that the modems are still properly connected and powered and attempt to connect with each station from remotely.

Appendix D: PSI Bridge Inspection Reports on Louetta and San Angelo HPC Structures

DRAFT

HIGH PERFORMANCE CONCRETE BRIDGE DECK INVESTIGATION

Tomball Parkway (S.H. 249) Bridge over Louetta Road
Houston, Texas

I. BACKGROUND

The Tomball Parkway (S.H. 249) Bridge over Louetta Road in Houston, Texas consists of two separate bridges, one carrying three lanes of the northbound traffic and the other carrying three lanes of the southbound traffic with an additional exit ramp (see photos 1 through 3). Both bridges consist of precast U-beam girders covered with precast concrete deck panels (3.5-inches thick \times 8-feet long), which are in turn covered with 3.75-inches of cast-in-place concrete (see photo 4). The substructures consist of concrete columns and concrete abutments at each end.

The Tomball Parkway Bridge is a major structure carrying heavy traffic. It is 391-feet long and consists of three spans in each direction. Span 1, Span 2 and Span 3 have approximate lengths of 121.5 ft., 135.5 ft. and 134.0 ft., respectively. The width of the bridge is variable and varies from 160 ft. at the ramp to 120 ft. in the middle. The bridge has a skew of 33° to 39° . Each span in the northbound bridge consists of five Texas U54 beams, and each span in the southbound bridge consists of six Texas U54 beams. Beams are prestressed. The specified compressive strength of the girders at release of prestressing and 56 days ranged from 6,900 to 8,800 psi and 9,800 to 13,100 psi, respectively. At the interior bents, each beam is supported by a single post-tensioned pier.

The bridge was designed in accordance with the AASHTO Standard Specifications for Highway Bridges (1992) using HS 20-44 design live load and an E_c value of 6,000 ksi. Prestress losses in the girder were calculated as 55,390 psi. Camber at release was calculated to be in the range of 4.06 in. to 5.64 in. The minimum concrete cover over the stirrups was specified to be 1.0 in.

All beams, piers, and precast deck panels were fabricated using high performance / high strength concrete. For comparison purposes, the southbound main-lane bridge has a high performance / high strength cast-in-place deck, whereas the northbound main-lane bridge has a high performance / normal strength cast-in-place concrete deck. The precast deck panels were prestressed utilizing $\frac{3}{8}$ in. diameter strands. The cast-in-place concrete overlay was reinforced with #5 bars at a spacing of 6 in. center-to-center in the transverse direction and #4 bars at a spacing of 12 in. center-to-center in the longitudinal direction. The rebar used in the cast-in-place deck was Grade 60 and uncoated. The concrete cover over #5 transverse reinforcing bars in the cast-in-place deck was specified as 2 in. The concrete cover below the $\frac{3}{8}$ in. diameter strands in the precast deck panels was specified as $1\frac{3}{4}$ in. The deck of each bridge was constructed simultaneously using similar construction techniques by the same personnel.

DRAFT

The Tomball Parkway (S.H. 249) Bridge over Louetta Road was the first of a series of demonstration projects for utilizing HPC in bridge structures, which were co-sponsored by the Federal Highway Administration (FHWA) and the Texas Department of Transportation (TxDOT). The construction of the bridge decks started in October 1996. After construction was completed, but before opening to traffic, both the northbound and southbound bridges were expanded by one lane on their left sides to accommodate an increase in the projected usage of the highway. In anticipation of the widening, the original bridge deck on the widened side was poured only to the center of the top flange of the original exterior girder. That is, the overhang on the widened side of each bridge was not constructed during the original deck pour and the parallel northbound and southbound bridges were several feet apart. After widening, the two bridges give the appearance of a single bridge, referred to Tomball Parkway (S.H. 249) Bridge in this report. The bridge was opened to traffic in both directions in June 1998.

II. SCOPE OF SERVICES

Professional Service Industries Inc. (PSI) is under contract with the Federal Highway Administration (FHWA) to conduct bridge deck inspections for HPC bridges. Our scope of services on this bridge included a series of tasks and sub-tasks, which are described as follows:

- Collect all available information relevant to the construction of each bridge, including;
 - Deck Concrete Properties
 - Specified Deck Concrete Construction Procedures
 - Approved Concrete Mixture Proportions
 - Measured Properties from QC Tests of Production Concrete
 - Measured Properties from Research Tests of Production Concrete
 - Actual Method of Deck Placement
 - Average Daily Traffic (ADT)
 - Average Daily Truck Traffic (ADTT)
 - Exposure Condition of the Bridge
 - Any Performed Maintenance
 - Any Inspection Reports
- Visually inspect the bridge, and obtain the following:
 - General condition of the deck top surface
 - Determination of the maximum crack width
 - General condition of the deck underside
 - General condition of the girders
 - Photograph areas of significant deterioration
 - Prepare drawings locating defects
 - Extract 8 concrete core samples

III. COMPILATION OF BRIDGE CONSTRUCTION INFORMATION

Information sources used for this report included bridge drawings, field inspection results, bridge summary data sheets, and technical information contained in FHWA's "Compilation and Evaluation of Results from High Performance Concrete Bridge Projects" version 3.

Deck Concrete Properties

Two HPC mixture designs were specified for use in the cast-in-place decks of the Tomball Parkway Bridge (class K, and class S Modified). The southbound cast-in-place decks utilized class K (HPC) and the northbound cast-in-place decks utilized class S (Modified). The class K (HPC) mixture design incorporated 32% fly ash by the weight of total cementitious materials and a high range water reducer (HRWR) for reduced water-to-cementitious material ratio (w/cm) and reduced permeability. The mixture had a specified maximum w/cm of 0.35. The class K (HPC) concrete may be classified as a high strength HPC. The class S (Modified) mixture design incorporated 28% fly ash by the weight of total cementitious materials without the use of a high or mid-range water reducer. A maximum w/cm of 0.43 was specified for this mixture. The class S (Modified) concrete may be classified as a normal strength HPC.

Table 1 lists the specified properties for concrete used in the cast-in-place decks of the two bridges. Limited information was available on the precast deck panels. For these panels, the slump of the mixture was specified as not to exceed 8 inches and the compressive strength at 28 days was specified as 8,000 psi (Table 1)

TABLE 1: Specified Concrete Properties for Precast Deck Panels and Cast-in-Place Decks

Property	Precast Deck Panels	Northbound Cast-in-Place Decks Class S (Modified)	Southbound Cast-in-Place Decks Class K (HPC)
Max. Water/Cementitious Material Ratio:	---	0.43	0.35
Percentage of Fly Ash:	---	28%	32%
Slump:	≤ 8 in.	3 - 4 in.	8 - 9 in.
Air Content:	---	5%	0%
Designed Compressive Strength:	8000 psi @ 28 days	4000 psi @ 28 days	8000 psi @ 28 days
Chloride Permeability (AASHTO T 277):	Guideline of 1500 coulombs at 56 days		

Specified Deck Concrete Construction Procedures

The procedures specified for deck concrete construction were in conformance with the current TxDOT specifications for casting of bridge decks. It should be noted that HPC

used in the construction of the Tomball Parkway overpass bridge incorporated a number of chemical and mineral admixtures. As a result, special attention was required during the concrete placement and curing, specifically for the HS/HPC mixture having a low water-to-cementitious material ratio (0.35). Since minimal bleeding water occurred from the mixture during concrete casting, plastic shrinkage cracking was a concern when the construction was done in conditions of high temperature and low relative humidity. Fogging of the deck while the concrete was still plastic was specified in the deck concrete construction procedures. Additionally, membranes such as curing compounds were specified after the surface finishing to help prevent moist loss.

For the cast-in-place deck a wet curing for 10 days was specified when fly ash was used and 8 days when no fly ash was used. Concrete cylinders 4 × 8 in. in dimensions and cured according to AASHTO T 23 were used for quality control testing.

Approved Concrete Mixture Proportions for Production Concrete

The Tomball Parkway Bridge has composite decks consisting of precast concrete deck panels (3.5-inches thick × 8-feet long), which are in turn covered with 3.75-inches of cast-in-place concrete. Table 2 provides the approved mixture proportions for the class S (Modified) normal strength HPC used in the northbound bridge decks and the class K (HPC) high strength concrete used in the southbound bridge decks.

TABLE 2: Approved Mixture Proportions for Precast Deck Panels and Cast-in-Place Decks

	Precast Deck Panels	Northbound Cast-in-Place Decks Class S (Modified)	Southbound Cast-in-Place Decks Class K (HPC)
Cement Brand:	Alamo	Capitol	Capitol
Cement Type:	III	I	I
Cement Quantity:	565 lb/yd ³	383 lb/yd ³	474 lb/yd ³
Fly Ash Type:	C	C	C
Fly Ash Quantity:	164 lb/yd ³	148 lb/yd ³	221 lb/yd ³
% Replacement by Weight:	22.5%	28%	32%
Fine Aggregate Type:	River Sand	River Sand	River Sand
Fine Aggregate FM:	2.60	2.54	2.54
Fine Aggregate Quantity:	1109 lb/yd ³	1243 lb/yd ³	1303 lb/yd ³
Coarse Aggregate, Max. Size:	¾ in.	1 ½ in.	1 in.
Coarse Aggregate Type:	No. 6 Crushed River Gravel	No. 4 Crushed Limestone	No. 5 Crushed Limestone
Coarse Aggregate Quantity:	1983 lb/yd ³	1856 lb/yd ³	1811 lb/yd ³
Water:	228 lb/yd ³	229 lb/yd ³	244 lb/yd ³
High-Range Water-Reducer Type:	F	--	F

DRAFT

High-Range Water-Reducer Quantity:	170 fl oz/yd ³	None	122 fl oz/yd ³
Retarder Type:	B and D	B and D	B and D
Retarder Quantity:	23 fl oz/yd ³	45 fl oz/yd ³	22 fl oz/yd ³
Air Entrainment Quantity:	None	2.1 fl oz/yd ³	None
Water/Cementitious Materials Ratio:	0.31	0.43	0.35

Measured properties of the approved concrete mixtures for precast deck panels and cast-in-place decks are summarized in Table 3.

TABLE 3: Measured Properties of Approved Mixture for Precast Deck Panels and Cast-in-Place Decks

Property	Precast Deck Panels	Northbound Cast-in-Place Decks	Southbound Cast-in-Place Decks
Slump, in	7 – 10	3 – 4	8 – 9½
Air Content, %	2.0%	5.0	0.9 – 1.4%
Unit Weight, lb/ft ³	149.9	143.2	150.2
Chloride Permeability (AASHTO T 277)	1430 coulombs @ 56 days	1730 coulombs @ 56 days	900 coulombs @ 56 days

The properties of the cement used in precast deck panels and cast-in-place decks are shown in Table 4.

TABLE 4: Properties of Cement used in the Construction of Precast Deck Panels and Cast-in-Place Decks

Property	Precast Deck Panels	Cast-in-Place Decks
Chemical, %		
SiO ₂	18.95	20.24
Al ₂ O ₃	6.50	5.66
Fe ₂ O ₃	2.97	2.11
CaO	64.57	64.63
MgO	0.71	1.27
SO ₃	3.79	3.16
Loss of Ignition	1.57	2.06
Insoluble Residue	0.24	0.19
Free Lime	1.70	N/A
C ₃ S	61.10	59.23
C ₃ A	1.80	11.43
Total Alkali	0.71	0.60
Specific Surface, cm ² /gm		
Blaine	6360	3430
Wagner	2933	1823

DRAFT

% Passing No. 325 Sieve	99.7	93.7
Compressive Strength, psi		
1 Day	4230	N/A
3 Day	5076	4085
7 Day	5930	5115
28 Day	N/A	N/A
Setting Time, min		
Vicat Initial	N/A	115
Vicat Final	N/A	180
Gilmore Initial	62	185
Gilmore Final	118	350

Measured Properties from QC Tests of Production Concrete

Precast Deck Panel

For precast deck panels, limited amount of information was available on the measured properties from QC tests of production concrete. The typical properties of precast deck panels are documented later in this report under the research test results.

Cast-in-Place Deck

Table 5 summarizes the measured properties from QC tests of class S (Modified) and class K (HPC) production concrete used in the cast-in-place decks of both northbound and southbound bridges.

TABLE 5: Measured Properties of Production Concrete for Cast-in-Place Decks

Property	Age, days	Northbound Class S (Modified)		Southbound Class K (HPC)	
		Standard Cured	Site Cured	Standard Cured	Site Cured
Slump, in.		4		7	
Air Content, %		3.8		0	
Unit Weight, lb/ft ³		143		150	

Measured Properties from Research Tests of Production Concrete

Precast Deck Panel

The measured properties from research tests of production concrete used in the precast deck panels are shown in Table 6.

DRAFT

TABLE 6: Measured Properties from Research Tests of Production Concrete Used in the Precast Deck Panels

Date Cast		9/12/96	9/12/96	9/16/96	9/16/96	9/18/96	9/18/96
Property	Specimen Curing	Standard Cured	Site Cured	Standard Cured	Site Cured	Standard Cured	Site Cured
	Age, days						
Compressive Strength, psi (AASHTO T 22)	1	6010	-	-	-	-	-
	3	-	-	7380 ⁽¹⁾	-	-	-
	7	6640	8260	8620	8870	-	-
	14	-	-	-	-	-	-
	28	8620	8440	9680	10050	-	-
	56	8810	9040	10330	10280	12370	11930
	90	-	-	-	-	12730	12290
Modulus of Elasticity, ksi (ASTM C 469)	1	5490	-	-	-	-	-
	3	-	-	4580 ⁽¹⁾	-	-	-
	7	6000	5280	5530	5910	-	-
	14	-	-	-	-	-	-
	28	6040	5500	5900	5330	-	-
	56	6450	5640	6390	5650	6210	5890
	90	-	-	-	-	6520	6110
Splitting Tensile Strength, psi (ASTM C 496)	7	680	720	730	750	-	-
	28	800	780	760	810	-	-
	56	850	870	820	910	660	810
	90	-	-	-	-	860	880
RCPT, Coulombs (AASHTO T 277)	56	1420	1860	1460	2580	1260	1550

⁽¹⁾ Tested at 2 days.**NOTES:** All tests were made using 4 × 8-in cylinders.

The creep and shrinkage data for production concrete used in the precast deck panels is shown in Table 7. All 4 × 20-in cylinders for the creep and shrinkage measurement were stored alongside the beams for 8 to 18 hours, stripped at approximately 24 hours after casting and loaded at an age of 2 days to 20 and 40 percent of the nominal design compressive strength of the mixture. Temperature and humidity were not controlled. Average relative humidity was 55 percent.

TABLE 7: Creep and Shrinkage Properties from Research Tests of Production Concrete Used in the Precast Deck Panels

Days after Loading	Creep Coefficient ⁽¹⁾	Specific Creep ⁽¹⁾ , millionths/psi	Shrinkage ⁽²⁾ , millionths
7	0.54	0.085	80
28	0.77	0.120	198

DRAFT

56	0.92	0.143	233
180	1.16	0.180	268

- (1) Reported creep values are the average values for specimens loaded to the 20 and 40 percent levels. Nine readings were taken on each specimen.
- (2) Shrinkage values include adjustments for one day of drying before initial readings were taken and for length changes caused by variation in concrete temperatures.

Cast-in-Place Deck

The compressive strength, modulus of elasticity, splitting tensile strength, and chloride permeability of production concrete used in the cast-in-place decks are shown in Table 8. In general class K (HPC) concrete has better strength properties compared to class S (Modified) concrete for both standard and site cured specimens.

TABLE 8: Measured Properties from Research Tests of Production Concrete Used in the Cast-In-Place Decks

Property	Age, days	Northbound Bridge Class S (Modified)		Southbound Bridge Class K (HPC)	
		Standard Cured	Site Cured	Standard Cured	Site Cured
Compressive Strength, psi	28	5600	4890	9630	9220
	56	5700	5090	9740	9100
Modulus of Elasticity, ksi	28	4520	4460	5170	4730
	56	4870	4010	5750	4990
Splitting Tensile Strength, psi	28	460	465	740	725
	56	540	550	820	730
Chloride Permeability, coulombs	56	1730	2120	900	1300

Table 9 provides the creep and shrinkage data for production concrete used in the cast-in-place decks.

Table 9: Measured Creep and Shrinkage Properties of Production Concrete Used in the Cast-in-Place Decks

Days after Loading	Creep Coefficient ⁽¹⁾		Specific Creep ⁽¹⁾ , millionths/psi		Shrinkage ⁽²⁾ , millionths	
	Northbound Class S (Modified)	Southbound Class K (HPC)	Northbound Class S (Modified)	Southbound Class K (HPC)	Northbound Class S (Modified)	Southbound Class K (HPC)
7	0.39	0.46	0.084	0.087	66	91
28	0.74	0.80	0.160	0.152	178	238

56	0.98	1.09	0.213	0.206	240	279
180	1.47	1.69	0.317	0.320	296	344

- (1) Reported creep values are the average values for specimens loaded to the 20 and 40 percent levels. Nine readings were taken on each specimen.
- (2) Shrinkage values include adjustments for one day of drying before initial readings were taken and for length changes caused by variation in concrete temperatures.

Compared to class S (Modified) HPC, the class K (HPC) has higher strength and low chloride permeability, however, it also shows greater shrinkage value. It is noted that a greater shrinkage value may be responsible for the cracking discussed in the following sections.

Actual Method of Deck Placement

Construction of the Tomball Parkway Bridge decks occurred in October 1996, with the concrete for the decks pumped from a truck or placed using a concrete bucket. Prior to placement of the cast-in-place decks, the precast deck panels were saturated to prevent the loss of mixing water.

Concrete was distributed by a mechanical spreader. The concrete was compacted using internal vibrators and a rolling screed to provide proper consolidation and avoid internal segregation. A final troweled finish was applied followed by tining for enhanced skid resistance. Surface finishing consisted of motorized screed pan with a burlap drag.

Fogging of the concrete decks started when the concrete was still in plastic state. A curing compound was applied in addition to the continuous fogging. The wet mats were kept moist for 10 days after casting for the HPC decks with pozzolans. This procedure was aimed at avoiding the surface moisture evaporation and plastic shrinkage cracks.

For each bridge all three spans of the cast-in-place portion of the decks were placed in a single pour. Shortly after placement of concrete, tooled control joints were placed at each interior bent to control cracking.

Average Daily Traffic (ADT) and Average Daily Truck Traffic (ADTT)

Average daily traffic for northbound lanes was calculated based on a count of all vehicles crossing the bridge during a 15 minute period beginning at 1000 hrs on August 25, 2003. These vehicle counts gave at an ADT of 27,360 and an ADTT of 8,784.

Average daily traffic for southbound lanes was calculated based on a count of all vehicles crossing the bridge during a 15 minute period beginning at 0836 hrs on August 26, 2003. These vehicle counts gave an ADT of 81,120 and an ADTT of 3,360.

Exposure Condition of the Bridge

The Tomball Parkway Bridge is on State Highway 249 in northwest Houston, Texas. The bridge improved the State Highway 249 from a non-freeway facility to a freeway facility in northwest Harris County. The National Weather Service reports that the average high temperature is 93.1°F in July and the average low temperature is 38.4°F in February. The minimum temperature varies between 75.8°F in July and 33.7°F in February. The normal precipitation varies between 14.65 inches per month in October to 0.89 inches per month in February. Based on the National Weather Service record there is minimal annual exposure to wet/dry and freeze/thaw cycles. There was no reported application of deicing salt on this bridge.

Performed Maintenance

No documents were found which would indicate any maintenance had been performed since bridge construction in 1994.

Inspection Reports

Several inspection trips to the Tomball Parkway Bridge had been made by the Construction Materials Research Group (CMRG) personnel from the University of Texas at Austin in June and July 1998. The inspections approximately 19 months after the decks were cast were to inspect and map crack patterns on the surface of the decks through visual observation. Further information is available through the Project report 7-3993 of the Center for Transportation Research at The University of Texas at Austin.

According to the report, similar crack patterns were noted for both the southbound and northbound bridge decks. However, the extent of longitudinal cracking was reported to be slightly higher on the southbound decks (constructed with class K high strength HPC). The crack widths were measured to be less than 0.031 in. on the surface of the concrete decks. Crack widths were similar for main spans of both the southbound and northbound bridges. Rectangular pattern cracking was observed on both the southbound and northbound bridges.

IV. Bridge Deck Inspection

PSI personnel performed a close visual inspection of the bridge deck during the week of August 25, 2003. The results of that inspection are summarized as follows.

General Condition of the Deck Top Surface

Figure 1 shows the general layout of the decks for the Tomball Parkway Bridge. Results of visual inspection of the decks of the two bridges are shown in Figure 2. Surface defects observed and documented during visual inspection primarily included transverse cracks, longitudinal cracks, and diagonal cracks (see photos 5 and 6). Other defects observed and documented included small spalls at joints and cracks; exposed reinforcing steel at one location; and inclusion of wood pieces at one location. Signs of abrasion

were visible on the decks, particularly in the wheel paths (see Photo 5). However, apparent signs of other serious damages such as freeze-thaw, D-cracking, alkali-silica reaction, and alkali-aggregate reaction were not observed. Small drilled holes ($\frac{3}{4}$ in. diameter) and core locations with failing patches, which resulted from previous investigation by others, were also observed.

A total of 1703 cracks (longitudinal, traverse, and diagonal) were recorded during visual survey of the bridge decks (see Figure 2). The sum of crack lengths was 11,098.4 ft. over a bridge deck area of 66,636 ft². Crack density (total crack length / deck area) for the northbound and southbound bridges combined was calculated to be 0.167 ft./ sq.ft.

No significant difference was noted in the magnitude and pattern of cracking in the northbound and southbound bridges where two different classes of HPC were used (see Figure 2). Note that in the southbound bridge class K (high strength HPC) was used and in the northbound bridge modified class S (Modified) normal strength HPC was used. Though the two bridges are exhibiting significant level of cracking, majority of the cracks are hairline cracks with a width of less than 0.031 in. A typical crack on the bridge decks is shown in photo 7. The number of cracks that were classified as hairline cracks totaled 1,671 with a combined total length of 10,810.2 ft. A relatively small number of cracks were classified as fine cracks with widths in the range of 0.031 to 0.063 in. The number of these cracks was 32 and their combined total length was 288.2 ft.

Figure 3 identifies the locations of the fine cracks along with other defects such as spalls, exposed rebar and wood inclusions. It can be noted that the fine cracks were limited at span ends along the skew. Small surface spalls, which either occurred due to breaking of tined edges or the crack edges, were observed at 23 locations (see Figure 3). Photo 8 illustrates typical spalling due to breaking of crack edges. A rebar was visible at one location in span 1 of the southbound bridge (see Figure 3). Also inclusion of wood pieces was observed at one location in span 3 of the southbound bridge (see Figure 3).

Figure 3 also illustrates the locations of drilled holes and cores, which resulted from previous investigation by others. Patching of most of the core holes was failing.

The number, length and density of cracks for each structure are shown in Tables 10 through 15, and described below according to the crack type.

Transverse Cracks: The transverse cracks in the northbound and southbound bridges were comparable. A total of 228 cracks were observed in three spans of the northbound bridge with a combined total length of 955 ft. A total number of 282 cracks with a combined total length of 1456.7 ft. were observed in the three spans of the southbound bridge (see Tables 10 and 11). The crack length per deck area for the northbound and southbound bridges was 0.03 ft./ sq.ft. and 0.04 ft./ sq.ft. respectively. A number of transverse cracks and also longitudinal cracks, as discussed in the following section, were at the boundaries of the precast deck panels, creating semi-rectangular patterns.

Longitudinal Cracks: The number and length of longitudinal cracks are significantly greater than those of the transverse and diagonal cracks. The length per deck area in the southbound and northbound bridges was estimated to be 0.11 ft./ sq.ft. and 0.13 ft./ sq.ft., respectively (see Tables 12 and 13). The span length did not appear to have a distinct correlation with the magnitude of cracking. In the southbound bridge, span 1, span 2, and span 3 with lengths of 121.5 ft., 135.5 ft., and 134 ft. had crack length per deck area of 0.11 ft./ft²., 0.14 ft./ft²., and 0.10 ft./ft²., respectively. In the northbound bridge, the corresponding crack length per deck area was 0.11 ft./ sq.ft., 0.13 ft./ sq.ft., and 0.16 ft./ sq.ft. Crack lengths as large as 131.5 ft. and 109.4 ft. were observed in the northbound and southbound bridges, respectively. Several of the longitudinal cracks were along the U beams and at the boundaries of the precast deck panels.

Diagonal Cracks: Diagonal cracks accounted for the least amount of total cracks and were comparable in the northbound and southbound bridge decks. These diagonal cracks were typically present in the acute corners and near the joints. The crack length per deck area was 0.009 ft./ sq.ft. in both the northbound and southbound bridges (see Tables 14 and 15).

TABLE 10: Measured Transverse Cracks on the Surface of Northbound Cast-in-Place Bridge Decks

Northbound Transverse Cracks	Count	Length Range (feet)	Total Length of Cracks (feet)	Deck Area (sq.ft.)	Crack Density: Crack Length / Deck Area (ft./sq.ft.)
Span 1	66	0.8 to 17.3	275.6	10340	0.027
Span 2	76	1.0 to 13.5	302.9	10735	0.028
Span 3	86	1.2 to 18.9	376.5	9805	0.038

TABLE 11: Measured Transverse Cracks on the Surface of Southbound Cast-in-Place Bridge Decks

Southbound Transverse Cracks	Count	Length Range (feet)	Total Length of Cracks (feet)	Deck Area (sq.ft.)	Crack Density: Crack Length / Deck Area (ft./sq.ft.)
Span 1	84	1.2 to 15.2	456.2	12348	0.037
Span 2	126	0.7 to 20.5	692.7	12530	0.055
Span 3	72	1.4 to 20.8	307.8	10879	0.028

TABLE 12: Measured Longitudinal Cracks on the Surface of Northbound Cast-in-Place Bridge Decks

Northbound Longitudinal Cracks	Count	Length Range (feet)	Total Length of Cracks (feet)	Deck Area (sq.ft.)	Crack Density: Crack Length / Deck Area (ft./sq.ft.)
Span 1	113	0.8 to 120.4	1088.3	10340	0.105

Span 2	216	0.8 to 131.5	1369.9	10735	0.128
Span 3	247	0.9 to 137.2	1581.0	9805	0.161

TABLE 13: Measured Longitudinal Cracks on the Surface of Southbound Cast-in-Place Bridge Decks

Southbound Longitudinal Cracks	Count	Length Range (feet)	Total Length of Cracks (feet)	Deck Area (sq.ft.)	Crack Density: Crack Length / Deck Area (ft./sq.ft.)
Span 1	205	0.8 to 105.5	1267	12348	0.103
Span 2	188	1.1 to 109.4	1719.9	12530	0.137
Span 3	125	1.1 to 55.9	1062	10879	0.098

TABLE 14: Measured Diagonal Cracks on the Surface of Northbound Cast-in-Place Bridge Decks

Northbound Diagonal Cracks	Count	Length Range (feet)	Total Length of Cracks (feet)	Deck Area (sq.ft.)	Crack Density: Crack Length / Deck Area (ft./sq.ft.)
Span 1	10	1.8 to 16.3	79	10340	0.008
Span 2	24	1.6 to 13.3	164.7	10735	0.015
Span 3	7	1.4 to 12.3	31.2	9805	0.003

TABLE 15: Measured Diagonal Cracks on the Surface of Southbound Cast-in-Place Bridge Decks

Southbound Diagonal Cracks	Count	Length Range (feet)	Total Length of Cracks (feet)	Deck Area (sq.ft.)	Crack Density: Crack Length / Deck Area (ft./sq.ft.)
Span 1	15	1.5 to 12.3	59.5	12348	0.005
Span 2	17	1.4 to 12.9	116.6	12530	0.009
Span 3	26	1.7 to 13.8	147.5	10879	0.014

Crack Widths

About 98% of the cracks on the two bridges were hairline cracks with a width of less than 0.031 in. The remaining 2% of the cracks were classified as fine cracks with widths in the range of 0.031 to 0.063 in. The fine width cracks were generally located at span ends along the skew and some exhibited spalling due to the breaking of the edges (see photo 8).

General Condition of the Deck Underside

The underside of the decks was inspected from the ground without the aide of any access equipment. The underside of the decks was generally in good condition with a few

exceptions. Cracks were visible on the underside of a few precast deck panels at span ends (see photo 9). Efflorescence was visible at these crack locations.

General Condition of the Girders

The girders were inspected from the ground without the aide of any access equipment. Visible cracks were observed in only one girder. A series of fine cracks approximately 2 to 5 inches long were observed on the northeastern most girder of the northbound bridge near Abutment 2 (see photo 10).

Concrete Core Samples

Eight core samples were retrieved from the decks during the inspection. Core sample locations are shown on Figure 1. The cores were 3 $\frac{3}{4}$ in diameter and were labeled as 1 through 8. The cores were transferred to FHWA for further analysis.

TABLE 13: Core Dimensions

Sample	1	2	3	4	5	6	7	8
Diameter (in.)	3 $\frac{3}{4}$	3 $\frac{3}{4}$	3 $\frac{3}{4}$	3 $\frac{3}{4}$	3 $\frac{3}{4}$	3 $\frac{3}{4}$	3 $\frac{3}{4}$	3 $\frac{3}{4}$
Length (in.)	4	2 $\frac{1}{2}$	2 $\frac{1}{8}$	3 $\frac{3}{4}$	3 $\frac{3}{4}$	3 $\frac{3}{4}$	3 $\frac{3}{4}$	3 $\frac{3}{4}$

Preliminary Conclusions

The construction of the Tomball Parkway (S.H. 249) Bridge was completed in 1997. Under a research project 7-3993, researchers from the University of Texas at Austin performed a visual inspection of the two bridges 19 months after the construction. It was reported that the two bridges exhibited longitudinal, transverse, and zigzag cracks at the time of this inspection and the crack widths were less than 0.031 in. The crack pattern in the two bridges was reported to be similar.

The visual inspection of the bridge decks as part of our study was performed about five years after the previous inspection. The northbound and southbound bridges are exhibiting comparable magnitude and pattern of cracking. A total of 1,703 longitudinal, transverse, and diagonal cracks were recorded on the two bridges with a combined total crack length of 11,098.4 ft. over a bridge deck area of 66,636 ft². However, 98% of these cracks were hairline cracks with width less than 0.031 in. The remaining 2% of the cracks were classified as fine cracks with widths in the range of 0.031 to 0.063 in.

The cast-in-place decks of the northbound and southbound bridges were constructed with two different classes of HPC. Normal strength class S (Modified) HPC was used in the northbound bridge, and high strength class K (HPC) was used in the southbound bridge. However, it appears that mixture proportions did not play a significant role in the

cracking of the decks. Class K (HPC) used in the southbound bridge was reported to have a low w/cm of 0.35 and a fly ash content of 32% by weight of the cementitious material content. This class K (HPC) mixture had a high shrinkage and cracking potential. However, the performance of this mixture was comparable to normal strength class S (Modified) HPC used in the northbound bridge, which was reported to have a w/cm of 0.43 and a fly ash content of 28% by weight of the total cementitious material content. This indicates that the curing procedures used during construction were probably effective.

Significant difference in the coefficient of thermal expansion of the precast deck panels and cast-in-place decks may partly be attributed to the shrinkage cracks observed in the two bridges. It was reported that the coefficient of thermal expansion of the cast-in-place deck was about $4.0 \mu\epsilon / ^\circ\text{F}$. On the other hand the coefficient of thermal expansion of the precast deck panels was reported to be about $7.3 \mu\epsilon / ^\circ\text{F}$.

It was also reported that the construction of all the spans of the northbound and southbound bridges was done as a single pour construction without properly locating the tooled control joints at the centerline of the skew. This single pour construction might have also contributed to the development of cracks observed at the northbound and southbound bridges.

At span ends along the skew, a number of fine width cracks (0.031 to 0.063 in.) were observed. Some of these cracks were exhibiting spalling due to breaking of the edges. The layout of the cast-in-place decks and precast deck panels at span ends may partly be attributed to the development and widening of these cracks. At span ends, the cast-in-place decks were skewed but precast deck panels had a straight geometry. Skewed deck panels at span ends might have helped control these cracks.

The structural system of the northbound and southbound bridges is flexible compared to conventional bridges considering the wide beam spacing, large span, and relatively thin deck used on these bridges. This relatively flexible structural system combined with the heavy ADT and ADTT on these bridges might have contributed to the development and widening of some cracks.

Another factor that could have contributed to the development of longitudinal cracks is shortening of the precast panels in the transverse direction. As the panels shorten because of creep and shrinkage, the cast-in-place portion of the deck has to accommodate the movement. This can lead to tensile stresses in the cast-in-place concrete. In addition, the Texas U-beam is stiffer than the same depth I-beam. This means that any transverse shortening of the deck has to encounter a lot more resistance with a U-beam than with an I-beam. This will thus lead to higher tensile stresses in the deck with a U-beam and greater likelihood of longitudinal cracking.

Petrographic analysis of the core samples retrieved from the decks of the northbound and southbound bridges would further explain the performance of HPC used in Tomball Parkway Bridge.

Photographic Documentation

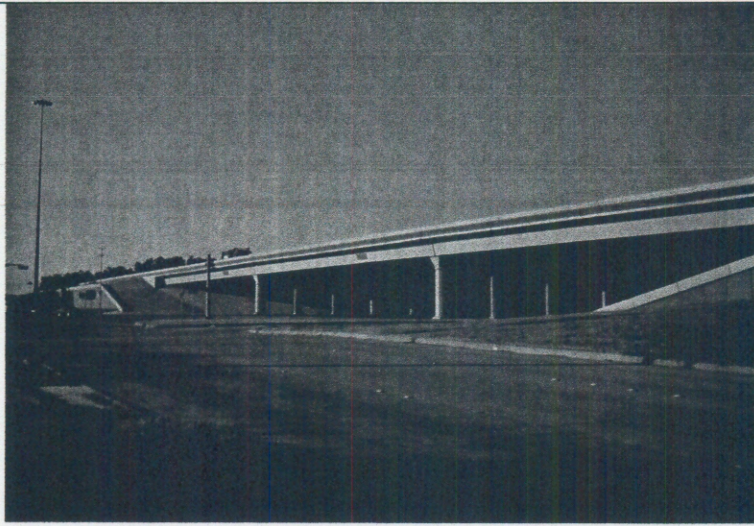


Photo 1: View looking south at the northbound bridge.

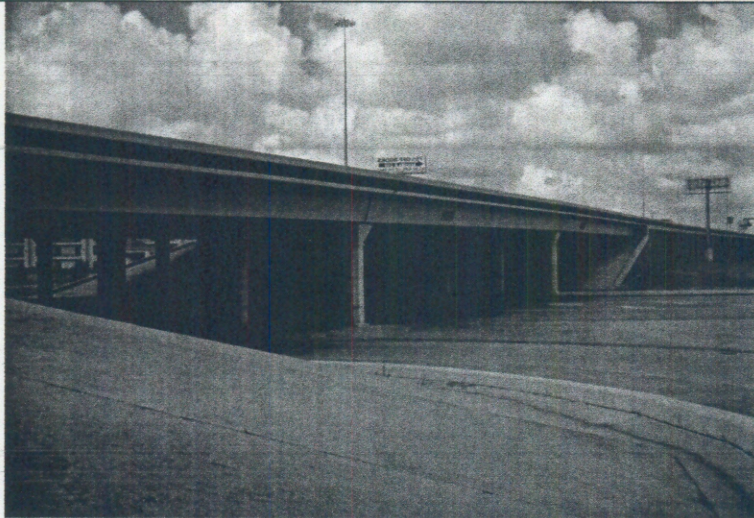


Photo 2: View looking south at the southbound bridge.



Photo 3: View looking north at the northbound bridge. The approach ramp is in foreground. Span 1 begins at mid-photo.



Photo 4: View showing bridge substructure consisting of U-beam girders and columns. Separation between northbound and southbound bridges is shown at the center.



Photo 5: View looking north at the left side of the northbound bridge.

DRAFT



Photo 6: View looking north at southbound bridge.



Photo 7: View showing typical crack in the bridge deck. Crack width is less than 0.031 in. and is categorized as hairline.



Photo 8: View showing spalling associated with cracks in the deck at span ends.

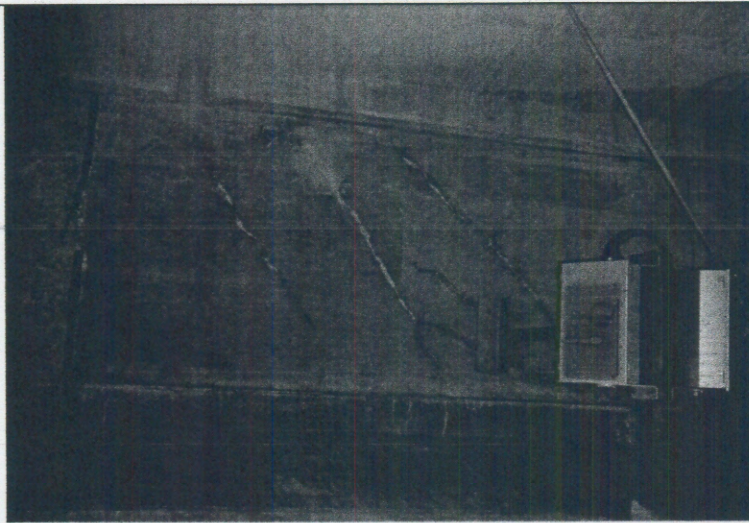


Photo 9: View showing underside of bridge at span end.

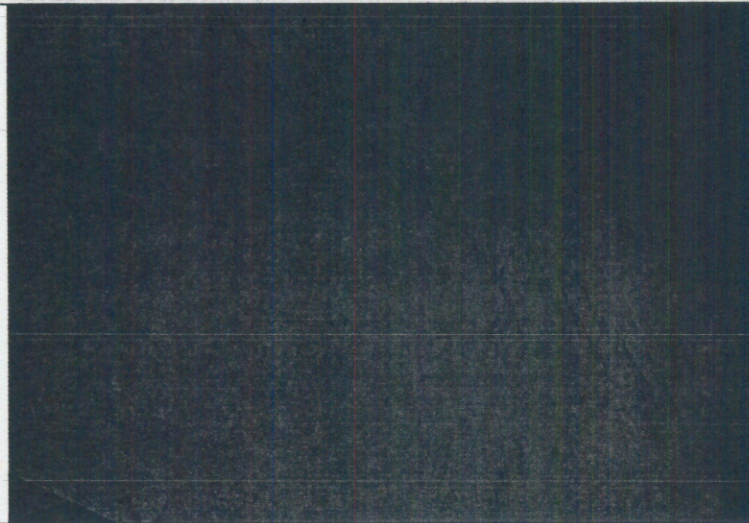
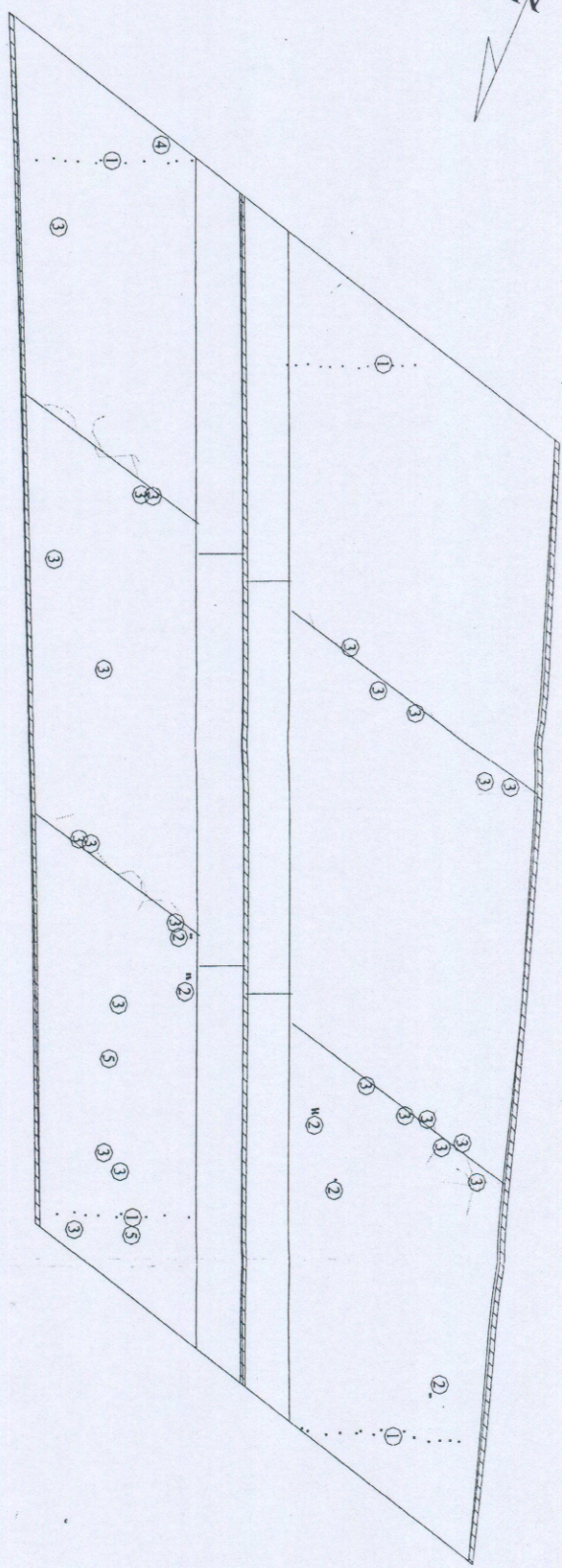
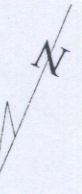





Photo 10: View showing close-up of fine cracks in the northeastern most girder of the northbound bridge.



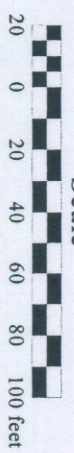
Legend

-  Parapet
-  Fine width crack (31)
-  Other Defects

Other Defects

- ① Drill holes, $\frac{3}{4}$ " diameter
- ② Former core locations with failing patches
- ③ Spall
- ④ Exposed rebar
- ⑤ Inclusion of woody material

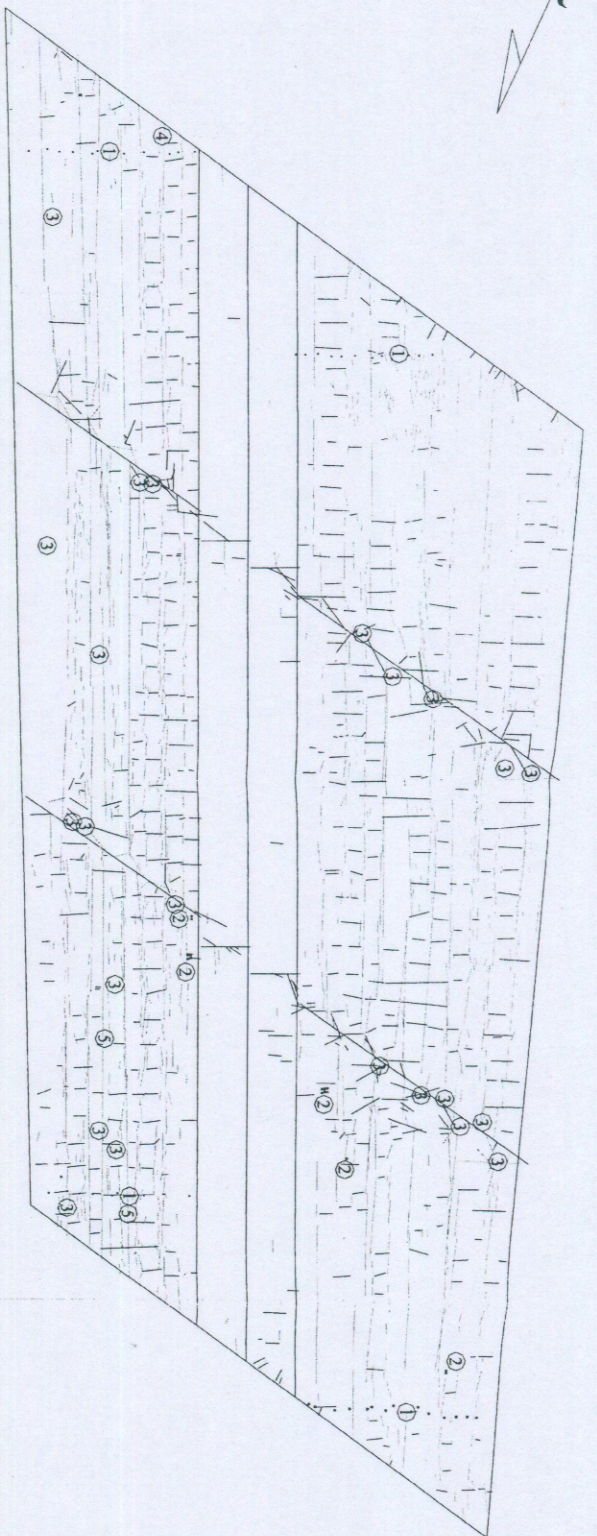
Scale



psi Information
To Build On
Engineering • Consulting • Testing

State Highway 249 (Tomball Pkwy)
Louetta Road Overpass
Houston, Texas

Figure 3:
Fine Cracks ($\frac{1}{32}$ to $\frac{1}{16}$ in.) and Other Defects

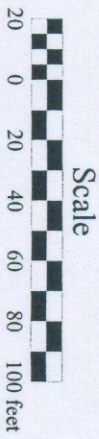


Legend

- ② Feature of Interest
- Longitudinal Crack (1094)
- | Transverse Cracks (510)
- / Diagonal Cracks (99)

Features of Interest

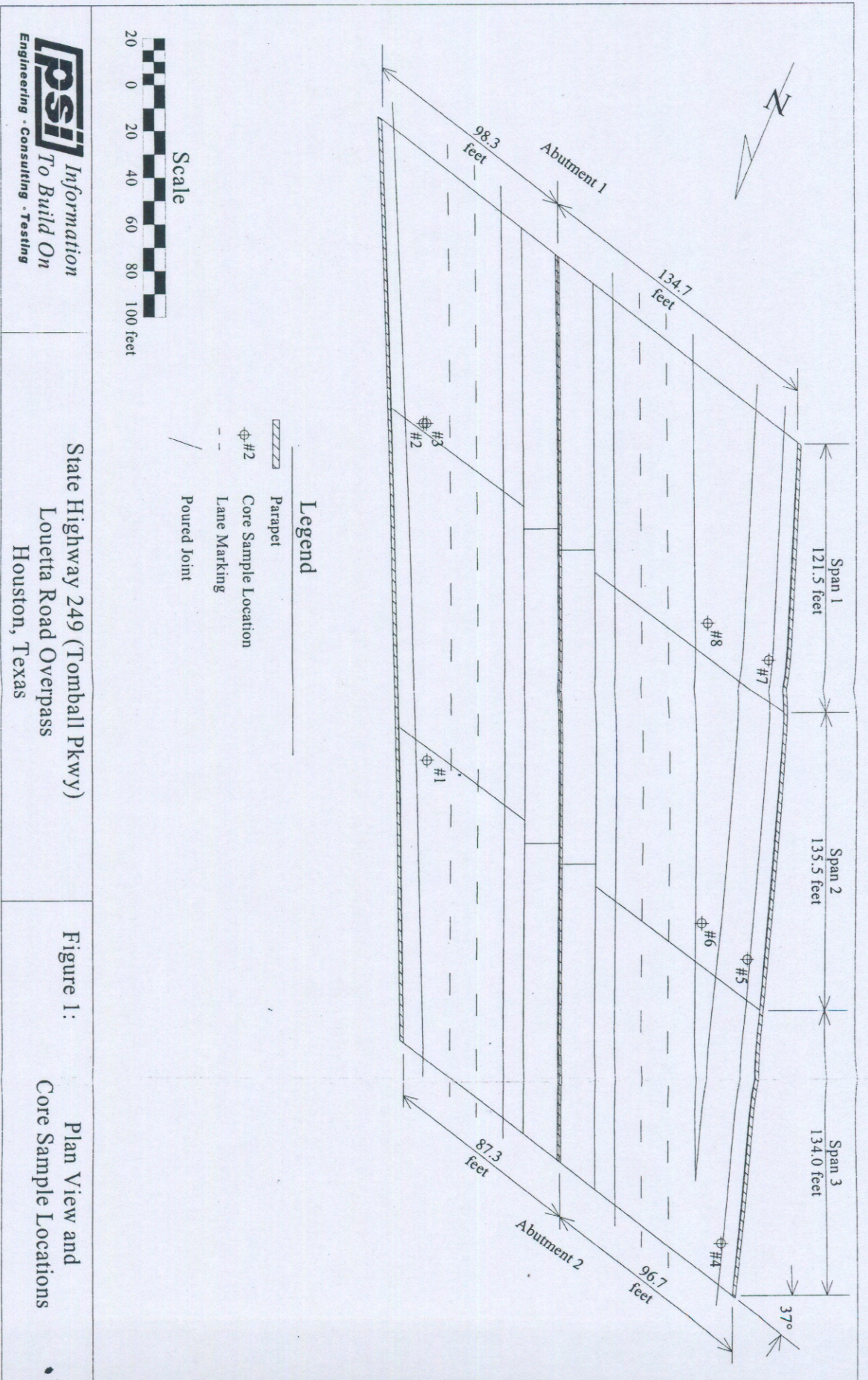
- ① Drill holes, $\frac{3}{4}$ " diameter
- ② Former core locations with failing patches
- ③ Spall
- ④ Exposed rebar
- ⑤ Inclusion of woody material



Information
To Build On
Engineering · Consulting · Testing

State Highway 249 (Tomball Pkwy)
Louetta Road Overpass
Houston, Texas

Figure 2: Visible Survey



Checklist

The following checklist is adapted from 201.1R-92, and provided to facilitate a thorough survey. The definition of terms and associated photographs in 201.1 R-92, are utilized to standardize the reporting of the condition of the concrete in the structures.

1. Description of structure or pavement
 - 1.1 Name, location, type, and size
The Tomball Parkway (S.H. 249) Bridge over Louetta Road in Houston, Texas consists of two separate bridges, one carrying three lanes of northbound traffic and the other carrying the three lanes of southbound traffic with an additional exit ramp. The overpass bridge is 391-feet long and consists of three spans for each direction.
 - 1.2 Owner, project engineer, contractor, when built
Owner-Texas Department of Transportation. This bridge is part of a demonstration project for HPC in bridge structures which were co-sponsored by the Federal Highway Administration (FHWA) and the Texas Department of Transportation (TxDOT). The bridge was constructed in 1996 and opened to traffic in June 1998. The contractor was William Brothers Inc. at Houston.
 - 1.3 Design
 - 1.3.1 Architect and/or engineer: The Texas Department of Transportation (TxDOT)
 - 1.3.2 Intended use and history of use: To carry traffic over the Louetta Road and improve the State Highway 249 from a non-freeway facility to a freeway facility. Opened to traffic in June 1998.
 - 1.3.3 Special features: Both structures consist of pre-cast Texas U54-beams. The structures are intended to be compared for relative durability and performance based on the extensive use of HS/HPC in the southbound structure and the use of normal strength HPC in the northbound structure.
 - 1.4 Construction
 - 1.4.1 Contractor-general William Brothers Inc. at Huston TX
 - 1.4.2 Subcontractors concrete placement: N/A
 - 1.4.3 Concrete supplier: Lopez-Gloria Construction Services at Huston TX
 - 1.4.4 Agency responsible for testing: N/A
 - 1.4.5 Other subcontractors: N/A
 - 1.5 Photographs
 - 1.5.1 General view Photos 1 through 4
 - 1.5.2 Detailed close up of condition of area Photos 5 through 10
 - 1.6 Sketch map-orientation showing sunny and shady and well and poorly drained regions N/A
2. Present condition of structure Date of Evaluation The week of August 25, 2003
 - 2.1 Overall alignment of structure No signs of misalignment
 - 2.1.1 Settlement
 - 2.1.2 Deflection
 - 2.1.3 Expansion
 - 2.1.4 Contraction
 - 2.2 Portions showing distress (beams, columns, pavement, walls, etc., subjected to strains and pressures) N/A

2.3	Surface condition of concrete	
2.3.1	General (good, satisfactory, poor, dusting, chalking, blisters)	<u>Good</u>
2.3.2	Cracks	<u>Transverse, Diagonal, and longitudinal</u>
2.3.2.1	Location and frequency	<u>See Figure 2 and Figure 3</u>
2.3.2.2	Type and size (see Definitions)	<u>See Figure 2 and Figure 3</u>
	Longitudinal	<u>Along the U-beam and panel boundaries</u>
	Width (from Crack comparator)	<u>Less than 0.03 in.</u>
	Hairline	(Less than 1/32 in.)
	Fine	(1/32 in. - 1/16 in.)
	Medium	(1/16 - 1/8 in.)
	Wide	(Greater than 1/8 in.)
	Transverse	<u>At the U-beam diaphragm and panel boundaries</u>
	Width (from Crack comparator)	<u>Less than 0.03 in..</u>
	Hairline	(Less than 1/32 in.)
	Fine	(1/32 in. - 1/16 in.)
	Medium	(1/16 - 1/8 in.)
	Wide	(Greater than 1/8 in.)
	Craze	N/A
	Width (from Crack comparator)	
	Hairline	(Less than 1/32 in.)
	Fine	(1/32 in. - 1/16 in.)
	Medium	(1/16 - 1/8 in.)
	Wide	(Greater than 1/8 in.)
	Map	N/A
	Width (from Crack comparator)	
	Hairline	(Less than 1/32 in.)
	Fine	(1/32 in. - 1/16 in.)
	Medium	(1/16 - 1/8 in.)
	Wide	(Greater than 1/8 in.)
	D-Cracking	N/A
	Width (from Crack comparator)	
	Hairline	(Less than 1/32 in.)
	Fine	(1/32 in. - 1/16 in.)
	Medium	(1/16 - 1/8 in.)
	Wide	(Greater than 1/8 in.)
	Diagonal	<u>In the acute corners and near the joints</u>
	Width (from Crack comparator)	<u>Less than 0.03 in.</u>
	Hairline	(Less than 1/32 in.)
	Fine	(1/32 in. - 1/16 in.)
	Medium	(1/16 - 1/8 in.)
	Wide	(Greater than 1/8 in.)
2.3.2.3	Leaching, stalactites	N/A
2.3.3	Scaling	N/A
2.3.3.1	Area, depth	
2.3.3.2	Type (see Definitions)	
	Light	(Less than 1/8 in.)
	Medium	(1/8 in. - 3/8 in.)

		Severe	(3/8 in. – 3/4 in.)	
		Very Severe	(Greater than 3/4 in.)	
2.3.4	Spalls and popouts	<u>Minor, associated with wider cracks</u>		
2.3.4.1	Number, size, and depth			
2.3.4.2	Type (see Definitions)			
	Spalls			
		Small	(Less than 3/4 in. depth)	
		Large	(Greater than 3/4 in. depth)	
	Popouts			
		Small	(Less than 3/8 in. diameter)	
		Medium	(3/8 in. – 2 in. diameter)	
		Large	(Greater than 2 in. diameter)	
2.3.5	Extent of corrosion or chemical attack, abrasion, impact, cavitation			
				N/A
2.3.6	Stains, efflorescence	<u>Efflorescence along a few cracks on the underside of the deck panels</u>		
2.3.7	Exposed reinforcement	<u>One location, see Figure 3</u>		
2.3.8	Curling and warping			N/A
2.3.9	Previous patching or other repair			N/A
2.3.10	Surface coatings			N/A
2.3.10.1	Type and thickness			N/A
2.3.10.2	Bond to concrete			N/A
2.3.10.3	Condition			N/A
2.3.11	Abrasion			N/A
2.3.12	Penetrating sealers			
2.3.12.1	Type			N/A
2.3.12.2	Effectiveness			N/A
2.3.12.3	Discoloration			N/A

2.4	Interior condition of concrete (in situ and samples)	N/A
2.4.1	Strength of cores	
2.4.2	Density of cores	
2.4.3	Moisture content	
2.4.4	Evidence of alkali-aggregate or other reactions	N/A
2.4.5	Bond to aggregate, reinforcing steel, joints	N/A
2.4.6	Pulse velocity	
2.4.7	Volume change	
2.4.8	Air content and distribution	
2.4.9	Chloride-ion content	
2.4.10	Cover over reinforcing steel	
2.4.11	Half-cell potential to reinforcing steel.	
2.4.12	Evidence of reinforcement corrosion	
2.4.13	Evidence of corrosion of dissimilar metals	
2.4.14	Delaminations	N/A
2.4.14.1	Location	N/A
2.4.14.2	Number, and size	N/A
2.4.15	Depth of carbonation	
2.4.16	Freezing and thawing distress (frost damage)	
2.4.17	Extent of deterioration	
2.4.18	Aggregate proportioning, and distribution	
3.	Nature of loading and detrimental elements	
3.1	Exposure	
3.1.1	Environment (arid, subtropical, marine, freshwater, industrial, etc.)	N/A
3.1.2	Weather-(July and January mean temperatures, mean annual rainfall and months in which 60 percent of it occurs)	
3.1.3	Freezing and thawing	
3.1.4	Wetting and drying	Minimal annual exposure
3.1.5	Drying under dry atmosphere	N/A
3.1.6	Chemical attack-sulfates, acids, chloride	N/A
3.1.7	Abrasion, erosion, cavitation, impact	N/A
3.1.8	Electric currents	N/A
3.1.9	Deicing chemicals which contain chloride ions	N/A
3.1.10	Heat from adjacent sources	N/A
3.2	Drainage	N/A
3.2.1	Flashing	
3.2.2	Weepholes	
3.2.3	Contour	
3.2.4	Elevation of drains	

3.3	Loading	<u>Research Test Data Available in Compilation CD Version 3</u>	
3.3.1	Dead		
3.3.2	Live		
3.3.3	Impact		
3.3.4	Vibration		
3.3.5	Traffic index		
3.3.6	Other		
3.4	Soils (foundation conditions)		
3.4.1	Compressibility		
3.4.2	Expansive soil		
3.4.3	Settlement		
3.4.4	Resistivity		
3.4.5	Evidence of pumping		
3.4.6	Water table (level and fluctuations)		
4.	Original condition of structure		Good
4.1	Condition of formed and finished surfaces		Good
4.1.1	Smoothness		
4.1.2	Air pockets ("bugholes")		
4.1.3	Sand streaks		
4.1.4	Honeycomb		
4.1.5	Soft areas (retarded hydration)		
4.1.6	Cold joints		
4.1.7	Staining		
4.1.8	Sand pockets		
4.2	Defects		N/A
4.2.1	Cracking		
4.2.1.1	Plastic shrinkage		
4.2.1.2	Thermal shrinkage		
4.2.1.3	Drying shrinkage		
4.2.2	Curling		
5.	Materials of Construction		See Table 2
6.	Construction Practices		See Report pg. 9

DRAFT

HIGH PERFORMANCE CONCRETE BRIDGE DECK INVESTIGATION

U.S. Route 67 Bridge
San Angelo, Texas

I. BACKGROUND

The U.S. Route 67 Bridge in San Angelo, Texas is part of a high-speed expressway and carries traffic over the North Concho River, U.S. Route 87, and South Orient Railroad tracks. It was constructed in 1997 and opened to traffic in January 1998. The bridge consists of two separate structures, one carrying two lanes of eastbound traffic and the other two lanes of westbound traffic (see photos 1 and 2). Both structures consist of prestressed concrete I-beam girders covered with precast concrete deck panels (4-inches thick \times 8-feet long), which in turn are covered with 3.5-inches of cast-in-place concrete. The substructures consist of concrete columns, concrete bent caps, and concrete abutments at each end.

The eastbound structure is 950-feet long and consists of eight spans (see photo 3). Spans 7 and 8 are skewed to accommodate the railroad tracks. The bridge decks at spans 1 through 4 are 38-feet wide. The decks progressively widen in spans 5, 6, 7, and 8 to accommodate an exit-ramp at the eastern end of the eastbound bridge. Except for the girders in spans 6 through 8, high performance concrete (HPC) was used for all girders, deck panels, and cast-in-place concrete in the eastbound structure.

The westbound structure is 960-feet long and consists of nine spans (see photo 4). Spans 7, 8, and 9 are skewed to accommodate the railroad tracks. The bridge deck at span 1 is 38-feet wide, and the decks progressively widen in spans 2 through 9 to accommodate an on-ramp at the eastern end of the westbound bridge. At the time of the inspection, traffic lanes on the western half of the westbound bridge merged down to a single lane to accommodate original construction of the expressway west of the bridge. In the westbound structure, HPC was used only for the cast-in-place decks of spans 1 through 5.

This bridge is part of a demonstration project for HPC in bridge structure which was co-sponsored by the Federal Highway Administration (FHWA) and the Texas Department of Transportation (TXDOT). It is evident that the structures were intended to be compared for relative durability and performance based on the extensive use of HPC in the eastbound structure and the limited use of HPC in the westbound structure. Span 1 of both structures is approximately of the same length and width, but the eastbound span uses 4 girders while the westbound span uses 7 girders. The eastbound structure has only 8 spans, while the westbound structure has 9 spans.

II. SCOPE OF SERVICES

Professional Service Industries Inc. (PSI) is under contract with the Federal Highway Administration (FHWA) to conduct bridge deck inspections for HPC bridges. Our scope of services on this bridge included a series of tasks and sub-tasks, which are described as follows:

- Collect all available information relevant to the construction of each bridge, including;
 - Deck Concrete Properties
 - Specified Deck Concrete Construction Procedures
 - Approved Concrete Mixture Proportions
 - Measured Properties from QC
 - Other Measured Properties
 - Actual Method of Deck Placement
 - Average Daily Traffic (ADT)
 - Exposure Condition of the Bridge
 - Any Performed Maintenance
 - Any Inspection Reports
- Visually inspect the bridge, and obtain the following:
 - General condition of the deck top surface
 - Determination of the maximum crack width
 - General condition of the deck underside
 - General condition of the girders
 - Photograph areas of significant deterioration
 - Prepare drawings locating defects
 - Extract 6 concrete core samples

DRAFT

III. COMPILATION OF BRIDGE CONSTRUCTION INFORMATION

Information sources used for this report include bridge drawings, inspection reports, bridge summary data sheets, and technical information contained in FHWA's "Compilation and Evaluation of Results from High Performance Concrete Bridge Projects" version 3.

Deck Concrete Properties

Three classes of HPC were specified for use in the decks of the San Angelo Bridge (class H, class K, and class S). Class H (HPC) was used in the precast panels of the eastbound bridge, whereas class K (HPC) was used in the cast-in-place deck of this bridge. As mentioned earlier, the use of HPC was limited in the westbound bridge. Class S (HPC) was used in the cast-in-place decks of spans 1 through 5. The other elements of this bridge were constructed with normal concrete. Table 1 lists the classes of concrete used on the San Angelo Bridge. Table 2 lists the specified properties for each class of HPC.

Table 1: Classes of Concrete Used in the Construction of San Angelo Bridge

Direction	Span	Component		
		Precast Girders	Precast Deck Panels	CIP Deck
Eastbound	1-5	H (HPC)	H (HPC)	K (HPC)
	6-8	H	H (HPC)	K (HPC)
Westbound	1-5	H	H	S (HPC)
	6-9	H	H	S

TABLE 3: Approved Mixture Proportions for Precast Panels

Mixture Parameters	Class H (HPC) Eastbound Deck Panels	Class H Westbound Deck Panels
Cement Brand:	Capitol	Capitol
Cement Type:	III	III
Cement Quantity:	658 lb/yd ³	564 lb/yd ³
Fine Aggregate Type:	River Sand	River Sand
Fine Aggregate FM:	2.63	2.63
Fine Aggregate SG:	Not available	Not available
Fine Aggregate Quantity:	1355 lb/yd ³	1457 lb/yd ³
Coarse Aggregate, Max. Size:	1-in.	1-in.
Coarse Aggregate Type:	No. 5 Crushed Limestone	No. 5 Crushed Limestone
Coarse Aggregate Quantity:	1844 lb/yd ³	1889 lb/yd ³
Water:	251 lb/yd ³	275 lb/yd ³
Water Reducer Type:	D	D
Water Reducer Quantity:	300 fl oz/yd ³	257 fl oz/yd ³
Retarder Type:	D	D
Retarder Quantity:	79 fl oz/yd ³	49 fl oz/yd ³
Air Entrainment Quantity:	None	None
Water/Cementitious Materials Ratio:	0.38	0.49

Measured properties of approved concrete mixtures for the precast deck panels are summarized in Table 4.

TABLE 4: Measured Properties of Approved Concrete Mixtures for Precast Deck Panels

Measured Concrete Properties	Class H (HPC) Eastbound Deck Panels	Class H Westbound Deck Panels
Slump:	5-6 in.	6-7 in.
Air Content:	1.5%	1.5%
Unit Weight	150.9 lb/ft ³	150.7 lb/ft ³
Rapid Chloride Permeability (AASHTO T 277):	1980 coulombs at 56 days	3230 coulombs at 56 days

The properties of the cement used in the deck panels are shown in Table 5.

TABLE 5: Properties of the Cement used in the Construction of Deck Panels

Chemical Composition, %		
SiO ₂		19.66
Al ₂ O ₂		5.38
Fe ₂ O ₃		2.06
CaO		64.05
MgO		1.26
SO ₃		4.09
Loss of Ignition		2.64
Insoluble Residue		0.27
Free Lime		N/A
C ₃ S		60.58
C ₃ A		10.77
Total Alkali		0.60
Specific Surface, cm ² /gm		
Blaine		5730
Wagner		2926
% Passing No. 325 Sieve		98.6
Compressive Strength, psi		
1 Day		4545
3 Day		5910
7 Day		6750
28 Day		N/A
Setting Time, min		
Vicat	Initial	75
	Final	120
Gilmore	Initial	135
	Final	255

Cast-in-Place Deck

Class K (HPC) was used in the cast-in-place deck of all the spans of the eastbound bridge. The HPC used in limited numbers of spans of the westbound bridge (span 1 through 5) was of class S. The remaining spans of the westbound bridge (spans 6 through 9) utilized normal class S concrete. The approved proportions for these mixtures are shown in Table 6.

TABLE 6: Approved Mixture Proportions for Cast-in-Place Deck

Mixture Parameters	Class K (HPC) Eastbound CIP Deck	Class S (HPC) Westbound CIP Deck (Spans 1 through 5)	Class S Westbound CIP Deck (Spans 6 through 9)
Cement Brand:	Lonestar	Lonestar	Lonestar
Cement Type:	II	II	II
Cement Quantity:	490 lb/yd ³	427 lb/yd ³	611 lb/yd ³
Fly Ash Type:	Class C	Class C	None
Fly Ash Quantity:	210 lb/yd ³	184 lb/yd ³	---
Fine Aggregate Type:	River Sand	River Sand	River Sand
Fine Aggregate FM:	2.70	2.70	2.70
Fine Aggregate Quantity:	1365 lb/yd ³	1240 lb/yd ³	1243 lb/yd ³
Coarse Aggregate, Max. Size:	1 1/4 in.	1 1/4 in.	1 1/4 in.
Coarse Aggregate Type:	No. 5 Crushed River Gravel	No. 5 Crushed River Gravel	No. 5 Crushed River Gravel
Coarse Aggregate Quantity:	1900 lb/yd ³	1856 lb/yd ³	1856 lb/yd ³
Water:	219 lb/yd ³	258 lb/yd ³	258 lb/yd ³
High Range Water Reducer Type:	F	---	---
HRWR Quantity:	156 fl oz/yd ³	---	---
Retarder Brand:	---	Plastocrete 161R	Plastocrete 161R
Retarder Type:	B and D	B and D	B and D
Retarder Quantity:	28 fl oz/yd ³	26 fl oz/yd ³	26 fl oz/yd ³
Air Entrainment Quantity:	3.1 fl oz/yd ³	3.1 fl oz/yd ³	3.1 fl oz/yd ³
Water/Cementitious Materials Ratio:	0.31	0.42	0.42

Measured properties of approved concrete mixtures for the cast-in-place deck are summarized in Table 7.

TABLE 7: Measured Properties of Approved Concrete Mixtures for Cast-in-Place Decks

Measured Concrete Properties	Class K (HPC) Eastbound CIP Deck	Class S (HPC) Westbound CIP Deck (Spans 1-5)	Class S Westbound CIP Deck (Spans 6-9)
Slump:	7-9 in.	3-4 in.	3-4 in.
Air Content:	6%	6%	6%
Unit Weight	149.4 lb/ ft ³	145.3 lb/ ft ³	145.6 lb/ ft ³
Rapid Chloride Permeability (AASHTO T 277):	690 coulombs at 56 days	1380 coulombs at 56 days	2490 coulombs at 56 days

Measured Properties from QC Tests of Production Concrete*Precast Deck Panels*

The measured properties from QC tests of class H (HPC) production concrete used in the precast deck panels of the eastbound bridge are shown in Table 8.

TABLE 8: Measured Properties from QC Tests of Class H (HPC) Production Concrete

Date Cast	Release		
	Slump (inches)	Age (hours)	Compressive Strength (psi)
8/16/96	8	14	4600
8/16/96	—	21	5590
8/19/96	4-1/2	19	5560
8/19/96	4	15-1/2	5080
8/20/96	3-1/2	20-1/4	5270
8/20/96	3-1/2	17	4960
8/20/96	5	16	4880
8/20/96	2-1/2	20	5450
8/22/96	7	20	5160
8/22/96	4	17	5560
8/23/96	4	20	4880
8/29/96	—	23	4790
9/4/96	4-1/4	24	4010
9/10/96	4	20	4570

NOTES: No information was available on the curing condition of the cylinders used in the above testing.

Cast-in-Place Deck

The measured properties from QC tests of class K (HPC) production concrete used in the cast-in-place deck of the eastbound bridge are shown in Table 9.

TABLE 9: Measured Properties from QC Tests of Class K (HPC) Production Concrete

Date Cast	Eastbound Span No.	Slump (inches)	Concrete Temp. (°F)	Air Content (%)	Compressive Strength (psi)		
					5 days	7 days	28 days
6/12/97	1	5-1/2	77	7	5181 ⁽¹⁾	5373	6680
		5	78	6.2	6103 ⁽¹⁾	6991	7358
6/25/97	2	7-1/2	80	6.0	4755	5815	--
		8	75	6.2	5986	5657	--
7/9/97	3	8	80	6.2	6216	5792	--
		7	88	6.2	5976	6357	--
7/23/97	4	8	81	6.0	6481	6056	8180
		8	83	6.3	5779	6245	7454
7/26/97	5	7-3/4	84	6.8	5746 ⁽¹⁾	6100	7269

		8-1/2	81	1.2	6586 ⁽¹⁾	5735	--
8/28/97	7	8	78	6.0	6253	6540	--
		8-1/4	82	6.0	5506	5804	--
9/4/97	8	7	80	6.0	4286 ⁽¹⁾	6247	7128
		6-1/4	82	5.2	5418 ⁽¹⁾	6049	--

(1) Tested at age 4 days.

(2) Tested at age 6 days.

NOTES: Concrete received a wet mat cure for 10 days. Test cylinders received AASHTO T 23 initial and standard curing. The unit weight of concrete was 149 lbs/ft³.

Limited amount of information was available on measured properties from QC tests of class S (HPC) production concrete used in spans 1 through 5 of the westbound bridge. It was reported that the unit weight of the concrete was 145 lb/ft³ and the concrete had a compressive strength of 6120 psi at 28 days.

Measured Properties from Research Tests of Production Concrete

Precast Deck Panels

The compressive strength, modulus of elasticity, and coefficient of thermal expansion of class H (HPC) production concrete used in the eastbound bridge and class H normal concrete used in the westbound bridge are shown in Table 10.

**TABLE 10: Measured Properties from Research Tests of Production Concrete
Used in the Precast Deck Panel**

Bridge	Compressive Strength ⁽¹⁾ , psi		Modulus of Elasticity ⁽¹⁾ , ksi		Coefficient of Thermal Expansion ⁽²⁾ , mill/ °F
	Release at 24 Hours	56 days HPC 28 days non HPC	Release at 24 Hours	56 days HPC 28 days non HPC	
Eastbound HPC	3140	10,100	2990	4620	4.7
Westbound non HPC	5310	8250	3990	4680	4.6

(1) Averaged values for all instrumented panels cast 2/5/97 for eastbound and 9/4/96 for westbound.

(2) Average of two increasing and two decreasing values between 40 and 20 °F at 60% relative humidity.

NOTES: All 4 × 8-in cylinders cured alongside the panels before and after release and tested using neoprene pads and steel caps.

The creep and shrinkage data for class H (HPC) production concrete used in the eastbound bridge

and class H normal production concrete used in westbound bridge is shown in Table 11. All 4×20 -in cylinders for the creep and shrinkage measurement were stored alongside the beams for 8 to 18 hours, stripped at approximately 24 hours after casting and loaded at an age of 2 days to 20 and 40% of the nominal design compressive strength of the mixture. Temperature and humidity were not controlled. Average relative humidity was 55 percent.

TABLE 11: Creep and Shrinkage Properties from Research Tests of Production Concrete Used in the Precast Deck

Days after Loading	Creep Coefficient ⁽¹⁾		Specific Creep ⁽²⁾ Millionths / psi		Shrinkage ⁽²⁾ millionths	
	Eastbound Class H (HPC)	Westbound Class H	Eastbound Class H (HPC)	Westbound Class H	Eastbound Class H (HPC)	Westbound Class H
7	0.58	0.74	0.133	0.168	135	249
28	1.12	1.07	0.257	0.244	330	360
56	1.41	1.37	0.324	0.310	404	387
180	1.95	1.97	0.445	0.444	528	428

⁽¹⁾ Reported creep values are the average values for specimens loaded to the 20 and 40 percent levels. Nine readings were taken on each specimen.

⁽²⁾ Shrinkage values include adjustments for one day of drying before initial readings were taken and for length changes caused by variation in concrete temperatures.

Cast-in-Place Decks

The compressive strength, modulus of elasticity, and coefficient of thermal expansion of class K (HPC) production concrete used in the eastbound cast-in-place deck, class S (HPC) used in spans 1 through 5 of the westbound bridge, and class S normal concrete used in the spans 6 and 7 of the westbound bridge are shown in Table 12.

TABLE 12: Measured Properties from Research Tests of Production Concrete Used in the Cast-In-Place Deck

	Compressive Strength ⁽¹⁾ , psi	Modulus of Elasticity, ksi	Coefficient of Thermal Expansion ⁽²⁾ , mill/ °F
Eastbound - Class K (HPC)			
1	7290	5500	4.6
2	8420	5230	
3	9060	6060	
4	7550	5790	
5	8220	5010	
6	8680	5380	
7	7460	4920	
8	7770	5570	
Westbound - Class S (HPC)			

1	6400	5170	4.4
2	5160	4670	
3	4450	4310	
4	4700	4670	
5	4560	4640	
Westbound - Class S			
6 and 7	5340	4930	4.9

- (1) At 56 days for HPC mixtures. At 28 days for non-HPC mixtures.
 (2) Average of two increasing and two decreasing values between 40 and 20 °F at 60% relative humidity.

The creep and shrinkage data for class K (HPC) production concrete used in the cast-in-place decks of the eastbound bridge, class S (HPC) production concrete used in the cast-in-place decks of spans 1 through 5 of the westbound bridge, and class S normal concrete used in spans 6 through 9 of the westbound bridge are shown in Table 13.

TABLE 13: Measured Creep and Shrinkage Properties from Research Tests of Production Concrete Used in the Cast-In-Place Deck

Days after Loading	Creep Coefficient ⁽¹⁾			Specific Creep ⁽¹⁾ , millionths/psi			Shrinkage ⁽²⁾ , millionths		
	Eastbound Class K (HPC)	Westbound		Eastbound Class K (HPC)	Westbound		Eastbound Class K (HPC)	Westbound	
		Class S (HPC)	Class S		Class S (HPC)	Class S		Class S (HPC)	Class S
7	0.72	0.65	0.53	0.108	0.212	0.106	138	125	118
28	1.07	1.21	0.94	0.161	0.390	0.186	251	269	258
56	1.25	1.51	1.43	0.188	0.488	0.284	285	371	340
180	1.59	2.23	1.96	0.240	0.722	0.389	265	462	434

- (1) Reported creep values are the average values for specimens loaded to the 20 and 40 percent levels. Nine readings were taken on each specimen.
 (2) Shrinkage values include adjustments for one day of drying before initial readings were taken and for length changes caused by variation in concrete temperatures.

The chloride ion penetration data for class K (HPC) production concrete used in the cast-in-place deck of the eastbound bridge, class S (HPC) production concrete used in the cast-in-place deck of spans 1 through 5 of the westbound bridge, and class S normal concrete used in the spans 6 through 9 of the westbound bridge are shown in Table 14.

TABLE 14: Chloride Ion Penetration (AASHTO T 259) Data for Production Concrete Used in the Cast-in-Place Deck

Concrete Class	K (HPC)	K (HPC)	S (HPC)	S
Casting Date	6/12/97	8/19/97	12/3/96	2/15/97
Depth, in				

0.25	0.201	0.156	0.269	0.368
0.75	0.000	0.000	0.000	0.058
1.25	0.000	0.000	0.000	0.000
Integral Chloride	0.56	0.44	0.85	1.17

NOTES: All specimens were moist cured. Values are chloride percentage by weight of concrete. Specimens were moist cured for 14 days followed by 42 days drying and ponding for 90 days.

For class K (HPC) used in the cast-in-place decks of the eastbound bridge, a linear relationship was established between the splitting tensile strength and the square root of compressive strength (Equation 1) for both ASTM moist cured cylinder specimens and the site/ field test specimens.

$$f_{sp} = 8.80\sqrt{f_c'} \quad \text{Eqn. (1)}$$

where f_c' is the compressive strength, and f_{sp} is the splitting tensile strength.

The class K (HPC) used in the cast-in-place decks of the eastbound bridge exhibited very low to low Coulombs value, in the range of 250 Coulombs to 1,500 Coulombs. When tested for freeze-thaw resistance utilizing the ASTM C 666, the class K (HPC) used in the cast-in-place decks of the eastbound bridge experienced a maximum weight loss of 1.30% after 300 freeze-thaw cycles. As a comparison, the class S normal concrete used in the cast-in-place decks of spans 6 through 9 of the westbound bridge experienced a maximum weight loss of 3.64% after 300 freeze-thaw cycles.

Actual Method of Deck Placement

Construction of the deck occurred in June 1997, with the concrete for the deck pumped from a truck or placed via a concrete bucket. Concrete was distributed by a mechanical spreader. A final troweled finish was applied followed by tining for enhanced skid resistance. Surface finishing consisted of motorized screed pan with a burlap drag. Prior to placement of the cast-in-place deck, the precast panels were saturated to prevent the loss of mixing water while the concrete was in plastic state. The concrete was internally vibrated to provide proper consolidation and avoid internal segregation. Fogging of the concrete deck started when the concrete was in the plastic state. A curing compound was applied in addition to the continuous fogging. This procedure avoided the surface moisture evaporation and plastic shrinkage cracks. The deck was cured using wet mat for 10 days when fly ash was used and 8 days when fly ash was not used. The wet mats were kept moist for 10 days after casting for the HPC decks with pozzolans.

Average Daily Traffic (ADT)

The district identifies this bridge as carrying 10,000 vehicles per day. This value appeared reasonable based on a cursory and subjective estimation of traffic flow made while the PSI inspection crew was on-site.

Exposure Condition of the Bridge

The area surrounding the bridge is developed with mixed residential and commercial land use. The National Weather Service reports that the normal maximum temperature varies between 94.4°F in

July and 57.9°F in January. The normal minimum temperature varies between 70.4°F in July and 31.8°F in January. The normal precipitation varies between 3.09 inches per month in May to 0.81 inch per month in January with between 4 to 7 days per month where precipitation is greater than 0.01 inches. There are normally 51 days per year when the temperature drops below 32°F. Based on this information, the bridge has minimal annual exposure to wet/dry and freeze/thaw cycles. There was no reported application of deicing salt on this bridge.

Performed Maintenance

No documents were found which would indicate any maintenance had been performed since the bridge was constructed in 1997.

Inspection Reports

A "Bridge Inspection Record", a "Bridge Inventory Record", and a "Bridge Appraisal Worksheet" dated November 2002 were obtained from TXDOT. The Bridge Inspection Report mentions "minor cracks in the deck" parallel to bent 9 at 18 to 24 inches from the control joint in the westbound bridge. These cracks were reported to relate to the deck discontinuity. The inspection report also indicates "the deck overhangs have minor transverse cracks with efflorescence, at the bottom side" of the westbound bridge.

IV. BRIDGE DECK INSPECTION

PSI personnel performed a visual inspection of the bridge decks during the week of July 14, 2003. The results of the inspection are summarized as follows.

General Condition of the Deck Top Surface

Figure 1 shows the general layout of the decks of the eastbound and westbound bridges. Results of our visual inspection of the decks of the two bridges are shown in Figure 2. Surface defects observed and documented during our visual inspection primarily included transverse cracks, longitudinal cracks, and diagonal cracks. All these cracks were hairline cracks with respective maximum widths of 0.014 in., 0.012 in., and 0.010 in. (see photos 5 and 6). The number and length of different type of cracks is summarized in Tables 15 through 20. Signs of abrasion were visible on the decks, particularly in the wheel paths (see Photo 3). However, apparent signs of other serious damages such as freeze-thaw, D-cracking, alkali-silica reaction, and alkali-aggregate reaction were not observed.

A distinct difference was noted in the number and length of cracks on the decks of the two bridges. The westbound bridge had significantly more cracks than the eastbound bridge (see photos 7 and 8). A comparison of the magnitude of cracking on the decks of the two bridges is presented below by crack type.

Transverse Cracks: Spans 1 through 4 of the eastbound bridge had relatively small number of transverse cracks. A total of 50 cracks were observed in these spans with a combined total length of 243.9 ft. Compared to this a total number of 56 cracks with a combined total length of 776.4 ft. were observed in spans 1 through 4 of the westbound bridge (see Tables 15 and 16). Since the number, length and width of the spans of the two bridges are variable, a comparison of crack length

per deck area is more useful. For spans 1 through 4, the crack length per deck area for the eastbound and westbound bridges is 0.11 ft./sq. ft. and 0.37 ft./sq. ft., respectively.

The eastbound bridge deck exhibited a relatively large number of short-length cracks in spans 5 through 8. The number of cracks in spans 5 through 9 of the westbound bridge was less but the cracks were of larger length. The crack length per deck area in spans 5 through 8 of the eastbound bridge was 0.54 ft./sq. ft. Compared to this, the crack length per deck area in spans 5 through 9 of the westbound bridge was 0.62 ft./sq. ft. In particular, span 5 of both of the eastbound and westbound bridges has exhibited large crack densities, 0.615 ft./sq. ft. and 0.752 ft./sq. ft. respectively.

Considering the total length of the two bridges, the crack length per deck area for the eastbound and westbound bridges was estimated to be 0.31 ft./sq. ft. and 0.50 ft./sq. ft. respectively.

A pattern which was clearly present in the westbound bridge and absent in the eastbound bridge was that in the westbound bridge deck the cracks appeared to be at the boundaries of the precast deck panels, creating rectangular patterns (see photo 8). Texas DOT reported that this pattern of cracking was observed along bents 7 and 9 of the westbound bridge soon after the construction was completed. The cracking was attributed to a single pour construction of spans 6 through 9 of the westbound bridge. A single pour construction was not reported at other locations of the westbound or eastbound bridges.

Longitudinal Cracks: The number and length of longitudinal cracks was significantly less than that of the transverse cracks. However, the westbound bridge decks again had more cracks compared to the eastbound bridge decks. The length per deck area of longitudinal cracks in the eastbound and westbound bridges was estimated to be 0.15 ft./sq. ft. and 0.24 ft./sq. ft., respectively (see Tables 17 and 18).

Diagonal Cracks: Relatively small number of short-length diagonal cracks was observed in both the eastbound and westbound bridges. These cracks were typically present in the acute corners and near the joints. The crack length per deck area was comparable in the two bridges, 0.009 ft./sq. ft. on the eastbound bridge and 0.01 ft./sq. ft. on the westbound bridge (see Tables 19 and 20).

TABLE 15: Measured Transverse Cracks on the Surface of Eastbound Bridge Decks

Eastbound Transverse Cracks	Count	Length Range (feet)	Total Length of Cracks (feet)	Deck Area (sq. ft.)	Crack Density: Crack Length / Deck Area (ft./sq.ft.)
Span 1	8	2.2 to 6.3	31.9	497	0.064
Span 2	4	3.0 to 11.6	26.1	595	0.044
Span 3	21	1.2 to 12.7	93.3	570	0.164
Span 4	17	1.9 to 25.5	92.6	567	0.163
Span 5	54	1.1 to 36.6	330.4	538	0.615
Span 6	33	1.7 to 19.2	193.7	393	0.493
Span 7	58	1.9 to 30.3	460.3	480	0.958
Span 8	9	2.6 to 6.2	33.3	478	0.070

NOTES: Transverse cracks include cracks oriented parallel to skewed joints

TABLE 16: Measured Transverse Cracks on the Surface of Westbound Bridge Decks

Westbound Transverse Cracks	Count	Length Range (feet)	Total Length of Cracks (feet)	Deck Area (sq. ft.)	Crack Density: Crack Length / Deck Area (ft./sq.ft.)
Span 1	17	1.7 to 33.5	209.8	516	0.407
Span 2	15	2.9 to 39.8	201.8	510	0.396
Span 3	10	3.1 to 35.1	180.4	525	0.344
Span 4	14	2.7 to 41.8	184.4	558	0.331
Span 5	33	2.8 to 29.6	349.6	465	0.752
Span 6	24	3.5 to 39.3	363.8	686	0.530
Span 7	2	6.1 to 10.2	16.2	126	0.129
Span 8	15	1.3 to 13.3	87.4	321	0.273
Span 9	49	2.4 to 39.4	521.4	560	0.932

NOTES: Transverse cracks include cracks oriented parallel to the skewed joints

TABLE 17: Measured Longitudinal Cracks on the Surface of Eastbound Bridge Decks

Eastbound Longitudinal Cracks	Count	Length Range (feet)	Total Length of Cracks (feet)	Deck Area (sq. ft.)	Crack Density: Crack Length / Deck Area (ft./sq.ft.)
Span 1	13	1.3 to 7.8	56.9	497	0.115
Span 2	17	1.1 to 75.6	134.6	595	0.226
Span 3	13	2.2 to 8.6	51.3	570	0.090
Span 4	7	4.4 to 7.1	37.5	567	0.066
Span 5	21	1.9 to 10.3	102.9	538	0.191
Span 6	2	3.8 to 6.6	10.4	393	0.026
Span 7	28	2.2 to 41.5	163.9	480	0.341
Span 8	14	1.9 to 7.8	68.1	478	0.142

NOTES: Longitudinal cracks include cracks that are oriented perpendicular to the skewed joints

TABLE 18: Measured Longitudinal Cracks on the Surface of Westbound Bridge Decks

Westbound Longitudinal Cracks	Count	Length Range (feet)	Total Length of Cracks (feet)	Deck Area (sq. ft.)	Crack Density: Crack Length / Deck Area (ft./sq.ft.)
Span 1	12	2.4 to 5.9	45.4	516	0.088
Span 2	16	1.7 to 37.6	127.6	510	0.250
Span 3	21	1.6 to 14.4	82.3	525	0.157
Span 4	58	0.6 to 25.9	191.6	558	0.343
Span 5	31	1.4 to 8.9	114.9	465	0.247
Span 6	10	1.9 to 55.2	82.0	686	0.120
Span 7	8	2.8 to 6.7	35.7	126	0.283
Span 8	9	1.9 to 31.7	87.8	321	0.274
Span 9	12	2.9 to 109.0	236.9	560	0.423

NOTES: Longitudinal cracks include cracks that are oriented perpendicular to the skewed joints

TABLE 19: Measured Diagonal Cracks on the Surface of Eastbound Bridge Decks

Eastbound Diagonal Cracks	Count	Length Range (feet)	Total Length of Cracks (feet)	Deck Area (sq. ft.)	Crack Density: Crack Length / Deck Area (ft./sq.ft.)
Span 1	0	-	-	497	-
Span 2	2	2.7 to 3.7	6.4	595	0.011
Span 3	1	2.1 to 2.1	2.1	570	0.004
Span 4	3	1.7 to 5.0	9.5	567	0.017
Span 5	5	2.3 to 6.6	18.2	538	0.034
Span 6	0	-	-	393	-
Span 7	0	-	-	480	-
Span 8	0	-	-	478	-

TABLE 20: Measured Diagonal Cracks on the Surface of Westbound Bridge Decks

Westbound Diagonal Cracks	Count	Length Range (feet)	Total Length of Cracks (feet)	Deck Area (sq. ft.)	Crack Density: Crack Length / Deck Area (ft./sq.ft.)
Span 1	0	-	0.0	516	-
Span 2	3	2.7 to 4.6	10.7	510	0.021
Span 3	4	2.4 to 5.2	14.6	525	0.028
Span 4	2	4.1 to 5.3	9.4	558	0.017
Span 5	0	-	0.0	465	-
Span 6	3	2.9 to 3.4	9.7	686	0.014
Span 7	0	-	0.0	126	-
Span 8	0	-	0.0	321	-
Span 9	0	-	0.0	560	-

Maximum Crack Width

The maximum width of longitudinal cracks and transverse cracks was measured to be 0.012 in. and 0.014 in., respectively. The maximum width of diagonal cracks was measured to be 0.010 in. According to ACI 201.R-92, these crack widths are classified as hairline cracks.

General Condition of the Deck Underside

The underside of the deck, inspected from ground without the aid of any access equipment, exhibited no visible signs of significant distress. However, a few minor transverse cracks along with efflorescence on the bottom side of the deck overhang of the westbound bridge, as noted in earlier inspection reports, were observed (see photo 10).

General Condition of the Girders

The girders were inspected from the ground, without the aide of any access equipment. No visible signs of any significant distress were noted.

Concrete Core Samples

Six cores, approximately 3.5 inches long and 4 inches in diameter, were retrieved from the decks. The core sample locations are shown in Figure 1. The locations were evenly distributed along shoulders of the bridges. The cores were labeled as TX-1 through TX-6 and transferred to FHWA for further analysis.

TABLE 21: Core Dimensions

Sample	TXS-1	TXS-2	TXS-3	TXS-4	TXS-5	TXS-6
Diameter (in.)	3 ³ / ₄	3 ³ / ₄	3 ³ / ₄	3 ³ / ₄	3 ³ / ₄	3 ³ / ₄
Length (in.)	5 ¹ / ₄	4 ³ / ₄	5 1/2	4 ³ / ₄	5	5

Preliminary Conclusions

Table 22 shows the various combinations of concretes in each span of the eastbound and westbound bridges and corresponding crack density for transverse cracks, longitudinal cracks, and diagonal cracks.

TABLE 22: Summary of Crack Density for Different Bridge Spans

	Span 1	Span 2	Span 3	Span 4	Span 5	Span 6	Span 7	Span 8	Span 9
Precast Girders	Class H								
Precast Deck Panels	Class H								
Cast-in-Place Decks	Class S (HPC)					Class S			
Transverse Crack Density (ft./sq.ft.)	0.407	0.396	0.343	0.331	0.752	0.530	0.128	0.273	0.932
Longitudinal Crack Density (ft./sq.ft.)	0.088	0.250	0.157	0.343	0.247	0.120	0.283	0.274	0.423
Diagonal Crack Density (ft./sq.ft.)	0	0.021	0.028	0.017	0	0.014	0	0	0

	Span 1	Span 2	Span 3	Span 4	Span 5	Span 6	Span 7	Span 8
Precast Girders	Class H (HPC)					Class H		
Precast Deck Panels	Class H (HPC)							
Cast-in-Place Decks	Class K (HPC)							
Transverse Crack Density (ft./sq.ft.)	0.064	0.044	0.164	0.163	0.615	0.493	0.958	0.070
Longitudinal Crack Density (ft./sq.ft.)	0.115	0.226	0.090	0.066	0.191	0.026	0.341	0.142
Diagonal Crack Density (ft./sq.ft.)	0	0.011	0.004	0.017	0.034	0	0	0

The eastbound bridge where both the precast deck panels and the cast-in-place decks were constructed utilizing HPC has exhibited better performance compared to the westbound bridge where HPC was used only in the cast-in-place decks of a limited number of spans (1 through 5). Comparing cast-in-place deck of spans 1 through 5 of the westbound bridge with that of the eastbound bridge, the performance of the eastbound cast-in-place deck is found to be superior. This could be attributed to a better quality HPC used in the cast-in-place deck of the eastbound bridge. The class K (HPC) used in the cast-in-place deck of the eastbound bridge was reported to have a lower water-to-cementitious material ratio compared to the class S (HPC) used in the cast-in-place deck of the westbound bridge. The water-to-cementitious material ratio of class K (HPC) was specified as 0.31 compared to 0.42 of class S (HPC).

It is noted that relatively large number of short-length transverse cracks were observed in spans 5 through 8 of the eastbound bridge. The consistent cracking pattern appeared to be related to two factors. First, the cracks may be caused by an inadequate moist curing less than that used in spans 1 through 4. Since the HPC used had a very low water-to-cementitious material ratio and contained 30% fly ash by weight of the total cementitious material content, this concrete needed a very careful attention to moist curing. Second, the eastbound bridge along the southern edge is also the side where the beams have a longer span and larger skew angle. This type of structural configuration makes the southern edge of the eastbound bridge relatively flexible. Combined with the heavy ADT and ADTT, this structural configuration might have contributed to a large number of short-length transverse cracks.

The rectangular pattern cracking particularly observed in spans 8 and 9 of the westbound bridge may be attributed to a combination of factors. These may include single pour construction of a

Photographic Documentation

Photo 1: View looking northeast. The eastbound bridge is in foreground, and the westbound bridge is in the background.

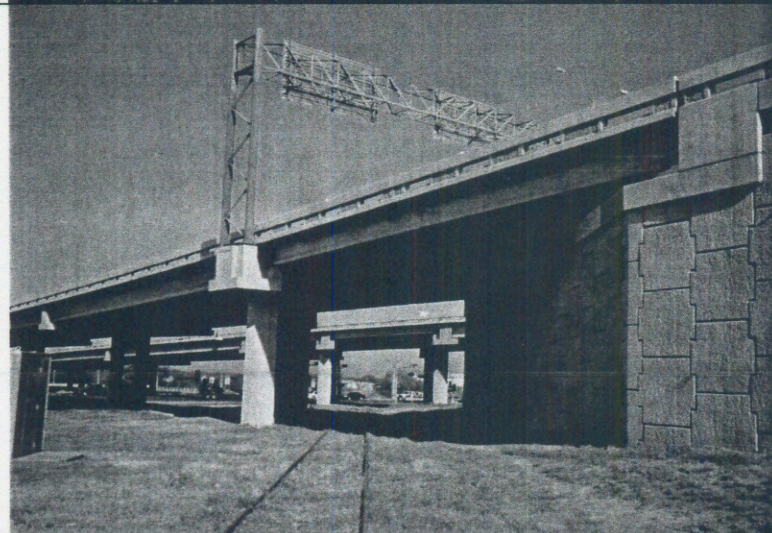


Photo 2: View looking northwest at the eastern end of the eastbound bridge.

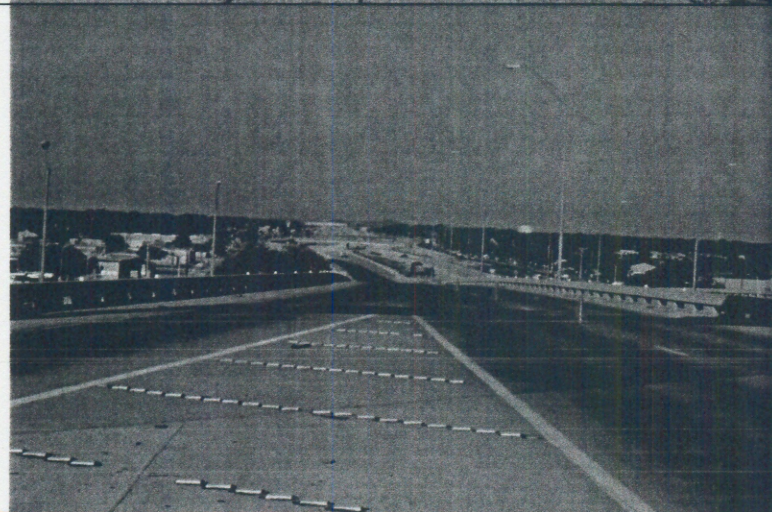


Photo 3: View looking west from the eastern end of the eastbound bridge.



Photo 4: View looking west from the eastern end of the westbound bridge.

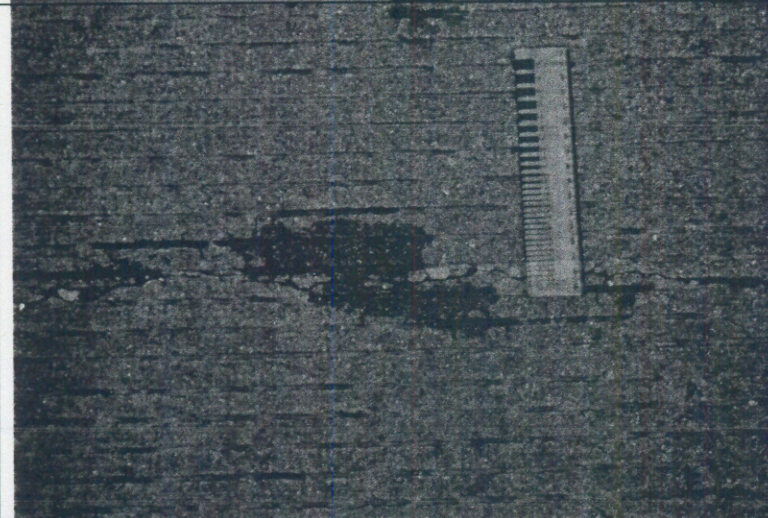


Photo 5: Closeup view of a transverse crack.



Photo 6: Closeup view of a longitudinal crack.



Photo 7: View of the eastbound bridge, the western end of Span 5, showing cracking pattern at the edge of span.



Photo 8: View of the westbound bridge, the western end of Span 4 showing the rectangular cracking pattern.

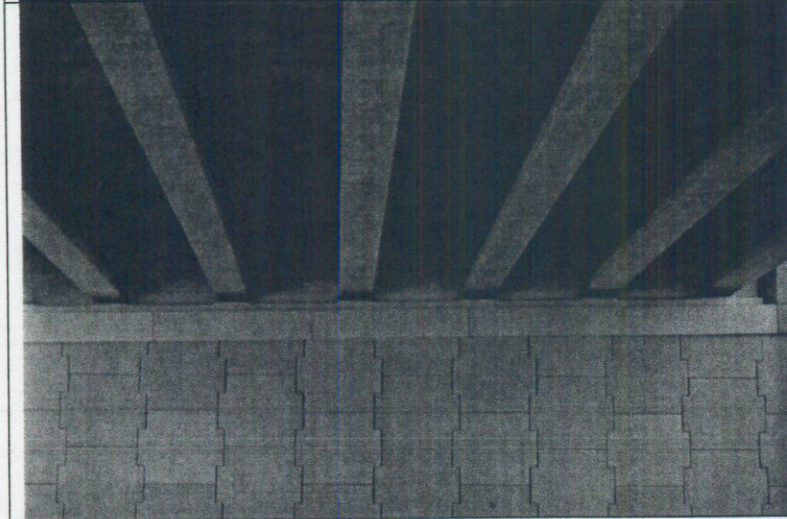


Photo 9: Typical condition of the underside of the deck.

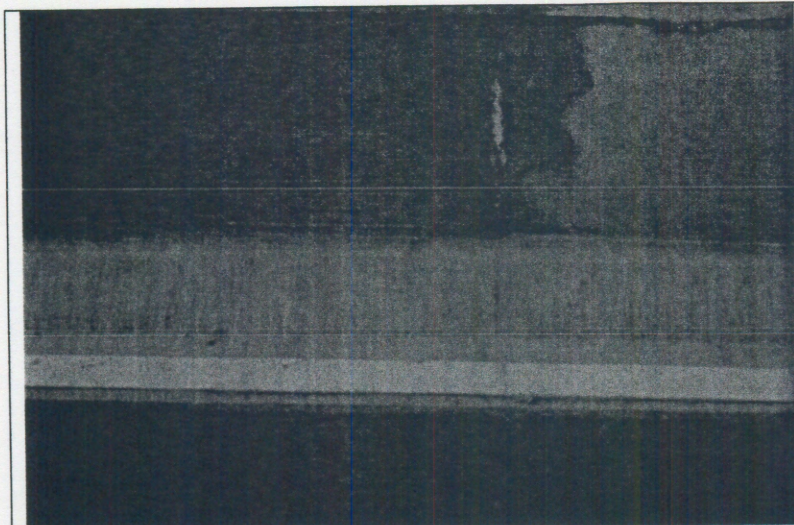


Photo 10: Cracks with efflorescence along the overhang on the westbound bridge.

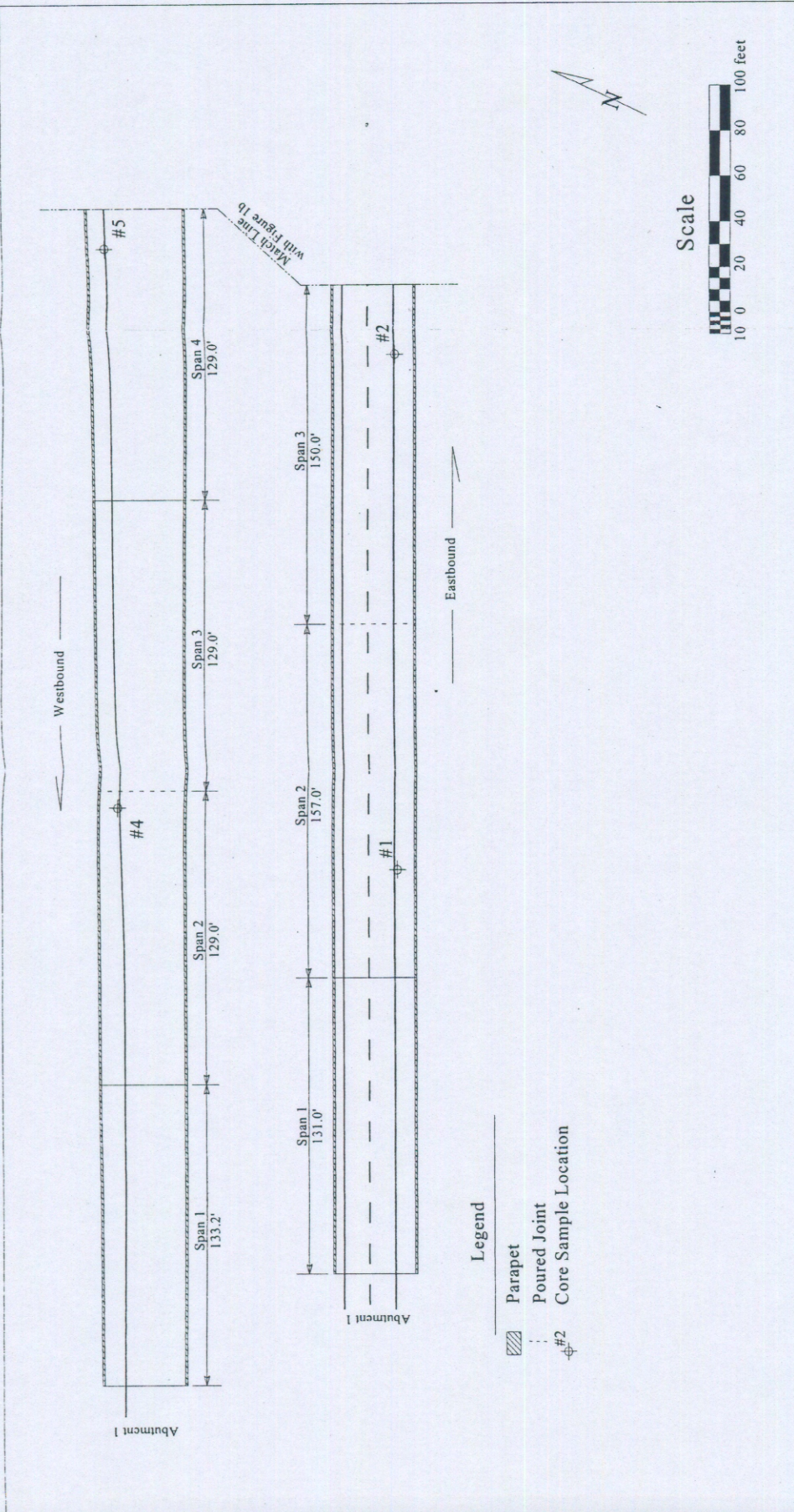


Figure 1a: Plan View and Core Sample Locations

US Route 67 Bridge
over US 87 and North Concho River
San Angelo, Texas

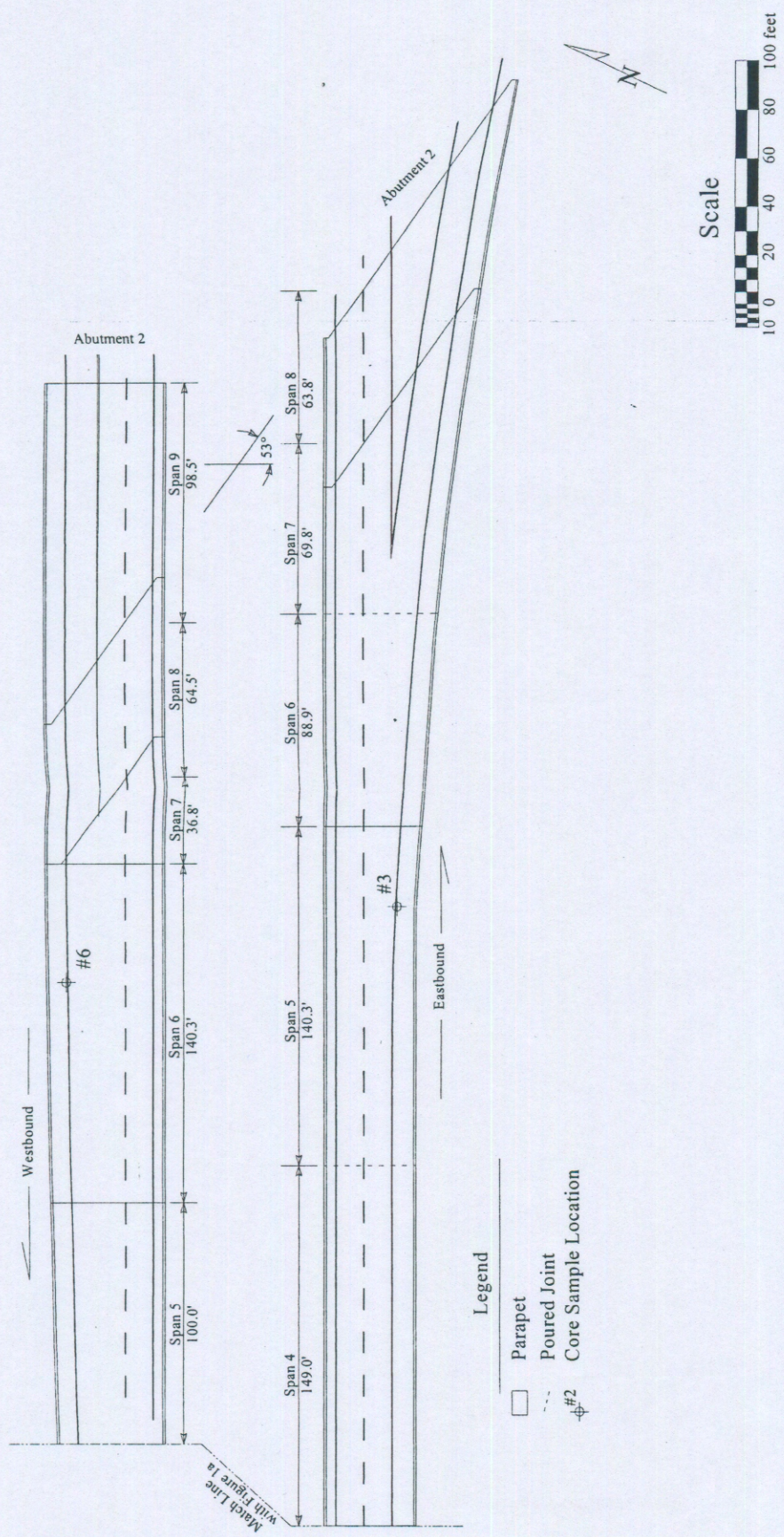


Figure 1b: Plan View and
Core Sample Locations

US Route 67 Bridge
over US 87 and North Concho River
San Angelo, Texas

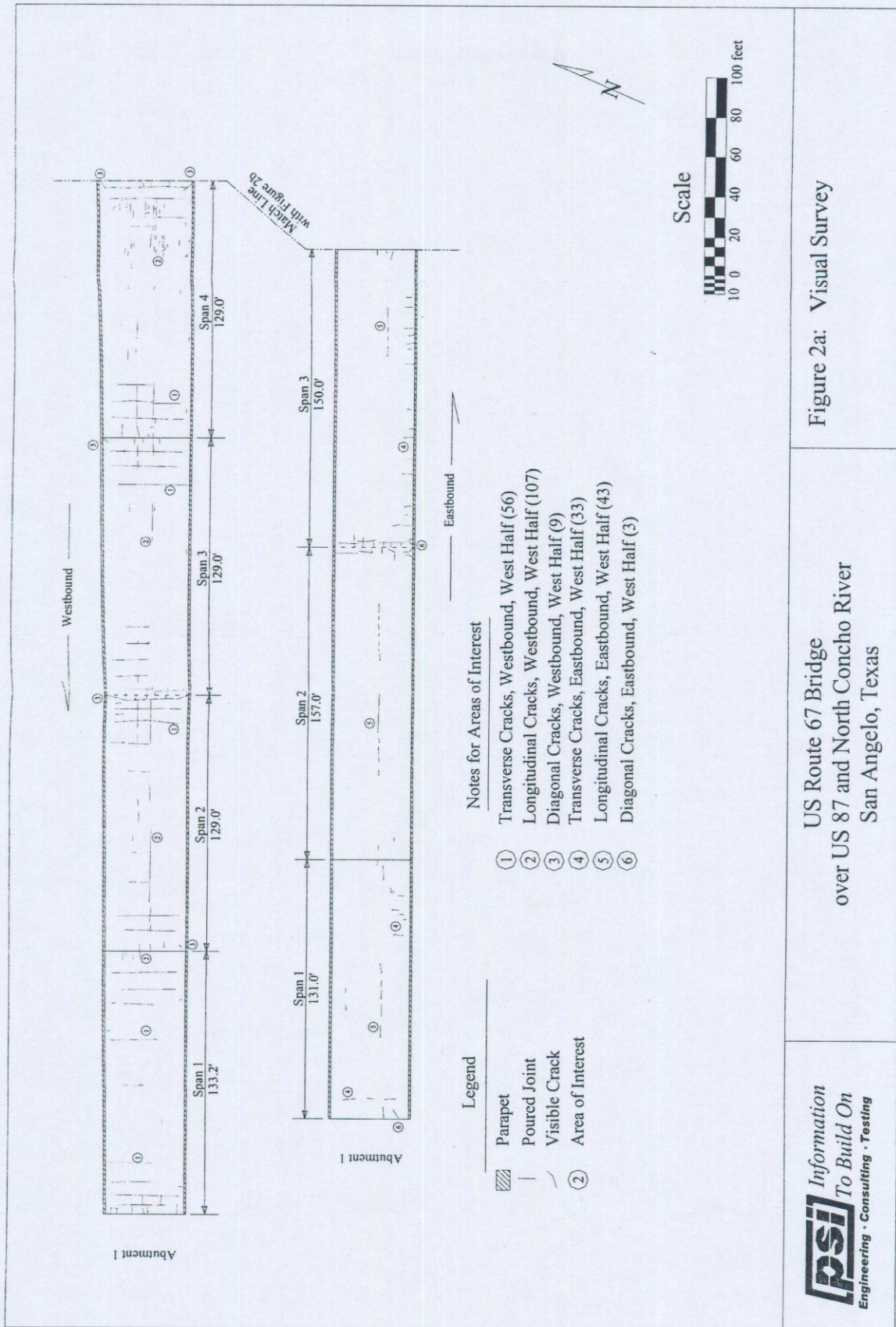


Figure 2a: Visual Survey

US Route 67 Bridge
over US 87 and North Concho River
San Angelo, Texas

psi Information
To Build On
Engineering • Consulting • Testing

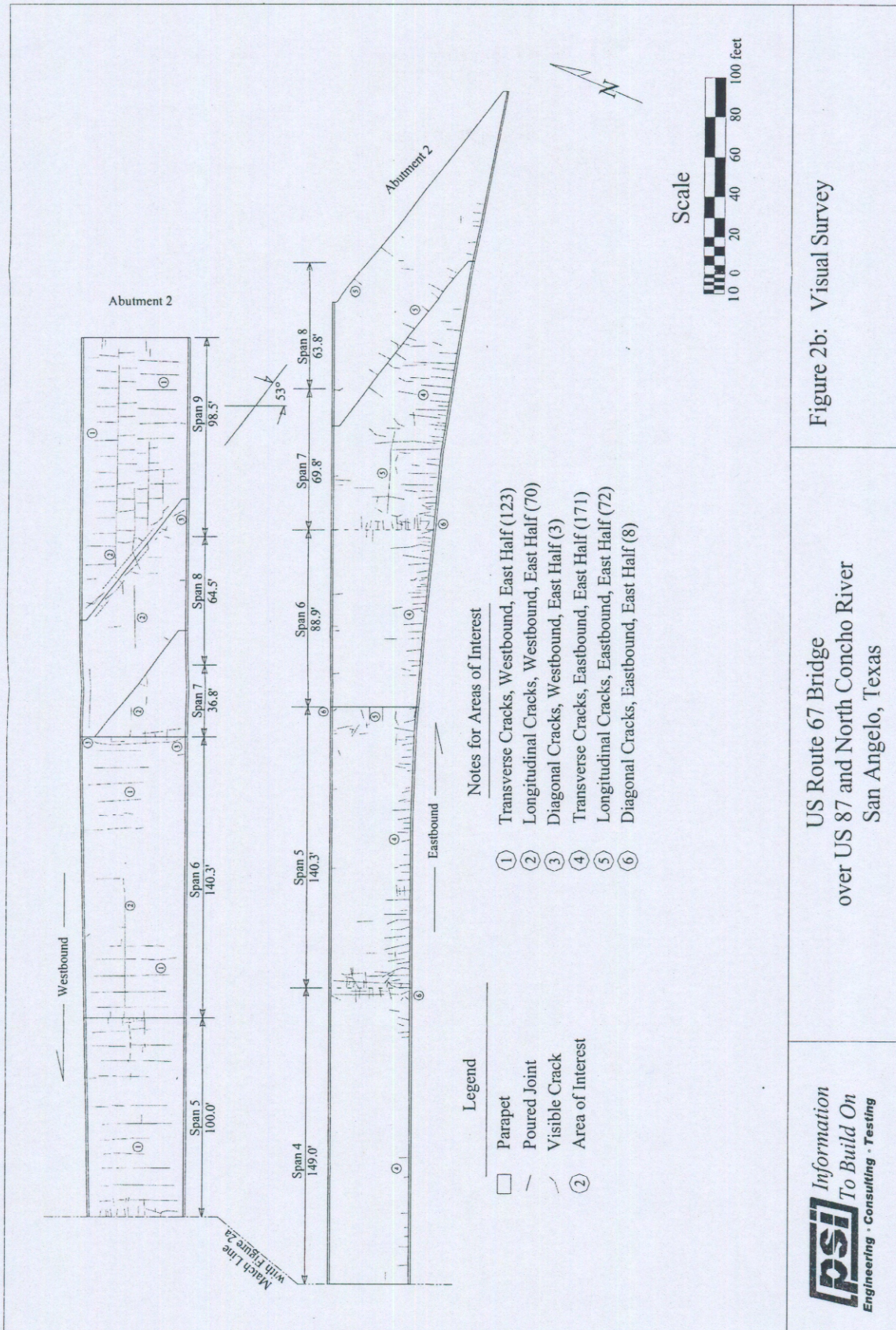


Figure 2b: Visual Survey

US Route 67 Bridge
over US 87 and North Concho River
San Angelo, Texas

Checklist

The following checklist is adapted from 201.1 R-92, and provided to facilitate a thorough survey. The definition of terms and associated photographs in 201.1 R-92, are utilized to standardize the reporting of the condition of the concrete in the structures.

1. Description of structure or pavement
 - 1.1 Name, location, type, and size
The U.S. Route 67 Bridge in San Angelo, Texas is part of a high-speed expressway and carries traffic over the North Concho River, U.S. Route 87, and South Orient Railroad tracks. The bridge consists of two separate structures, one carrying two lanes of eastbound traffic and the other two lanes of westbound traffic. The eastbound structure is 950-feet long and consists of eight spans. The westbound structure is 958-feet long and consists of nine spans.
 - 1.2 Owner, project engineer, contractor, when built
Owner-Texas Department of Transportation. This bridge is part of a demonstration project for HPC in bridge structures which was co-sponsored by the Federal Highway Administration (FHWA) and the Texas Department of Transportation (TXDOT). The bridge was constructed in 1997 and opened to traffic in January 1998.
 - 1.3 Design
 - 1.3.1 Architect and/or engineer: The Texas Department of Transportation (TXDOT)
 - 1.3.2 Intended use and history of use: To carry traffic over the North Concho River, U.S. Route 87, and South Orient Railroad tracks. Opened to traffic in January 1998. No documents were found which would indicate any maintenance had been performed since bridge construction in 1997.
 - 1.3.3 Special features: Certain spans are skewed to accommodate the railroad tracks, the exit-ramp at the eastern end of the eastbound bridge, and the on-ramp at the eastern end of the westbound bridge. The structures are intended to be compared for relative durability and performance based on the extensive use of HPC in the eastbound structure and the limited use of HPC in the westbound structure.
 - 1.4 Construction
 - 1.4.1 Contractor-general Jascon Inc. of Uvalde TX and Reece Albert Inc. of San Angelo TX
 - 1.4.2 Subcontractors concrete placement: N/A
 - 1.4.3 Concrete supplier: Cast-in-place concrete provided by Concho Concrete Inc. of San Angelo TX
 - 1.4.4 Agency responsible for testing: N/A
 - 1.4.5 Other subcontractors: N/A
 - 1.5 Photographs
 - 1.5.1 General view Photos 1 through 2
 - 1.5.2 Detailed close up of condition of area Photos 3 through 6
 - 1.6 Sketch map-orientation showing sunny and shady and well and poorly drained regions: N/A
2. Present condition of structure Date of Evaluation The week of July 14, 2003
 - 2.1 Overall alignment of structure No signs of misalignment
 - 2.1.1 Settlement

2.1.2	Deflection	
2.1.3	Expansion	
2.1.4	Contraction	
2.2	Portions showing distress (beams, columns, pavement, walls, etc., subjected to strains and pressures)	<u>N/A</u>
2.3	Surface condition of concrete	
2.3.1	General (good, satisfactory, poor, dusting, chalking, blisters)	<u>Good</u>
2.3.2	Cracks	<u>Transverse, Diagonal, and longitudinal</u>
2.3.2.1	Location and frequency	<u>See Figure 2</u>
2.3.2.2	Type and size (see Definitions)	<u>See Figure 2</u>
	Longitudinal	<u>Over each of the girder lines</u>
	Width (from Crack comparator)	<u>Less than 0.012 in.</u>
	Hairline	(Less than 1/32 in.)
	Fine	(1/32 in. - 1/16 in.)
	Medium	(1/16 - 1/8 in.)
	Wide	(Greater than 1/8 in.)
	Transverse	<u>Throughout the length</u>
	Width (from Crack comparator)	<u>Less than 0.014 in..</u>
	Hairline	(Less than 1/32 in.)
	Fine	(1/32 in. - 1/16 in.)
	Medium	(1/16 - 1/8 in.)
	Wide	(Greater than 1/8 in.)
	Craze	<u>N/A</u>
	Width (from Crack comparator)	<u></u>
	Hairline	(Less than 1/32 in.)
	Fine	(1/32 in. - 1/16 in.)
	Medium	(1/16 - 1/8 in.)
	Wide	(Greater than 1/8 in.)
	Map	<u>N/A</u>
	Width (from Crack comparator)	<u></u>
	Hairline	(Less than 1/32 in.)
	Fine	(1/32 in. - 1/16 in.)
	Medium	(1/16 - 1/8 in.)
	Wide	(Greater than 1/8 in.)
	D-Cracking	<u>N/A</u>
	Width (from Crack comparator)	<u></u>
	Hairline	(Less than 1/32 in.)
	Fine	(1/32 in. - 1/16 in.)
	Medium	(1/16 - 1/8 in.)
	Wide	(Greater than 1/8 in.)
	Diagonal	<u>At Skew Ends and acute corners</u>
	Width (from Crack comparator)	<u>Less than 0.010 in.</u>
	Hairline	(Less than 1/32 in.)
	Fine	(1/32 in. - 1/16 in.)
	Medium	(1/16 - 1/8 in.)
	Wide	(Greater than 1/8 in.)
2.3.2.3	Leaching, stalactites	<u>N/A</u>
2.3.3	Scaling	<u>N/A</u>
2.3.3.1	Area, depth	<u></u>

2.3.3.2	Type (see Definitions)	_____
	Light	(Less than 1/8 in.)
	Medium	(1/8 in. – 3/8 in.)
	Severe	(3/8 in. – 3/4 in.)
	Very Severe	(Greater than 3/4 in.)
2.3.4	Spalls and popouts	<u>Very minor, insignificant at the base of few columns</u>
2.3.4.1	Number, size, and depth	_____
2.3.4.2	Type (see Definitions)	_____
	Spalls	
	Small	(Less than 3/4 in. depth)
	Large	(Greater than 3/4 in. depth)
	Popouts	
	Small	(Less than 3/8 in. diameter)
	Medium	(3/8 in. – 2 in. diameter)
	Large	(Greater than 2 in. diameter)
2.3.5	Extent of corrosion or chemical attack, abrasion, impact, cavitation	N/A
2.3.6	Stains, efflorescence	<u>Minor, around the Deck overhangs at the bottom side of the westbound bridge</u>
2.3.7	Exposed reinforcement	N/A
2.3.8	Curling and warping	N/A
2.3.9	Previous patching or other repair	N/A
2.3.10	Surface coatings	N/A
2.3.10.1	Type and thickness	N/A
2.3.10.2	Bond to concrete	N/A
2.3.10.3	Condition	N/A
2.3.11	Abrasion	N/A
2.3.12	Penetrating sealers	N/A
2.3.12.1	Type	N/A
2.3.12.2	Effectiveness	N/A
2.3.12.3	Discoloration	N/A

2.4	Interior condition of concrete (in situ and samples)	N/A
2.4.1	Strength of cores	
2.4.2	Density of cores	
2.4.3	Moisture content	
2.4.4	Evidence of alkali-aggregate or other reactions	N/A
2.4.5	Bond to aggregate, reinforcing steel, joints	N/A
2.4.6	Pulse velocity	
2.4.7	Volume change	
2.4.8	Air content and distribution	
2.4.9	Chloride-ion content	
2.4.10	Cover over reinforcing steel	
2.4.11	Half-cell potential to reinforcing steel.	
2.4.12	Evidence of reinforcement corrosion	
2.4.13	Evidence of corrosion of dissimilar metals	
2.4.14	Delaminations	N/A
2.4.14.1	Location	N/A
2.4.14.2	Number, and size	N/A
2.4.15	Depth of carbonation	
2.4.16	Freezing and thawing distress (frost damage)	
2.4.17	Extent of deterioration	
2.4.18	Aggregate proportioning, and distribution	
3.	Nature of loading and detrimental elements	
3.1	Exposure	
3.1.1	Environment (arid, subtropical, marine, freshwater, industrial, etc.)	
3.1.2	Weather-(July and January mean temperatures, mean annual rainfall and months in which 60 percent of it occurs)	82°F/45°F 20.9 in. May- Oct. 68%
3.1.3	Freezing and thawing	51 days per year below 32°F. Minimal annual exposure to F-T
3.1.4	Wetting and drying	Minimal annual exposure
3.1.5	Drying under dry atmosphere	N/A
3.1.6	Chemical attack-sulfates, acids, chloride	N/A
3.1.7	Abrasion, erosion, cavitation, impact	N/A
3.1.8	Electric currents	N/A
3.1.9	Deicing chemicals which contain chloride ions	N/A
3.1.10	Heat from adjacent sources	N/A
3.2	Drainage	N/A
3.2.1	Flashing	
3.2.2	Weepholes	
3.2.3	Contour	
3.2.4	Elevation of drains	

3.3 Loading		Research Test Data Available in Compilation CD Version 3
3.3.1	Dead	
3.3.2	Live	
3.3.3	Impact	
3.3.4	Vibration	
3.3.5	Traffic index	
3.3.6	Other	
3.4	Soils (foundation conditions)	
3.4.1	Compressibility	
3.4.2	Expansive soil	
3.4.3	Settlement	
3.4.4	Resistivity	
3.4.5	Evidence of pumping	
3.4.6	Water table (level and fluctuations)	
4.	Original condition of structure	Good
4.1	Condition of formed and finished surfaces	Good
4.1.1	Smoothness	
4.1.2	Air pockets ("bugholes")	
4.1.3	Sand streaks	
4.1.4	Honeycomb	
4.1.5	Soft areas (retarded hydration)	
4.1.6	Cold joints	
4.1.7	Staining	
4.1.8	Sand pockets	
4.2	Defects	
4.2.1	Cracking	
4.2.1.1	Plastic shrinkage	
4.2.1.2	Thermal shrinkage	
4.2.1.3	Drying shrinkage	
4.2.2	Curling	
5.	Materials of Construction	See Tables 1, 2,4, and 5
6.	Construction Practices	See Report pg. 11and 12

Appendix E: Collecting and Downloading Strain and Temperature Data from the Louetta Bridge and San Angelo HPC Bridge Data Loggers

**Collecting and Downloading Strain and Temperature Data
From the Louetta Bridge and San Angelo HPC Bridge
Data Loggers**

By Shawn Gross, PhD.

CHAPTER 1. INTRODUCTION

CHAPTER 2. DOWNLOADING RAW DATA FILES

CHAPTER 3. GAUGE DURABILITY

CHAPTER 4. MEAN BRIDGE TEMPERATURES

CHAPTER 5. LONG-TERM PRESTRESS LOSSES

CHAPTER 6. LONG-TERM CAMBER AND DEFLECTION

CHAPTER 1: INTRODUCTION

The purpose of this document is to provide researchers and TxDOT personnel with some guidance in any future attempts to resume the collection and analysis of field data for evaluations of long-term performance of the State Highway 249 HPC Bridges over Louetta Road in Harris County near Houston, Texas and the US 67 HPC bridges over the Concho River, US 87 and S.O. Rail Road in San Angelo, Texas. Earliest data for such performance indications included methods for evaluating rapidly changing structural and material properties in the prestressed and post tensioned HPC beams. As these early larger changes gradually diminished, however, so did the need for and the interest in continued monitoring of them. Since all structures, even durable ones, eventually begin to deteriorate at an accelerated pace, the research team provides this guide for possibly monitoring the final years of performance and modes of failure for these first TxDOT HPC bridges.

The guide is organized to address interests in the order of their availability to the monitoring personnel. Chapter 1 provides introductory material; Chapter 2 provides the proper procedure for collecting any logger-stored raw data from remaining sensors. Chapter 3 addresses gage durability, since the meaningless processed data lines in the data tables will be the result of gage failures. Chapter 4 discusses mean temperature considerations for the bridge data. The final two chapters address questions regarding long-term stress and strain. Prestress losses are covered in Chapter 5, and chapter 6 is focused on long-term camber and deflection changes.

CHAPTER 2. DOWNLOADING RAW DATA FILES

This chapter covers the downloading of raw data files from the Campbell Scientific (CS) SM716 storage module. Raw data files must be downloaded via cable and interface module to a computer, manipulated by CS's proprietary PC 208 SORTDATA sorting program, and converted into a spreadsheet format before further processing. Once in the spreadsheet format, the data can be reduced and analyzed for determination of thermal gradients, concrete strains, prestress losses, and other types of structural behavior according to the methods described in subsequent chapters.

Transferring Data from the Storage Modules to the Computer

After the SM716 storage module has been transported back to the laboratory (or any other location) from the jobsite, the following steps should be followed to download the raw data files from the storage module to the computer.

- **Connect the SM716 to the serial port of the computer** using the CS SC532 interface and associated cables. In some cases, a 9-to-25 pin or male-to-female adapter may be required, depending upon the serial port connection at the computer. Note that the SC532 must be plugged in (powered) to operate.
- From the SORTDATA\PC208 directory, **run** the **SMCOM** DOS-based program. For the program to run, you must choose the proper serial port configuration (COM1, COM2, COM3, or COM4).
- The program gives the user several options. First, collect all of the data from the storage module using the **COLLECT ALL** option. The data should be saved in comma separated value (CSV) format and in the current directory with the filename starter: NEWx (where x is the letter corresponding to that storage module). The computer will consecutively number the data files with the same starter automatically.

Example: A data set is to be downloaded from storage module G, and seven previous data sets have been collected from module G. You enter the filename starter NEWG, and the computer writes to the file NEWG008.DAT.

- After downloading is complete, **erase the data** from the storage module using the ERASE option. It is strongly recommended that the existence of a data file (from the above step) be verified prior to this erasing the data. This file verification is easily checked by (HOW????)
- **Reset the storage module** using the RESET option. This reformats the storage module as a sort of "cleaning" process.
- **Upload the data collection (datalogger) programs** to the storage module. Programs have been customized to each data acquisition box, and are stored in the directory SORTDATA\PC208. Backup copies of the programs are stored in the subdirectory PROGRAMS. All program files have the extension .DLD. Programs may be stored in any of

eight program storage "slots" on the storage module. All four programs listed below should be uploaded to the storage module by following the instructions on the screen.

LOU_N_1.DLD should be stored in "slot" 1 (Program for the Louetta NB Box)
LOU_S_1.DLD should be stored in "slot" 3 (Program for the Louetta SB Box)
SANANG_1.DLD should be stored in "slot" 5 (Program for the SA EB Boxes)
SANANG_C.DLD should be stored in "slot" 7 (Program for the SA WB Box)

It is essential that the correct program be installed in the correct slot, so that in the field the correct program can be uploaded from the storage module to the datalogger.

Once the programs have been uploaded to the storage module, the storage module is ready to be used for data collection in the field (Chapter 3).

Conversion of the Raw Data Files into Sorted Form

The raw data file downloaded from the storage module is now ready for further processing. The SORTDTA1 program, written in the PASCAL computer language, is used to manipulate the data. The program is a DOS-based .EXE file and can be found in the directory SORTDATA\PROGRAM. The program takes a data file and performs a sorting operation based on a specified instruction text file. The resulting modified data file is in a form that can then be directly incorporated into a Microsoft Excel spreadsheet.

- **Locate the raw data file** to be modified. If the downloaded raw data file has the extension .CSV (What does this CSV mean or indicate? Comma-separated Values?), rename the file .DAT.
- **Create a duplicate (backup) copy of the raw data file** in the same directory. **Move the backup copy** to the directory SORTDATA\DOWNLOAD\DOWNLD5. This directory contains (will contain) only raw, unprocessed data files that can be reclaimed in case of lost data.
- **Move the other (original) raw data file** to the appropriate directory as listed below. A permanent copy of the unmodified raw data file will be stored in this location.

LOUFILES\NBRIDGE for the Northbound Louetta Bridge
LOUFILES\SBRIDGE for the Southbound Louetta Bridge
SANFILES\EBRIDGE for the Eastbound San Angelo Bridge, Spans 1-2
SANFILES\XBRIDGE for the Eastbound San Angelo Bridge, Spans 3-4
SANFILES\WBRIDGE for the Westbound San Angelo Bridge

- **Rename the raw data file** using the following convention. The numbers xx should be selected as the next available number for the raw data file. Thus, if fourteen raw data files already exist in the appropriate directory, use the number 15 for the current file.

LNB000xx.DAT for the Louetta NB Bridge
LSB000xx.DAT for the Louetta SB Bridge

SEB000xx.DAT for the San Angelo EB Bridge, Spans 1-2
SXB000xx.DAT for the San Angelo EB Bridge, Spans 3-4
SWB000xx.DAT for the San Angelo WB Bridge

- **Move the renamed raw data file** to the SORTDATA\PROGRAM directory.
- **Run the SORTDTA1.EXE DOS Program.** This executable program will use the "alignment" (ALNxxxx.TXT) and "zero" (ZERO.TXT) to manipulate the raw data. Data will be converted from voltages to strains and temperatures, and sorted into a predetermined form. The zero file is used in the conversion process, and must not be erased or changed. For this reason, a backup of the ZERO.TXT file should be kept in the same directory. The alignment files are used to tell the program the desired order of sorted data, and also must not be erased or damaged.

Note that the program will need to be run twice for all cases except the Northbound Louetta bridge using the same raw data file. One run of the program will manipulate strain data, and a second run of the program will collect temperature data. Each run will create a different modified output file (one for strain and one for temperature).

- **At the "Which beam is this data from?" prompt**, enter:

LNB for the Louetta NB Bridge
LSS for the Louetta SB Bridge strain data
LST for the Louetta SB Bridge temperature data
SES for the San Angelo EB Bridge Spans 1-2 strain data
SET for the San Angelo EB Bridge Spans 1-2 temperature data
SXS for the San Angelo EB Bridge Spans 3-4 strain data
SXT for the San Angelo EB Bridge Spans 3-4 temperature data
SWS for the San Angelo WB Bridge strain data
SWT for the San Angelo WB Bridge temperature data

- **At the "Which box is this data being read from?" prompt**, enter:

N for the Louetta NB Bridge
S for the Louetta SB Bridge
E for the San Angelo EB Bridge Spans 1-2
X for the San Angelo EB Bridge Spans 3-4
W for the San Angelo WB Bridge

- **At the "name of the data file to be sorted" prompt**, enter the raw data file name for the file being processed, such as LSB00014.DAT.
- **At the "Use this data file for zero values?" prompt**, enter N. This is extremely important, and if you enter Y by mistake, the program asks you if you are sure that you want to modify zero values. Zero values should not be modified under any condition.

- **At the "Name of the output file?" prompt**, type in the filename for the modified file. The modified file's name should be the same as the raw data file with the .MOD extension instead of .DAT, and with the following replacement for the first three zeros.

STR for a file with strain data (Louetta SB or San Angelo)

TMP for a file with temperature data (Louetta SB or San Angelo)

000 for a Louetta Northbound file

Example: To modify the strain data for a raw data file LSB00026.DAT, enter:

```
LSS
S
LSB00026.DAT
N
LSBSTR26.MOD
```

- The program lists the number of data entries being modified. Then the **program terminates**.
- **Move the original and modified files** to the appropriate directory as given below. The original and modified data files are permanently stored in these locations.

LOUFILES\NBRIDGE for the Northbound Louetta Bridge

LOUFILES\SBRIDGE for the Southbound Louetta Bridge

SANFILES\EBRIDGE for the Eastbound San Angelo Bridge, Spans 1-2

SANFILES\XBRIDGE for the Eastbound San Angelo Bridge, Spans 3-4

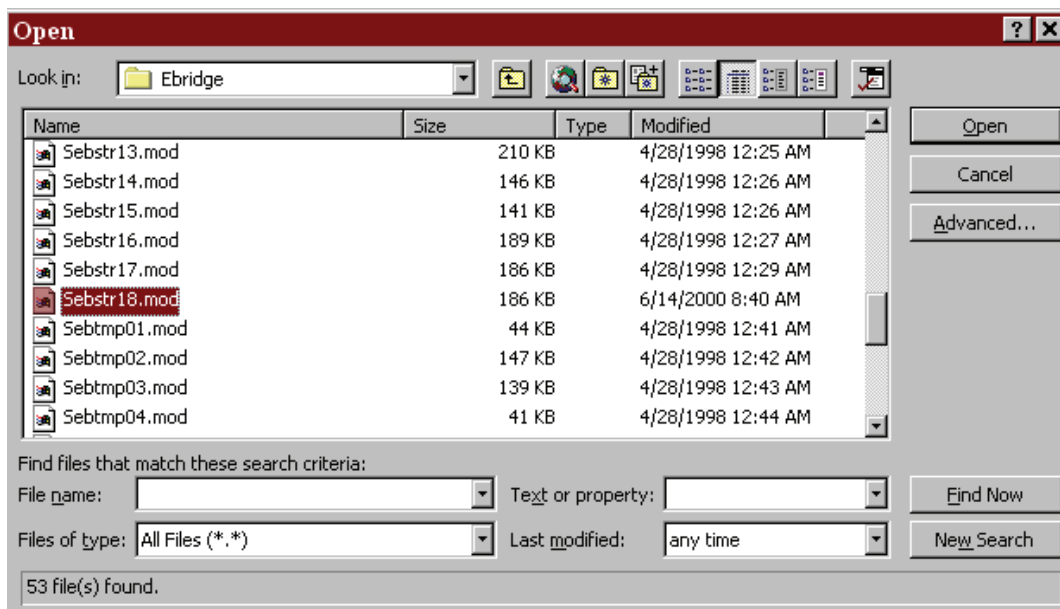
SANFILES\WBRIDGE for the Westbound San Angelo Bridge

The modified data file is now ready to be incorporated into an Excel spreadsheet.

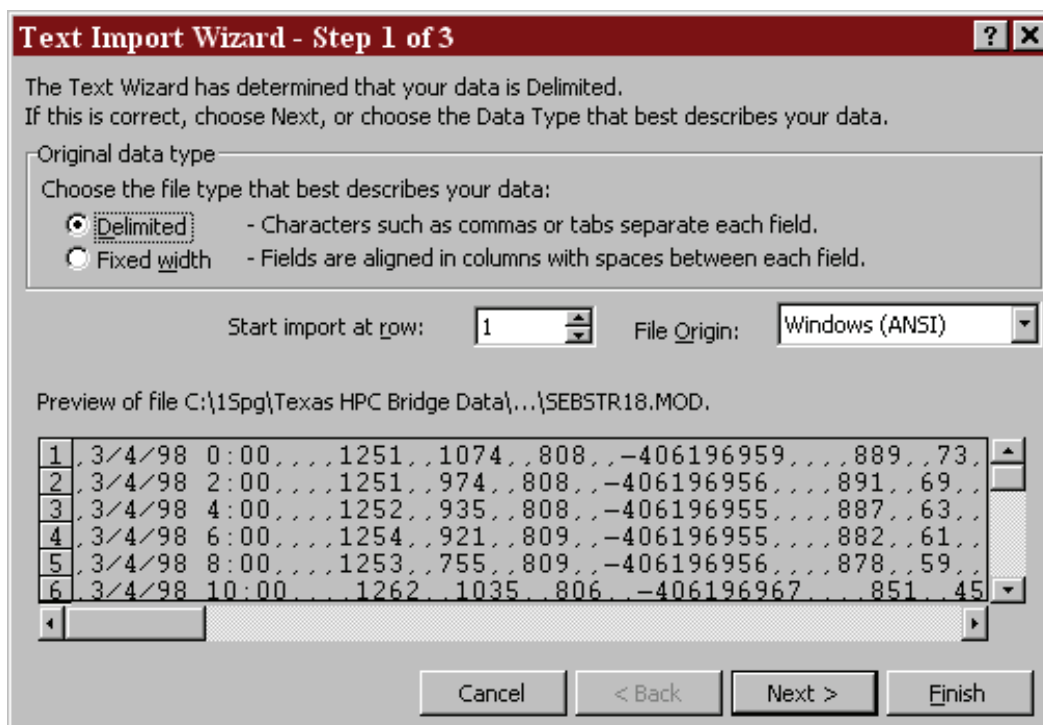
Transfer of the Modified Data Files into Excel Spreadsheets

The modified data files will now be inserted into formatted Excel spreadsheets that allow for easier lookup of data. This standardized spreadsheet format will also facilitate later interpretation of data for prestress losses, temperature gradients, etc.

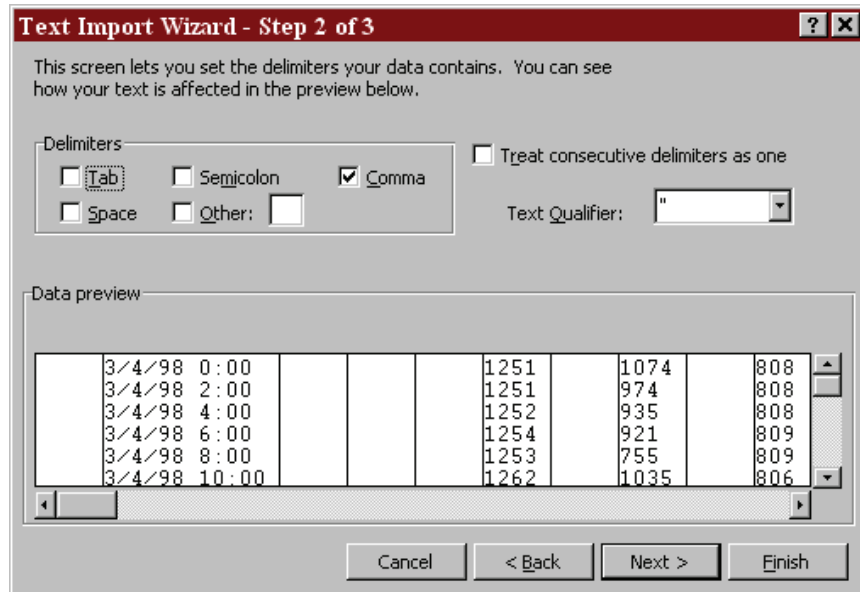
- **Locate the .MOD file** that has been modified in one of directories listed in the final step of the previous section.
- **Open the modified file in Excel as a text file.** Because the data files have the .MOD extension, "All Files" must be selected in the "Files of Type" box.



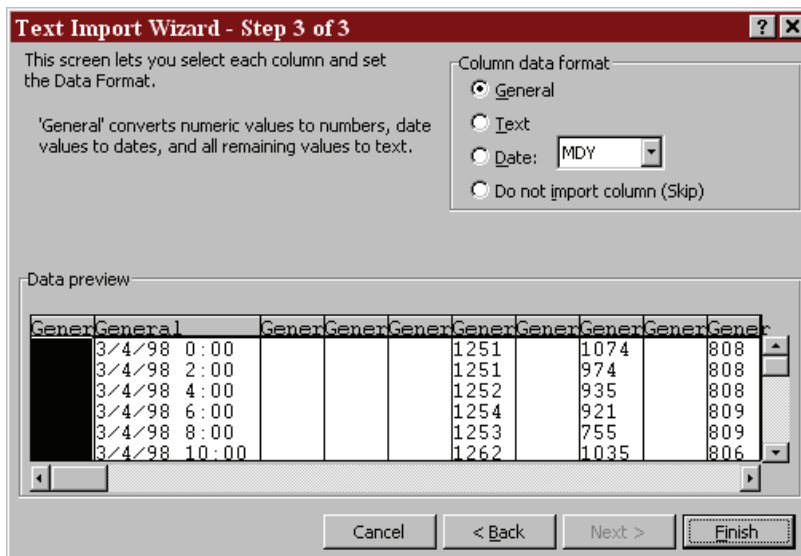
- The text file import wizard (as shown below) should appear. On the first screen, select the options as shown below (these should be the default options) and press "Next".



- Select "Comma" as the delimiter on the second screen. The data should now appear in columns, as shown below. Press the "Next" button.



- Select the default values on the final screen of the wizard (as shown below), and press the "Finish" button.



- The data is now incorporated into spreadsheet form, as shown below. Note that the width of column B (and possibly other columns) may have to be widened to see the data values.

	A	B	C	D	E	F	G	H	I	J	K	L	M	N
1		3/4/1998 0:00				1251		1074		808		-4.1E+08		
2		3/4/1998 2:00				1251		974		808		-4.1E+08		
3		3/4/1998 4:00				1252		935		808		-4.1E+08		
4		3/4/1998 6:00				1254		921		809		-4.1E+08		
5		3/4/1998 8:00				1253		755		809		-4.1E+08		
6		3/4/1998 10:00				1262		1035		806		-4.1E+08		
7		3/4/1998 12:00				1275		1035		799		-4.1E+08		
8		3/4/1998 14:00				1285		1004		798		-4.1E+08		
9		3/4/1998 16:00				1281		1075		799		-4.1E+08		
10		3/4/1998 18:00				1264		1057		801		-4.1E+08		
11		3/4/1998 20:00				1249		1052		803		-4.1E+08		
12		3/4/1998 22:00				1243		1005		805		-4.1E+08		
13		3/5/1998 0:00				1240		1065		805		-4.1E+08		
14		3/5/1998 2:00				1241		981		806		-4.1E+08		
15		3/5/1998 4:00				1241		1057		807		-4.1E+08		
16		3/5/1998 6:00				1241		1068		806		-4.1E+08		
17		3/5/1998 8:00				1242		1045		807		-4.1E+08		
18		3/5/1998 10:00				1250		1048		801		-4.1E+08		
19		3/5/1998 12:00				1265		975		790		-4.1E+08		
20		3/5/1998 14:00				1281		1043		786		-4.1E+08		
21		3/5/1998 16:00				1277		1044		787		-4.1E+08		
22		3/5/1998 18:00				1258		1036		789		-4.1E+08		
23		3/5/1998 20:00				1247		1007		794		-4.1E+08		
24		3/5/1998 22:00				1244		1057		797		-4.1E+08		
25		3/6/1998 0:00				1244		1022		799		-4.1E+08		
26		3/6/1998 2:00				1244		1047		800		-4.1E+08		
27		3/6/1998 4:00				1246		1062		799		-4.1E+08		
28		3/6/1998 6:00				1249		1074		801		-4.1E+08		
29		3/6/1998 8:00				1250		1074		801		-4.1E+08		
30		3/6/1998 10:00				1254		1078		801		-4.1E+08		
31		3/6/1998 12:00				1258		1066		802		-4.1E+08		
32		3/6/1998 14:00				1263		1055		800		-4.1E+08		

- **Examine the spreadsheet**, especially the dates and times in column B. Each row corresponds to one data collection point, and the columns correspond to gauges sorted in a particular order. The values in the columns should be relatively constant, and should appear in every other column. Some of these values represent strains, while others represent temperatures. In particular, check the dates and times at the beginning and end of the file (first and last row). Delete any rows that appear to have incomplete data at the end of the file (these incomplete data lines occasionally appear).

The data must now be copied into a template file that includes headers, so that the data is labeled.

- In Excel, **open the appropriate template file** from those listed below.

LOUFINAL\NBRIDGE\LNBMODEL.XLS for the NB Louetta
 LOUFINAL\SBRIDGE\STRAINS\LSSMODEL.XLS for the SB Louetta strains
 LOUFINAL\SBRIDGE\TEMPS\LSTMODEL.XLS for the SB Louetta temperatures
 SANFINAL\EBRIDGE\STRAINS\SESMODEL.XLS for the EB SA Span 1-2 strains
 SANFINAL\EBRIDGE\TEMPS\SETMODEL.XLS for the EB SA Span 1-2 temperatures
 SANFINAL\XBRIDGE\STRAINS\SXSMODEL.XLS for the XB SA Span 3-4 strains
 SANFINAL\XBRIDGE\TEMPS\SXTMODEL.XLS for the XB SA Span 3-4 temperatures
 SANFINAL\WBRIDGE\STRAINS\SWSMODEL.XLS for the WB San Angelo strains
 SANFINAL\WBRIDGE\TEMPS\SWTMODEL.XLS for the WB San Ang. temperatures

- **Copy (CTRL+C) all of the data rows from the .MOD file.** Be sure that you are copying rows and not individual cells. The selected data should appear as shown below. Note that the row numbers on the left margin are highlighted.

	A	B	C	D	E	F	G	H	I	J	K	L	M	N
1		3/4/1998 0:00				1251		1074		808		-4.1E+08		
2		3/4/1998 2:00				1251		974		808		-4.1E+08		
3		3/4/1998 4:00				1252		995		808		-4.1E+08		
4		3/4/1998 6:00				1254		921		809		-4.1E+08		
5		3/4/1998 8:00				1253		755		809		-4.1E+08		
6		3/4/1998 10:00				1262		1035		806		-4.1E+08		
7		3/4/1998 12:00				1275		1035		799		-4.1E+08		
8		3/4/1998 14:00				1265		1004		798		-4.1E+08		
9		3/4/1998 16:00				1281		1075		799		-4.1E+08		
10		3/4/1998 18:00				1264		1057		801		-4.1E+08		
11		3/4/1998 20:00				1249		1062		803		-4.1E+08		
12		3/4/1998 22:00				1243		1005		805		-4.1E+08		
13		3/5/1998 0:00				1240		1065		805		-4.1E+08		
14		3/5/1998 2:00				1241		981		806		-4.1E+08		
15		3/5/1998 4:00				1241		1057		807		-4.1E+08		
16		3/5/1998 6:00				1241		1068		806		-4.1E+08		
17		3/5/1998 8:00				1242		1045		807		-4.1E+08		
18		3/5/1998 10:00				1250		1049		801		-4.1E+08		
19		3/5/1998 12:00				1265		975		799		-4.1E+08		
20		3/5/1998 14:00				1281		1043		786		-4.1E+08		
21		3/5/1998 16:00				1277		1044		767		-4.1E+08		
22		3/5/1998 18:00				1258		1036		769		-4.1E+08		
23		3/5/1998 20:00				1247		1007		794		-4.1E+08		
24		3/5/1998 22:00				1244		1057		797		-4.1E+08		
25		3/6/1998 0:00				1244		1022		799		-4.1E+08		
26		3/6/1998 2:00				1244		1047		800		-4.1E+08		
27		3/6/1998 4:00				1246		1062		799		-4.1E+08		
28		3/6/1998 6:00				1249		1074		801		-4.1E+08		
29		3/6/1998 8:00				1250		1074		801		-4.1E+08		
30		3/6/1998 10:00				1254		1078		801		-4.1E+08		
31		3/6/1998 12:00				1258		1066		802		-4.1E+08		
32		3/6/1998 14:00				1263		1055		800		-4.1E+08		

- **Paste the copied data into the template (model) spreadsheet.** Start by selecting only Row 14 as the location to insert the text (see below), and then paste the data (CTRL+V).

Microsoft Excel - Labmodel.xls

File Edit View Insert Format Tools Data Window Help

75%

Paste Special...

Arial 10

B I U

10/28/1996 16:50 -2.793

697

1002

4221

N21-E HORIZONTAL CGS PROFILE

14

15

16

17

18

19

20

21

22

23

24

25

26

27

28

29

30

31

32

33

34

35

36

37

38

39

40

Draw

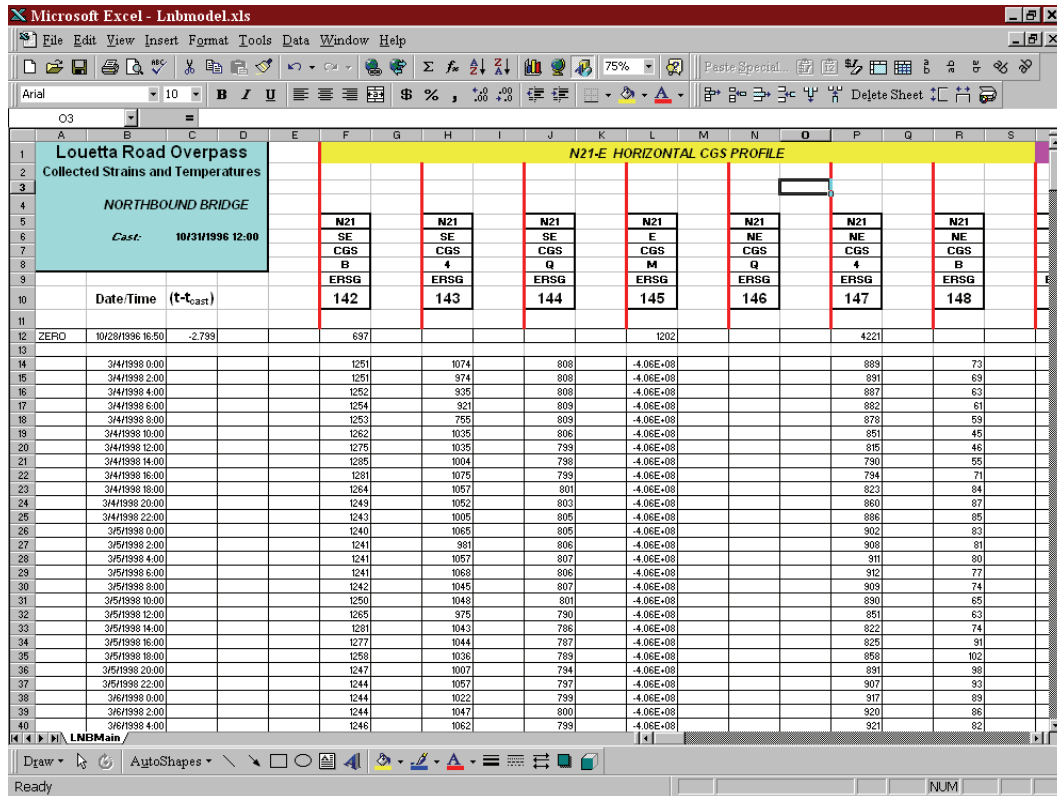
AutoShapes

Ready

NUM

- **Format the spreadsheet by copying the formats from row 12 to the rest of the spreadsheet.** Select Row 12, then Copy (CTRL+C). Select Rows 14 through the end of the spreadsheet and select Paste Special under the Edit menu. Select Formats to copy the format

from row 12 to all of the other rows. When completed, the spreadsheet should look like the picture below.



- **Save the new Excel data file with a filename other than the template name** using the Save As command. Save files using the convention below, and in the directories given below. Choose xx as the next sequential number over the files already existing in the appropriate directory.

LOUFINAL\NBRIDGE\LNBDATxx.XLS for the NB Louetta
 LOUFINAL\SBRIDGE\STRAINS\LSBSTRxx.XLS for the SB Louetta strains
 LOUFINAL\SBRIDGE\TEMPS\LSBTMPxx.XLS for the SB Louetta temperatures
 SANFINAL\EBRIDGE\STRAINS\SEBSTRxx.XLS for the EB SA Span 1-2 strains
 SANFINAL\EBRIDGE\TEMPS\SEBTMPxx.XLS for the EB SA Span 1-2 temperatures
 SANFINAL\XBRIDGE\STRAINS\SXBSTRxx.XLS for the XB SA Span 3-4 strains
 SANFINAL\XBRIDGE\TEMPS\SXBTMPxx.XLS for the XB SA Span 3-4 temperatures
 SANFINAL\WBRIDGE\STRAINS\SWBSTRxx.XLS for the WB San Angelo strains
 SANFINAL\WBRIDGE\TEMPS\SWBTMPxx.XLS for the WB San Ang. Temperatures

- **As a backup, print a copy of the .XLS data file.** The print setup will already be set from the model template files. Printing is set at 40% in landscape mode. Store the hardcopy in a safe location.

The formatted Excel spreadsheets have several key features. The upper left hand corner of the spreadsheet identifies the bridge which data is from, whether data is composed of strains, temperatures, or both, and lists the date on which the bridge deck was cast. Across the top of the spreadsheet are gauge identifiers, including the gauge number and several pieces of information

as to the location of the gauge. Descriptions of each identifier may be found in Section 3.4.1 (Table 3.4) of the comprehensive report.

Also across the top of the spreadsheet is a line of alternating colors which identifies a group of gauges that are used together in data analysis. Typically, this group of gauges would be oriented in a single horizontal or vertical profile across a beam or bridge deck. Sketches depicting the gauge locations may also be found in Appendices A and B of the comprehensive report. The print setup has been organized to display these rows at the top of each page.

It is again emphasized that the reader must be familiar with the contents of Chapters 2 and 3 of the comprehensive report to facilitate understanding of the meaning of these locations and gauge groupings. These chapters describe the details of each bridge and the overall instrumentation plans and procedures for the research projects.

CHAPTER 3. GAUGE DURABILITY

This chapter discusses the method of determining which of the 518 embedded gauges used in the Louetta and San Angelo bridges are performing in a consistent, reliable manner over the long-term. A manual investigation must be periodically performed to examine the behavior of each individual gauge. A summary of the durability of gauges, organized by gauge type, must then be compiled.

Durability of Gauge Types - Data through March 1998

The types of embedded gauges used in the Louetta and San Angelo bridges include vibrating wire gauges (including integral thermistors), electric resistance strain gauges, and thermocouples. Each type of gauge is described in detail in Section 3.2.2 of the comprehensive report. Past experience on this and other projects has generally shown vibrating wire gauges (VW/TR) and thermocouples (TC) to be quite durable, while electrical resistance strain gauges (ERSG) have been more susceptible to damage and long-term decay. The durability of all gauges through March 1998 is shown graphically in Figure 3.1.

Embedded gauges are lost or become unstable for a variety of reasons. As discussed in Section 3.7 of the comprehensive report, most damage to vibrating wire gauges and thermocouples was observed to occur during casting, transportation, or other aspects of construction. In some cases, an entire group of gauges was disconnected *intentionally* to make room for additional gauges in the deck. The survey of gauges in March 1998 reflected the durability after a few months to a few years of data collection. Additional surveys are needed to establish the long-term durability over several years. It is recommended that a survey be conducted once a year to establish the durability trend for each gauge type.

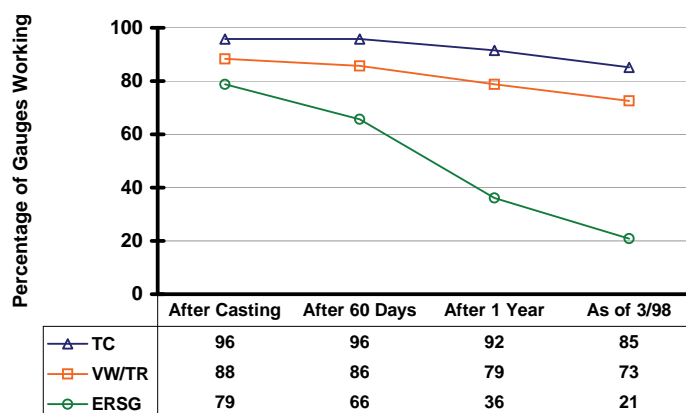


Figure 3.1 - Durability of Embedded Gauges as of March 1998

How to Conduct a Durability Survey

A typical durability survey worksheet is shown in Figure 3.2. In the Excel file GAUGEDURABILITY.XLS, a worksheet has been established for each beam, precast panel, and cast-in-place deck slab. Each of the 518 embedded gauges is listed once among the series of worksheets. The purpose of the worksheets is to identify which gauges are working at each listed time stage. The status of each gauge was reviewed at the following stages:

- Initial hookup of the gauges prior to concrete placement
- Just after concrete placement
- Just prior to transportation (if gauge is in a beam or precast panel)
- Just after placement of the cast-in-place deck
- 1 year after initial hookup of the gauge
- in March 1998

It is again suggested that the durability of each gauge be reviewed on an annual basis. Additional columns have been provided in the worksheets to facilitate recording of gauge status at future dates.

When a gauge is in proper working condition, a + symbol should be placed in the proper cell within the new column. (This can be done by typing in: '+' into as the cell contents.) The worksheets are setup to automatically count the total number of working gauges (+ symbols) per beam, panel, or deck span. In the example shown in Figure 3.2, gauges 1029, 1030, 1034, 1233, 1613, 1614, 1616, 1617, and 1618, were working properly as on March 1998. A total of 9 of the 14 gauges installed in Beam E24 were working properly as of this date.

If a gauge is working properly, readings should be both present and stable. If a gauge is not working properly, it will be blank, read -6999 or -99999, or may read erratically. Readings should make sense depending upon the type of gauge: for strains, values up to 2000 microstrain or higher may be reasonable, while for temperatures values should range from approximately 20 to 120 degrees. When a gauge is reading a value that appears somewhat unstable, a subjective decision must be made regarding the acceptability of gauge readings. In certain cases, especially within the deck, values that appear unstable are actually reasonable because the readings (strains or temperatures) reflect significant changes due to temperature variations throughout the course of a day. If there is any uncertainty as to the stability of an individual gauge, its performance over *several consecutive days* should be examined.

Persons performing the durability survey may wish to examine the March 1998 readings as a guide. The Excel durability worksheets for each beam, panel, or deck span were constructed using readings from the following sorted data files for the completed bridges:

Loufiles\Nbridge\Lnbdat16.xls
Loufiles\Sbridge\Strains\Lsbstr16.xls
Loufiles\Sbridge\Temps\Lsbtmp16.xls
Sanfiles\Wbridge\Strains\Swbstr18.xls
Sanfiles\Wbridge\Temps\Swbtmp18.xls
Sanfiles\Ebridge\Strains\Sebstr17.xls
Sanfiles\Ebridge\Temps\Sebtmp17.xls

Beam/Panel/Deck:		E24						
Casting Date:		3/8/1997						
General Comments:								
Total Counts								
ERSG	7	5	5	5	4	3	3	0
VW/TR	1	1	1	1	1	1	1	0
TC	6	6	6	6	6	5	5	0
	14	12	12	12	11	9	9	0
Gauge Type	Gauge #	Initial Hookup	Working After Casting	Working Before Shipment	Working After Deck Casting	Working After 1 Year	Working As of March 1998	Working As of
ERSG	1028	+	+	+				
	1029	+	+	+	+	+	+	
	1030	+	+	+	+	+	+	
	1031							
	1032	+	+	+	+			
	1033							
	1034	+	+	+	+	+	+	
VW/TR	1233	+	+	+	+	+	+	
TC	1613	+	+	+	+	+	+	
	1614	+	+	+	+	+	+	
	1615	+	+	+	+			
	1616	+	+	+	+	+	+	
	1617	+	+	+	+	+	+	
	1618	+	+	+	+	+	+	

Figure 3.2 Example Excel Worksheet for Gauge Durability

Creating a Summary for the Durability Study

After all of the durability worksheets have been completed by a manual inspection of data files, a tabular summary should be created to allow for analysis of where gauges are demonstrating good long-term durability and where gauges are demonstrating poor long-term durability. Summaries

should be compiled for each project (Louetta and San Angelo), as well as for the overall research program. The summaries should provide a total count of the number of working gauges, as well as subcounts by bridge and gauge type. An example summary is shown in Figure 3.3 for the Louetta bridges. Summary tables for durability studies through March 1998 are provided in the Excel file GAUGEDURABILITY.XLS.

Additionally, charts should be created that provide a graphical representation of the summarized data. Charts will facilitate the analysis of durability data and the identification of durability trends. At a minimum, a chart similar to that shown in Figure 3.1, which shows the long-term durability for the entire research program by gauge type, should be created. Similar charts may be constructed for each bridge (Louetta-N, Louetta-S, San Angelo-E, and San Angelo-W), and for each gauge type (VW/TR, TC, and ERSG). New charts may easily be adapted from the existing charts in the Excel file GAUGEDURABILITY.XLS.

A brief Gauge Durability Summary Report should be written at the conclusion of each durability study, and distributed to proper project personnel. This report should consist of a brief discussion of the techniques used in the study (reference may be made to this document where appropriate) and should identify any trends observed regarding the durability of embedded gauges. The report should include all summary tables and charts created as part of the durability study.

	ERSG						VW/TR						TC						Total					
	Total	Initial Hookup	After Casting	After 60 Days	After 1 Year	As of 3/98	Total	Initial Hookup	After Casting	After 60 Days	After 1 Year	As of 3/98	Total	Initial Hookup	After Casting	After 60 Days	After 1 Year	As of 3/98	Total	Initial Hookup	After Casting	After 60 Days	After 1 Year	As of 3/98
Louetta NB Beams	59	49	47	31	18	6	14	14	13	12	7	7	12	11	11	11	11	12	85	74	71	54	36	25
Louetta NB CIP Deck	24	23	22	22	0	0	2	2	2	2	2	2	4	4	4	4	4	4	30	29	28	28	6	6
Louetta SB Beams	49	39	36	32	24	5	27	27	27	25	23	16	24	22	22	22	22	17	100	88	85	79	69	38
Louetta SB Panels	0	0	0	0	0	0	6	6	6	6	6	6	4	4	4	4	4	4	10	10	10	10	10	10
Louetta SB CIP Deck	4	3	3	3	0	0	17	15	14	14	14	14	10	10	10	10	10	10	31	28	27	27	24	24
TOTAL	136	114	108	88	42	11	66	64	62	59	52	45	54	51	51	51	51	47	256	229	221	198	145	103
Louetta NB	83	72	69	53	18	6	16	16	15	14	9	9	16	15	15	15	15	16	115	103	99	82	42	31
Louetta SB	53	42	39	35	24	5	50	48	47	45	43	36	38	36	36	36	36	31	141	126	122	116	103	72
Total Percentages		84	79	65	31	8.1		97	94	89	79	68		94	94	94	94	87		89	86	77	57	40
Louetta NB		87	83	64	22	7		100	94	88	56	56		94	94	94	94	100		90	86	71	37	27
Louetta SB		79	74	66	45	9		96	94	90	86	72		95	95	95	95	82		89	87	82	73	51
Louetta NB Beams		83	80	53	31	10		100	93	86	50	50		92	92	92	92	100		87	84	64	42	29
Louetta NB CIP Deck		96	92	92	0	0		100	100	100	100	100		100	100	100	100	100		97	93	93	20	20
Louetta SB Beams		80	73	65	49	10		100	100	93	85	59		92	92	92	92	71		88	85	79	69	38
Louetta SB Panels								100	100	100	100	100		100	100	100	100	100		100	100	100	100	100
Louetta SB CIP Deck		75	75	75	0	0		88	82	82	82	82		100	100	100	100	100		90	87	87	77	77

Figure 3.3 - Example Tabular Summary for Gauge Durability

CHAPTER 4. MEAN BRIDGE TEMPERATURES

This chapter discusses the measurement of mean bridge temperatures in the Louetta and San Angelo Bridges. Temperature data is being recorded continuously at several locations within the beams and decks of each bridge using embedded thermocouples and thermistors. This chapter explains the analytical process used to compute mean bridge temperatures from raw temperature data. Guidelines for comparison of measured data to ambient and design temperatures are also provided.

Background

Mean bridge temperature can be defined as the average, or mean temperature through the entire depth of the bridge superstructure. Essentially, the mean bridge temperature is a weighted average of the temperatures at all depths, including different locations within the beams and deck. This mean temperature is important in design because it is related to axial movements of the superstructure and thus must be considered in the design of bearings and expansion joints.

Mean bridge temperatures were determined in each bridge (Louetta Northbound, Louetta Southbound, San Angelo Eastbound, and San Angelo Westbound) for 1997 upon completion of construction at the jobsites. Data is needed for 1998, 1999, 2000, and future years. Mean bridge temperatures are computed using a composite beam (beam and portion of the deck) from each bridge. These beams were selected on the basis of their location within the span, the location of gauges in the deck above the beams, and the reliability of gauge measurements. These beams are identified in Figure 4.1, along with important beam and deck dimensions that are used in the analytical process of computing mean bridge temperatures. Additional background data is provided in the Excel file Meanbrtempsummary.xls.

The mean bridge temperature is computed as a weighted average by considering the measured temperatures at each gauge location within the composite beam, and assigning that temperature to a specific area or *layer*. The gauge locations and layers used for calculation of mean bridge temperatures can be seen in Figure 4.2 for a U54 beam and an AASHTO Type IV beam. Depending upon relative dimensions within the beam and deck, a certain weight factor is assigned to the temperature at each layer. These weight factors for the composite beams used in this study are listed in Figure 4.3. These weight factors have already been incorporated into the calculation spreadsheets, but are listed here for reference purposes. Note that the contribution of the deck to the mean bridge temperature ranges from 39 to 52 percent (sum of weights for layers 7 and 8), as a function of the type of beam cross-section, deck thickness, beam spacing, and the moduli of elasticity of the various concretes.

	Louetta NB	Louetta SB	S. Ang. WB	S. Ang. EB
Beam / Web ¹	N33-W	S14-E	W15	E25
Beam Type	U54A	U54A	IV	IV
Depth of CIP Deck Gauge Below Surface	2.25	2.25	2.00	2.25
CIP Deck Thickness	3.75	4.00	4.75	4.00
Precast Panel Thickness	3.50	3.50	4.00	4.00
Haunch Thickness	1.50	1.50	1.50	3.50
Total Deck Thickness Above Beam Flange	8.75	9.00	10.25	11.50
Total Deck Thickness Between Beams	7.25	7.50	8.75	8.00
Beam Spacing (Width of Tributary Deck)	150.36	194.40	68.00	79.20
Gap Between Precast Panels	14.63 [#]	14.63 [#]	9.00	9.00
Width of Haunch	23.50 [#]	23.50 [#]	16.00	16.00
All dimensions in inches. (1 in. = 25.4 mm)				
¹ See Section 3.4.1 for notation. [#] Total for top flanges above both webs.				

Figure 4.4 - Deck Dimensions and Gauge Depths for Selected Composite Beams

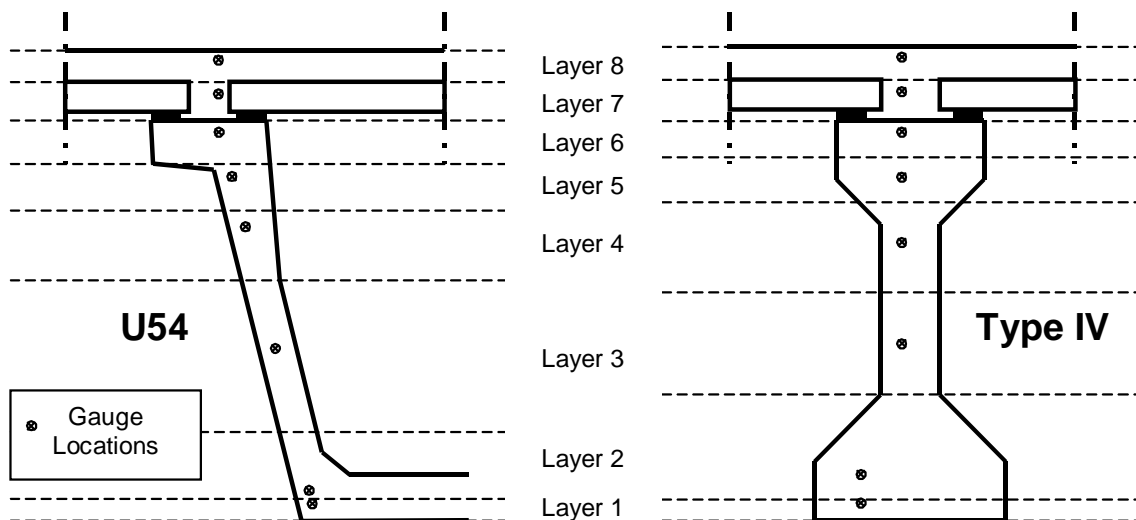


Figure 4.5 - Gauge Locations and Layers Used for Calculation of Average Bridge Temperature

	Louetta NB	Louetta SB	San Angelo WB	San Angelo EB
Beam / Web	N33-W	S14-E	W15	E25
Weight, Layer 1	.090	.078	.060	.057
Weight, Layer 2	.138	.119	.218	.208
Weight, Layer 3	.112	.096	.086	.082
Weight, Layer 4	.060	.052	.081	.077
Weight, Layer 5	.054	.046	.086	.081
Weight, Layer 6	.100	.086	.077	.073
Weight, Layer 7	.242	.264	.183	.220
Weight, Layer 8	.205	.260	.208	.201

Figure 4.6 - Weights Used for Calculation of Average Bridge Temperature

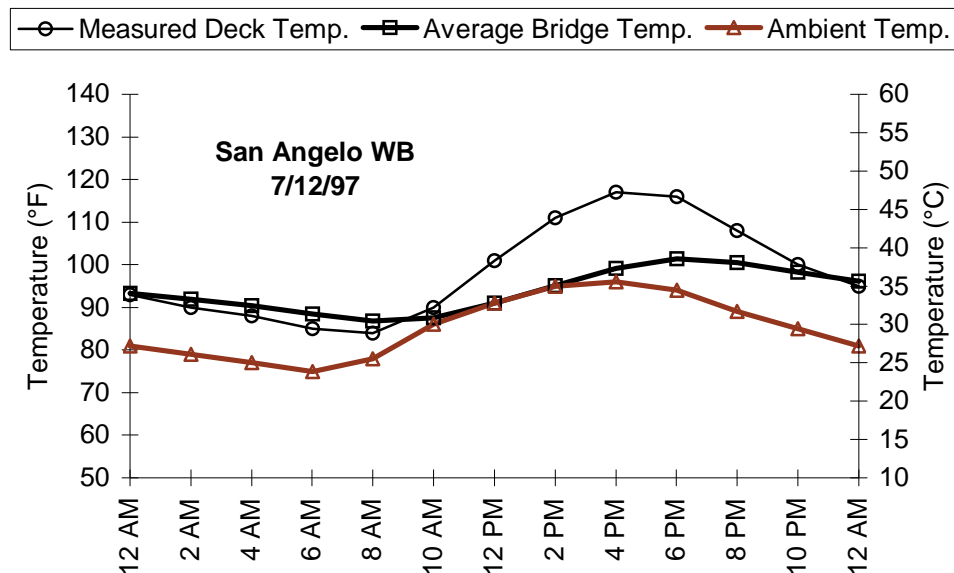


Figure 4.7 - Typical Temperature Behavior on a Sunny Summer Day

Measurements

In addition to measuring the mean bridge temperature, it is important to compare this temperature to the measured ambient temperature and measured deck temperature (at a gauge location approximately 2.00 to 2.25 in. below the deck surface). This comparison allows for a better understanding of the thermal behavior of the bridge superstructures. As an example, these three temperatures are compared in Figure 4.4 for the San Angelo non-HPC Westbound Bridge on a sunny summer day. The three temperatures can be seen to show similar increases and decreases in sense, but not in magnitude. The deck clearly heats up and cools down much more quickly than the bridge structure as a whole, though both remain at or above ambient temperature

throughout the day. Similar hourly comparisons are made for selected days in Section 5.3.2 of the comprehensive report.

For purposes of long-term data collection, it is more important to determine these temperatures on a daily basis, and to determine monthly averages. A comparison of the *daily maximum* deck, mean bridge, and ambient temperatures is shown in Figure 4.5. In Figure 4.6, these daily maximum temperatures are averaged on a monthly basis. Similar plots can be constructed for *daily minimum* temperatures. The steps below provide guidance in creating these plots and in summarizing the data.

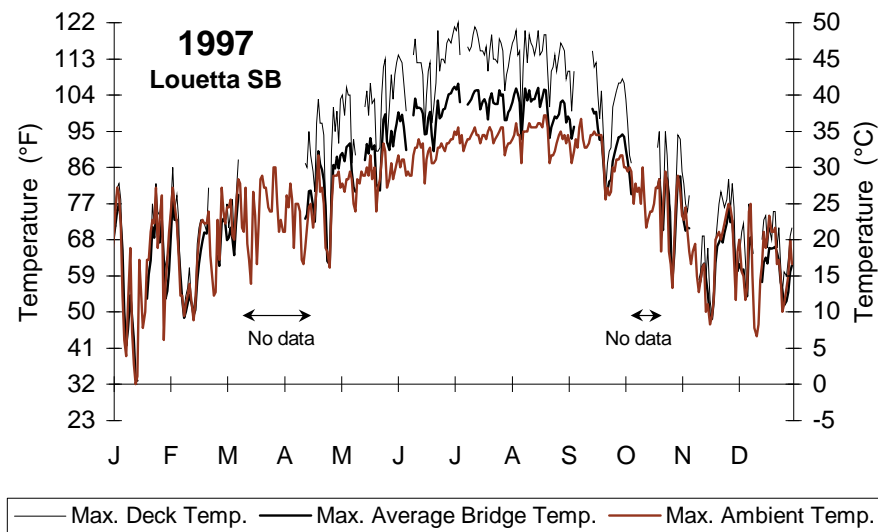


Figure 4.8 - Maximum Daily Temperatures for Composite Beam S14-E in 1997

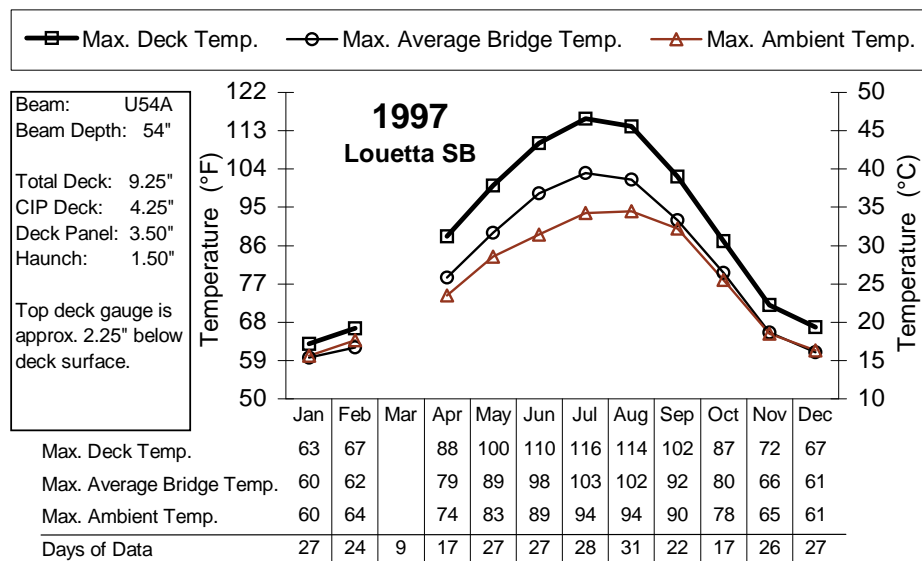


Figure 4.9 - Average Maximum Daily Temperatures by Month for Beam S14-E in 1997

- 1** Copy an old TG file (such as this one) and rename the new copy.
- 2** Input data for the cross-section layers on the [Coefficients](#) sheet. Cells with required input are shaded in yellow.
- 3** On [DataSort](#) sheet, input the first gauge number (BF gauge) and the number of gauges to be read at the top left corner of the sheet.
- 4** Calculate the entire workbook.
- 5** Open a raw data file (such as LSBTMP06). Select all and copy values into the [Data](#) sheet of this workbook.
- 6** Copy all rows with data from [DataSort](#) into [TGCalc](#). Do not leave blank rows between new sections of data.
- 7** Repeat the previous two steps for all raw data files associated with the period of study.
- 8** Copy the equations in row 13, columns O through AT, of the sheet [TGCalc](#) to all subsequent rows with data.
- 9** Copy the equations in row 10, columns G through AD, of the sheet [TGSummary](#) to all subsequent rows.
- 10** Input/adjust the ambient temperature data in columns AE and AF of the sheet [TGSummary](#).
- 11** Copy the formulas in rows 376 and 396, columns G through AD, of the sheet [TGSummary](#) to rows 377 through 387 and 397 through 407, respectively. Delete data from rows with data for less than half of the month's days.
- 12** Calculate the entire workbook.
- 13** Print the sheet [TGSummary](#) and look for odd values, especially in the Maximum and Minimum temperatures.
- 14** Correct data in the sheet [TGCalc](#) as necessary.
- 15** Delete calculated values in appropriate columns G through AD of the sheet [TGSummary](#) for days where data is incomplete or missing.
- 16** Calculate the entire workbook.
- 17** Print the sheet [TGSummary](#), and all sheets with charts.

Figure 4.10 - Step-by-Step Instructions for Analysis of Mean Bridge Temperatures and Thermal Gradients

Step -by-Step Instructions for Computation and Analysis of Mean Bridge Temperatures

The steps described in detail below are listed in Figure 4.7. The steps are used in conjunction with the Excel files TGxxyyyy.xls where xx is the particular bridge in question and yyyy is the calendar year. This sequence of steps should be followed for each calendar year on each bridge, with a new Excel file created each time.

(Note: The procedure outlined here also computes thermal gradient data.)

Step 1: Copy an old TG file and rename the new copy.

This step allows for a new file to be created using an old file as a template. An existing file from the same bridge should be used for this purpose (i.e. create a new Louetta SB file from an existing Louetta SB file, not from a file for a different bridge).

Step 2: Input data for the cross-section layers on the "Coefficients" sheet. Cells with required input are shaded in yellow.

This step may be skipped when an old file is used as a template, as suggested in Step 1. The "Coefficients" worksheet computes the weights of each layer within the composite beam based on a set of input properties.

Step 3: On "DataSort" sheet, input the first gauge number (BF gauge) and the number of gauges to be read at the top left corner of the sheet.

This step may be skipped when an old file is used as a template, as suggested in Step 1. These cells identify which gauges the temperatures will be selected from. The Excel workbook is programmed to locate these gauges automatically and to disregard other temperature data.

Step 4: Calculate the entire workbook.

It is highly recommended that the workbook be calculated manually since it is so large. If calculations are done automatically, extremely slow performance can be expected on some computers. This can be done by selecting Tools-Options on the menu bar, and setting the calculation option to Manual as shown in Figure 4.8. When it is desired to have formulas evaluated, F9 should be pressed.

Step 5: Open a raw data file (such as LSBTMP06). Select all and copy values into the "Data" sheet of this workbook.

This process imports raw data from temperature files that will be processed. Data is imported from the raw modified (.mod) data files that are created using the method outlined in Chapter 2. To copy all data from the .mod file to the "Data" worksheet, follow the instructions in Figure 4.9. The worksheets should look identical after copying.

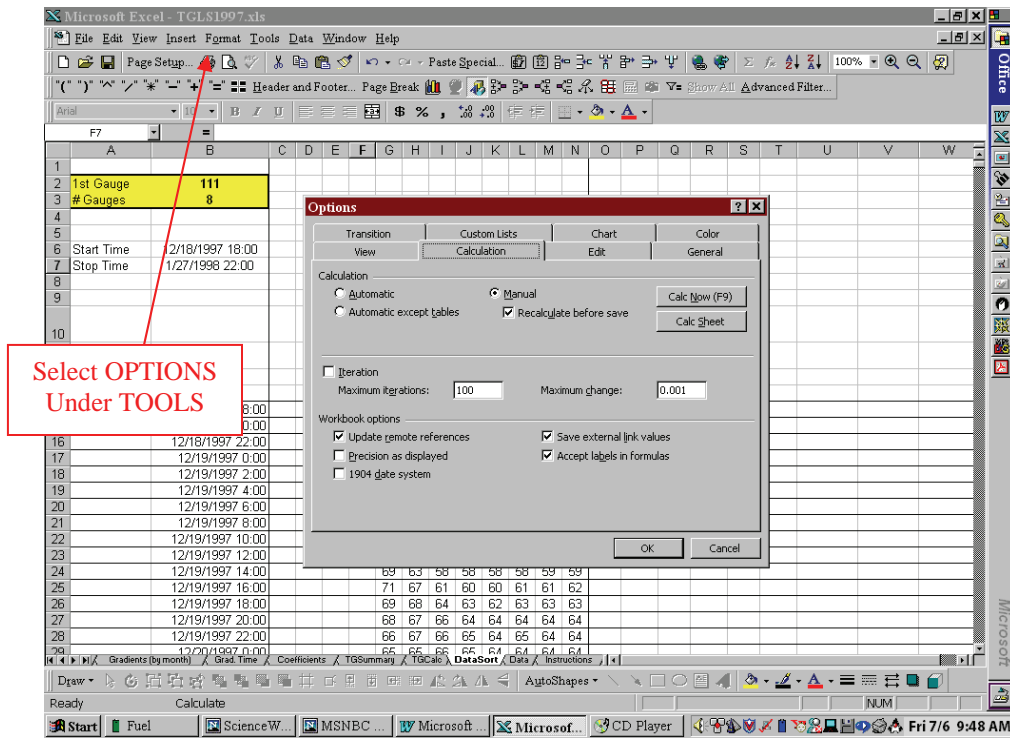


Figure 4.11 - Changing Excel Calculation Options to Manual

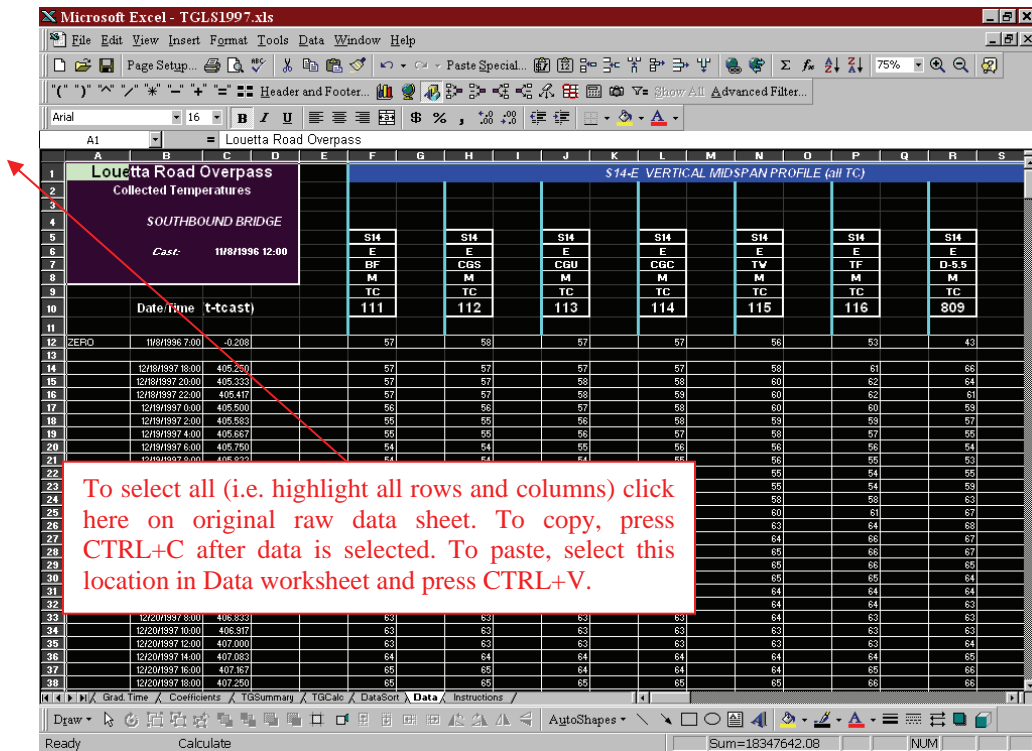


Figure 4.12 - Selecting Raw Data to Copy Into Data Worksheet

Step 6: Copy all rows with data from "DataSort" into "TGCalc" Do not leave blank rows between new sets of data.

The worksheet TGCalc is used to compile and analyze temperature data for the period of study (typically a calendar year). Data is to be copied into TGCalc from DataSort, which is a worksheet that automatically "weeds out" the temperature data of interest from the Data sheet to which the raw data has just been copied. It is important that the DataSort worksheet not be modified in any way (except as described in Step 3 when appropriate). To copy data from DataSort to TGCalc:

- Select all rows (it is easiest to select complete rows by clicking on the row number) from Row 14 down to the end of the data in DataSort. Alternatively, if this is data from the very beginning or very end of the calendar year, only the appropriate rows should be selected.
- Press CTRL+C to copy these rows to the clipboard.
- Highlight the beginning row on which to place the data within TGCalc by clicking on the row number. This should be Row 14 on TGCalc, or the next sequential row number if appending data to existing data in TGCalc. Do not paste anything over Row 13 in TGCalc!!!
- Press CTRL+V to paste the rows that were copied to the clipboard.

Step 7: Repeat the previous two steps (Steps 5 and 6) for all raw data files associated with the period of study.

The period of study will typically be a calendar year. Once Steps 5 and 6 have been repeated the appropriate number of times, the end result should be that all of the temperature data from the correct gauges for the entire period of study (calendar year) has been pasted into Rows 14 and below in the TGCalc worksheet. It is important that this data be pasted sequentially with earliest dates at the top. However, if gaps in the data exist because the data acquisition systems malfunctioned or because the data is missing, these problems are addressed in subsequent steps.

Step 8: Copy the equations in Row 13, Columns O through AT, of the sheet "TGCalc" to all subsequent rows with data.

Pasting these formulas in rows 14 and higher will allow for the maximum and average temperatures to be calculated, as well as for thermal gradients to be computed. These equations must be present in Columns O through AT for all rows with temperature data on the TGCalc sheet. The equations in row 13 should not be deleted even though they are "dummy" equations and do not correspond to specific data.

Step 9: Copy the equations in Row 10, Columns G through AD, of the sheet "TGSummary" to all subsequent rows.

The worksheet TGSummary is the main worksheet on which all average bridge temperature (and thermal gradient) data is summarized. The data should appear for a calendar year in Rows 10 through 374. The equations in Row 10, Columns G through AD, should be copied down through

row 374 such that data is calculated for each individual day. Columns B through F in TGSummary are automatically filled and should not be modified. Data computed in the TGSummary worksheet for each day includes:

- Maximum temperature (and time and location at which it occurred)
- Minimum temperature (and time and location)
- Maximum positive thermal gradient (and time and location)
- Maximum negative thermal gradient (and time and location)
- Maximum average bridge temperature (and time)
- Minimum average bridge temperature (and time)
- Maximum deck temperature (and time)
- Minimum deck temperature (and time)
- Maximum ambient temperature
- Minimum ambient temperature

(For a leap year, a single row should be inserted between rows 68 and 69. The equations in Columns B through F should be copied from the row above into the new row. The value of 28 in Cell A377 should also be changed to 29, representing the number of days in February.)

Step 10: Input/adjust the ambient temperature data in Columns AE and AF of the sheet "TGSummary".

The ambient daily maximum and minimum temperature data for each site (Louetta or San Angelo) must be obtained and input manually into Columns AE and AF of the TGSummary worksheet. This data can be downloaded from the National Climatic Data Center (NCDC) web site (www.ncdc.noaa.gov). This data can be downloaded free of charge (as of July 2001). For the Louetta Bridge, data from Houston Intercontinental Airport (Station #414300) should be used. For the San Angelo Bridge, data from San Angelo Mathis Field (Station #417943) should be used. This data has already been accumulated for the 1998, 1999, and 2000 calendar years, and can be found in the Excel workbook AmbientTemps199819992000.xls.

Step 11: Copy the formulas in Rows 376 and 396, Columns G through AD, of the sheet "TGSummary" to rows 377 through 387 and 397 through 407, respectively. Delete data from rows with data for less than half of the month's days.

The data in these rows summarizes the computed temperature values on a *monthly* basis. For example, the average maximum daily average bridge temperature in January is reported. Data in these rows is used in the monthly summary plots described in the next section. The values in Rows 376 through 387 are identical to the values in rows 396 through 407, but are presented to a different number of significant digits. The values in Rows E and F correspond to the number of days in that month with complete morning and afternoon data, respectively. When data is incomplete for a month (i.e. data exists for less than half of the days in that month), then an "x" appears in Rows C and/or D. In this situation, average data should not be reported for the month and the data in Rows G through AD should be deleted for that row so that the data does not appear in the monthly summary plots.

Step 12: Calculate the entire workbook

The entire workbook is calculated at this point; to be sure that data is updated. This process is explained in Step 4. (Note: The workbook should be calculated at several points during the process of creating a new workbook. This step is listed at this point as a reminder in case the workbook has not been calculated after performing earlier steps.)

Step 13: Print the sheet "TGSummary" and look for odd values, especially in the Maximum and Minimum temperatures.

The purpose of this step, which relies on the judgment of the reader, is to "weed out" bad data that results from error values in the raw data files.

In addition to the identification of basic trends in the data, a few specific conclusion statements should be developed similar to conclusions 1 through 7 for "Total Prestress Losses" in Section 7.5 of the comprehensive report. At a minimum, the following questions should be addressed:

- What are the ranges of values long-term prestress loss for each bridge?
- What is the most significant component of prestress loss for the beams in each bridge?
- Is there generally agreement between measured total prestress loss values for identical (or nearly identical) beams within a single span?
- How do the measured total net prestress loss values compared with the actual design predictions?
- How do the measured total net prestress loss values compare with the predictions from the detailed time-step model based on measured material properties and construction parameters?
- How do the measured total net prestress loss values compare with the predictions from other loss prediction methods (AASHTO and PCI)?
- How do the measured total net prestress losses values compare with the predictions from the prediction method suggested in Table 7.11 of the comprehensive report?

CHAPTER 5. LONG-TERM PRESTRESS LOSSES

This chapter discusses the collection of long-term prestress loss data for the Louetta and San Angelo Bridges. Long-term data is being collected for fifteen different beams between the two projects using embedded vibrating wire strain gauges. The selection of raw data and the correction for thermal effects are discussed in this chapter. Guidelines for analysis and comparison of measured data to predicted prestress losses are also presented.

Measurement of Prestress Losses

Prestress loss is defined in simple terms as a stress reduction in the prestressing strand over time. Prestress loss is caused by a number of factors; sources of loss in bonded pretensioned strands include elastic shortening, creep, shrinkage, and relaxation. Pre-release effects, including thermal effects, may also contribute to long-term prestress loss. A comprehensive discussion of sources of prestress loss may be found in Section 7.1.1 of the comprehensive report.

Prestress losses are essentially being measured continuously in the completed Louetta and San Angelo Bridges using embedded vibrating wire strain gauges. The measurement of losses is indirectly carried out by collecting long-term data on concrete strains at the level of the strand. As strain compatibility between the strand and surrounding concrete is assumed, the change in strain over time in the strand is taken to be equal to the measured change in strain over time in the surrounding concrete (at the level of the strand). The change in stress of the strand, or prestress loss, can then be calculated by multiplying this strain by the modulus of elasticity of prestressing steel.

This simple approach requires two other considerations. First, the component of loss associated with relaxation of the strand is *not* measured by the embedded gauges. Thus, the small component of loss associated with relaxation is computed analytically and added to the measured values. Secondly, this research program revealed an apparent loss of prestress *before release* for beams in the San Angelo and Louetta Bridges. Since the "zero" readings for the embedded gauges were taken at the time just before release of prestress, this component of loss is also not included in the measurements. Therefore, this pre-release loss must also be added analytically to the measured values.

Finally, it is important to note that temperature effects play an important role in the measurement of prestress losses because measured losses are computed from measured concrete strains. Both the seasonal temperature variations and daily temperature gradients that develop through the depth of the bridge beams affect the measured strains (and thus, the measured losses). Methods for addressing the role of these effects are presented in the next section.

A more complete discussion of the methodology employed in this research program for measurement of prestress losses is provided in Section 7.1.2 of the comprehensive report. It is highly recommended that the reader refer to this section prior to following the steps outlined in the next section.

Because readings are being recorded continuously, prestress loss data can, in theory, be reported at any time for the beams in the Louetta and San Angelo Bridges. As discussed in subsequent sections, it is recommended that data be reported annually for each bridge. In each annual report, data should be identified at approximately three month intervals. For example, an annual report written in December might present prestress loss measurements for each beam at four times throughout that year: March, June, September, and December. This will provide a somewhat continuous record of prestress loss data over the service lives of the structures.

Data Reduction - Determination of Measured Prestress Losses

The determination of prestress losses can be separated into two steps. First, raw concrete strain and temperature data is identified at the time of interest. Subsequently, corrections are made for thermal effects. The following sections address each of these steps in depth.

Identification of Raw Concrete Strain and Temperature Data

Raw strain and temperature data is obtained from the comprehensive modified data files (.MOD) created using the methods outlined in Chapter 2. Strain data for prestress losses is measured using **vibrating wire strain gauges (VW)** at the **center-of-gravity of prestressing strands (CGS)**. Temperatures corresponding to these gauge locations are measured using **thermistors (TR)** that are integrally attached to the vibrating wire gauges. One strain gauge and one temperature gauge at the CGS location at midspan are used for each of the fifteen beams in which long-term prestress loss data is being monitored, except for Louetta Beam S15 in which strains and temperatures are each measured with two embedded gauges at midspan.

For the date on which prestress losses are to be determined, strain and temperature data should be selected from early morning readings, such as 7:00 AM or 8:00 AM. The selection of raw data at these times will minimize the effect of daily thermal gradients, and will lead to more "stable" readings of prestress loss. If data is not available at these times on the day in question, then a different date should be selected for the raw data rather than taking earlier or later readings on the original day.

The Excel file LossesRawData.xls, shown in Figure 5.1, should be used to document the raw strain and temperature data. In this worksheet, gauge numbers corresponding to the vibrating wire gauges and thermistors that should be used for raw data are provided. The cells highlighted in yellow - measurement date, recorded strain, and recorded temperature - should be updated for each new set of readings (every three months or so). A new worksheet should also be created within this Excel file for each new set of readings to document these raw data values.

Microsoft Excel - LossesRawData.xls

File Edit View Insert Format Tools Data Window Help

Page Setup... Paste Special... Header and Footer... Page Break

Arial 10 B I U

J13 = 58

	A	B	C	D	E	F	G	H	I	J
1	LONG-TERM PRESTRESS LOSS RAW DATA SHEET									
2										
3	Beam	Measurement Date	Deck Casting Date	Release Date	Days After Deck Casting	Days After Release	Strain Gauge Ilo.(s)	Recorded Strain	Temp. Gauge Ilo.(s)	Recorded Temp.
4	Louetta HPC									
5	N32	3/18/1998	10/31/1996	2/16/1996	503	761	181	946	481	64
6	S15 #	3/16/1998	11/8/1996	2/27/1996	493	748	29, 35	770, 752	329, 335	64
7	S16	3/16/1998	11/8/1996	10/1/1994	493	1262	24	904	324	63
8	S25	3/16/1998	11/8/1996	11/11/1994	493	1221	78	663	378	63
9	San Angelo EB HPC									
10	E13	4/18/1998	6/12/1997	2/20/1997	310	422	1222	1078	1422	58
11	E14	4/18/1998	6/12/1997	2/20/1997	310	422	1228	1481	1428	58
12	E24	4/18/1998	6/25/1997	3/10/1997	297	404	1233	1247	1433	59
13	E25	4/18/1998	4/2/1996	3/10/1997	746	404	1202	1213	1402	58
14	E34	2/3/1998	7/9/1997	3/24/1997	209	316	1236	1401	1436	52
15	E35	2/3/1998	7/9/1997	3/31/1997	209	309	1238	1437	1438	52
16	E44	2/3/1998	8/2/1997	4/14/1997	185	295	1244	1332	1444	52
17	San Angelo WB Non-HPC									
18	W14	4/18/1998	12/3/1996	3/8/1996	501	771	1207	758	1410 *	56
19	W15	4/18/1998	12/3/1996	3/8/1996	501	771	1208	753	1410 *	56
20	W16	4/18/1998	12/3/1996	3/8/1996	501	771	1210	684	1410	56
21	W17	4/18/1998	12/3/1996	3/13/1996	501	766	1216	596	1416	56
22	# For Beam S15, record strains and temperatures for both East and West sides									
23	* Gauges 1407, 1408 assumed not to be working - if these gauges are working, use them for temperatures									
	Last Readings									

Draw AutoShapes

Ready NUM

Figure 5.13 - Long-Term Prestress Loss Raw Data Worksheet

It is important to note that strain values should be relatively stable long-term. There may be seasonal variations and will be some change due to long-term prestress loss, but these values should not change *significantly* over the three month period between readings. (The reader may wish to examine the plots of measured losses shown in Appendix G of the comprehensive report to see the relative stability of prestress loss measurements over time.) If the strain values appear to be changing drastically, it is likely that the gauge is damaged or not working properly. The gauge should be checked for long-term stability by examining the readings over a continuous period of time. The data should then either be taken from an earlier date when the gauge was working properly, or no data should be reported for that beam.

Correction for Temperature Effects / Updating of Plots and Prediction Models

The correction for *seasonal* temperature effects is performed as part of the process of updating data plots and long-term prediction models for prestress losses. (Note that the prediction models are the same models used for prediction of long-term camber and deflection.) These prediction models use a detailed time-step computer analysis that considers measured parameters such as the actual concrete strengths, measured moduli of elasticity, measured deck thicknesses, actual

construction schedule, etc. Explanation of the background of the model is beyond the scope of this report, but a brief description is found at the beginning of Appendix G of the comprehensive report.

The plots in Appendix G, which show measured and predicted prestress losses as a function of time, were created and should be updated using the Excel files FullTDxxx.xls. These files only need to be updated for the fifteen beams in which long-term prestress loss data is successfully being collected. For each of these files, three worksheets will be of interest for updating prestress loss measurements (Input, Measured Loss, and Loss Chart). All other worksheets are associated with camber and deflection or are simply used in performing the complicate calculations required for the time-step prediction models. These other sheets should not be modified!

Microsoft Excel - FullTDW16.xls

File Edit View Insert Format Tools Data Window Help

Page Setup... Paste Special...

Header and Footer... Page Break

Arial 10 B I U \$ % , .00 +.00

F7 =

	A	B	C	D	E	F	G	H	I	J	K	L	M	N	O	P
1	W16															
2						Release	After PT	Deck Only	Composite			Creep	Shr	Modulus	Strength	Slab Shr
3	Main	f_{jack}	202.50	A	820	818	532	1363		Ultimate	0.96	284	30.9	10200	525	
4		f_o	195.41	I	271470	270910	4004	744720		Power	0.8	1.6	2860	0.231	0.8	
5		# strand	52	ybot	24.00	24.04	5.86	37.81		Time	4.9	42.4		0.992	11.8	
6		A_{st}	0.153							VSRH	0.630	0.601			0.217	
7		cgs	5.46					t_{facking}	3.00		Multiplier	0%	0%	0%	0%	0%
8	Top	f_{jack}	202.50					t_{casing}	1.19			0.96	284.0	30.9	10200	525
9		f_o	193.39					t_{slitting}	0.25					2860		
10		# strand	0					$t_{\text{deck cut}}$	7.00							
11		A_{st}	0.217							L	127.79			Drape	0.883	0.117
12		cgs	52.00				Date	Age	Crp Adj.	d	54			Debond	1.000	0.000
13	Top PT	f_{jack}	202.50			Release	#####			harp	57.4			D+D		0.117
14		f_o	185.72			PT	#####	28	0.84	cgs,end	13.54			PT-Top	0.683	0.317
15		# strand	0			Cut Top	#####	89	0.74	Msw	1713			PT-Bot	0.841	0.159
16		A_{st}	0.217			Panels	#####	214	0.66	Mpanels	504			Cut Top	0.931	0.069
17		cgs	10.00			CIP	#####	270	0.65	MCIP	824			Panels	0.833	0.167
18	Bot PT	f_{jack}	202.50			Rails	#####	313	0.63	Mrails	0			CIP	0.833	0.167
19		f_o	191.82					375		Eslab	5120			Rails	0.833	0.167
20		# strand	0					500								
21		A_{st}	0.217					700								
22		cgs	4.63					1000								
23																

Change this age value to update prediction model

Input Measured Camber Camber Chart Measured Loss Loss C

Draw AutoShapes

Ready

NUM

Figure 5.14 - Time-Step Prediction Analysis "Input" Worksheet

The Input worksheet may be seen in Figure 5.2. All cells shaded green on the worksheets indicate input values which are linked throughout the spreadsheet and must be used in the calculations. The only value that needs to be changed for purposes of updating the prediction analysis to a new "ending date" is cell H22, which is circled in Figure 5.2. This cell represents the last date of the analysis, and should be modified to reflect the number of days between the release of prestressing strands and the date of prestress loss measurements in the completed bridge. This value is calculated in the LossesRawData.xls worksheet shown in Figure 5.1 (Column F). For example, if the beam was released on March 8, 1996 and (reported) prestress loss measurements are taken on April 18, 1998 (as for Beams W14, W15, and W16), then 771 would be entered for cell H22. Once this value is changed, the spreadsheet will automatically update other cells such that the prestress loss at the date in question is predicted. Release dates for all beams may be found on the Input worksheet, the LossesRawData.xls file, or in Appendix F of the comprehensive report.

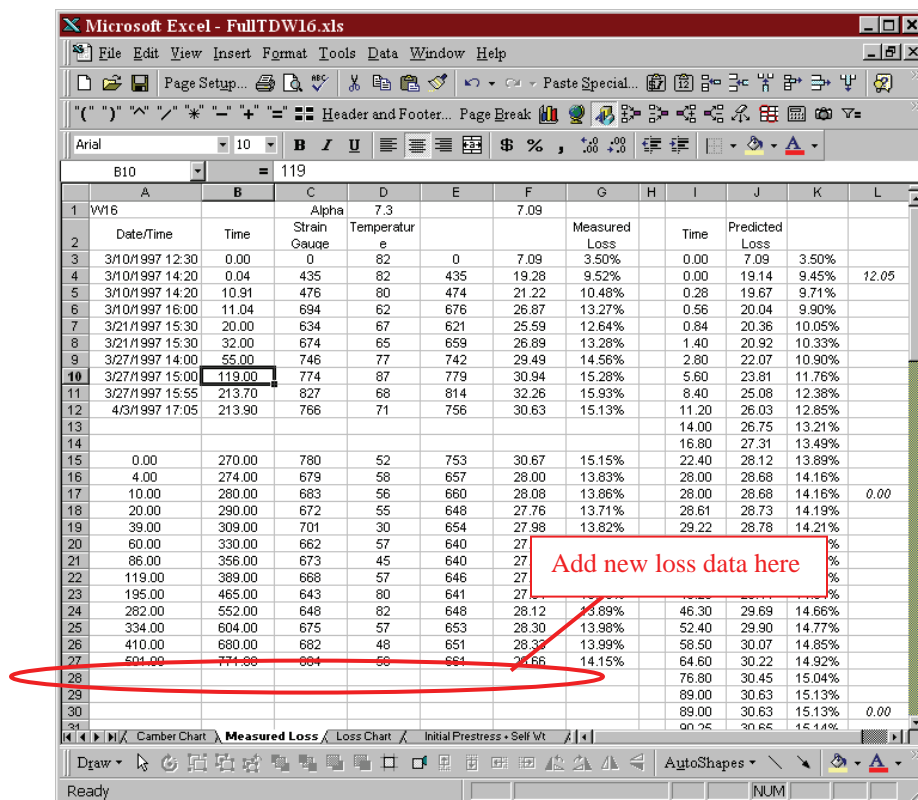


Figure 5.15 - Time-Step Prediction Analysis "Measured Loss" Worksheet

Once this input value is changed, the Measured Loss worksheet should then be used to enter the measured raw strain and temperature data for prestress losses in the beam. Seven values or formulas should be entered in the location shown in Figure 5.3, including:

- Days after cast-in-place deck placement (copy value from Column E in Fig. 5.1)
- Days after release of prestressing strands (copy value from Column F in Fig. 5.1)

- Raw strain measurement (copy value from Column H in Fig. 5.1)
- Raw temperature measurement (copy value from Column J in Fig. 5.1)
- Calculated temperature-corrected strain reading (copy formula from row above)
- Calculated net prestress loss, ksi (copy formula from row above)
- Calculated net prestress loss, % of jacking stress (copy formula from row above)

The second and fifth values - number of days after release and corrected long-term strain reading - should both be noted, as these values will be entered into a summary table (described in the next section). The predicted prestress loss at the date in question should also be noted; this predicted loss (in ksi) can be found by scrolling down to the bottom of column J.

Finally, the prestress loss plots should be updated. The plot may be found on the Loss Chart worksheet as shown in Figure 5.4. Although the plots are linked to the values on the Measured Loss Worksheet, the data series should be checked to ensure that all values including new data are properly plotted. Time scales on the x-axis may also need to be adjusted. For each beam, the measured and predicted loss plot should be presented in an appendix of the prestress loss measurement summary report (discussed in the next section).

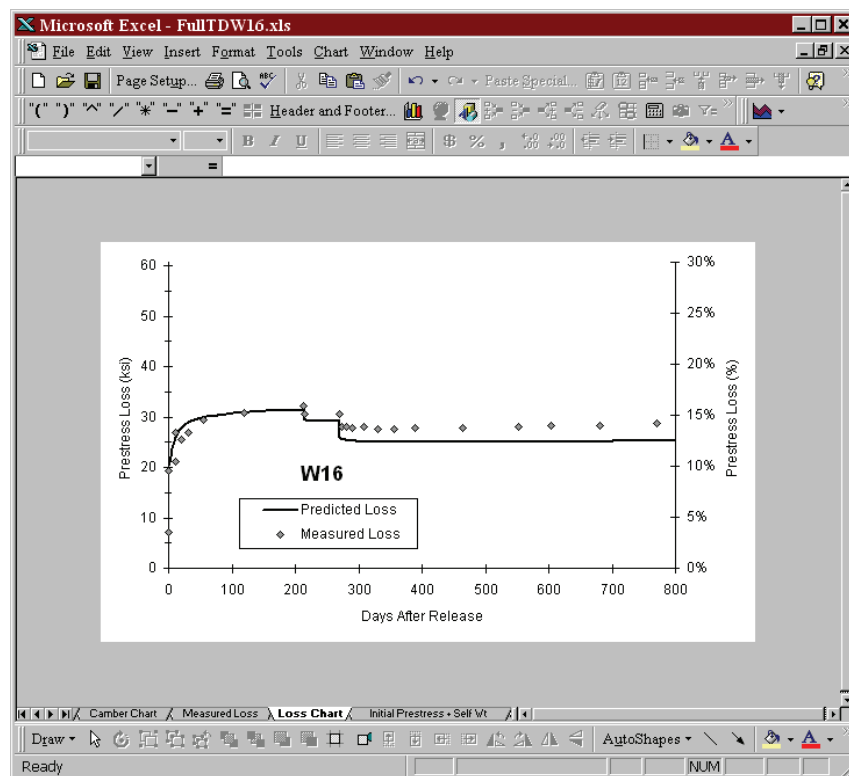


Figure 5.16 - Time-Step Prediction Analysis "Loss Chart" Worksheet

Beam	Days After Release	Loss Components (ksi)				Total Loss (ksi)	Total Loss (% of f_{jack})
		PR	ES	CR+SH *	RE		
Louetta HPC Beams							
N32	761	8.10	17.75	14.47	2.78	43.11	21.29
S15	748	8.10	16.38	10.61	2.77	37.86	18.70
S16	1262	8.10	17.16	11.93	3.06	40.26	19.88
S25	1221	8.10	12.96	9.70	3.04	33.81	16.70
Average		8.10	16.07	11.68	2.92	38.76	19.14
San Angelo Eastbound HPC Beams							
E13	422	8.10	25.03	15.02	2.46	50.61	24.99
E14	422	8.10	24.58	22.10	2.46	57.24	28.27
E24	404	9.11	20.19	19.78	2.43	51.51	25.44
E25	746	8.10	22.46	18.63	2.77	51.95	25.66
E34	316	9.11	30.86	15.17	2.30	57.43	28.36
E35	309	9.11	30.52	16.26	2.28	58.17	28.73
E44	305	9.11	26.15	18.09	2.28	55.63	27.47
Average		8.68	25.68	17.86	2.42	54.65	26.99
San Angelo Westbound Non-HPC Beams							
W14	771	7.09	13.94	10.84	2.79	34.67	17.12
W15	771	7.09	14.73	9.81	2.79	34.41	16.99
W16	771	7.09	12.18	10.62	2.79	32.68	16.14
W17	766	7.09	12.80	7.84	2.79	30.51	15.07
Average		7.09	13.41	9.78	2.79	33.07	16.33
1 ksi = 6.895 MPa							
* Includes compensation for measured elastic change in stress due to superimposed dead load							
See general notes at beginning of Appendix H.							
PR: Pre-release (See Section 7.2); ES: Elastic Shortening; CR: Creep; SH: Shrinkage; RE: Relaxation							

Figure 5.17 - Measured Total Prestress Losses in Individual Beams by Component

Beam	Total Prestress Losses (ksi)								
	Measured #	Incremental Time-Step (Meas. Parameters) #	Actual Beam Designs (PSTRS14 or ADAPT) #	AASHTO LRFD Time-Dependent Lump-Sum (Design Parameters) ##	AASHTO LRFD Components (Design Parameters) ##	AASHTO LRFD Components (Meas. Parameters) ##	PCI Design Handbook Components (Design Parameters)	PCI Design Handbook Components (Meas. Parameters)	Suggested Method # (Meas. Parameters)
Louetta HPC Beams									
N32	43.11	42.30	57.79	38.72	67.05	57.71	50.57	38.79	40.02
S15	37.86	44.36	57.79	40.65	72.53	61.25	55.99	40.85	41.60
S16	40.26	46.32	52.99	38.29	69.92	59.88	55.78	41.64	41.65
S25	33.81	40.99	52.99	36.68	62.12	52.46	46.27	34.27	36.83
Avg.	38.76	43.49	55.39	38.59	67.91	57.83	52.15	38.89	40.03
San Angelo Eastbound HPC Beams									
E13	50.61	54.48	49.36	57.21	102.35	88.19	81.73	63.81	55.51
E14	57.24	54.76	49.36	57.21	104.46	89.40	84.84	65.40	56.27
E24	51.51	54.17	49.83	56.43	103.96	89.09	83.02	65.16	55.67
E25	51.95	49.74	42.26	51.50	89.31	77.32	70.00	55.23	49.63
E34	57.43	54.79	50.85	57.67	105.45	90.91	83.87	66.48	56.80
E35	58.17	54.73	50.85	57.67	106.27	90.69	85.06	65.93	56.71
E44	55.63	55.70	51.01	57.85	105.83	91.90	84.40	67.32	57.75
Avg.	54.65	54.05	49.07	56.51	102.52	88.21	81.85	64.19	55.48
San Angelo Westbound Non-HPC Beams									
W14	34.67	30.52	47.91	41.02	51.91	45.54	39.18	31.76	28.68
W15	34.41	30.52	47.91	41.02	51.91	45.54	39.18	31.76	28.68
W16	32.68	30.52	47.91	41.02	51.91	45.54	39.18	31.76	28.68
W17	30.51	30.49	47.91	41.02	51.71	43.98	38.87	29.55	28.15
Avg.	33.07	30.51	47.91	41.02	51.86	45.15	39.10	31.21	28.55
1 ksi = 6.895 MPa For individual loss components, see Appendix H. # Includes pre-release losses. ## Includes pre-release relaxation losses only.									

Figure 5.18 - Comparison of Measured and Calculated Total Prestress Losses

Analysis of Data

For each beam, measured prestress losses should be compared with values predicted by several methods. Prestress loss summary tables, like those shown in Figures 5.5 and 5.6, should be prepared as part of an annual summary report. Measured values should be summarized in a table

such as that shown in Figure 5.5 for each set of readings (every three months), while a measured vs. predicted summary table such as that shown in Figure 5.6 should be prepared only for the last set of readings each year.

The Excel file LossesSummary_XXXX.xls (where XXXX is the date or number of the summary report [LossesSummary_LastReadings.xls is the final summary file from the original research project, dated April 1998]) should be used in this process. This file contains nine worksheets, one of which is used to calculate components of total measured loss for reporting in Figure 5.5, and eight prediction calculation sheets that are used for determining the predicted values to report in Figure 5.6. The purpose of each key worksheet is described below. Any modifications required for each sheet are also noted.

Measured - This worksheet is used to calculate the components of measured prestress loss. The worksheet can be seen in Figure 5.7. The yellow cells in columns B and D, containing the number of days after release and the corrected measured long-term strain (Columns B and E, respectively from Figure 5.3) should be updated with each new reading. Other cells contain constant values or are computed automatically. Column C contains the measured strain at release, which is used to calculate the elastic shortening loss. Column E contains the percentage gain in prestress caused by elongation of the strand when the precast deck panels and cast-in-place concrete deck are added. Column F contains the number of days between stressing of the strands and release, and is used in the calculation of relaxation loss. Column G contains the estimated pre-release loss, which is discussed in Section 7.2 of the comprehensive report.

	A	B	C	D	E	F	G	H	I	J	K	L	M	N	O
1															
2		Days	Rel ε	LT ε	EL %	RE Days	PR	ES	CR+SH	RE	EL	Measured Total Net	Measured Total		
3															
4	N32	761	634	947	2.82	5	8.10	17.75	14.47	2.78	-5.71	37.40	18.47%	43.11	21.29%
5	S15	748	585	773	2.64	5	8.10	16.38	10.61	2.77	-5.35	32.52	16.06%	37.86	18.70%
6	S16	1262	613	919	1.66	5	8.10	17.16	11.93	3.06	-3.36	36.89	18.22%	40.26	19.88%
7	S25	1221	463	672	1.90	5	8.10	12.96	9.70	3.04	-3.85	29.96	14.80%	33.81	16.70%
8															
9	E13	422	894	1082	4.82	5	8.10	25.03	15.02	2.46	-9.76	40.85	20.17%	50.61	24.99%
10	E14	422	878	1485	2.52	5	8.10	24.58	22.10	2.46	-5.10	52.14	25.75%	57.24	28.27%
11	E24	404	721	1251	2.44	5	9.11	20.19	19.78	2.43	-4.94	46.57	23.00%	51.51	25.44%
12	E25	746	802	1217	3.46	5	8.10	22.46	18.63	2.77	-7.01	44.95	22.20%	51.95	25.66%
13	E34	316	1102	1405	3.30	5	9.11	30.86	15.17	2.30	-6.68	50.75	25.06%	57.43	28.36%
14	E35	309	1090	1440	3.19	5	9.11	30.52	16.26	2.28	-6.46	51.71	25.54%	58.17	28.73%
15	E44	305	934	1335	3.39	5	9.11	26.15	18.09	2.28	-6.86	48.77	24.08%	55.63	27.47%
16															
17	W14	771	498	737	2.05	3	7.09	13.94	10.84	2.79	-4.15	30.52	15.07%	34.67	17.12%
18	W15	771	526	733	1.98	3	7.09	14.73	9.81	2.79	-4.01	30.40	15.01%	34.41	16.99%
19	W16	771	435	661	2.12	3	7.09	12.18	10.62	2.79	-4.29	28.39	14.02%	32.68	16.14%
20	W17	766	457	549	2.60	3	7.09	12.80	7.84	2.79	-5.27	25.25	12.47%	30.51	15.07%
21															
22	Lou							16.07	11.68	2.92	-4.57	34.19	16.89%	38.76	19.14%
23	SAEB							25.68	17.86	2.42	-6.69	47.96	23.68%	54.65	26.99%
24	SAWB							13.41	9.78	2.79	-4.43	28.64	14.14%	33.07	16.33%
25															

Figure 5.19 - Losses Summary "Measured" Worksheet

In columns H, I, J, and K, the actual components of loss are computed (ES = elastic shortening, CR+SH = creep & shrinkage combined, RE = relaxation, EL = gain in prestress due to deck loads). It is important to note that the CR+SH components cannot be separated in the measurement because they occur simultaneously. As mentioned previously, relaxation losses are computed analytically. Columns L, M, N, and O contain the measured *total net* and measured *total* losses. The *total net* losses represent the actual losses that occur over time when the reduction in losses (or prestress "gain") due to the precast deck panel and cast-in-place deck loads are considered. The *total* losses conservatively ignore this gain in prestress. Both values are used in comparisons with predicted values; the detailed time-step analysis computes prestress losses on the *total net* basis, while the more simplified methods compute losses on the *total* basis.

Relevant data from the *Measured* worksheet shown in Figure 5.7 should be placed in the measured losses summary table to be included in the summary report. Comparison of Figures 5.5 and 5.7 will show which values should be copied over.

	A	B	C	D	E	F	G	H	I	J	K	L	M	N
1		Days	Time-Step Total Net	Measured Total Net				EL	PR		Time-Step Total	Measured Total		
2														
3														
4	N32	761	35.98	17.77%	37.40	18.47%		6.32	8.10		42.30	20.89%	43.11	21.29%
5	S15	748	37.50	18.52%	32.52	16.06%		6.86	8.10		44.36	21.91%	37.86	18.70%
6	S16	1262	41.92	20.70%	36.89	18.22%		4.40	8.10		46.32	22.87%	40.26	19.88%
7	S25	1221	34.20	16.89%	29.96	14.80%		6.79	8.10		40.99	20.24%	33.81	16.70%
8														
9	E13	422	46.68	23.05%	40.85	20.17%		7.80	8.10		54.48	26.90%	50.61	24.99%
10	E14	422	47.66	23.54%	52.14	25.75%		7.10	8.10		54.76	27.04%	57.24	26.27%
11	E24	404	47.88	23.64%	46.57	23.00%		6.29	9.11		54.17	26.75%	51.51	25.44%
12	E25	746	43.19	21.33%	44.95	22.20%		6.55	8.10		49.74	24.56%	51.95	25.66%
13	E34	316	47.83	23.62%	50.75	25.06%		6.96	9.11		54.79	27.06%	57.43	28.36%
14	E35	309	47.42	23.42%	51.71	25.54%		7.31	9.11		54.73	27.03%	58.17	28.73%
15	E44	305	48.83	24.11%	48.77	24.08%		6.87	9.11		55.70	27.51%	55.63	27.47%
16														
17	W14	771	25.40	12.54%	30.52	15.07%		5.12	7.09		30.52	15.07%	34.67	17.12%
18	W15	771	25.40	12.54%	30.40	15.01%		5.12	7.09		30.52	15.07%	34.41	16.99%
19	W16	771	25.40	12.54%	28.39	14.02%		5.12	7.09		30.52	15.07%	32.68	16.14%
20	W17	766	24.17	11.94%	25.25	12.47%		6.32	7.09		30.49	15.06%	30.51	15.07%
21														
22	Lou		37.40	18.47%	34.19	16.89%					43.49	21.48%	38.76	19.14%
23	SAEB		47.07	23.24%	47.96	23.68%					54.05	26.69%	54.65	26.99%
24	SAWB		25.09	12.39%	28.64	14.14%					30.51	15.07%	33.07	16.33%
25														

Figure 5.20 - Losses Summary "Time-Step" Worksheet

Time-Step - This worksheet, shown in Figure 5.8, is used to summarize the results of the detailed time-step prediction analyses carried out using the FullTDxxx.xls files. Only the yellow cells in column B must be updated using the results from the time-dependent analyses (values from the bottom of Column J of the Measured Loss worksheet in the FullTDxxx.xls files) shown in Figure 5.3. Other cells contain constants or are computed automatically. Values corresponding to the *total* measured and predicted losses (Columns K and M) should be copied to the appropriate

columns of the measured vs. predicted summary table that will be included in the summary report. This summary table is shown in Figure 5.6.

Actual Design - 1 yr. - This worksheet shows the predicted prestress losses from computer programs used in the actual design of the bridges (PSTRS14 for Louetta and San Angelo WB, ADAPT for San Angelo EB). The values for *total* measured loss from this worksheet should be copied over to the summary table (Figure 5.6) only if the number of days after release for a particular measurement is less than 1000 days. Otherwise, the values from the worksheet *Actual Design - 5 yr.* should be copied over. Neither worksheet needs to be updated.

The other worksheets correspond to additional various prediction models used for comparison with the measured data. These worksheets do not require any modification since the values predicted by these methods are only for general "long-term" behavior, and not for a specific age after release. The values from these tables are already included in the version of Figure 5.6 shown in this chapter, so the last six columns of this figure may be copied directly when assembling the summary report. These methods are listed briefly below:

- AASHTO LRFD Time-Dependent Lump-Sum - Design (computations included on the AASHTO LRFD Components - Design worksheet)
- AASHTO LRFD Components - Measured
- AASHTO LRFD Components - Design
- PCI Handbook - Measured
- PCI Handbook - Design
- Suggested - Measured

Parameter(s)	"Design" Parameters	"Measured" Parameters
Section Properties	Gross section properties	Transformed section properties
Concrete Unit Weights / Dead Loads	Based on assumed deck dimensions and 150 pcf (3.29 kg/m ³) for all concrete.	Based on measured deck thickness and measured unit weights, with approx. weight of steel included for beams.
Concrete Strength	Nominal design concrete strength	Based on tests of companion specimens.
Modulus of Elasticity	Eq. 4.2 (non-HPC) or Eq. 4.4 (HPC) from comprehensive report, using nominal design strengths.	Based on tests of companion specimens.

Figure 5.21 - Summary of Design and Measured Parameters Used in Calculations of Prestress Losses

The reader is referred to Section 7.4 or the introduction to Appendix H in the comprehensive report for a detailed description of each of these methods. The difference between *measured* and *design* properties is summarized in Figure 5.9. In general, design properties are assumed values

that would be used in the design process, while measured properties are based on parameters obtained during the construction process.

Once the summary tables have been constructed, a brief written summary report should be created. The report should include the summary tables shown in Figure 5.5 for each measurement (approximately three months apart), the summary table shown in Figure 8.6 for the most recent data, and a commentary on the measured and predicted values. Plots of measured vs. predicted prestress losses (based on the detailed time-step analyses) should be included in an appendix to the report.

Comments should briefly summarize any observations regarding the new prestress loss measurements. In particular, measurements should be compared to previous measurements and any trends in the long-term prestress loss behavior noted (e.g. Have the prestress losses increased slightly for all beams, decreased slightly, or remained relatively stable?). As mentioned previously, it is generally expected that any changes in prestress loss should be small.

In addition to the identification of basic trends in the data, a few specific conclusion statements should be developed similar to conclusions 1 through 7 for "Total Prestress Losses" in Section 7.5 of the comprehensive report. At a minimum, the following questions should be addressed:

- What are the ranges of values long-term prestress loss for each bridge?
- What is the most significant component of prestress loss for the beams in each bridge?
- Is there generally agreement between measured total prestress loss values for identical (or nearly identical) beams within a single span?
- How do the measured total net prestress loss values compared with the actual design predictions?
- How do the measured total net prestress loss values compare with the predictions from the detailed time-step model based on measured material properties and construction parameters?
- How do the measured total net prestress loss values compare with the predictions from other loss prediction methods (AASHTO and PCI)?
- How do the measured total net prestress loss values compare with the predictions from the prediction method suggested in Table 7.11 of the comprehensive report?

CHAPTER 6. LONG-TERM CAMBER AND DEFLECTION

This chapter covers the measurement of long-term camber and deflection in the Louetta and San Angelo HPC Bridges. The system suggested for data collection and described herein is the precise surveying system. Planning issues are discussed, and the method of raw data collection is described in detail. Processing of raw data, including corrections for measurement errors and temperature effects are discussed. Guidelines for analysis of processed camber and deflection data are also provided.

Precise Surveying System

Several systems of deflection measurement may be used for collection of long-term data on bridges, with various levels of difficulty and varying degrees of accuracy. Examples of deflection measurement systems include tensioned wire systems, precise surveying, inclinometers, and GPS-based systems. Because it has successfully been used in the past at both the Louetta and San Angelo bridge locations, the precise surveying system is recommended here. This is not intended to discourage the use of more advanced systems at a later date, especially as more advanced systems become more available, less expensive, and more reliable.

The precise surveying system is described in detail in Section 3.2.2.7 of the comprehensive report. The reader should be familiar with this section. Essentially, the "precise" surveying system is a simple rod-and-level surveying system, with three special considerations intended to make the system more precise. First, sight distances are limited such that the instrument cross hairs can be read relative to a more magnified target (the rod). In general, sight distances should be limited to 30 to 40 feet, unless the instrument has a very powerful magnification that permits greater setup distances. Secondly, precision scales with 1/50 and 1/100 inch divisions are fixed to the rod using adhesive tape. Finally, a post level is used to keep the rod perfectly level during measurement. These considerations may be seen in Figures 6.1 through 6.3.

The precise surveying system may be either a relative or absolute system. In an absolute system, actual *elevations* of key points on the bridge are determined using a network of pre-established benchmarks. In the relative system, the *change in elevation* between support points and midspan of a given beam are measured; benchmarks are not required for a relative system. The selection of a relative or absolute system depends upon many considerations, which are discussed in the comprehensive report. Because it is not dependent upon any pre-established benchmarks, a relative system is suggested for all long-term camber and deflection readings in the Louetta and San Angelo bridges. A relative system is unaffected by changes at the jobsite, and each relative reading essentially stands alone. Depending upon project constraints, a relative system may involve readings on top of or below the superstructure.

(Note: If the original network of benchmarks can be located at the Louetta jobsite, or if a new network of benchmarks is established, an *absolute* precise surveying system may be implemented for the Louetta bridges.)



Figure 6.22 - Measurement of Camber Using the Precise Surveying System

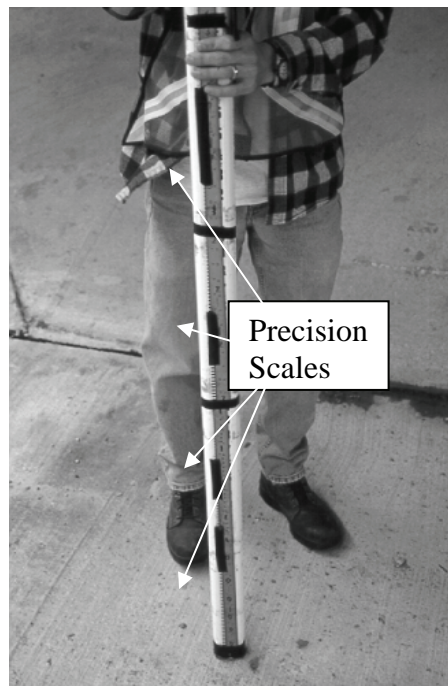


Figure 6.23 - Surveying Rod with Precision Scales Attached

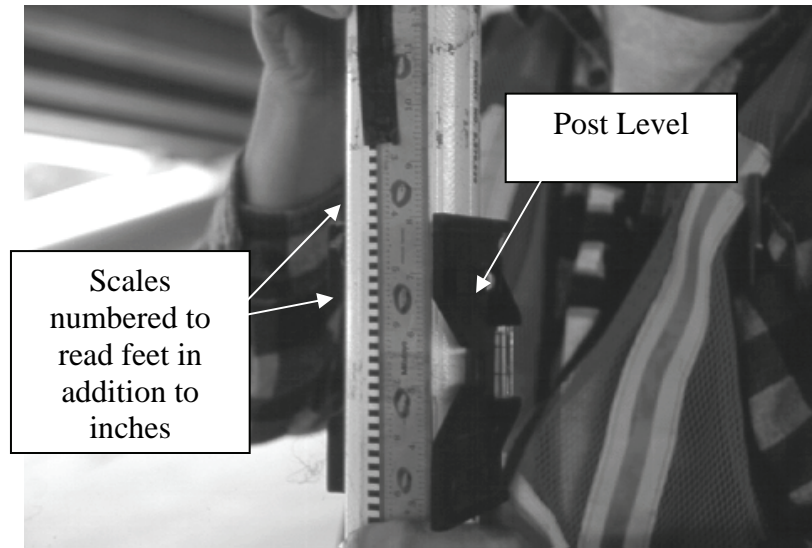


Figure 6.24 - Use of Post Level with Surveying Rod

Long-Term Camber and Deflection Readings - San Angelo

Camber and deflection measurements should be performed on the San Angelo bridges annually. Camber data was collected on fourteen San Angelo beams (ten HPC and four non-HPC), identified in Tables 3.7 and 3.8 of the comprehensive report, from fabrication of the beams through completion of bridge construction. However, in the completed bridge camber measurements were performed on *all* beams in the five instrumented spans. Camber measurements should therefore continue to be performed for all 27 beams located in Eastbound Spans 1 through 4 and Westbound Span 1.

Because of the site characteristics, the San Angelo bridges sit high above the ground elevation. In addition, the bridges cross the North Concho River. For these reasons, continuing camber measurements cannot practically be performed from below the superstructure. Camber must therefore be measured using precise surveying on the *top* surface of the deck. Benchmarks that are appropriate and usable cannot be established at the San Angelo jobsite in locations that are at a fixed elevation and not on the superstructure. Therefore, a *relative* precise surveying system is most appropriate for camber measurements at the San Angelo bridges.

Planning

Because measurements will be taken on the top surface of the bridge decks, the bridges will have to be closed to all traffic during the system setup and reading procedures. This will require coordination between the researchers and the TxDOT district or local offices. The ideal time for camber measurements is during the early morning hours on the weekend. On either Saturday or Sunday mornings, it is assumed that the impact of traffic closures will be least significant. Early morning readings also help to minimize the impact of thermal gradients on camber. Readings should essentially begin at dawn, or as soon as enough daylight is available to use the surveying equipment. If at all possible, readings during the midday and afternoon hours should be avoided.

It is recommended that two crews of three persons each be involved in the system setup and camber measurements. Depending on whether or not surveying points must be located (as described in the next section); there are two possibilities for the distribution of tasks between crews:

- If surveying points must be located, one crew should be responsible for locating these points and should move sequentially between spans. The second crew should follow on each span and be responsible for the actual surveying measurements. With this procedure, it is estimated that each span could be setup and measured in 30 to 45 minutes. The total time for this entire process is *estimated* to be approximately 3 to 4 hours.
- If surveying points do not need to be located, each crew should be responsible for measurements on two or three spans. Measurements on each span should take approximately 20 to 30 minutes. With two crews, all instrumented spans should be surveyed in about 1 1/2 to 2 hours. Alternatively, a single crew may be able to record all camber measurements in about 3 hours.

If enough personnel cannot be located, crews can be reduced to two persons. All system setup and camber measurement work can still be completed using two person crews, but the total amount of time for the entire process would be expected to increase. If five persons are available, three persons should be assigned to the system setup crew (if surveying points must be located), and two to the surveying measurement crew.

Setup of Surveying Points

The first work at the jobsite must be to establish the locations of points at which surveying readings will be taken. Typically, fluorescent marking paint is used to identify these locations. Depending upon exposure conditions and time between consecutive readings, these points may or may not need to be remarked each time measurements are to be taken. In an effort to reduce the need for locating points each time camber measurements are performed, points should be remarked using marking paint at the completion of each set of readings.

Extreme care must be taken such that the points are marked in the correct locations. Points are to be marked on the deck at three critical locations along the centerline of each beam: midspan, and directly above the center of *bearing* at each end. Fortunately, locating these points is not difficult because the San Angelo bridges have a perpendicular alignment. A 100' tape, 25' tape, chalk line, marker, and marking paint can facilitate the process of marking points.

The following considerations should be kept in mind in order to lay out points in the correct locations:

- The total width of the bridge(s) from *outside* edge of guardrail to *outside* edge of guardrail is 40 feet.
- Beam spacing (between centerlines of adjacent beams) are given in Tables 2.9 and 2.10 of the comprehensive report.

- The distance from the centerline of the exterior beam to the *outer* edge of the guardrail is 36 and 42 inches, respectively in the Westbound and Eastbound Bridges. (See Figure 2.26 of comprehensive report.)
- The width of the guard rail at the top of the deck is 9.75 inches.
- The construction joints *do not* coincide with the bearing locations for the beams. Instead, the construction joints are located above the centerline of the piers, as shown in Figure 9.4 (or at the face of the abutment back wall). For interior bents, the distance between center of bent and center of bearing may be taken as 29 inches. For abutments, this distance may be taken as 9.5 inches.
- Because of the above consideration, midspan of beams may not exactly coincide with midspan of the deck span (between construction joints). To be consistent with previous readings, midspan of *beams* should be marked. Distances between centerline of bearing at end of each beam are given in Tables 2.9 and 2.10 of the comprehensive report.

It is extremely important that each of the distances mentioned above be verified by a detailed examination of the bridge design drawings.

An example of the layout points can be seen in Figure 6.5 for an example span with five beams. For this situation, a total of 15 survey points would need to be marked.

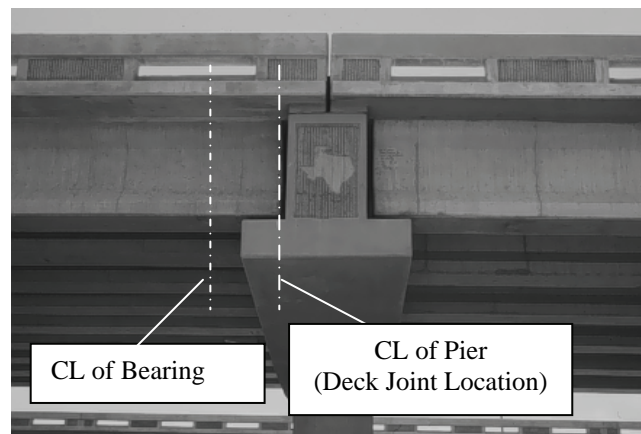


Figure 6.25 - Typical Pier Cap in San Angelo Bridges

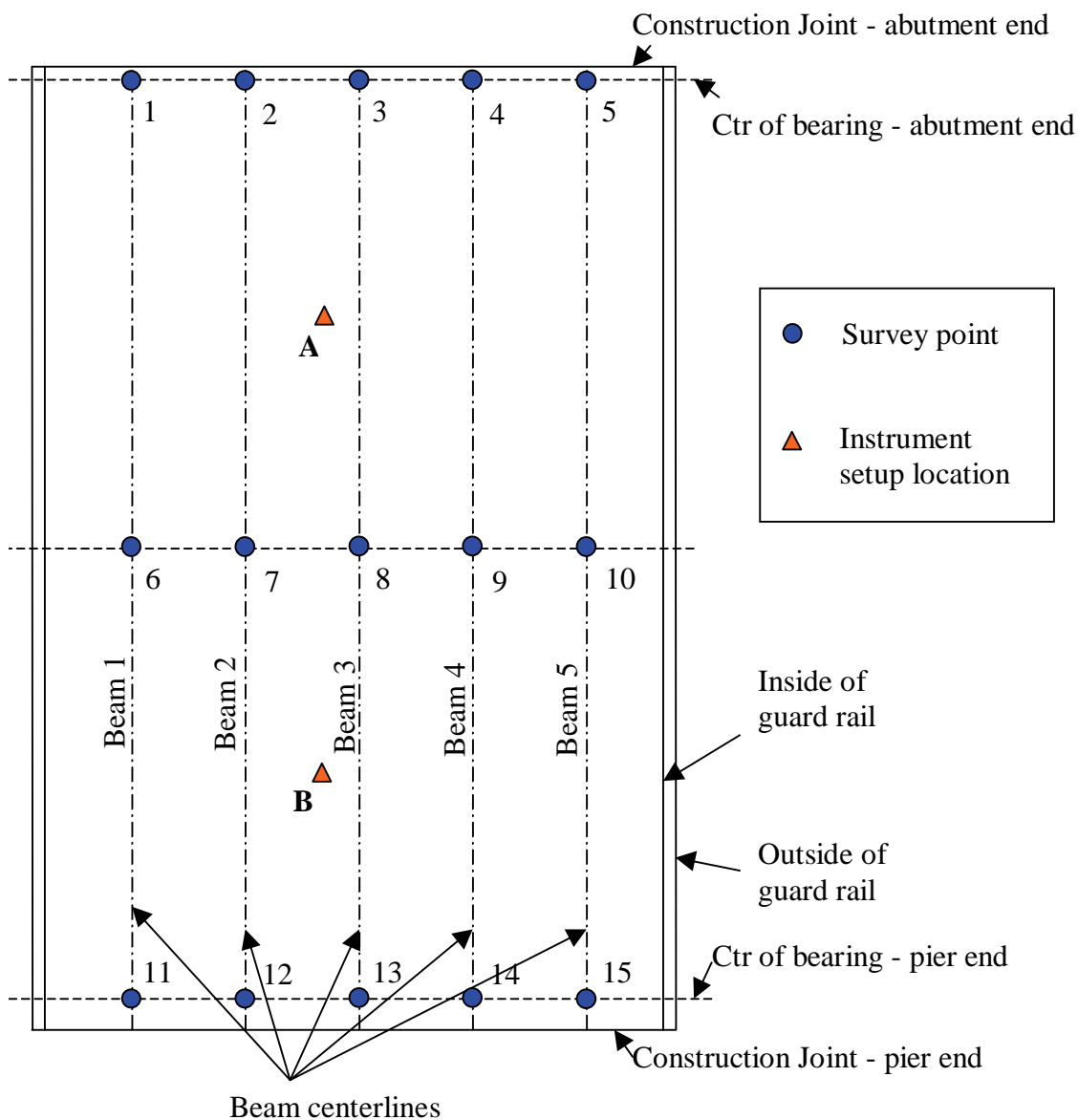


Figure 6.26 - Typical Precise Surveying Scheme for a San Angelo 5-Beam Span

Recording Raw Data in the Field by Precise Surveying (Relative Method)

For each span in the San Angelo bridges, measurement of camber requires setup of the instrument at two locations. From each location, a number of readings (relative elevations at survey points) are recorded. The elevation at one of the survey points is used to determine the elevation of the instrument after it is moved between setup locations.

Microsoft Excel - SATopofDeckReadings.xls

File Edit View Insert Format Tools Data Window Help

Arial 12 B I U

F2 =

	A	B	C	D	E	F	G	H
1	Span Example							
2								
3	4/20/2001 7:55							
4								
5			Beam No.					
6		Benchmark	1	2	3	4	5	
7								
8	West	100.00						HI
9	Bent		71.46	73.48	75.60	77.66	79.78	- Reading
10	Line		28.54	26.52	24.40	22.34	20.22	= Elevation
11		100.00						HI
12	Midspan		48.90	50.66	52.62	54.82	57.04	- Reading
13			51.10	49.34	47.38	45.18	42.96	= Elevation
14	East	122.28						HI
15	Bent		51.46	53.34	55.20	57.20	59.16	- Reading
16	Line		70.82	68.94	67.08	65.08	63.12	= Elevation
17								
18	Camber @ Deck Surface		1.42	1.61	1.64	1.47	1.29	
19	(Offset)					-0.25	-0.36	
20	@ Bottom of Beam					1.72	1.65	
21								

Example 1E Raw Data Sheet 2E Raw Data Sheet 3E Raw

Draw AutoShapes

Ready NUM

Figure 6.27 - Example of Raw Data Calculations for San Angelo Camber Readings

An example of the suggested procedure to be used for measurements on the example span in Figure 6.5 is given below. The raw data sheet shown in Figure 6.6 is used in conjunction with the example.

- Set up and level the instrument at Location **A**. The height of instrument (HI) is arbitrarily assumed to be 100.00 inches.
- Using the instrument, determine the distance (to a precision of 1/50 inch) that survey point **1** is below the instrument. (Assume this value is 71.46 in.)
- Without moving the instrument, repeat this procedure for points **2** through **5**. (Values = 73.48 in., 75.60 in., etc.)
- Without moving the instrument, repeat this procedure for points **6** through **10**.

- Move the instrument to location **B**. Set up and level the instrument.
- Measure the distance that point **10** is below the *new* height of instrument. Using the previously determined elevation of point **10**, determine the new height of instrument. (The elevation of point 10 was determined to be 42.96 in. The distance between point 10 and the new HI was found to be 79.32 in. Thus, the new HI is 122.28 in.)
- With the instrument at location **B**, determine elevations at points **11** through **15**. (Values = 51.46 in., 53.34 in., etc.)
- Determine the raw, uncorrected, top-of-deck camber for each beam. The camber is simply the elevation of the midspan point minus the average of the elevations above the bearings. (Beam 1: $51.10 - [(28.54 + 70.82)/2] = 1.42$ in.)

The Excel files SATopofDeckReadingsxx.xls (xx = 1E, 2E, 3E, 4E, 1W) can be used to check and store calculations. In each file, multiple worksheets will be found corresponding to previous readings. A new worksheet should be added for each new measurement. Raw data sheets for use in the field may be found in the file SATopofDeckReadings.xls.

Correction of Raw Camber Measurements

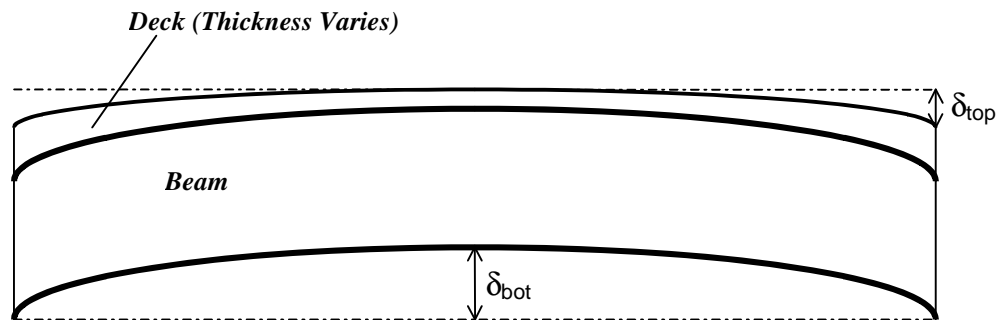
Measurement Location Correction (Top of Deck Correction)

As described in Sections 3.2.2.7 and 3.4.3.2 of the comprehensive report, camber measurements on the San Angelo bridges were performed on the bottom surface of the beam prior to the completion of construction at the jobsite. The system described in the previous section measures camber using the top surface of the deck, however. Because the deck is of varying thickness, these measurements are *not* identical. These two measurements are illustrated in Figure 6.7.

Camber of the deck surface is an important measurement that describes the profile of the actual deck surface. This value relates more to construction practices than to structural design calculations. Camber measurements for the top surface of the deck are recorded directly by the method described in the previous section.

To determine camber of the beams, the offset between the beam profile and deck profile must be known. In essence, this offset describes the average difference in deck thickness between the supports and midspan for each beam. These offsets were determined for all San Angelo beams using the readings on November 6, 1997. On this date, camber measurements were recorded on the bottom surface of the beams and subsequently on the top surface of the deck. Offsets are listed in Figure 6.7. Offsets are also provided in the raw data sheets found in the Excel files SATopofDeckReadingsxx.xls (xx = 1E, 2E, 3E, 4E, 1W). In most cases, camber was found to be larger when measured along the beams than when measured along the deck surface. Note that offsets are only provided for the 19 beams in which measurements were recorded on the bottom surface of the beam prior to completion of the bridges. Offsets are not known for Beams E21, E22, E23, E31, E32, E41, E42, or E43.

For all beams with offsets, two camber measurements should be reported - the "Top of Deck Camber" and the "Beam Camber".



$Offset = \delta_{top} - \delta_{bot}$	
Beam	Offset (in.)
E11	-2.73
E12	-2.11
E13	-2.24
E14	-3.00
E24	-0.35
E25	-0.01
E26	+0.28
E33	-0.27
E34	+0.19
E35	-1.19

Beam	Offset (in.)
E44	-1.18
E45	-0.74
W11	+0.04
W12	-0.54
W13	+0.12
W14	-0.36
W15	-0.28
W16	-0.42
W17	+0.04

Figure 6.28 - Difference between Top of Deck and Bottom of Beam Camber Readings

Thermal Gradient Correction

Thermal gradients are discussed in extensive detail in Section 5.4 of the comprehensive report. It is imperative that the reader be familiar with the contents of that section.

Thermal gradients within the depth of composite prestressed concrete beams affect the deflection behavior of such beams. In general, when the surface of the deck is at a higher temperature than the beam (which is shaded by the deck), an increase in camber is observed. On the other hand, when the surface of the deck is at a lower temperature, a decrease in camber is typically observed.

Thermal gradients are affected by environmental conditions at the bridge site, and are thus highly variable. However, thermal gradients can be *measured* quite easily using embedded instrumentation such as thermocouples and thermistors. Thermal gradients are being measured

on several beams in the Louetta and San Angelo bridges at one or two hour intervals as part of the long-term data collection on these bridges.

These thermal gradient measurements can be used to perform an analytical correction on measured camber data. Raw camber measurements must be adjusted to a "uniform temperature" or "no thermal gradient condition so that values at different ages can be meaningfully compared. As can be seen in Figure 6.8, camber may vary by as much as 0.50 inches or more over the course of a single day as a result of the changes in thermal gradients at different times of the day. Although the analytical correction described in this section is an approximation, it provides a rational method for "removing" the camber associated with thermal gradients.

To obtain the best camber measurements, both of the following considerations should be met:

- Avoid measuring camber in the midday and afternoon hours, when thermal gradients are highest.
- Correct all measurements by computing the theoretical thermal camber using the procedure described below. The thermal camber should be subtracted from the measured camber.

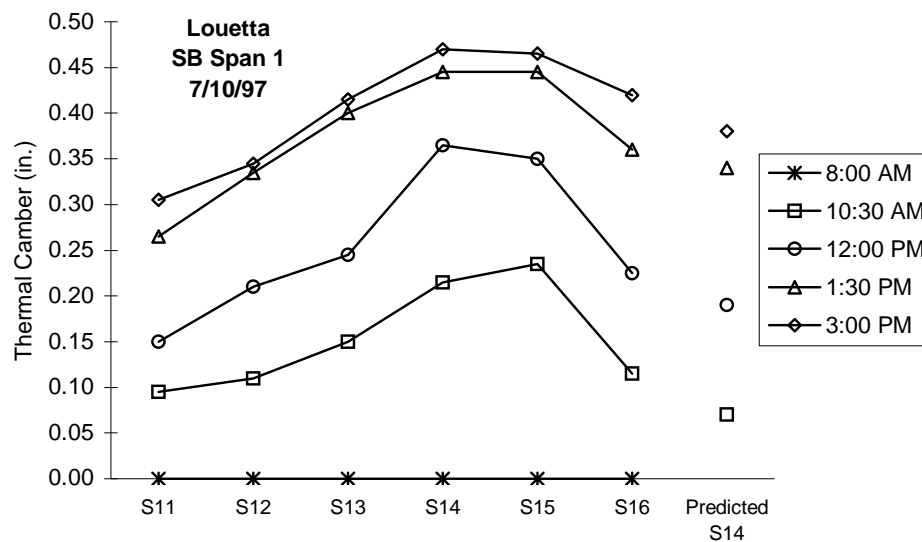


Figure 6.29 - Example of Measured and Analytically Predicted Thermal Camber

The computation of a camber caused by thermal gradients, or "thermal camber" is performed using a mechanics-based procedure that is described in detail in Section 5.4.1 of the comprehensive report. Essentially, the composite beam cross-section is divided into a series of layers of known width and thickness. The temperature of each layer must also be known. Using equilibrium and "plane sections remain plane" theory, elastic strains and self-equilibrating stresses are computed for each layer. The cross-sectional curvature can be determined from the strain distribution, and the thermal camber or deflection can then be computed by integrating the curvature along the length of the span.

Thermal camber for thermal gradient corrections in the San Angelo bridges can be calculated using the Excel file SATHermalCorrections.xls. This file consists of a single worksheet dedicated toward input and output, and multiple worksheets used to perform extensive calculations. The input/output worksheet can be seen in Figure 6.9. The reader will need only this sheet to perform calculations, but may wish to examine the more detailed calculation sheets to better understand the thermal gradient calculations. These worksheets contain important data for beams in each span, including span length, section properties, and material properties. *No cells should be modified in these detailed calculation sheets.*

Microsoft Excel - SATHermal Corrections.xls											
File Edit View Insert Format Tools Data Window Help											
Times New Roman 10 B I U											
K13 = 81											
To use, enter BLUE values. Calculations are performed on separate worksheets.											
Date and Time		11/6/1997 13:20	11/6/1997 12:40	11/6/1997 13:00	11/6/1997 13:10	11/6/1997 13:30					
Uses Measured TG for Beam(s)		E13	E24/E25	E34	E34 **	W14/W15/W16					
Span		1-E	2-E	3-E	4-E	1-W					
TEMPERATURES (deg F)	BF	63	62	64	65	63					
	CGS	62	60	62	62	62					
	CGU/I	61	60	61	61	61					
	CGC	61	60	61	62	61					
	TW	62	62	62	62	62					
	TF	62	62	64	63	62					
	D-5.5	71	68	72	74	72					
Thermal Camber (in.)	D-2	79	75	81	82	81					
		0.34	0.32	0.38	0.38	0.45	0.44	0.46	0.45	0.31	0.31
		Interior	Exterior	Interior	Exterior	Interior	Exterior	Interior	Exterior	Interior	Exterior
** No complete measured thermal gradient for Span 4-E											

Figure 6.30 - Input/Output Worksheet for Thermal Gradient Camber Calculations

The first step in using the thermal gradient camber worksheet is to identify the temperatures recorded using embedded gauges. These temperatures are identified using the sorted data files for embedded instrumentation gauges that were developed using the procedure described in Chapter 2. The temperatures selected to determine the thermal camber for each beam should meet the following criteria:

- Temperatures should be collected from a set of gauges comprising a vertical temperature profile for an interior composite beam in the same span as the beam for which thermal camber is being computed. (For example, when correcting the camber for Beam E22, temperatures from either Beam E24 or E25 should be used.)
- An alternate approach of averaging temperature data from several interior composite beams in the same bridge may be used. (For example, Beam E22 corrections may be based on average temperatures from Beams E13, E24, E25, and E34.)
- Temperatures from exterior beams should not be used, except when data is not available for interior beams. (Exterior beam temperatures exhibit much greater fluctuation based on the angle of the sun in the sky.)
- Temperature profiles must consist of a complete set of eight temperature measurements, including six through the depth of the beam and two in the slab directly above the beam.
- Temperature measurements should match, as close as possible, the time of camber readings. When the time does not match exactly, an interpolation of temperature data based on readings (scans) before and after the time of camber readings is appropriate, provided that the readings are reasonably close enough in time to the actual time of camber measurements.

The selection of temperatures for thermal gradient camber discussion is subjective and is ultimately left to the judgment of the reader. Because the analytical computation of thermal camber is approximate in nature, small variations in temperatures should not significantly impact the validity of making such a correction.

For simplicity, it is assumed that the same thermal camber occurs across all beams in a span, so temperatures are input on a span-by-span basis rather than a beam-by-beam basis. The computation worksheets will automatically use the eight temperatures input on the input/output worksheet and use them to assign temperatures to each layer of the composite beam. Slightly different calculations are performed for interior and exterior beams within a span because of the difference in section properties between interior and exterior beams. Once temperatures are input for a span, the computed thermal camber is shown on the same input/output worksheet.

In the thermal camber calculations, the baseline temperature against which the gradient is determined is always taken as the minimum temperature recorded through the depth of the cross-section. Therefore, it should be noted that this thermal camber computation only accounts for the effects of *daily* thermal gradients. This camber correction does not address the effect of seasonal fluctuations in the average bridge temperature. If the bridge were made of a single material, uniform temperature changes of any magnitude (for example, a change from 60 F through the entire cross-section to 80 F through the entire cross-section) would produce axial movements but not deflections. However, because the bridges are made of three different concretes (beam, panel, and cast-in-place deck) with different sets of material properties (coefficient of thermal expansion, elastic modulus), even uniform changes in temperature throughout the entire depth of

the cross-section can result in a slight upward camber or negative deflection. There is no simple, rational way to account for these seasonal effects. It is important for the researcher to keep in mind that reporting raw data will do the structural analyst no good, so meaningful reports will require other data against which the new data is to be compared. Any report of camber measurements should provide some comparisons with previous data and any predicted data (strains at the same locations calculated from predicted behavior).